INFORMATION TO USERS

This manuscript has been reproduced from the microfilm master. UMI films the text directly from the original or copy submitted. Thus, some thesis and dissertation copies are in typewriter face, while others may be from any type of computer printer.

The quality of this reproduction is dependent upon the quality of the copy submitted. Broken or indistinct print, colored or poor quality illustrations and photographs, print bleedthrough, substandard margins, and improper alignment can adversely affect reproduction.

In the unlikely event that the author did not send UMI a complete manuscript and there are missing pages, these will be noted. Also, if unauthorized copyright material had to be removed, a note will indicate the deletion.

Oversize materials (e.g., maps, drawings, charts) are reproduced by sectioning the original, beginning at the upper left-hand corner and continuing from left to right in equal sections with small overlaps. Each original is also photographed in one exposure and is included in reduced form at the back of the book.

Photographs included in the original manuscript have been reproduced xerographically in this copy. Higher quality 6" x 9" black and white photographic prints are available for any photographs or illustrations appearing in this copy for an additional charge. Contact UMI directly to order.

UMI

A Bell & Howell Information Company
300 North Zeeb Road, Ann Arbor MI 48106-1346 USA
313/761-4700 800/521-0600

The Synthesis and Characterization of Macrocyclic Ligands and Investigations of the Thermo and Photo Reactivity of Their Transition Metal Ion Complexes

by

Ian Mackay

B.Sc., University of Victoria, 1992

A Dissertation Submitted in Partial Fulfillment of the
Requirements for the Degree of

DOCTOR OF PHILOSOPHY

in the Department of Chemistry

We accept this dissertation as conforming
to the required standard

Dr. Alexander D. Kirk, Supervisor (Department of Chemistry)

Dr. Alexander McAuley, Department Member (Department of Chemistry)

Dr. Cornelia Bohne, Department Member (Department of Chemistry)

Dr. George Beer, Outside Member (Department of Physics)

Dr. William L. Waltz, External Examiner (Department of Chemistry, University of Saskatchewan)

Supervisors: Dr. A. D. Kirk and Dr. A. McAuley

Abstract

The mono protection of 1,4,7-triazacyclononane ([9]-aneN$_3$) was accomplished efficiently through the formation of an orthoamide derivative. The orthoamide was used to form three mono protected derivatives of [9]-aneN$_3$ which contained either a formyl, methyl, or benzyl protecting group attached to one of the nitrogen donors. The macrobicyclic complexes bicycloN$_5$, Me-bicycloN$_5$, and Bz-bicycloN$_5$ were synthesized through the Michael addition of two functional arms to the mono protected derivatives of [9]-aneN$_3$ followed by a ring closure template reaction around copper with glyoxal. Incomplete reduction by BH$_3$.THF led to the isolation of an enamine intermediate. The solution behavior of the Ni(II) and Ni(III) complexes of these macrobicyclic ligands is presented. The methyl and benzyl derivatives were found to have similar abilities as the parent bicycloN$_5$ ligand to stabilize the Ni(III) metal ion. Removal of the benzyl protecting group was achieved by reaction with formic acid in the presence of a Pd/C catalyst.

Attempts to couple two mono protected nonane molecules through the addition of functional acid chloride arms under conditions of high dilution were unsuccessful. Reaction of the benzyl protected bicyclic ligand Bz-bicycloN$_5$ with a bridging ligand in a high dilution reaction did provide evidence for the formation of a small amount of the novel macrotricyclic ligand tricyclo[9.14.9]N$_6$.

The Ni(II) complexes of the macrobicyclic ligands, and a series of other macrocyclic and related Ni(II) complexes having varying $Ni^{III/II}$ redox potentials, were used to study the quenching of the excited state of the platinum(II) dimeric complex $Pt_2(pop)_4^{4-}$. The quenching rate constants k_q were determined, and quenching of the excited state $^*Pt_2(pop)_4^{4-}$ by the nickel complexes was found to proceed by reductive

electron transfer. These results are discussed in terms of Marcus Theory. A plot of $\log k_q$ versus the ΔG for electron transfer was found to exhibit classic Rehm-Weller behavior. The excited state potential $Pt_2(pop)_4^{4-*/5-}$ was estimated from this series of quenching reactions and a range of 1.24 to 1.34 V (vs. NHE) was identified.

The photochemical and photophysical properties of the macrocyclic complex $Cr([18]\text{-}aneN_6)^{3+}$ ([18]-$aneN_6$ = 1,4,7,10,13,16-hexaazacyclooctadecane) were investigated and compared to the properties of the photoreactive Cr(III) complex $Cr(sen)^{3+}$ (sen = 4,4',4"-ethylidynetris(3-azabutan-1-amine)). The complex $Cr([18]\text{-}aneN_6)^{3+}$ was found to be unreactive ($\Phi_{rxn} < 10^{-3}$) while the photoreactivity of $Cr(sen)^{3+}$ was confirmed ($\Phi_{rxn} = 0.10$). Both of these complexes have very short ambient ^2E emission lifetimes and this is discussed in terms of distortions imposed on the complexes by the coordination of the ligands.

Direct irradiation into the doublet excited state of $Cr(sen)^{3+}$ at 675 nm resulted in a decrease in the quantum yield for the photoreaction of this complex from $\Phi_{rxn} = 0.10$ for quartet irradiation to $\Phi_{rxn} = 0.08$ for doublet irradiation. A model is suggested in which there are two competitive processes deactivating the doublet excited state; reverse intersystem crossing to the lowest quartet excited state and nonradiative decay back to the ground state. The temperature dependence of the ^2E emission lifetime was fitted to a two-term Arrhenius function to give estimates for the pre-exponential factors and activation energies of these two deactivation processes. Values of $A_1 = (1.2 \pm 0.9) \times 10^{15}\ s^{-1}$ and $E_{a1} = 45 \pm 1\ kJ\ mol^{-1}$, and $A_2 = (5.4 \pm 1.2) \times 10^{11}\ s^{-1}$ and $E_{a2} = 29 \pm 1\ kJ\ mol^{-1}$ were obtained.

The photostereochemistry of $Cr(sen)^{3+}$ was investigated using a modified reversed phase HPLC technique. A total of four photoproducts were identified from the photolysis of the resolved stereoisomers of $Cr(sen)^{3+}$and a loss of optical activity was found to be associated with the photoreaction. These results are discussed in terms of current models for predicting photostereoreactivity of Cr(III) complexes

Examiners:

Dr. Alexander D. Kirk, Co-Supervisor (Department of Chemistry)

Dr. Alexander McAuley, Co-Supervisor (Department of Chemistry)

Dr. Cornelia Bohne, Department Member (Department of Chemistry)

Dr. George Beer, Outside Member (Department of Physics)

Dr. William L. Waltz, External Examiner (Department of Chemistry, University of Saskatchewan)

Table of Contents

List of Tables

List of Figures

List of Schemes

List of Abbreviations

[9]-aneN_3	1,4,7-triazacyclononane
[10]-aneN_3	1,4,8-triazacyclodecane
maptacn	1-(3-aminopropyl)-1,4,7-triazacyclononane
daptacn	1,4-di-(3-aminopropyl)-1,4,7-triazacyclononane
taptacn	1,4,7-tri-(3-aminopropyl)-1,4,7-triazacyclononane
Me-daptacn	1-methyl-1,4-di-(3-aminopropyl)-1,4,7-triazacyclononane
Bz-daptacn	1-benzyl-1,4-di-(3-aminopropyl)-1,4,7-triazacyclononane
BicycloN_5	1,5,8,12,17-pentaazabicyclo[10.5.2]-nonadecane
Me-BicycloN_5	1-methyl-1,5,8,12,17-pentaazabicyclo[10.5.2]-nonadecane
Bz-BicycloN_5	1-benzyl-1,5,8,12,17-pentaazabicyclo[10.5.2]-nonadecane
[18]-aneN_6	1,4,7,10,13,16-hexaazacyclooctadecane
sen	4,4',4"-ethylidynetris(3-azabutan-1-amine)
sep	1,3,6,8,10,13,19-octaazabicyclo-[6-6-6]-eicosane
sar	3,6,10,13,16,19-hexaazabicyclo[6.6.6]-eicosane
diamsar	1,8-diamino-3,6,10,13,16,19-hexaazabicyclo[6.6.6]-eicosane
bipy	2,2'-bipyridine
CI	chemical ionization
cyclam	1,4,7,11-tetraazacyclotetradecane
CV	cyclic voltammetry
dmso	dimethyl sulfoxide
en	ethylenediamine
ESR	electron spin resonance
FAB	fast atom bombardment
ferrioxalate	trisoxalatoferrate(III), $[Fe(C_2O_4)_3]^{3-}$
Flu	fluorescence

HPLC	high performance liquid chromatography
L	ligand
LFP	laser flash photolysis
MS	mass spectroscopy
NMR	nuclear magnetic resonance
NHE	normal hydrogen electrode
ORD	optical rotary dispersion
Phos	phosphorescence
$[Pt_2(pop)_4]^{4-}$	tetrakis(μ-pyrophosphite-P,P')diplatinate(II) anion, $[Pt_2(\mu\text{-}P_2O_5H_2)_4]^{4-}$
phen	1,10-phenanthroline
pop	pyrophosphite^{2-}
ppm	parts per million
R	alkyl
tacn	1,4,7-triazacyclononane
THF	tetrahydrofuran
tosyl	p-tolyl-sulfonyl
t_R	retention time
SCE	saturated calomel electrode
SV	Stern-Volmer
trityl	triphenyl methyl
UV/Vis	ultra violet and visible
VC	Vanquickenbourne-Ceulemans

Acknowledgments

I wish to express my sincere appreciation to my supervisors Dr. A.D. Kirk and Dr. A. McAuley for their guidance and assistance throughout this research project. I would like to thank Mr. G. Irwin for providing LFP conductivity detection data fof $Cr(NH_3)_6^{3+}$ and $Cr(sen)^{3+}$, as well as many helpful discussions. I would also like to thank Dr. R. Fernando and Dr. L. Cai for their assistance and friendship.

I would like to thank Mrs. C. Greenwood for NMR spectra, and Dr. D. McGillvary for providing the mass spectra. I appreciate the cooperation from the technical staff in the instrument, mechanical and glass shops, and I would also like to thank my fellow graduate students for creating an enjoyable working environment.

This dissertation is dedicated to

My Family

CHAPTER ONE

INTRODUCTION

1.1 General

The unifying theme of this dissertation is the investigation of macrocyclic ligands and their transition metal complexes. The goals of this project were to design and synthesize novel macrocyclic ligands, and to use existing macrocyclic systems to study the chemistry of their transition metal complexes, both in the ground state, and in the excited state.

1.2 The Origins of Macrocyclic Chemistry

A macrocyclic ligand, as defined by Melson,[1] is a cyclic compound with nine or more members (including all hetero atoms) and with at least three or more donor (ligating) atoms. One of the simplest, most commonly studied macrocycles is the nine member ring 1,4,7-triazacyclononane, having three donor nitrogen atoms. From this small molecule, the range of complexity of macrocyclic ligands, both naturally occurring and synthetic in origin, includes examples of ligands containing many atoms and having mixed donors and multiple ring systems.

1.2.1 Historical

The development of coordination chemistry can be traced back to the work of such pioneers as Tassaert, who in 1798 reported that solutions of a cobalt salt reacted with ammonia to yield an orange color crystalline material containing 6 molecules of ammonia.[2] S. M. Jorgensen (1837 - 1914) was the first to systematically study the synthesis of such "complexes", and it was Alfred Werner (1866 - 1914) who correctly interpreted their true nature. Werner showed that neutral molecules were bound directly to the metal so that complex salts such as $CoCl_3 \cdot 6NH_3$ should be correctly formulated as $[Co(NH_3)_6]Cl_3$, thus developing the concept of a coordination complex. He also demonstrated that the ligands

occupy positions that describe the corners of an octahedron or a square. In the classic example $[Pt(NH_3)_2Cl_2]$ was shown to have a square planar arrangement giving rise to its two existing isomers. Werner's coordination theory,[3] for which he was awarded the Nobel Prize in 1913, led to the development of new theories of chemical bonding, and opened the door to the study of many other, more complicated, inorganic coordination complexes. It is from these humble beginnings that the field of macrocyclic chemistry has developed.

The discovery and study of coordination compounds containing macrocyclic ligands date back as early as the beginning of this century. The first macrocyclic compounds studied were unsaturated nitrogen containing rings with 14 - 16 members. The special nature of the synthetic macrocycle phthalocyanine and its metal complexes has been well documented[4] and the properties of these intensely colored compounds have been used in many commercial applications including dyes and pigments. Other naturally occurring macrocycles such as the porphyrins, chlorin, and corrin have been isolated and studied for their relationship with important biological systems such as haeme, chlorophyll, and vitamin B_{12} (Figure 1.2).

The first synthetic macrocycle to be isolated was by Curtis in 1960 [5] when he tried to recrystallise a nickel (II) tris ethylenediamine salt from acetone and produced an unexpected tetraaza macrocycle in what was also the first example of a "template" synthesis (Figure 1.1).

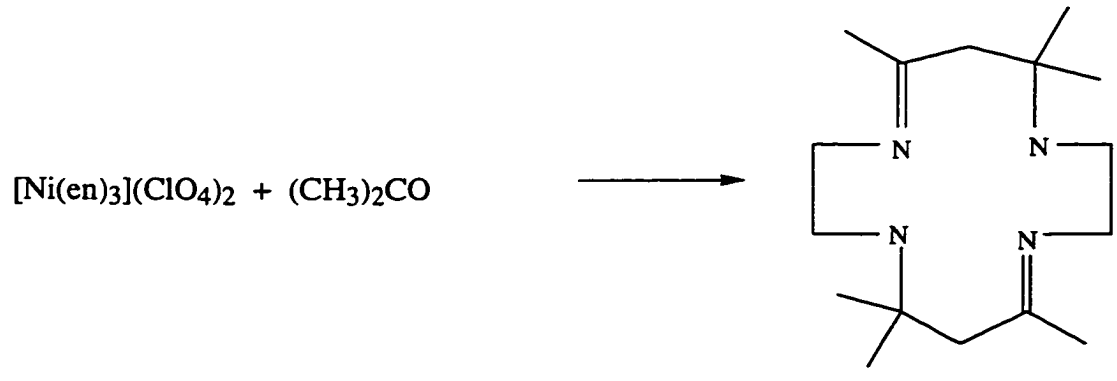

Figure 1.1 Template synthesis of Curtis macrocycle

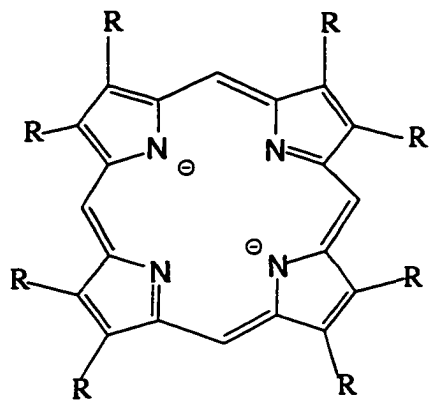

Porphyrin

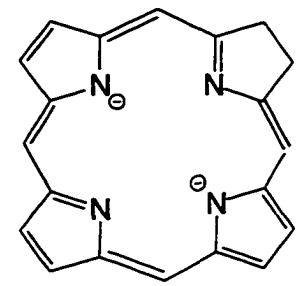

Chlorin

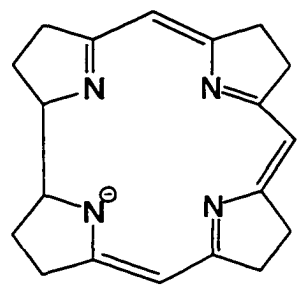

Corrin

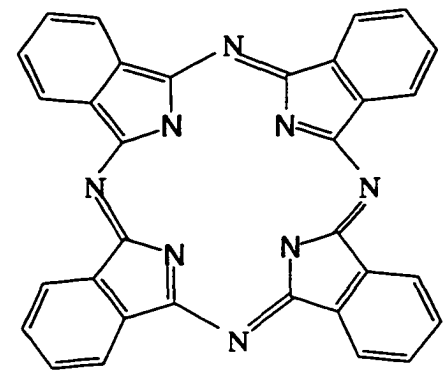

Phthalocyanine

Figure 1.2 Structures of some well known macrocyclic rings

After 1960, new synthetic methods were developed for the synthesis of macrocyclic ligands.[5,6] This has led to the formation of many new saturated and unsaturated macrocycles containing, nitrogen, oxygen and sulfur donor ligands. The natural consequence of this development was the current trend toward the study of more complex systems. The possibility of using synthetic macrocyclic complexes to mimic biological systems has been the driving force for much of this work. In addition to the biological

implications, macrocyclic ligands have found applications in many other areas. They have been developed for metal-ion catalysis, organic synthesis, metal-ion discrimination and analytical methods, and a number of industrial and medical applications.[7] More recently, macrocyclic complexes have been developed for uses in photochemical and photophysical processes; the design of many light induced devices such as 'switches', 'relays', and 'antennas' incorporate a macrocyclic ligand. The quest for efficient solar energy conversion as an alternative fuel source has provided much of the impetus for this research work. In this new class of molecule the macrocyclic component retains its own set of intrinsic properties while at the same time contributing to produce the unique properties of a larger molecular device. The study of the photochemical and photophysical properties of such "supermolecules" constitutes the new and exciting area of *supramolecular* photochemistry.

1.2.2 The Macrocyclic Effect

Macrocyclic complexes have been shown to have very different properties when compared to their open chain analogs. These properties include: 1) greater thermodynamic stability, 2) kinetic inertness of the complex towards demetallation, 3) greater ligand field strength, 4) the stabilization of less common oxidation states.

The term "macrocyclic effect" was first introduced by Cabbiness and Margerum[8] in 1969 to account for the enhanced thermodynamic stability of complexes containing macrocyclic ligands. An example of this is shown in Table 1.1.[9] The stabilization observed for the macrocyclic copper complex in this series is greater than what would be expected solely from the presence of an additional chelate ring (the "chelate" effect). The origins of the macrocyclic effect has been found to be both thermodynamic and kinetic in nature.

Table 1.1 Thermodynamic properties of Cu^{2+} complexes of tetraamine ligands in water

Ligand	log K	ΔH (kcal mol^{-1})	TΔS (kcal mol^{-1})
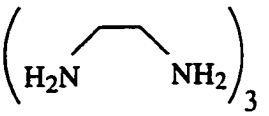 (en)	19.7	-25.2	1.7
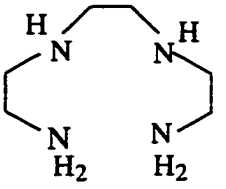 (2,2,2-tet)	20.1	-21.6	5.8
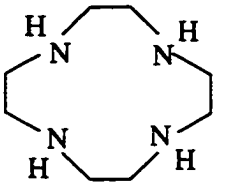 (cyclen)	24.8	-18.3	15.3

1.2.2.1 Thermodynamic Stability

The thermodynamic stability of macrocyclic complexes has been attributed to both entropic and enthalpic factors. The formation of a macrocyclic complex can almost always be associated with a favorable entropy change. This is comparable to the "chelate" effect,[10] where a favorable entropy results from the displacement of monodentate ligands by polydentate chelating ligands. Upon coordination, desolvation occurs, and in the case of multidentate ligands more molecules of solvent are released per unit of chelated ligand complexed, hence there is an increase in the translational and rotational entropy.

The role of the enthalpic term in the macrocyclic effect has been the topic of much debate.[11] The contribution from this term tends to vary depending on the nature of the macrocycle and on the nature of the metal. Some of the factors thought to play a role include: preorientation of the ligand, metal ion - hole size match, intrinsic basicity effects, ligand desolvation enthalpies, and dipole-dipole repulsion within the cavity of the macrocyclic ligand.[12]

1.2.2.2 Kinetic Stability

The kinetic contribution of the macrocyclic effect can be attributed to "multiple juxtapositional fixedness", a term which was introduced by Busch and co-workers[13] to explain the kinetic inertness of macrocyclic complexes. This is illustrated by the fact that $Ni(NH_3)_6^{2+}$ and $Ni(en)_3^{2+}$ complexes decompose within seconds in strongly acid solutions, $Ni(3,2,3\text{-tet})^{2+}$ decomposes within minutes, and $Ni(cyclam)^{2+}$ has a half life of approximately 30 years.[14] The open chain ligand can undergo successive predominantly dissociative displacement of the nitrogen donors by solvent molecules. In acid media, the amine donors become protonated and can no longer coordinate to the metal. In the case of the macrocyclic ligand there is no "open" end at which this displacement mechanism may commence. Dissociation of one of the nitrogen donors in the macrocyclic ring requires extensive rearrangement of the cyclic ligand, as illustrated in Figure 1.3. In order to achieve dissociation, the ligand would have to fold. This is not a favorable process and protonation is therefore retarded. In addition, the dissociated macrocyclic donor is kept in close proximity to the metal ion by the remaining coordinated ring system which increases the chances that recomplexation will occur.

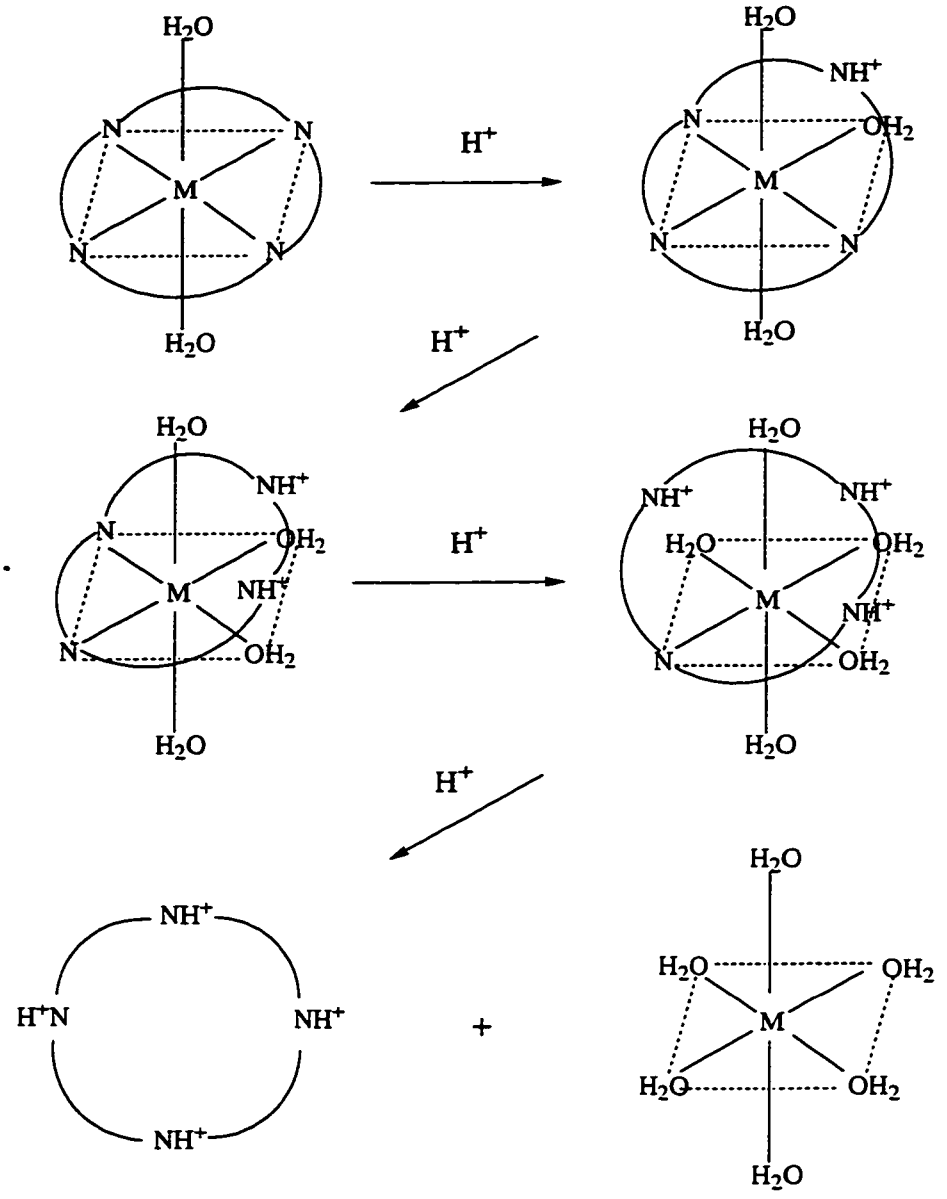

Figure 1.3 Acid catalyzed dissociation mechanism for macrocyclic ligands

1.2.2.3 Ligand Field Strength

Macrocyclic ligands have been shown to have stronger ligand field strengths than their non cyclic counter parts. This has been attributed to constrictive effects imparted on the metal ion by the macrocyclic ligand.[15] One can view the macrocyclic ligand as a stiff elastic band, which, if it is too small, must be stretched to accommodate the metal ion. This distortion exerts a force that enhances the metal-donor interaction and increases the ligand field splitting. More recently however, this increase in ligand field strength has been attributed to the increase in the intrinsic basicity of the secondary donor nitrogen atoms in the macrocyclic complexes, compared to primary donor nitrogen in the non macrocyclic complexes.[16] In the case of the secondary nitrogen donors, it has been proposed that a stronger M-N bond combined with low M-N bond strain results in the larger ligand field.

1.2.2.4 Stabilization of Unusual Oxidation States

The ability of macrocyclic ligands to stabilize less common oxidation states of a coordinated metal ion has been well documented.[17] For example, both the high-spin and low-spin Ni(II) complexes of cyclam are more easily oxidized to Ni(III) than are their corresponding open chain analogs. Unlike the open chain analogs, macrocyclic complexes of the nickel(III) ion have been found to persist long enough to allow for spectroscopic and kinetic studies.[18]

The stabilization of high oxidation states can be explained by both the thermodynamic and kinetic stability of the macrocyclic ligand. The thermodynamic contribution results from an increase in the ligand field splitting. This increased ligand field strength raises the energy of the electrons in the antibonding HOMO orbitals which makes it easier for these electrons to be removed. This results in a lowering of the redox potential to the higher oxidation states.

The kinetic contribution arises due to the fact that once the higher oxidation state is obtained, it is harder for any reducing influence, such as solvent, to reach the metal ion which is trapped in the ligand's closed framework.

A detailed study of the factors influencing the redox properties of twenty-seven nickel(II) tetraaza macrocycles was carried out by Busch and co-workers.[15] For a series of different macrocyclic ligands, a range of nearly two volts can be observed (Figure 1.4) for the Ni^{III}/Ni^{II} couple. The structural factors which favor higher oxidation states for the metal ion include having a negative charge on the ligand, and a match between the oxidized metal size and the ligand cavity. Lower oxidation states are favored by an increase in ligand unsaturation, and by increasing the number of substituents on the macrocyclic ring. The nature of the donor atom can also have an effect on the stability of oxidation states. As the donor type is changed from S, O, to N the Ni(III) state becomes more stable.

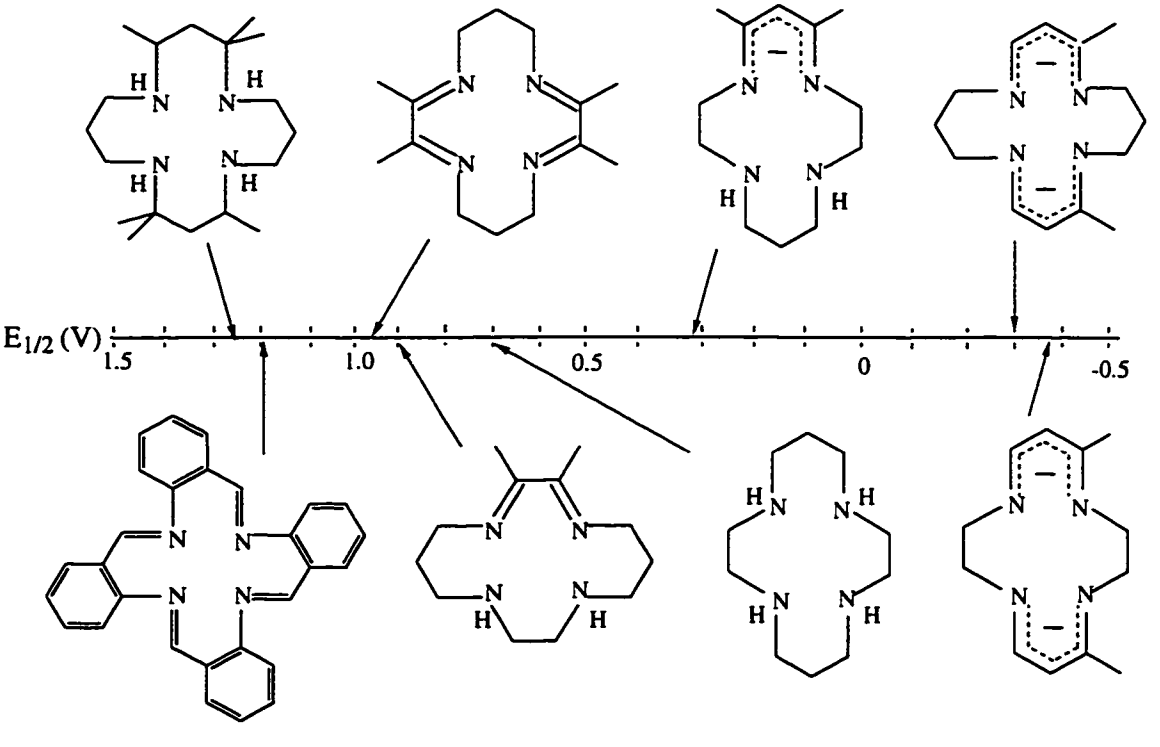

Figure 1.4 The effect of macrocyclic structure on the Ni^{III}/Ni^{II} redox potential.[15]

1.3 Synthesis of Macrocyclic Ligands

The formation of macrocyclic ligands presents many synthetic challenges, due largely to their cyclic nature, and quite often normal organic synthetic procedures cannot be used. A typical macrocyclic synthesis is shown in scheme 1.1. Three synthetic procedures are commonly utilized in the formation of macrocyclic ligands, they are: 1) high dilution reactions,[19] 2) template synthesis,[20] and 3) Richman/Atkins synthesis.[21] Each of these techniques acts to promote the formation of the desired cyclic product by increasing the rate of intramolecular cyclisation, ie. enhancing k_{intra} over k_{inter}, thus minimizing the formation of unwanted side products and polymers.

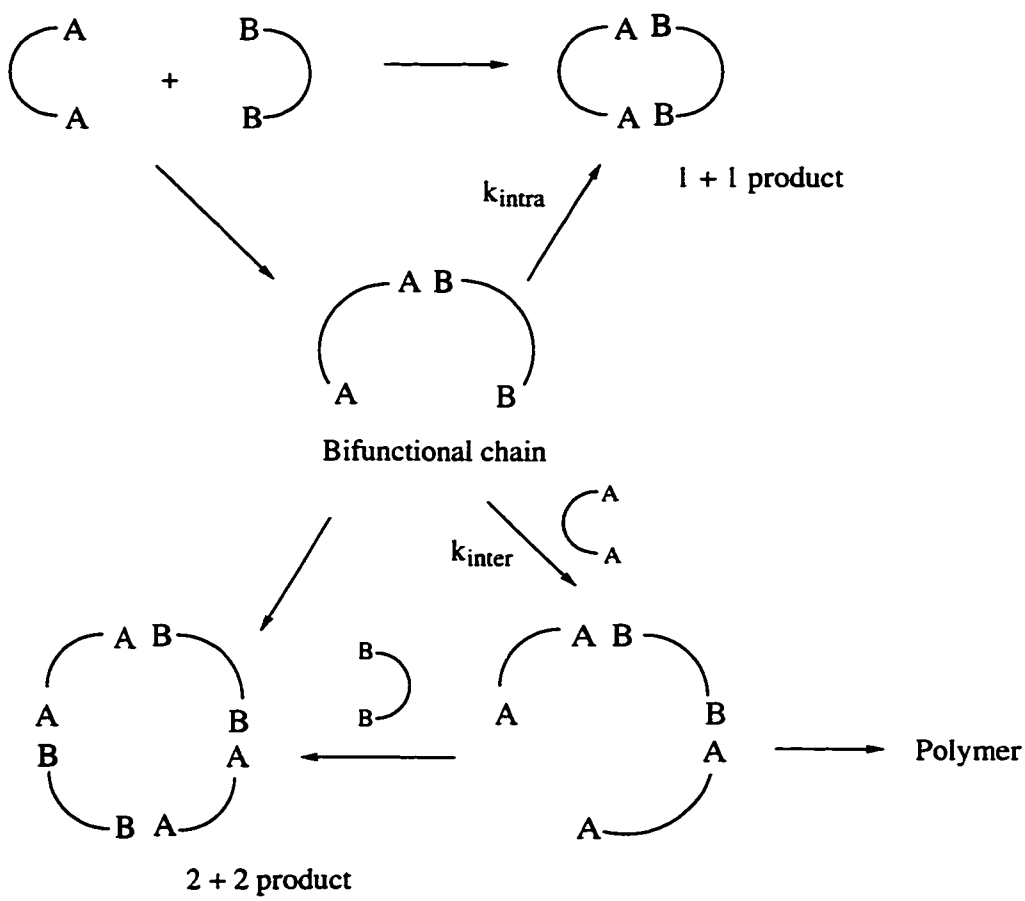

Scheme 1.1 The synthesis of macrocyclic ring systems.

1.3.1 High Dilution Techniques

By carrying out reactions under high dilution conditions the number of contacts between bifunctional reagents is decreased. This strategy promotes intramolecular reactions which lead to macrocycle formation over polymerization. Disadvantages with this technique however, include the need for very pure solvents, since reagent concentrations must be low and they become comparable to the impurity levels which may be present in the solvent. Also, specialized equipment is required to carry out high dilution reactions, primarily to allow for efficient mixing of the reagents and to accommodate the large volumes of solvent involved. The yields of the macrocycle obtained from this type of reaction are often quite low, even when reaction conditions have been optimized.

1.3.2 Template Reactions

Template reactions, as shown in section 1.2.1, involve the use of a metal ion, usually a cation, which acts as a "template" to assist in the cyclisation reaction. By holding the reactants in very specific orientations the metal ion can direct the steric course of the reaction thus favoring the formation of the cyclic product - this is known as the *kinetic template effect.* The *thermodynamic template* effect occurs when the metal ion perturbs an existing equilibrium in the reaction, favoring the formation of the macrocycle.

1.3.3 Richman/Atkins Synthesis

The Richman/Atkins synthesis[22] involves the use of rigid tosyl amide ($RTsN^-$) and tosylated alcohol (ROTs) functional groups. In this condensation reaction, the bulky tosyl groups are believed to prevent free bond rotation and hence reduce the number of conformational degrees of freedom. This reduces the number of possible condensation products and consequently favors ring closure.

A comparison of the three alternative synthetic routes described above for the formation of the macrocycle 1,4,8,11-tetraazacyclotetradecane (cyclam), giving the comparative yields, is shown in Figure 1.5.

1) High dilution Method : Yield

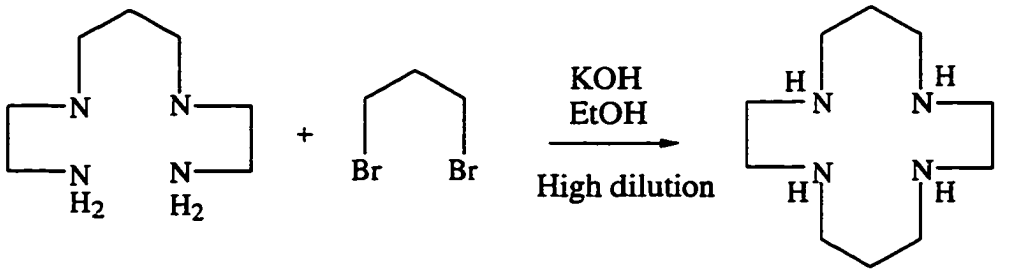

2) Template synthesis :

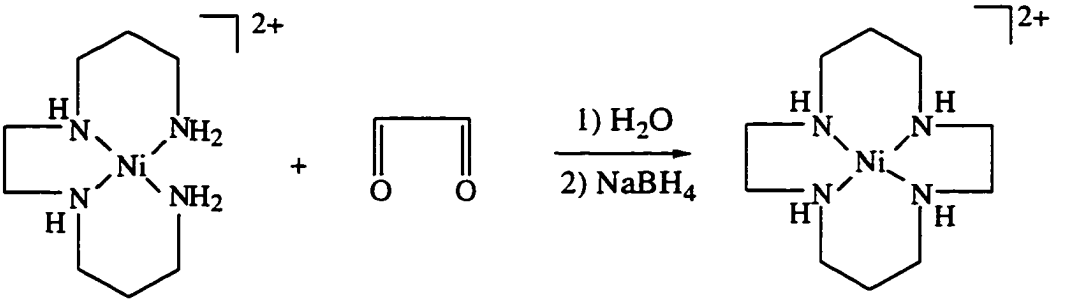

3) Richman/Atkins synthesis :

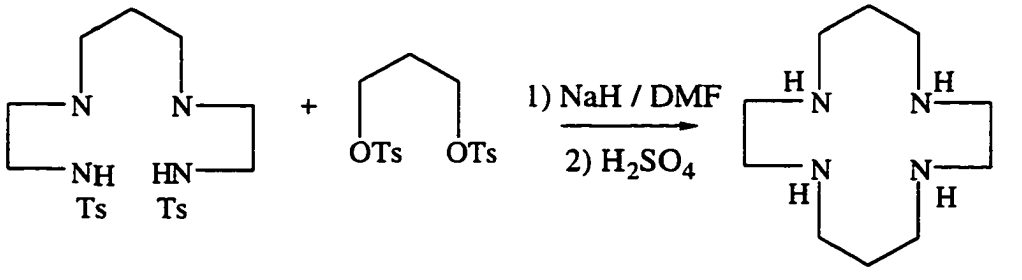

Figure 1.5 Comparison of synthetic methods used for the formation of macrocyclic ligands.

1.3.4 Emerging Strategies

A variety of synthetic strategies[23] have been utilized to form more complex macrocyclic ligands, namely compounds containing two and three fused ring systems, referred to here as bi- and tricyclic ligands. One strategy involves the functionalization of small macrocyclic ligands by the addition of pendant arms.[24] A second ring can then be fused to these pendant arms under high dilution conditions to form a tricyclic ligand (Scheme 1.2a). A second strategy which has been used is the "capping" of a parent ring system with a bifunctional bridging molecule (Scheme 1.2b).[25]

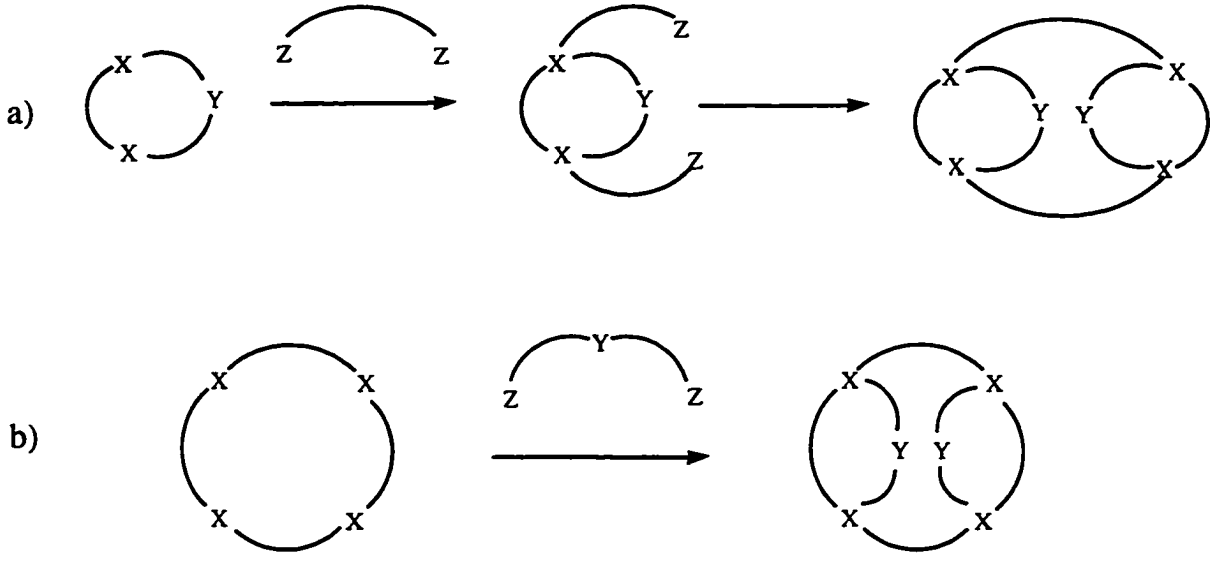

Scheme 1.2 Synthetic strategies to bi- and tri- cyclic macrocyclic ligands

1.4 Use of Macrocyclic Ligands to Study Thermal Reactions

Owing to their kinetic and thermodynamic stability, macrocyclic ligands have been used extensively for the study of ground state inorganic reaction mechanisms. The kinetic stability of macrocyclic complexes ensures that their chemistry is not complicated by ligand

dissociation reactions.[26] Macrocyclic complexes are ideally suited for the study of outer-sphere electron transfer reactions,[27] since they may impose the same coordination geometry on both oxidation states involved, so that minimal rearrangement accompanies the redox change. Also, the ligand may effectively block all of the coordination sites of the metal center, thus inhibiting inner-sphere electron transfer paths. Macrocyclic ligands have also been used in the study of inorganic substitution reactions. The advantages of using macrocyclic complexes are two-fold. First, substitution reactions at uncommon oxidation states may be studied, second, the macrocyclic ligand may be used to block possible coordination sites at the metal center, thereby simplifying the kinetics and allowing for easier analysis.

1.5 Photochemistry of Coordination Complexes

Photochemistry is a branch of science which deals with the interaction of matter and light. Photochemical reactions differ from thermal reactions in that they are initiated by the absorption of light rather than by the application of heat. Indeed, the very origins of life on earth are intimately linked to photochemical processes initiated by the sun.[28] Today, photochemistry plays an important role in many aspects of science, including chemistry, physics, and biology. Photochemistry of coordination compounds has drawn much attention due to its potential for industrial applications.[29-31] One can envisage the conversion of solar energy in the photochemical production of hydrogen from water as an alternative fuel source, or the photocatalytic destruction of harmful materials in the atmosphere to maintain the ozone layer. These are just a few of the possible applications currently being explored.

Macrocyclic complexes have found importance in photochemical studies of metal ion complexes for the same reasons they are important in ground state studies (as described

in the preceding sections of this chapter). These ligands provide increased thermal stability, compared to their non cyclic analogs, which can be used to eliminate ground state reactions (decomposition) and allow for easier analysis of the photochemical products. The macrocyclic ligand may also block coordination sites on the metal ion, placing constraints on the complex for photosubstitution of its ligands. As well, there may be an associated change in stereochemistry of the macrocyclic ligand which may provide a useful way to probe the details of the photochemical reaction.

1.5.1 Excited States

In the simplest case, at ordinary light intensities, the interaction of light with a molecular system is very generally an interaction between one molecule and one photon, and can be written in the form:

$$A + h\nu \rightarrow A^* \qquad (1.1)$$

A molecule (A) is promoted from the ground electronic state to an electronically excited state by absorption of a quantum of light. The necessary condition is that the photon energy (hν) matches the energy gap between the ground and excited state. In the case of transition metal complexes, this corresponds to light in the visible or near ultraviolet regions of the electromagnetic spectrum.

The nature of any photochemical and photophysical processes which result from the formation of an excited state by the absorption of light is strongly dependent on the type of electronic transition involved. These transitions can be metal centered (MC) or ligand field (LF) bands, ligand to metal charge transfer (LMCT), or metal to ligand charge transfer (MLCT) bands, ligand centered (LC), ion pair charge transfer (IPCT), or charge transfer to

solvent (CTTS) transitions. Figure 1.6 summarizes some of these transitions for an octahedral coordination complex.

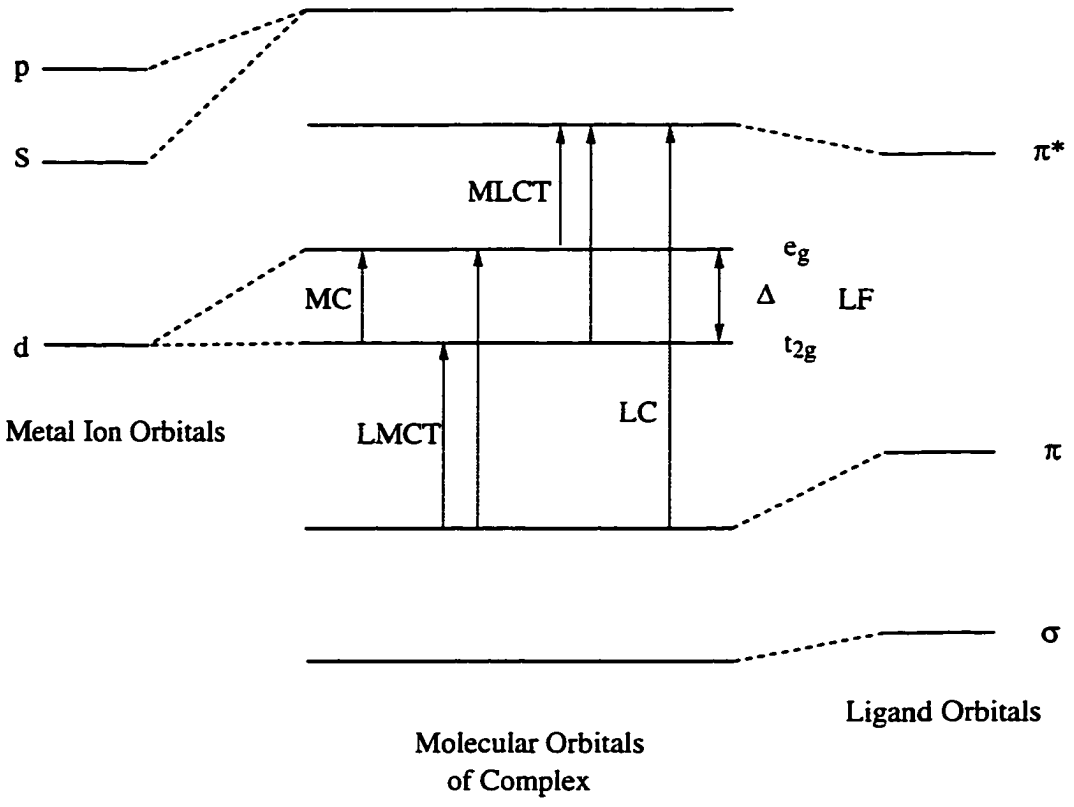

Figure 1.6 Molecular orbital diagram and possible electronic transitions for an octahedral coordination complex.

The intensity associated with an electronic transition is governed by a set of rules known as *selection rules* for light absorption and emission.[32-34] These rules are summarized below:

(i) Transitions between states of different spin multiplicity are forbidden ($\Delta S \neq 0$, spin forbidden transition). Therefore, $S \leftrightarrow T$ is forbidden, while $S \leftrightarrow S$ and $T \leftrightarrow T$ are allowed transitions (while S and T represent single and triplet electronic states respectively it should be noted that these selection rules also apply for doublet (D) and quartet (Q) electronic states).

(ii) For molecules which possess a center of symmetry (commonly found in transition metal complexes), electric dipole transitions between states of the same parity are forbidden (parity forbidden or Laporte forbidden transition). Therefore $g \leftrightarrow g$, $u \leftrightarrow u$ are forbidden, but $g \leftrightarrow u$ is an allowed transition (g and u represent those states which are symmetric (g, gerade) and antisymmetric (u, ungerade) with respect to inversion).

In reality, relaxation of these selection rules results from perturbations such as spin-orbit coupling and vibronic coupling, and formally forbidden transitions can be observed. These transitions become weakly allowed because of static or dynamic (vibrational) distortions of geometry. In solution, the power of light transmitted (P_t) through a sample of pathlength 1 (cm) and molar concentration c (mol L^{-1}) at a given wavelength can be represented by the Beer-Lambert Law:

$$P_t = P_o \, 10^{-\varepsilon c l} \qquad (1.2)$$

or

$$A = \varepsilon c l \qquad (1.3)$$

where P_o is the incident light power, ε the molar absorptivity (L mol^{-1} cm^{-1}), and A the absorbance which is defined as:

$$A = -\log\left(\frac{P_t}{P_o}\right) \qquad (1.4)$$

As a consequence of the selection rules, allowed transitions have large molar absorptivities (ε: 10^4 - 10^5 M^{-1} cm^{-1}), while forbidden transitions have low molar absorptivities (ε: 0.1 - 10^2 M^{-1} cm^{-1}).

1.5.2 Deactivation Pathways of Excited States

An electronically excited molecule is energetically unstable with respect to the ground state, and will efficiently lose its excess energy to return to the ground state. This may occur through a number of physical processes, both radiative and nonradiative, or by reaction to form new chemical species (photoproducts). A Jablonski diagram, shown in Figure 1.8, depicts all of the unimolecular deactivation pathways available to the molecule. This includes the radiative processes of phosphorescence ($\Delta S \neq 0$) and fluorescence ($\Delta S = 0$), and the nonradiative processes of vibrational relaxation (VR), internal conversion (IC), and intersystem crossing (ISC). Internal conversion occurs between electronic levels of identical spin states, while intersystem crossing occurs between electronic levels having different spin states.

The excited state molecules can also be deactivated (quenched) by other species in a bimolecular interaction as shown in Figure 1.7. Here k_d is the diffusion controlled rate constant for the formation of an encounter pair; k_{-d} is the encounter pair dissociation rate constant; k_{en}, and k_e are the rate constant for energy transfer and electron transfer quenching processes in the encounter complex respectively.

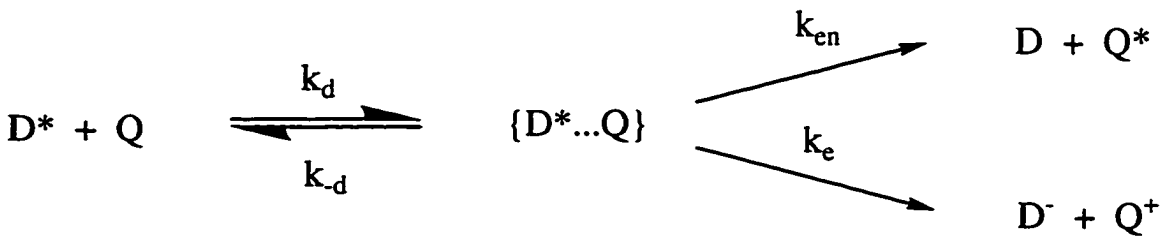

Figure 1.7 Typical bimolecular deactivation processes of an excited state molecule.

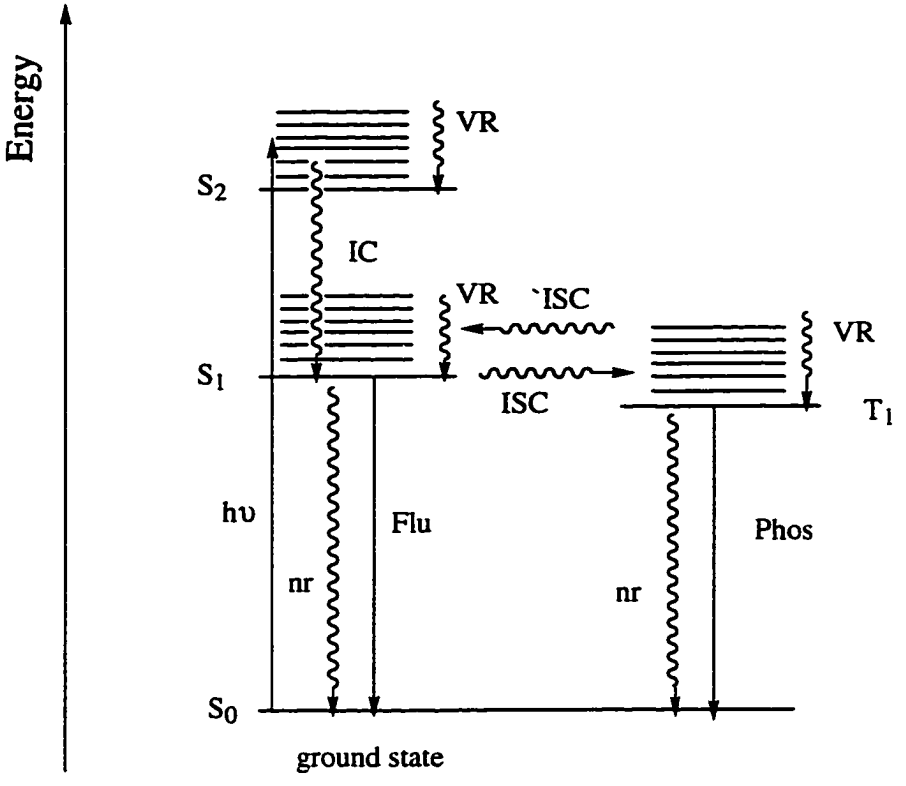

Figure 1.8 Jablonski diagram showing decay pathways available to an excited state complex.

(Radiative transitions are shown as straight lines, nonradiative transitions as wavy lines. S_0, ground state; S_1 and S_2 excited states with the same multiplicity as S_0; T_1, excited state with different multiplicity than S_0; VR, vibrational relaxation; ISC, intersystem crossing; `ISC, reverse intersystem crossing; IC, internal conversion; Flu, fluorescence; Phos; phosphorescence; nr, non-radiative)

1.6 Quenching Mechanisms Involving Transition Metal Complexes

1.6.1 Quenching Mechanisms

The most important types of bimolecular quenching are energy transfer processes and electron transfer reactions. In an energy transfer process (eq. 1.5), the excited state D^* is deactivated with the simultaneous promotion of the quencher Q to its excited state. In an electron transfer reaction an electron is transferred between the excited state D^* and the quencher. This can occur both oxidatively and reductively (eqs. 1.6-7).

$$D^* + Q \rightarrow D + Q^* \qquad \textit{energy transfer} \qquad (1.5)$$

$$D^* + Q \rightarrow D^+ + Q^- \qquad \textit{oxidative electron transfer} \qquad (1.6)$$

$$D^* + Q \rightarrow D^- + Q^+ \qquad \textit{reductive electron transfer} \qquad (1.7)$$

1.6.2 Thermodynamic Aspects

The ability of an excited state to undergo energy transfer is related to the excited state energies, often referred to as the zero-zero energy E^{00}, of the donor-acceptor pair. For energy transfer to be thermodynamically allowed, the excited state energy level of the acceptor (Q) must be less than that of the donor (D): $E^{00}(D^*/D) > E^{00}(Q^*/Q)$.[35]

The ability of an excited state to undergo electron transfer is related to the reduction and oxidation potentials of the excited state couples, D^+/D^* and D^*/D^-. Assuming that changes in size, shape, and solvation of the excited state are minimal relative to the ground state, the Stokes shift between absorption and emission will be small, and changes in entropy may be neglected. In such a case, the free energy change of the redox process can be readily calculated from the redox potentials:

$$E^0(D^+/D^*) = E^0(D^+/D) - E^{00} \qquad (1.8)$$

$$E^0(D^*/D^-) = E^0(D/D^-) + E^{00} \qquad (1.9)$$

Where $E^0(D/D^-)$ and $E^0(D^+/D)$ are the reduction and oxidation potentials of the ground state molecule, and can be obtained by cyclic voltammetry.[36]

It should be noted that, as shown quantitatively by equations (1.8) and (1.9), an excited state molecule is both a stronger reductant and a stronger oxidant than the corresponding ground state molecule. Compared to its ground state, the excited state molecule has an electron in a higher energy orbital which is more easily removed ($E^0(D^+/D^* > E^0(D^+/D)$) thus making it a better reductant. It also has a "hole" in a low lying orbital which can readily accept an electron ($E^0(D^*/D^-) < E^0(D/D^-)$) thus making it a better oxidizing agent. This is shown pictorially in Figure 1.9.

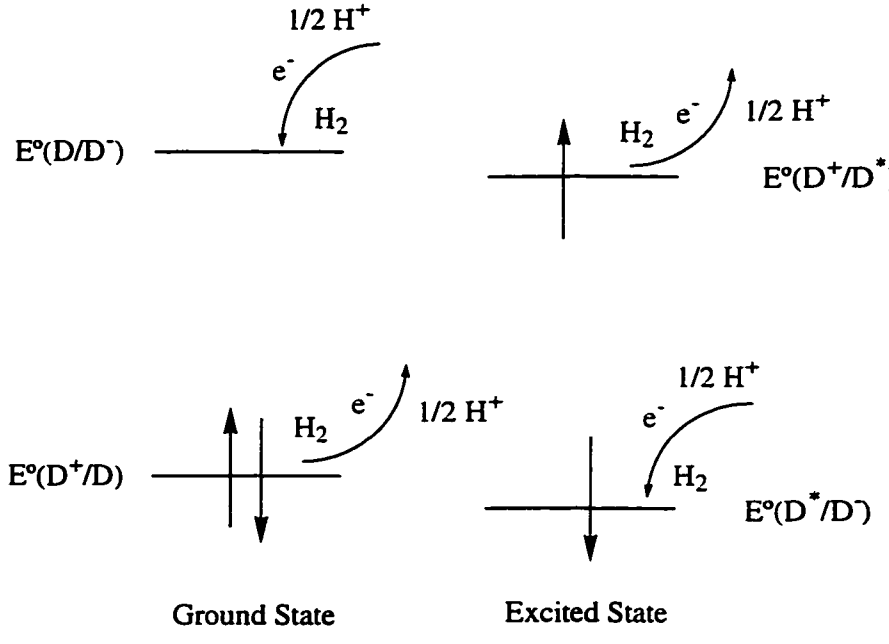

Figure 1.9 Comparison of redox potentials for ground state and excited state electronic configurations.

1.6.3 Kinetic Aspects

The kinetic aspects of the bimolecular reaction between an excited state molecule and a quencher have been investigated in detail.[37] Both continuous irradiation and pulse excitation (laser flash photolysis) have been utilized to measure quantities such as quantum yield for the photoreaction, emission intensity, and lifetime. In the absence of a quencher, the lifetime (τ°) of the excited state is given by the expression:

$$\tau^\circ = \frac{1}{\Sigma k_i} \tag{1.10}$$

where Σk_i represents the summation of the first order rate constants for all the pseudo unimolecular processes by which the excited state decays. In the presence of quencher Q, the number of deactivation modes for the excited state increases, therefore the lifetime is shortened, as given by the expression:

$$\tau = \frac{1}{(\Sigma k_i + k_q[Q])} \tag{1.11}$$

where k_q is the bimolecular rate constant for the quenching reaction. Dividing eq. (1.10) by eq. (1.11) gives the well known Stern-Volmer equation:

$$\frac{\tau^\circ}{\tau} = 1 + k_q\tau^\circ[Q]) \tag{1.12}$$

A plot of τ°/τ vs [Q] gives a straight line with slope equal to $k_q\tau^\circ$. The bimolecular quenching rate constant, k_q, can thus be obtained from the slope divided by τ°. The Stern-Volmer equation can also be expressed as the ratios of quantum yields (Φ°/Φ), or emission intensities (I°/I) in the absence and presence of quencher. The quantum yield is defined as

the ratio between the number of moles of species produced (photons or molecules) and the number of moles of photons (1 mole of photons = 1 einstein) absorbed. eq. (1.13).

$$\emptyset = \frac{\text{(moles of product formed)}}{\text{(moles of photons absorbed)}} \tag{1.13}$$

If the excited state is populated directly by irradiation, the quantum yield for a specific process i ($\phi_i°$) can be expressed as:

$$\emptyset_i° = \frac{k_i}{\Sigma k_i} = \tau° k_i \tag{1.14}$$

If the excited state is not directly populated by absorption then the expression for the quantum yield becomes more complicated. For example, the quantum yield for emission from the lowest spin-forbidden excited state (phosphorescence, $\emptyset_{phos}$) can be expressed by the following expression:

$$\emptyset°_{phos} = \eta_{isc} k_{phos} \tau°_{phos} \tag{1.15}$$

where η_{isc} is the efficiency of population of the emitting excited state by the state being populated by absorption, through intersystem crossing, eq. (1.17).

$$\eta_{isc} = \frac{k_{isc}}{\Sigma k_i} \tag{1.16}$$

The rate constant k_q of the bimolecular quenching process is controlled by many factors, and can be expressed in terms of the rate constants for the individual processes which occur in the quenching mechanism. For a reductive excited state electron transfer process of the type shown in eq. (1.7), the reaction rate can be discussed on the basis of

the mechanism shown in Figure 1.10, where k_d, k_{-d}, k'_d, and k'_{-d} are the rate constants for the formation and dissociation of the outer-sphere encounter complex, k_e and k_{-e} are the unimolecular rate constants for the electron transfer step involving the excited state, and $k_{e(g)}$ and $k_{-e(g)}$ are the corresponding rate constants for the ground state electron transfer step.

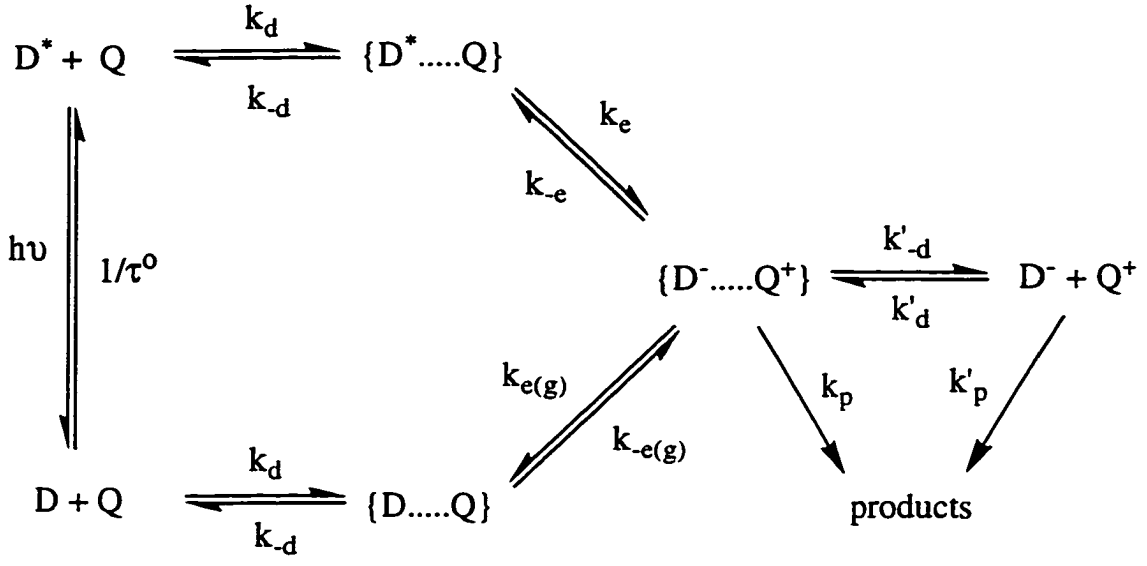

Figure 1.10 Kinetic mechanism for a reductive electron transfer process.

A steady state analysis of this kinetic scheme[38,39] shows that the observed quenching rate constant (k_{exp}) can be expressed as a function of the rate constants of the various steps:

$$k_{exp} = \frac{k_d}{1 + \frac{k_{-d}}{k_e} + \frac{k_{-d}\,k_{-e}}{k'_{-d}\,k_e}} \qquad (1.17)$$

In a classical approach, k_{-e}/k_e is given by $\exp(\Delta G^\circ/RT)$, where ΔG° is the standard free energy change of the electron transfer step.

$$k_{exp} = \frac{k_d}{1 + \frac{k_{-d}}{k_e} + \frac{k_d}{k'_{-d}} e^{\Delta G^\circ/RT}} \qquad (1.18)$$

At the heart of this process is the unimolecular electron transfer step (k_e), within the encounter complex. When an electron is transferred between the excited state molecule and the quencher in solution, there may be associated with it changes in bond lengths, angles, and solvent reorganization.[39,40] This quantity is given the term *reorganizational energy*, λ, which is usually divided into two parts:

$$\lambda = \lambda_{in} + \lambda_{out} \qquad (1.19)$$

The solvent independent term λ_{in} arises from structural differences between the equilibrium configurations of the reactant and product states. The outer term λ_{out} is called the solvent reorganizational energy because it arises from differences between the orientation and polarization of solvent molecules around {D*..Q} and {D^-..Q^+}. The quantity has been approximated using both spherical reagent models,[41] and an ellipsoidal model.[42]

Since electronic motions are faster than nuclear motions (the Franck-Condon principle), an adjustment of the nuclear configuration prior to electron transfer is required. This gives rise to an activation barrier, $\Delta G^\ddagger$, as shown in Figure 1.11.

The unimolecular rate constant for the electron transfer step is given by:

$$k_e = k_e^\circ \exp^{-\Delta G^\ddagger/RT} = (\kappa kT/h) \exp^{-\Delta G^\ddagger/RT} \qquad (1.20)$$

where k_e° is the effective frequency factor and κ is the electronic transmission coefficient. The transmission coefficient is usually taken as unity ($\kappa = 1$) for bimolecular electron

transfer processes.[43] Combining eq. 1.18 and 1.20 leads to an expression which relates the rate of the electron transfer step to its activation barrier and free energy change:

$$k_{exp} = \frac{k_d}{1 + \frac{k_d}{k_e^\circ e^{\Delta G^\ddagger/RT}} + \frac{k_d}{k'_{-d}} e^{\Delta G^\circ/RT}} \qquad (1.21)$$

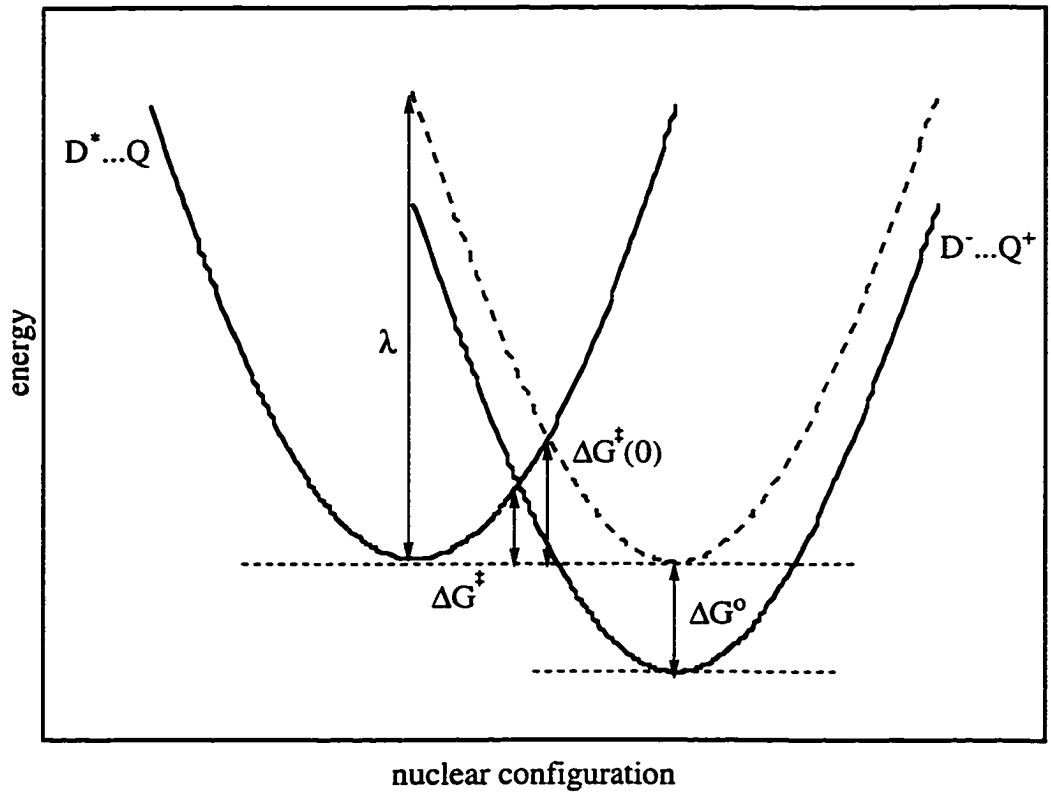

Figure 1.11 Energy surfaces for the initial and final states of an electron transfer reaction.

The free energy of activation, $\Delta G^{\ddagger}$, may be expressed by the classical Marcus quadratic free energy relationship:[43]

$$\Delta G^{\ddagger} = \Delta G^{\ddagger}(0)\left\{ 1 + \left[\frac{\Delta G^{\circ}}{4\,\Delta G^{\ddagger}(0)}\right]\right\}^2 \qquad (1.22)$$

where $\Delta G^{\ddagger}(0)$ is the so-called intrinsic nuclear barrier (when $\Delta G = 0$, the activationless case) and is equivalent to one quarter of the reorganizational energy (λ), as derived from the theory of intersecting parabolas.

$$\Delta G^{\ddagger}(0) = \frac{\lambda}{4} \qquad (1.23)$$

For a homogeneous series of reactants that have varying redox potentials but the same size, shape, electronic structure, and electronic charge, one can assume that the reaction parameters k_d, k_{-d}, k'_{-d}, and k_e°, and $\Delta G^{\ddagger}(0)$ are constant.[44] Under these assumptions k_{exp} only depends on ΔG°, the free energy change, and a plot of $\log k_{exp}$ vs ΔG° should produce a bell shaped curve involving (i) a "normal" region for endergonic reactions, where $\log k_{exp}$ increases with increasing driving force, ii) an "inverted" region for strongly exergonic reactions, where $\log k_{exp}$ decreases with increasing driving force (Figure 1.12). In practice, the inverted region has proven quite difficult to observe experimentally because the top of the bell-shaped curve often gives k values that are higher than the diffusion limit and the curve is therefore 'cut off'. The curve that results from the failure to observe the Marcus Inverted Region has come to be what is known as "Rehm-Weller" behavior,[39] shown by the dashed line in figure 1.12a. The first experimental evidence for the inverted region ("Marcus Behavior") came in the 1980's with some elegant studies in rigid media.[45] Conclusive evidence for the inverted region has now been found for both bimolecular and covalently linked systems.[46,47]

a)

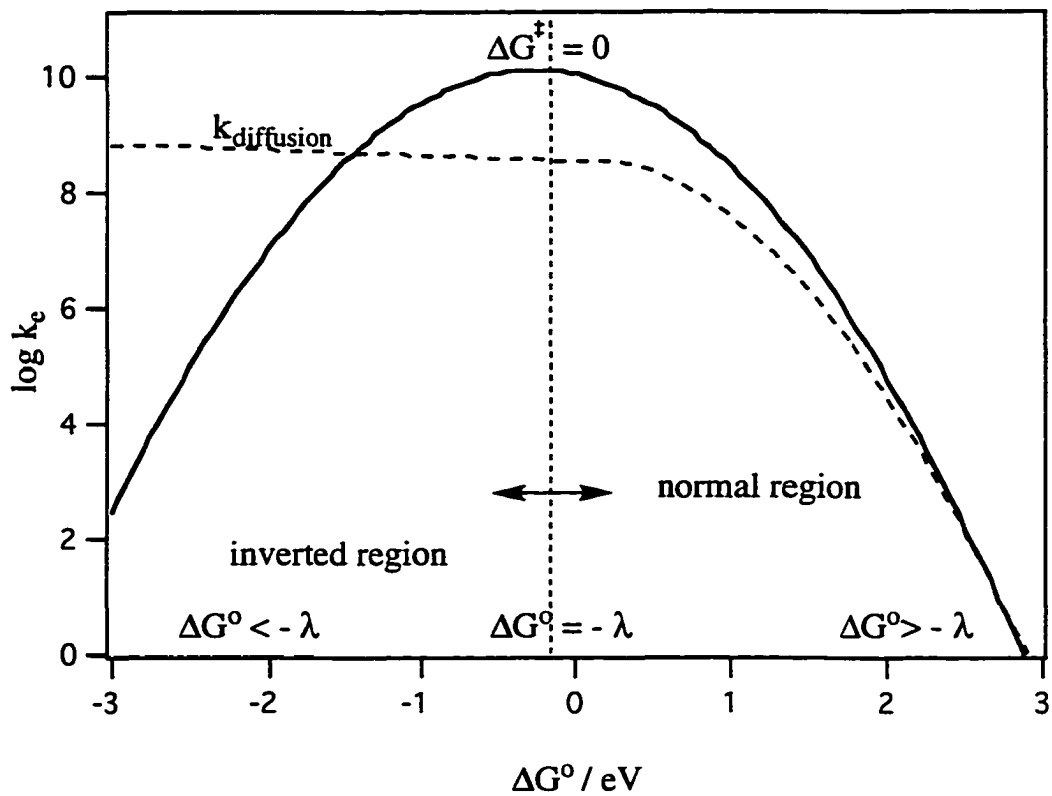

b)

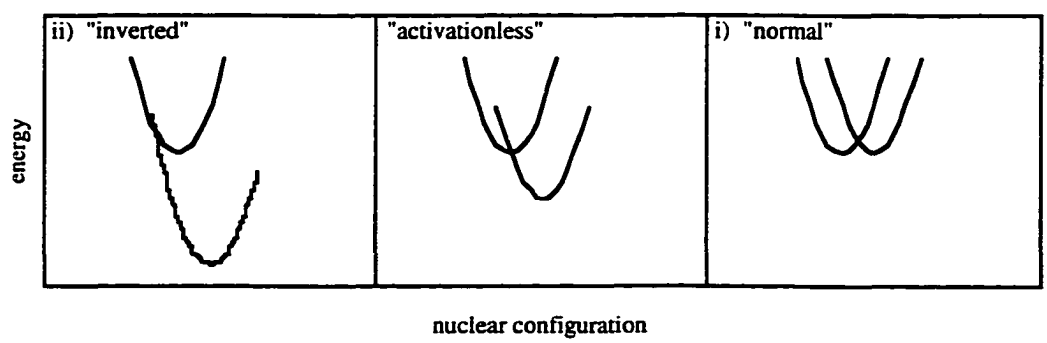

Figure 1.12 Marcus type plot: a) Variation of log k_e with the exergonicity (ΔG°) of the electron transfer reaction; b) potential energy curves for the reactant and product states in the normal, activationless, and inverted regions.

1.7 Photochemistry and Photophysics of Cr(III) Complexes

The effect of light on Cr(III) complexes was first noticed over seventy years ago, but it was in the 1960's that systematic studies of the photochemistry of Cr(III) complexes began. Since then, the investigation of Cr(III) photochemistry and photophysics has been one of the more intensely studied areas of transition metal photochemistry, and the topic of many reviews.[48-56] Despite this considerable research effort, there still remains today uncertainty about several of the details of the excited state participation in Cr(III) photochemical reactions. The focus of much of the current work in the field is to clarify these uncertainties and allow one to better understand, and indeed predict Cr(III) photochemical behavior.

1.7.1 Electronic Configuration and States of Cr(III) Complexes

Octahedral complexes of Cr(III) have a quartet ground state arising from the $t_{2g}^3e_g^0$ electronic configuration. Electronic excitation produces an excited state quartet with $t_{2g}^2e_g^1$ configuration. This can convert by intersystem crossing (section 1.5.2) to a doublet excited state with spin paired $t_{2g}^3e_g^0$ configuration. Figure 1.13 shows a simple ligand field representation of these states. The group theoretical term symbols for these states are $^4A_{2g}$, $^4T_{2g}$, and ^2E_g respectively. A typical absorption spectrum of an octahedral Cr(III) complex exhibits a weak but sharp band in the 650 - 750 nm range which can be assigned to the $^2E_g \leftarrow {}^4A_{2g}$ doublet transition. This transition is symmetry as well as spin forbidden, resulting in a very low molar absorptivity ($\varepsilon < 1\ M^{-1}cm^{-1}$). Spin pairing within the t_{2g} subshell results in the doublet state (D) having the same electronic configuration as the ground state ($t_{2g}^3e_g^0$) and therefore similar metal-ligand bond distances. This results in the characteristically sharp absorption band with small Stokes shift, as well as a narrow

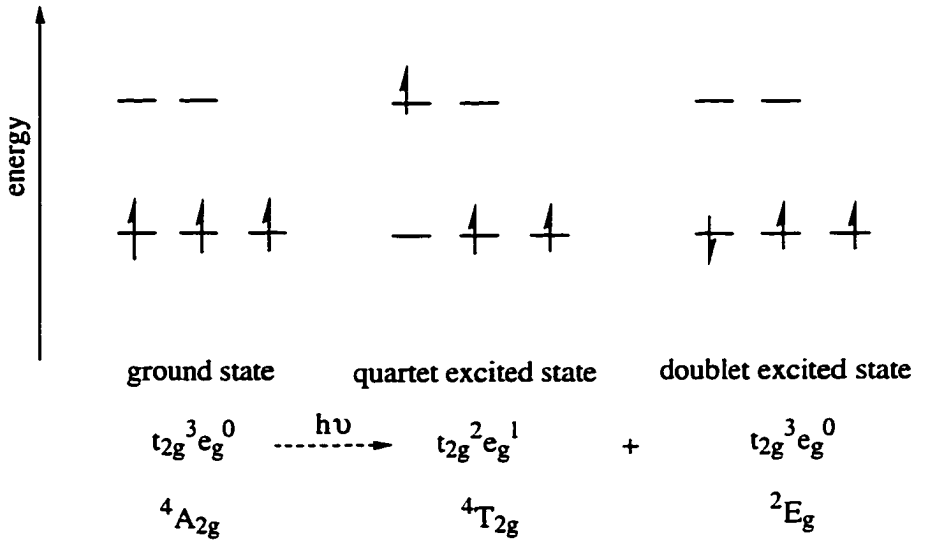

Figure 1.13 Simple ligand field representation of the orbital electron distribution of the ground state, and quartet and double excited states of Cr(III).

emission band for phosphorescence. Two other ligand field bands, involving d-d transitions, arise from the promotion of an electron from the nonbonding t_{2g} orbitals to the antibonding e_g orbitals. Here, the equilibrium distances in the excited states are larger than those in the ground state and as a result, the absorption bands are broadened. The lowest energy quartet band (Q) is assigned to the transition $^4T_{2g} \leftarrow {}^4A_{2g}$, while the higher energy band is assigned to a transition to a higher energy quartet state $^4T_{1g} \leftarrow {}^4A_{2g}$. These transitions are symmetry forbidden but spin allowed and have molar absorptivities in the range 10 to 100 M^{-1} cm^{-1}. The exact position of these bands depends on the ligand field strengths of the ligands coordinated to the chromium metal ion. Determining the 0-0 energy of the lowest lying quartet state can be difficult, due to the lack of any observable direct emission (fluorescence). It has been suggested[57] that the energy corresponding to the wavelength at the red end of the absorption spectrum at which the absorptivity is 5% of the band maximum is a reliable estimate of the relaxed quartet excited level.

1.7.2 Excited State Processes of Cr(III) Complexes

As already shown in section (1.5.2) a Jablonski diagram can be used to represent the possible deactivation pathways for an excited state. This diagram can be modified to show the excited state processes for a Cr(III) octahedral complex (Figure 1.14)

The doublet excited state is relatively long lived and usually has a lifetime on the order of μs, while the quartet excited state is short lived, with a lifetime in the picosecond or sub-picosecond domain. The doublet deactivation processes are therefore quenchable while the quartet processes are not. Photoreactions that go via the doublet state are referred to as "slow" reactions, while reactions that go via the quartet state are called "fast", or "prompt" reactions. The percentage of photoreaction that proceeds by each of these states can be determined either by measuring the quantum yield in the presence and absence of a suitable quencher, or by following the reaction directly by monitoring changes in conductivity of the chromium complex in solution, on the timescale of the doublet lifetime. For the chromium (III) hexamine complex $Cr(en)_3^{3+}$, it has been found that 30% of the reaction occurs on the timescale of the quartet state (prompt), while 70% occurs with the 1.7 μs lifetime of the doublet state (slow).[58]

A good understanding of the photophysical properties of the excited states of Cr(III) complexes is essential for analysis of the photochemical behavior . Studies have included investigation of the dependence of temperature and medium (or solvent), and the effect of $^4T_{2g}$ - ^2E_g energy separation on emission lifetime, activation energy (E_a), and emission quantum yield (or intensity).[59]

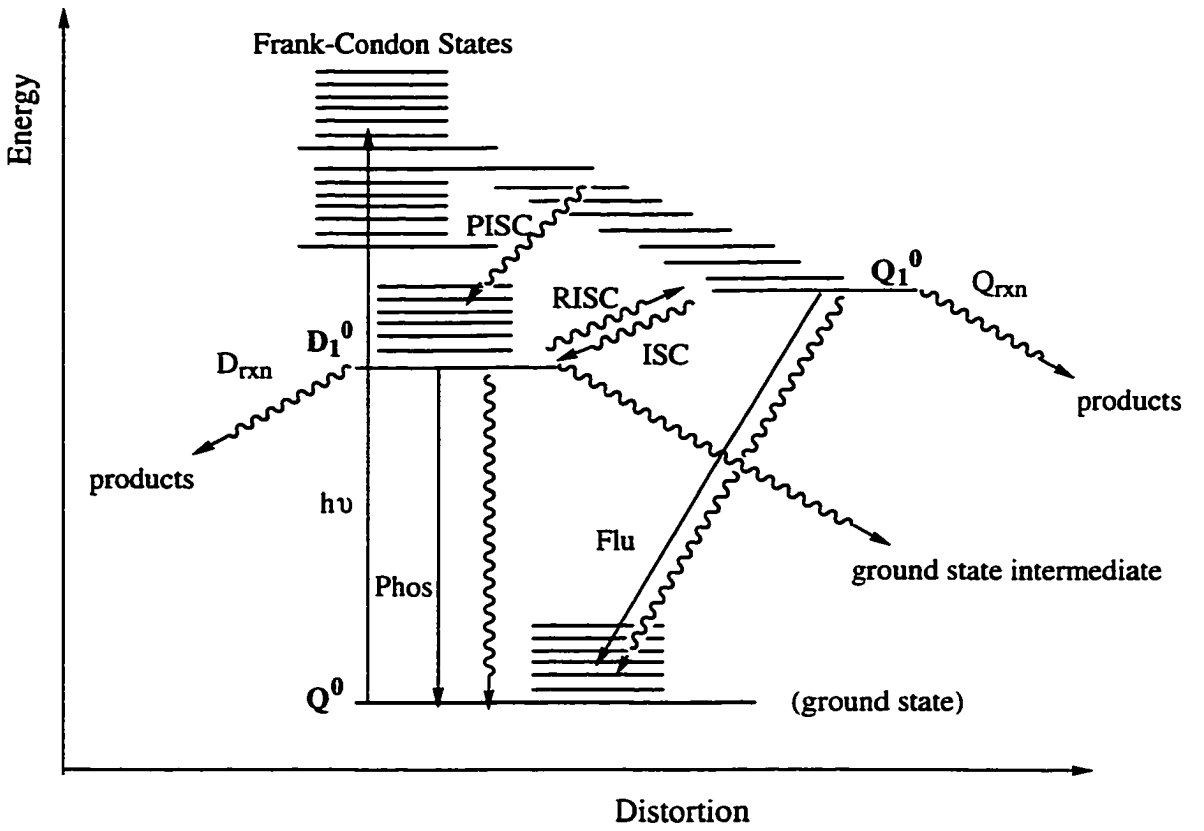

Figure 1.14 The excited state processes of Cr(III) complexes:
(Q^0 = ground state, $D_1{}^0$ and $Q_1{}^0$ = zero vibrational level of the lowest energy doublet and quartet excited states; Flu = fluorescence; Phos = phosphorescence; ISC = intersystem crossing; RISC = reverse intersystem crossing; PISC = prompt intersystem crossing; D_{rxn} = direct doublet reaction; Q_{rxn} = direct quartet reaction).

1.7.3 Photoreactive Pathways of Cr(III) Complexes

The predominant reaction mode observed for the photolysis of Cr(III) complexes in the ligand field bands is photosubstitution by solvent; a coordinated ligand is displaced from the chromium metal center and replaced by a solvent molecule, usually water (photoaquation). It is often found that the photochemical reactions are in contrast to the observed thermal reactions. An example of this is found for the complex $Cr(NH_3)_5(NCS)^{2+}$ which thermally aquates thiocyanate while in the photochemical reaction, ammonia is lost.[60] Analysis of this type of result led to a set of rules,[61] proposed by Adamson, which rationalize the photoreaction modes of mixed-ligand Cr(III) complexes:

Rule 1: "Consider the six ligands to lie in pairs at the ends of three mutually perpendicular axis. That axes having the weakest average crystal field will be the one labilized."

Rule 2: "If the labilized axis contains two different ligands, then the ligand of greater field strength preferentially aquates."

While these rules are successful for predicting the photochemistry of many Cr(III) complexes, there are exceptions, particularly in compounds containing fluoride ligands. These rules did however provide a foundation on which other models, by Zink,[62] Kirk,[63] and Vanquickenbourne and Ceulemans,[64-66] would be based.

1.7.4 Photostereochemistry of Cr(III) Complexes

Adamson's rules raised the question as to whether or not there were any stereochemical implications associated with the photochemistry of Cr(III) complexes.[67,68] It is well established that the photoaquation reaction of Cr(III) complexes exhibits

stereochemical change,[69] and many examples can be found where the stereochemistry of the photoproduct is different from that of the starting material. These observation were rationalized by Kirk's rule,[63] which states: "The entering ligand will stereospecifically occupy a position corresponding to entry into the coordination sphere *trans* to the leaving ligand." In this model, once a ligand is lost, one of its adjacent ligands ("cis") moves to take up its position and the substituting ligand occupies the vacated position. This specific ligand migration, also known as the "Edge displacement mechanism", is confined to any one of the three orthogonal planes within the coordination sphere of the molecule.

Vanquickenbourne and Ceulemans (VC) developed an angular overlap model[64] that predicts the identity of the ligand preferentially lost and provides a symmetry based rule to rationalize the photostereochemical behavior of mixed-ligand Cr(III) complexes. Their symmetry rule shows that the substituting ligand enters the coordination sphere *trans* to the leaving ligand. Excitation of the lowest energy quartet state corresponds to 45° rotation of charge density in one of the three orthogonal planes, namely $d_{xy} \rightarrow d_{x^2-y^2}$, $d_{xz} \rightarrow d_{x^2-z^2}$, $d_{yz} \rightarrow d_{y^2-z^2}$. The latter two upper state orbitals are linear combinations of d_{z^2} and $d_{x^2-y^2}$.

This population of a sigma antibonding orbital in the excited state will labilize the four ligands in the excitation plane. If the four ligands are not the same, the electron distribution between the orbital lobes will not be equal, the different ligands will be labilized to different extents, depending on their ligand field strengths. VC theory predicts that the ligand *trans* to the weakest field ligand is lost preferentially. It should also be recognized that there is, in the same plane, a vacant t_{2g} orbital which can interact with the substituting nucleophile, thus facilitating substitution. The importance of this vacant t_{2g} orbital was first pointed out by Zink[62] and Kirk.[63] Once the leaving ligand has been lost the square planar (SP) excited state which results will minimize its energy by rearranging to a ground state trigonal bipyramidal intermediate (TBP) which can then undergo nucleophilic attack. The course of this process has been illustrated for the complex $CrCl(NH_3)_5^{2+}$ and this is shown in Figure 1.15. Solvent attack on the TBP formed by this complex is allowed only at the two edges

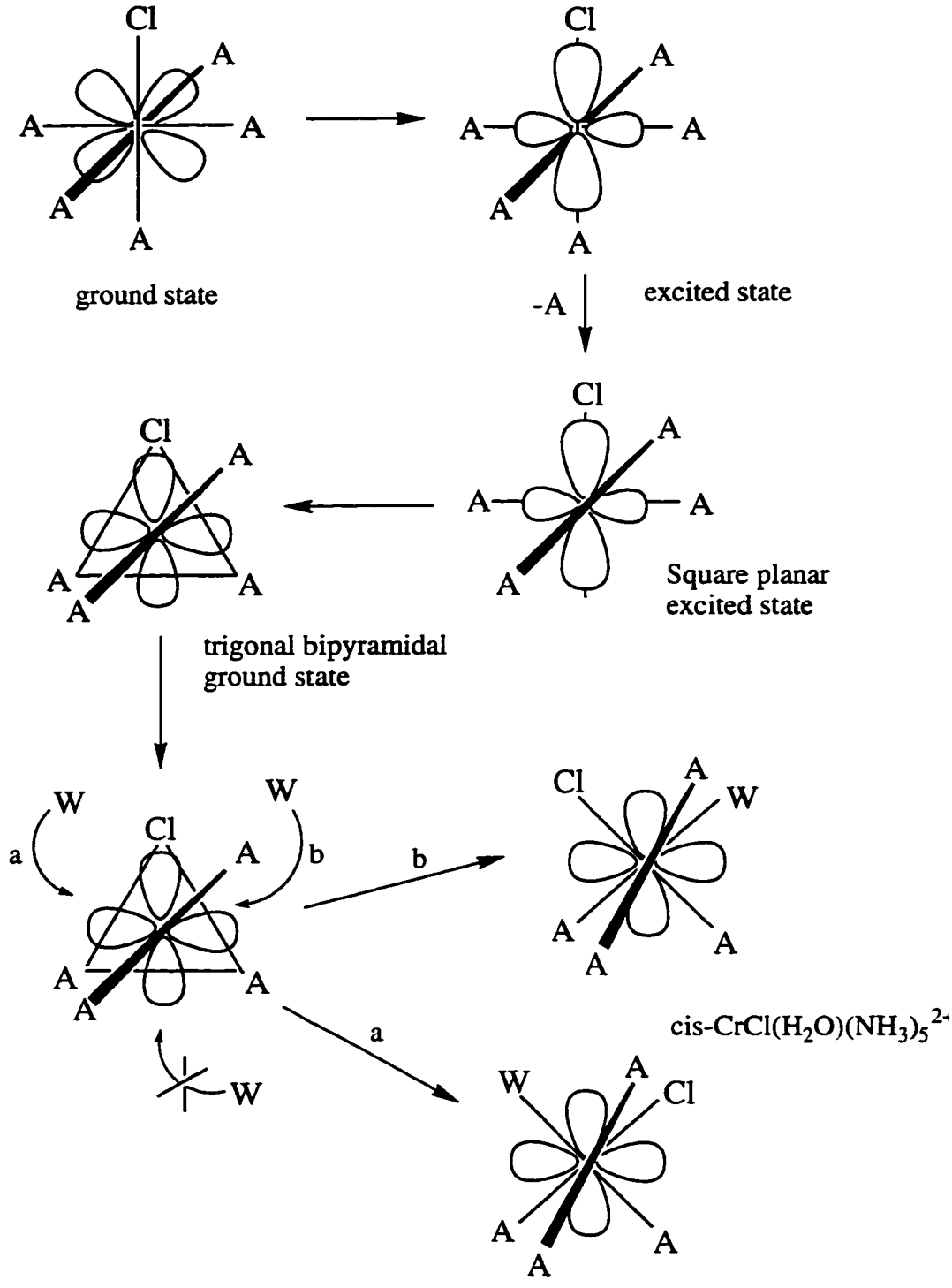

Figure 1.15 Pictorial representation of the photostereochemistry of the Cr(III) complex $CrCl(NH_3)_5^{2+}$ according to the Vanquickenbourne/Ceulemans theory: A = NH_3, W = H_2O.

"cis" to the chloride, this leads to the ground state *cis* product, *cis*-$CrCl(H_2O)(NH_3)_4^{2+}$. Entry of the solvent molecule trans to the chloride is not allowed as this would lead to the formation of an electronically excited state of the *trans* product, hence the stereoretentive pathway is forbidden.

1.7.5 Stereochemical Constraints

The existence of the stereochemical change associated with Cr(III) photosubstitution raises two interesting questions:

1) What happens to the photochemistry if the ligand imposes steric constraints?
2) Is stereochemical change a requirement of the photoreaction via the excited state?

Kutal and Adamson[70] found that incorporation of the macrocyclic ligand cyclam in the equatorial plane of $Cr(Cl)_2(cyclam)^+$ inhibited photochemical reaction. The quantum yield for photoaquation of the chloride ligand was found to be low ($\Phi = 3.3 \times 10^{-4}$) and the small amount of photoproduct that was formed had the stereoretentive *trans* configuration. In contrast, the analogous 2,3,2-tet complex, where there is no complete ring in the equatorial plane was photoreactive, showing stereochemical change but with a reduced yield compared to unconstrained analogs. In the case of the cyclambisammine complexes, $Cr(NH_3)_2(cyclam)^{3+}$, the *trans* complex has a much lower quantum yield ($\Phi \sim 0.01$)[71a] for photoaquation than the *cis* complex($\Phi = 0.15$).[71b] These observations would seem to support the claim that stereochemical change is a requirement for efficient photosubstitution to occur. When a constrained ligand such as cyclam is present, which can not easily

rearrange to allow for this change, the normal photoreactive pathway is blocked and the quantum yield for photoreaction decreases markedly.

There has been an on going controversy in Cr(III) photochemistry as to the exact pathway of the reaction that proceeds via the doublet state (the "slow" component).[52] Three hypothesis have been proposed:

(a) Direct doublet reaction

(b) Reverse intersystem crossing followed by quartet reaction

(c) Crossing to a reactive ground state intermediate

This problem has been investigated by: kinetic evidence, spectroscopic findings, temperature dependence and medium studies of the emission lifetime and intensity, volumes of activation , and deuterium isotope effects. The consensus of this evidence rules out (a) as a viable pathway in support of either reverse intersystem crossing and reaction via the quartet state, or tunneling to a ground state transition state for reaction. A good criterion for distinguishing (b) from (c) (and (a)) is the stereochemistry of the photoproducts. Photoaquation of Cr(III) complexes usually occurs with stereochemical change, facilitated by the vacant t_{2g} orbital of the quartet excited state. Reaction from a ground state intermediate (pathway (c)), or directly from the doublet state (pathway (a)), is expected to show similar stereochemistry to the ground state (thermal) reactions which are stereoretentive in nature. Only pathway (b) can easily explain the observed stereochemical results associated with the photoreactions of Cr(III) complexes.

Clearly, the identification of more examples of Cr(III) complexes which exhibit stereochemical change associated with their photoreaction would be useful. In particular, the study of constrained systems where the migration of the ligands can be controlled and the stereochemistry of the photoproducts unambiguously identified may be used to probe

the details of the photochemical reaction . This may lead to resolving the question of the excited state reaction pathway in chromium(III) complexes once and for all.

1.8 Summary

In the following chapters, the chemistry of macrocyclic transition metal complexes is explored. Details of the synthetic and instrumental techniques used throughout this dissertation are given in chapter two. Chapter three deals with the synthetic route to macrobicyclic ligands, with the ultimate goal being the synthesis of the macrotricyclic target ligand. The characterization of the copper and nickel complexes of these ligands is also included. In chapter four, quenching studies of the excited state of the platinum dimeric complex tetrakis(μ-pyrophosphite-P,P')-diplatinate(II) ($Pt_2(pop)_4^{4-}$) by a series of Ni(II) macrocyclic complexes are explored. Finally, in chapter five, the photophysical and photostereochemical properties of Cr(III) macrocyclic complexes are discussed, the goal being the elucidation of the photorective pathways involved in the photochemistry of these Cr(III) complexes.

CHAPTER TWO

EXPERIMENTAL

2.1 Materials

All chemicals used were analytical grade reagents purchased from Aldrich, ACP Chemicals Inc., BDH Chemicals, Fischer Scientific Company Ltd., Sigma, or Strem. Most of these chemicals were used without further purification. Acetonitrile was dried over calcium hydride and distilled prior to use. Organo pure water was prepared using a SYBRON/ Barnstead Nanopure-A purifying system.

CAUTION: Perchlorate salts used in the synthesis are potentially explosive. Extreme care should be taken while working with these compounds; solutions containing these salts should never be heated to dryness.

2.2 Instruments and Techniques

2.2.1 Elemental Analysis

Elemental analysis for C, H, N were performed by Canadian Microanalytical Services Ltd. (Delta, Vancouver, British Columbia).

2.2.2 Chromatography

2.2.2.1 HPLC

A Varian 5000 liquid chromatograph with 25 cm octadecylsilane RP-HPLC column was employed to separate cationic mixtures by ion interaction chromatography. Eluents consisted of 25 mM tetraethylammonium ion as the competing cation, 25 mM hexanesulfonate as the anion interaction agent, and 50 mM of the chiral resolving agent d-tartaric acid. Eluents were made up with a mixture of 7.5% methanol (HPLC grade) in organo pure water. The pH of the solution was adjusted to ~ 3.6 either by adding base

(NaOH), or additional d-tartaric acid. A flow rate of 1.5 mL/minute was used, and peaks were detected by UV absorption at a wavelength of 250 nm using a Vari-Chrom variable wavelength detector.

2.2.2.2 Ion Exchange Chromatography

SP-sephadex C-25 in Na^+ form and Dowex 50W-X2 ion exchange resins were used to separate metal cationic complexes. The details, and column dimensions are given under each experiment.

2.2.3 Electrochemistry

A Princeton Applied Research Model 273 potentiostat/galvanostat interfaced to an IBM PC computer was used for electrochemical measurements. Cyclic voltammograms were obtained using the Headstart program (Princeton). A standard three electrode electrochemical cell was used, with a Pt microelectrode as the working electrode, a Pt bead as the counter electrode, and a Ag^+/Ag wire as the reference electrode. All electrochemistry was performed in dry acetonitrile solutions containing supporting electrolyte 0.1 M (usually $^tBu_4NClO_4$). These solutions were degassed with argon prior to obtaining the cyclic voltammograms. The ferrocinium/ferrocene (Fc^+/Fc) couple was used as an external standard. The $E_{1/2}$ value for the Fc^+/Fc couple was found at 0.1 V vs Ag^+/Ag.

2.2.4 Spectroscopy

2.2.4.1 UV/Vis Spectra

UV-Visible spectra were run on either a Cary-1 or Cary-5 UV-Vis-NIR spectrophotometer coupled with a Compaq Deskpro 386s micro computer. Spectroscopic

data was evaluated using the program IGOR PRO(3) (Wavemetrics, Inc.) run on a Macintosh IIci computer.

2.2.4.2 Emission Spectra

Emission spectra were obtained with excitation by a Hanovia xenon lamp / Bausch and Lomb monochromator / intra-red filter (Balzers) source, with detection using a Jarrel-Ash 0.25 monochromator preceded by a Corning 3-71 red filter and a 1 cm path of concentrated potassium dichromate solution to remove light of wavelengths shorter than 650 nm. The detector was an RCA 31034 photomultiplier with a modified Keithley 410 electrometer. Spectra were recorded on an HP Moseley 7035B X-Y recorder.

2.2.4.3 Mass Spectroscopy

Mass spectra of organic compounds were run on a Finnegan GC 330 mass spectrograph using standard chemical ionization methods. Mass spectra of metal salts were obtained as liquid secondary ion mass spectra using a Kratos Concept double focusing magnetic instrument. Ions were produced by fast atom bombardment (FAB) in a matrix of meta-nitrobenzylalcohol (mNBA). All spectra were run in the positive ion mode.

2.2.4.4 NMR

Spectra involving ^{1}H NMR, ^{13}C NMR, and ^{13}C DEPT were run on a Bruker B-ACS60 300 MHz NMR spectrophotometer. The chemical shifts (δ ppm) are reported relative to tetramethylsilane (TMS) at 0 ppm.

2.2.4.5 ESR

Electron spin resonance was performed on a Bruker ER200tt instrument. Microwave radiation used was in the X-band region (9.2 GHz). Diphenylpicrylhydrazyl (DPPH, g = 2.0037) was used as an external standard. Spectra were recorded in solution either at ambient temperatures or at 77 K. Spectra recorded at 77 K were obtained in a frozen glass medium using a quartz dewar filled with liquid nitrogen.

2.2.5 Polarimetry

Optical rotation measurements were made on a Rudolph Research Autopol III automatic polarimeter using a micropolarimeter cell (path length = 10 cm, volume = 2.0 mL). Optical rotational values $[\alpha]_\lambda$ where measured at wavelengths of: λ = 365, 405, 435, 546, 589, and 633 nm.

2.2.6 Photochemical Procedures

2.2.6.1 Light Intensity Measurements

Ferrioxalate actinometry[72-75] was used for steady state light intensity measurement at 436 and 365 nm photolysis wavelengths. In a quartz cell, 3.0 mL aliquots of 0.050 M ferrioxalate (filtered through a 0.45 μm Micron Sep membrane filter) were irradiated for appropriate lengths of time (10 to 120 seconds), depending on the light intensity. A 'dark' blank solution, undergoing no irradiation, was also carried out. After irradiation, these solutions were mixed with 6.00 mL of developer (0.1% 1,10-phenanthroline, 0.75 M sodium acetate in 0.2 M H_2SO_4) and made up to 25.00 mL in actinic glass volumetric flasks. After storage in the dark for 30 minutes, the $Fe(phen)_3^{2+}$ product absorbance was measured at 510 nm, where $\varepsilon_{510} = 1.105 \times 10^4\ M^{-1}\ cm^{-1}$. The incident light intensity (einstein s^{-1}) was calculated using the following equation:

$$I_0 = \left[\frac{A_p - A_d}{\varepsilon_{510}\, l}\right]\left[\frac{V_T}{\emptyset\, f_a\, t}\right] \qquad (2.24)$$

where A_p and A_d are the absorbances of the photolysed and the blank solution at 510 nm respectively, $V_T = 2.500 \times 10^{-2}$ L is the total volume, L = 1 cm is the path length of the cell, t is the time of photolysis in seconds, Ø is the quantum yield for the production of Fe^{2+} at the appropriate wavelength, and $f_a = (1 - 10^{-A})$ is the fraction of the light absorbed (where A is the absorbance of the ferrioxalate solution at the irradiation wavelength). A typical lamp intensity was 2.0×10^{-8} Einstein s^{-1}. Light intensity was continually monitored using an Alphametrics Model P111OS silicon diode detector and Model 1020 power meter.

2.2.6.2 Photolysis

An HBO 1000 W mercury lamp (Universal Instruments AH6-1B) was used as the light source for steady state photolysis at 365 nm (Corning CS 7-60 colored glass filter), and 436 nm (Balzers interference filters). A 10 cm water filter was used to remove the infra-red components. Radiation at 488 nm was obtained from a Spectraphysics 2000 Argon ion laser. The laser beam was expanded to a diameter of about 1 cm using a beam expander in order to avoid possible errors due to any local secondary photolysis effects. Radiation at 675 nm was obtained from a tunable Coherent 590 Standing Wave Dye laser pumped by the Argon ion laser at 514 nm, and using Rhodamine 640 dye. The laser output intensity was measured using a power meter (Scientific 36-5002-365 Digital Power and Energy Indicator), with a typical power reading between 30 and 50 mW. Unless indicated otherwise, all solutions were prepared in 1×10^{-3} M $HClO_4$, thermostated to 22 ±

1 °C, and mixed efficiently with magnetic stirring. Solutions were photolyzed to conversions of less than 15% (unless otherwise specified) in order to avoid secondary photolysis.

2.2.6.3 Quantum Yield Determinations

The pH stat method was used to determine the absolute quantum yields of the chromium(III) complexes $[Cr([18]\text{-}aneN_6)]Br_3$ and $[Cr(sen)]Br_3$. Solutions were prepared by dissolving the complex in 1 x 10^{-3} M $HClO_4$, (filtered through a 0.45 μm Micron Sep membrane filter) and adjusting the absorbance at 436 nm to about 0.3 (3 mL, 0.5 - 1.0 x 10^{-2} M). The efficiently stirred solutions were irradiated at 22 ± 1 °C and the pH was monitored by an Ingold LOT combination electrode interfaced to a PDP-11 computer using a program in PASCAL ('Work') written by Dr. A. D. Kirk. Standard acid (9.427 x 10^{-2} M) was added from a 200 μL stepping motor burette to maintain a constant pH as photolysis proceeded. By this method a plot of the volume of acid added versus photolysis time was obtained and the quantum yield Ø for generation of the protonated photoproducts could be calculated. Sample calculations for the determination of Ø are given in Appendix I.

For the measurement of the quantum yield of photoreaction of $[Cr(sen)]Br_3$ at 675 nm irradiation, a specially designed flow cell (10.26 cm path length and 2 mm diameter), fitted with quartz windows, was positioned along the axis of the irradiation beam. This cell was used in conjunction with the dye laser apparatus described in section 2.2.6.2. The thermostatted (22 ± 1 °C) cell was connected to a glass solution reservoir using Tygon tubing (13 mm diameter). A filtered (0.45 μm) aqueous solution of the complex (~ 4 x 10^{-2} M) in 1 x 10^{-3} M $HClO_4$ was cycled through both the reservoir and the cell using a peristaltic pump at ~ 40 mL min^{-1} (the total volume of solution required to fill the cell, tubing, and reservoir was ~ 5 mL). Standard acid was added to the reservoir from a stepping motor buret to maintain a constant pH. Both magnetic stirring and cycling of the

solution ensured that the solution was being efficiently mixed. The pH of the solution was monitored by placing the combination electrode into the reservoir. This was used in conjunction with the PDP-11 computer as described above (the pH stat method) to obtain a plot of volume of acid added versus photolysis time. From this, the quantum yield of the photoreaction, $\emptyset_{rxn}$, was determined. The Light intensity was monitored using an Alphametrics Model P111OS silicon diode detector and Model 1020 power meter by reflecting at right angles to the laser beam. The intensity of the light transmitted through the back of the flow cell was monitored using a Scientech 365 power meter. Typically, laser powers of ~ 30 mW were used for irradiation. The complete experimental set up is shown in Figure 2.1.

2.2.6.4 Laser Flash Photolysis

A Spectra-Physics GCR-12 Nd/YAG laser, frequency tripled to 355 nm, with a 7 ns half-width, was used for flash photolysis studies. The laser pulse energy, measured by a thermal detector (Molectron J50) / tektronix 2445 oscilloscope, ranged from 1 to 70 mJ. To study the dependence of $Pt_2(pop)_4^{4-}$ photolysis on the laser pulse energy, $NiSO_4 \cdot 6H_2O$ filters (0.25 M, 0.5M, and 1.0 M) were placed in the laser beam in order to decrease the laser pulse energy used to irradiate the complex. For the $Pt_2(pop)_4^{4-}$ quenching experiments, the $Pt_2(pop)_4^{4-}$ complex was dissolved in 1 x 10^{-3} M $HClO_4$ to give an absorbance of about 1.0 at 370 nm. These solutions were then excited in a 7.0 by 7.0 mm Suprasil quartz cell, with nitrogen bubbling between laser shots for degassing and mixing. Transient absorption measurements were made with right angle geometry using an Oriel/Osram 150 W Xe lamp, which could be optionally intensified by pulsing, and a Digichrom 240 computer-controlled monochromator, with appropriate color filters mounted in filter wheels to remove scattered light. Detection was achieved by a Hamamatsu R928 photomultiplier and Tektronix 520A digital oscilloscope. The system is controlled by a

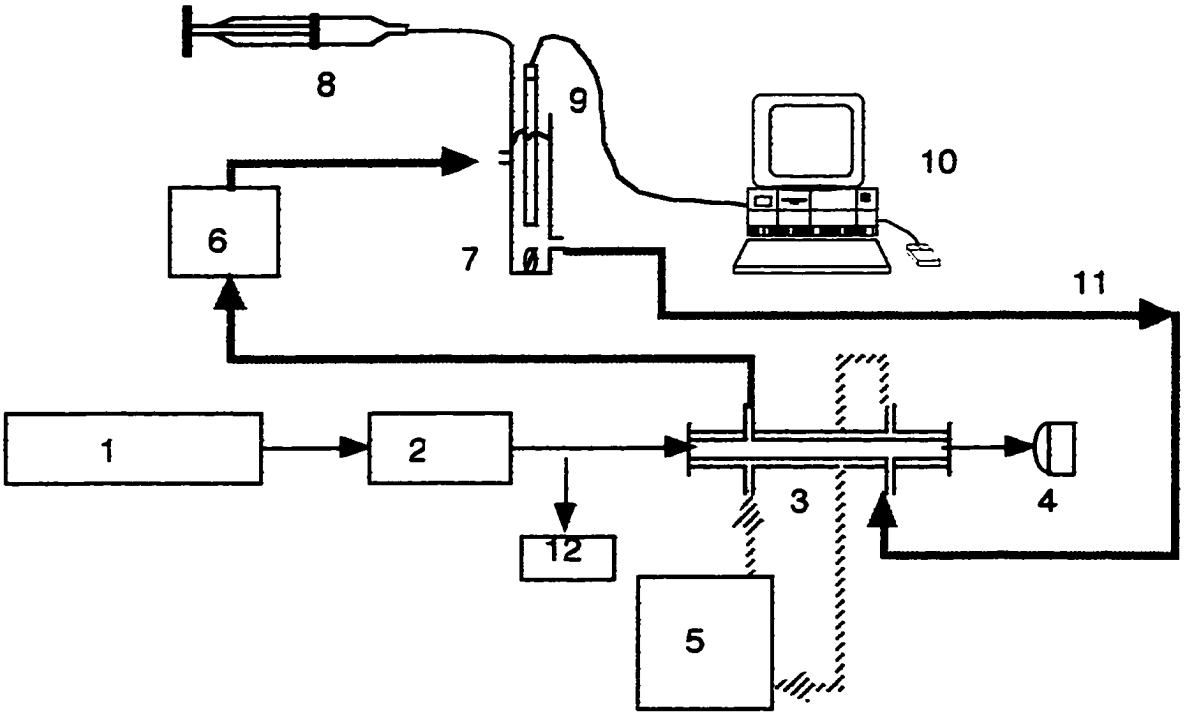

Figure 2.1 Experimental set-up for quantum yield measurement at λ = 675 nm irradiation: 1) argon ion laser; 2) dye laser; 3) thermostatted flow cell; 4) Scientech power meter; 5) temperature controller; 6) peristaltic pump; 7) Solution reservoir/magnetic stirring; 8) stepping motor burette; 9) combination electrode; 10) PDP-11 computer; 11) Tygon tubing; 12) Model 1020 power meter.

Mac IIsi computer program written using Labview 4.0 and is capable of transient spectroscopic measurements over the time-scale from tens of ns to 0.1 s and the wavelength range 260 to 800 nm.

Photolysis studies of the chromium metal ion complexes were carried out using conductivity detection. The DC-conductivity quartz flow cell has three equally spaced (0.7 cm apart) Pt electrodes each 0.5 mm in diameter. The dimensions of the cell are 0.7 x 0.7 x 3 cm. The two outer electrodes are connected to a 50 ohm resistor and a variable resistor, producing a Wheatstone bridge network in conjunction with the resistance of the solution as shown in Figure 2.2. A 150 V square wave DC pulse of approximately 4 ms duration was applied to the central electrode, and the Wheatstone bridge balanced through the use of the variable resistor. The baseline signal was further controlled by varying the timing of the laser pulse relative to the potential pulse so that the photolysis event occurs on the flattest portion of the 4 ms pulse. The laser beam was directed through a 0.6 x 0.4 cm window irradiating the solution between the two upper electrodes. The resulting change in conductivity, due to proton uptake with photoreaction, was detected through the imbalance of the bridge and measured as voltage. The transient conductivity data after excitation was amplified using a two-stage amplifier with gain settings of 1, 10, 30 before being relayed to a Tektronix TDS-520 digital scope. The timing for the laser and data acquisition was set by a custom pulse generator and synchronizer in conjunction with a Stanford Research Systems DG-535 delay generator. The experimental system is integrated to a Macintosh IIci computer and the data acquisition and data analysis programs were written by L. Netter, and A. D. Kirk using Labview 4.0 (National Instruments).

The absorbance of the solution used was adjusted to about 0.3 at 355 nm, and the pH adjusted to 3.5. About 50 mL of the solution was cycled from a reservoir through the cell using a peristaltic pump with a flow rate of approximately 40 mL min^{-1}.

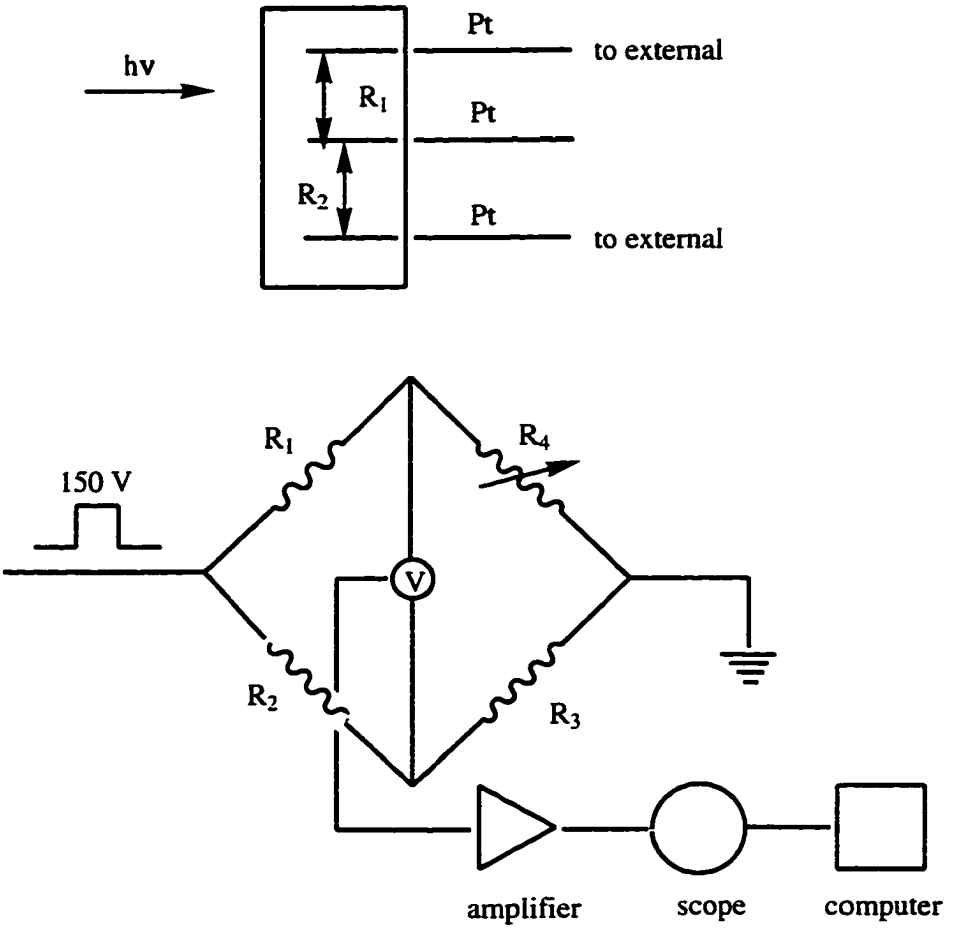

Figure 2.2 Wheatstone Bridge arrangement of cell used for flash conductivity detection

2.2.6.5 Emission Lifetime Measurements

Thermostated (Brickmann Lauda RC 3 thermostat) solutions, usually at 22 ± 0.1 °C, in 3 mL fluorescence cells were irradiated at 337 nm by a PTI PL 2300 Nitrogen Laser (1.5 mJ pulse, 3 Hz) and the emission decay was detected at right angles to the laser beam by a Jarrel-Ash 0.25 M monochromator / Hamamatsu R928 photomultiplier / Tektronix 2230 oscilloscope system with GPIB interface to an ATARI 1040 computer. Lifetimes were evaluated by weighted linear regression[76] on a plot of log(intensity) versus time over 1024 channels of decay using a GFABasic fitting program (written by Dr. A. D. Kirk). Solutions were deaerated by bubbling nitrogen through the cell for 30 minutes just prior to measuring the lifetime. Emission lifetimes were repeated five times and the average value was taken to be the lifetime of the complex. Low temperature emission lifetimes (below -30 °C) were measured in a dmso/H_2O (1:1) glassy medium by cooling the cell with liquid nitrogen in a Dewar sample compartment holder, fitted with orthogonal double walled evacuated quartz windows. As the liquid nitrogen slowly evaporated the sample warmed from -196 °C to ambient temperature and the lifetime could be measured over this temperature range. A calibrated Chromel-Alumel thermocouple connected to a mv potentiometer and a Perkin-Elmer Coleman 165 chart recorder was inserted into the sample cell to allowed for an accurate determination of the mean temperature over the lifetime measurement. In all cases, the temperature difference between the first emission lifetime measurement and the fifth measurement was found to be no more than 1 °C as the sample warmed up.

For the lifetime quenching studies of $Pt_2(pop)_4^{4-}$, pulse irradiation at its absorption maximum of about 370 nm was achieved, with the N_2 laser, by use of a quinine sulfate wavelength shifter. The absorbance of the quinine sulfate solution (in ethanol) at 337 nm was adjusted to 3.0 (ca. 3 x 10^{-4} M), and a fresh solution was used for each experiment. Two 1 cm rectangular glass spectrophotometer cells were placed in a thermostated cell

compartment, maintained at 22 ± 1 °C. The sample cell closest to the laser contained the quinine solution while the cell behind this contained 2.6 mL of a solution containing $Pt_2(pop)_4^{4-}$ in 0.010 M $HClO_4$ (see Figure 2.3). Nitrogen was presaturated by the same solvent and bubbled into the working solution for degassing and mixing after the addition of quencher. By focusing the laser on the quinine sulfate solution, 370 nm fluorescence was generated which in turn excited preferentially the $Pt_2(pop)_4^{4-}$ component solution. The resulting emission from the $Pt_2(pop)_4^{4-}$ solution was filtered through a Corning CS 3-72 glass filter, then a $K_2Cr_2O_7$ solution filter to remove any radiation of wavelengths shorter than 500 nm, and finally a neutral density filter to avoid overloading the photomultiplier by the intense $Pt_2(pop)_4^{4-}$ emission, even under quenched conditions. A schematic diagram of this experimental setup is shown in Figure 2.3.

$Pt_2(pop)_4^{4-}$ solution was freshly prepared by dissolving the complex in 0.010 M $HClO_4$ until an absorbance of about 0.3 at 370 nm was obtained (~ 1 x 10^{-5} M). Nitrogen was then bubbled through the solution until the lifetime reached a constant upper limit value. The quencher, also dissolved in 0.010 M $HClO_4$, was delivered into the $Pt_2(pop)_4^{4-}$ solution in 5 - 20 μL aliquots from a microburet fitted with a capillary tube. For each aliquot of quencher added, the lifetime τ was determined a minimum of 5 times. The quenching rate constant k_q was obtained from a Stern-Volmer plot of τ^o/τ vs [Q]. Each quenching experiment was carried out 2 times and the average rate constant was reported.

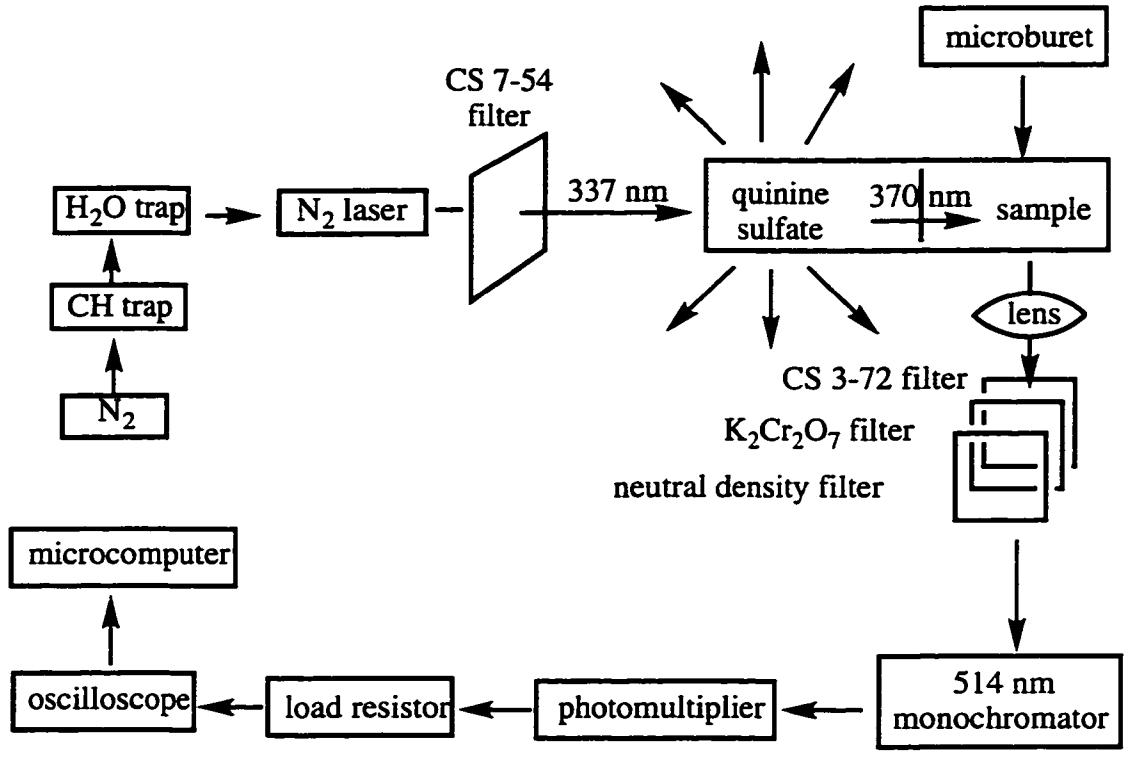

Figure 2.3 Experimental set-up for emission lifetime measurement

2.3 Synthesis of Macrocyclic Ligands and Their Transition Metal Complexes

2.3.1 1,4,7-triazacyclononane ([9]-aneN$_3$) (1)

The trihydrochloride salt [9]-aneN$_3$·3HCl, was prepared by a procedure described in literature[77], based on a modification of the Richman-Atkins synthesis.[78] Care was taken in this procedure to ensure that the tritosylated intermediate [9]-aneN$_3$·Ts$_3$, formed in the cyclisation reaction, was rigorously dried prior to detosylation. This can be achieved by grinding this white powder with a mortar and pestle, and placing in an oven (80 °C) for several days to dry.

The trihydrochloride (50 g, 17.1 mmol), was dissolved in water (200 mL), and the pH of the solution was adjusted to ~ 12 with NaOH (23 g, 0.58 mmol, 2.8 equiv.). The solution was then placed in a large continuous extractor, and extracted with $CHCl_3$ for 40 hr. The chloroform layer was dried over Na_2SO_4 and the solvent was removed on a rotary evaporator to give a yellow oil which was further dried under vacuum.

Yield: 14 g (52 %)

^{13}C NMR (300 MHz) ($CDCl_3$) : δ 47.1 ($\mathbf{C}H_2NR_2$).

MS (CI): 130 (M + 1), 158 (M + 29), 170 (M + 41).

2.3.2 Mono Protection of [9]-aneN$_3$

2.3.2.1 1-trityl-1,4,7-triazacyclononane (2)

The ligand 1,4,7-triazacyclononane (2.0 g, 15.5 mmol) was dissolved in 100 mL of chloroform (dried over 4A molecular sieves). To this solution was added Li_2CO_3 (1.3 g, 16.5 mmol, 1.1 equiv.) and the mixture was stirred at room temperature under an N_2 atmosphere for 30 minutes. Triphenylmethyl chloride (4.7 g, 16.5 mmol, 1.1 equiv.),

dissolved in 20 mL of chloroform, was added dropwise to this solution and stirring was continued for 24 hrs. The Li_2CO_3 was filtered off and the solvent was removed under reduced pressure to leave a yellow oil. This oil was redissolved in ether (50 mL) and the undissolved solid (unreacted triphenylmethyl chloride) was filtered off. The solution was again taken to dryness giving the desired product as a white solid.

Yield: 3.3 g (60 %)

^{13}C NMR (300 MHz) ($CDCl_3$) : δ 44.3, 45.8, 51.2 (CH_2NR_2); 79.5 (($C_6H_5)_3CNR_2$; 126.2, 127.7, 129.5 (($C_6H_5)_3CNR_2$.

2.3.2.2 1-formyl-1,4,7-triazacyclononane (3)

The free ligand 1,4,7-triazacyclononane (5.5 g, 42.6 mmol) was dissolved in N,N'-dimethylformamide dimethyl acetal (5.4 mL, 42.6 mmol), with stirring, under an N_2 atmosphere. This solution was refluxed at 85 °C for 3 hours, it was then cooled and dried under vacuum, leaving a light yellow solid material identified as the orthoamide of nonane.

Yield: 5.9 g (99 %)

^{13}C NMR (300 MHz) ($CDCl_3$) : δ 51.8 (CH_2NR_2); 103.9 (CH).

MS (CI): 140 (M + 1), 168 (M + 29), 180 (M + 41).

Nonane orthoamide (5.5 g) was dissolved in aqueous 3 M HCl (20 mL) and left to stir at 25 °C overnight. This solution was then made basic (~ pH 10) with NaOH and continuously extracted with $CHCl_3$ for 24 hours. The chloroform layer was collected, dried with Na_2SO_4, filtered, and evaporated to dryness. The white solid product was dried further under vacuum.

Yield: 5.0 g (80 %)

^{13}C NMR (300 MHz) ($CDCl_3$) : δ 46.0, 46.7, 48.4, 49.5, 50.2, 52.8 (CH_2NR_2); 163.9 (CHO).

MS (CI): 158 (M + 1), 186 (M + 29), 198 (M + 41).

2.3.2.3 1-methyl-1,4,7-triazacyclononane (4)

The formyl product, 1-CHO-1,4,7-triazacyclononane (3.5 g, 22.0 mmol) was dissolved in dry THF (50 mL). $LiAlH_4$ (2.6 g, 66.0 mmole, 3 equiv.) was added slowly, under an N_2 atmosphere, while cooling in an ice bath at 0 °C. This solution was refluxed overnight under N_2. The reaction mixture was again cooled in ice and water was added dropwise, with stirring, in order to react the excess $LiAlH_4$. After the effervescence had subsided, the insoluble material which had formed was filtered, washed with THF, and the combined THF filtrate was taken to dryness using a rotary evaporator. The residue was redissolved in distilled water (10 mL) and made basic (pH ~ 12) with by adding NaOH pellets. This solution was then extracted continuously with $CHCl_3$ for 24 hours. The chloroform layer was dried over Na_2SO_4, filtered, and taken to dryness, leaving the product as a yellow oil.

Yield: 2.2 g (68 %)

^{13}C NMR (300 MHz) ($CDCl_3$) : δ 43.8 (CH_3); 45.7, 49.9, 51.1, 57.4, 58.0, 60.9 (CH_2NR_2).

MS (CI): 144 (M + 1).

2.3.2.4 1-benzyl-1,4,7-triazacyclononane (5)

The nonane orthoamide (6.7 g, 48.3 mmol) was dissolved in $CHCl_3$ (25 mL) and benzylbromide (8.0 mL, 53.1 mmol, 1.1 equiv.) was added dropwise. This solution was stirred at 25 °C for 2 hours after time which the solvent was removed under reduced pressure. The residue was redissolved in 20 mL of distilled water and stirred for 2 additional hours. This solution was made basic (~ pH 10) with NaOH and extracted

continuously with $CHCl_3$ for 24 hours. The chloroform layer was collected, dried over Na_2SO_4, filtered, and taken to dryness under vacuum. This left a yellow oil product.

Yield: 11.9 g (99 %)

^{13}C NMR (300 MHz) ($CDCl_3$) : δ 39.6, 46.1, 50.4, 55.1, 56.3, 58.6 (CH_2NR_2); 64.8 (CH_2-ϕ); 128.7, 129.4, 130.6, 131.1, 132.2,133.4 (CH (phenyl)); 163.9 (CHO).

MS (CI): 248 (M + 1).

The oil (9.0 g, 36.7 mmol), prepared as described above, was dissolved in an aqueous solution (50 mL) of NaOH (37 g, 25 equiv.) and refluxed for 24 hours. This solution was then extracted continuously with $CHCl_3$, overnight. The chloroform extract was dried with Na_2SO_4, filtered, and the solvent removed under reduced pressure. The product 1-Bz-1,4,7-triazacyclononane, obtained as a slightly yellow solid, was dried under vacuum.

Yield: 7.1 g (88 %)

^{13}C NMR (300 MHz) ($CDCl_3$) : δ 46.1, 46.3, 52.6 (CH_2NR_2); 64.4 (CH_2-ϕ); 126.7, 126.9, 128.2, 129.1 (CH (phenyl)).

MS (CI): 220 (M + 1), 248 (M + 29), 260 (M + 41).

2.3.3 Functionalization of Mono Protected [9]-aneN$_3$

2.3.3.1 1-methyl-1,4,7-triazacyclononane (Me-daptacn) (6)

The compound 1-Methyl-1,4,7-triazacyclononane (2.1 g, 14.8 mmol) was dissolved in acrylonitrile (50 mL) and the solution was refluxed for 1 hour. The excess acrylonitrile was removed under reduced pressure, yielding a pale yellow oil, which was further dried under vacuum. This crude oil was suspended in 1 M BH_3·THF (400 mL) and refluxed overnight. Ethanol (150 mL) was added to destroy any excess BH_3. The solution was then taken to dryness under reduced pressure, leaving a crusty residue which in turn

was dissolved in aqueous 4M HCl (450 mL) and refluxed overnight. The solution was again taken to dryness under reduced pressure and the residue redissolved in distilled water (20 mL). The solution was made basic (~ pH 12) with NaOH, and extracted continuously for 48 hours. The chloroform layer was dried over Na_2SO_4, filtered, and taken to dryness, leaving the product as a yellow oil.

Yield: 2.8 g (74 %)

^{13}C NMR (300 MHz) ($CDCl_3$) : δ 42.8 ($\mathbf{C}H_3$); 28.5 ($CH_2\mathbf{C}H_2CH_2$); 38.9 ($CH_2CH_2\mathbf{C}H_2NH_2$); 48.5, 49.9, 52.7, 62.1 ($\mathbf{C}H_2NR_2$).

MS (CI): 258 (M + 1), 286 (M + 29), 298 (M + 41).

2.3.3.2 1-benzyl-1,4,7-triazacyclononane (Bz-daptacn) (7)

The compound 1-Bz-1,4,7-triazacyclononane (2.5 g, 11.4 mmol) was refluxed in acrylonitrile (50 mL) and the same procedure as described above (2.3.2.2) was followed, to give Bz-daptacn as a yellow oil.

Yield: 3.8 g (100 %)

^{13}C NMR (300 MHz) ($CDCl_3$) : δ 30.9 ($CH_2\mathbf{C}H_2CH_2$); 40.5 ($CH_2CH_2\mathbf{C}H_2NH_2$), 55.2, 55.3, 55.6, 56.4 ($\mathbf{C}H_2NR_2$); 64.5 ($\mathbf{C}H_2$-ϕ); 126.8, 127.2, 128.1, 129.0 (**C**H (phenyl)).

MS (CI): 334 (M + 1), 362 (M + 29), 374 (M + 41).

2.3.4 BicycloN$_5$ Complexes

2.3.4.1 1-benzyl-1,5,8,12,17-pentaazabicyclo[10.5.2]-nonandecane (Bz-BicycloN$_5$) (8)

The ligand Bz-daptacn (3.0 g, 9.0 mmol) was dissolved in 100% ethanol (100 mL) and a solution of $Cu(ClO_4)_2 \cdot 6H_2O$ (3.15 g, 9.9 mmol, 1.1 equiv.) in 100% ethanol (20 mL) was added dropwise at 25 °C. The solution immediately turned dark royal blue, and a purple/blue precipitate formed. Stirring was continued for 30 minutes and then the precipitate was filtered off, washed with ethanol, and dried under vacuum. The filtrate was collected, reduced in volume to 25 mL, and a second crop of $[Cu(Bz\text{-}daptacn)](ClO_4)_2$ was obtained.

Yield: 4.5 g (84 %)

UV-Vis (H_2O) λ (nm), (ε, L mol^{-1} cm^{-1}): 571 (149).

MS (FAB): 495.1 ($[Cu(L)(ClO_4^-)]^+$.

Analysis for $[Cu(C_{19}H_{35}N_5)](ClO_4)_2$

Calc (%):	C: 37.29;	H: 5.92;	N: 11.75
Found (%):	C: 36.66;	H: 5.76;	N: 11.20

To a solution of $[Cu(Bz\text{-}daptacn)](ClO_4)_2$ (2.0 g, 3.4 mmol) in a mixture of water (80 mL) and methanol (1500 mL) was added glyoxal (650 µL of a 40% solution, 3.9 mmol, 1.1 equiv.) The solution was refluxed overnight then cooled to room temperature. To this solution was added $NaBH_4$ (0.38 g, 7.5 mmol, 2.5 equiv.). The solution was then refluxed for 1 hour, over which time the color was observed to change to wine red/purple. The volume was reduced to 50 mL and the precipitate was filtered off, rinsed with methanol, and air dried. The filtrate was collected, evaporated to dryness under reduced

pressure, and suspended in methanol (25 mL) to give a second crop of [Cu(Bz-bicycloN$_5$)](ClO$_4$)$_2$.

Yield: 1.2 g (57 %)

UV-Vis (H_2O) λ (nm), (ε, L mol^{-1} cm^{-1}): 278 (5618), 546 (149).

MS (FAB): 521.1 ([Cu(L)(ClO_4^-)]$^+$, 360 (LH^+).

Analysis for [Cu($C_{21}H_{39}N_5$)](ClO$_4$)$_2$

Calc (%):	C: 40.42 ;	H: 6.30;	N: 11.22
Found (%):	C: 40.43;	H: 5.80;	N: 10.95

The free ligand 1-Benzyl-1,5,8,12,17-pentaazabicyclo[10.5.2]nonadecane (Bz-bicycloN$_5$) was obtained by dissolving [Cu(Bz-bicycloN$_5$)](ClO$_4$)$_2$ (1.0 g, 1.6 mmol) in distilled water (250 mL) and adding Na_2S (5 - 10 g). This solution was refluxed overnight. The resulting solution was colorless apart from a black precipitate of CuS. After filtration of the cooled mixture through a fine glass frit, the supernatant was taken to dryness. The residue was redissolved in aqueous 3 M NaOH (20 mL) and continuously extracted with $CHCl_3$ for 24 hours. The chloroform extract was dried over Na_2SO_4, filtered, and evaporated to dryness leaving a yellow oil which was further dried under vacuum. The free Bz-bicycloN$_5$ ligand was not stored, but rather used immediately to form the nickel complexes.

Yield: 0.52 g (90 %).

^{13}C NMR (300 MHz) ($CDCl_3$) : δ 26.1 ($CH_2CH_2CH_2$); 47.6, 49.0, 52.3, 53.9, 56.7, 56.9 (CH_2NR_2); 61.4 (CH_2-ϕ); 126.0, 128.1, 128.4, 129.2 (CH (phenyl)).

MS (CI): 362 (M + 1), 390 (M + 29), 402 (M + 41).

2.3.4.2 [Ni(Bz-bicycloN$_5$)](ClO$_4$)$_2$ (9)

The free ligand Bz-bicycloN$_5$ (0.11 g, 0.31 mmol) was dissolved in 100% ethanol (50 mL) and a solution of Ni(ClO$_4$)$_2$·6H$_2$O (124 mg, 0.34 mmol, 1.1 equiv.) in ethanol (10 mL) was added. The mixture was refluxed for 30 minutes, and after cooling to room temperature, the pink precipitate formed was filtered off, rinsed with ethanol, and air dried.

Yield: 110 mg (58 %)

UV-Vis (CH_3CN) λ (nm), (ε, L mol^{-1} cm^{-1}): 328 (sh), 523 (13.6).

Analysis for [Ni($C_{21}H_{39}N_5$)](ClO$_4$)$_2$

Calc (%):	C: 40.74;	H: 6.35;	N: 11.31
Found (%):	C: 40.68;	H: 6.35;	N: 11.31

2.3.4.3 1-methyl-1,5,8,12,17-pentaazabicyclo[10.5.2]-nonandecane (Me-BicycloN$_5$) (10)

The ligand Me-daptacn (1.1 g, 4.2 mmol) was dissolved in 100% ethanol (30 mL) and a solution of Cu(ClO$_4$)$_2$·6H$_2$O (1.47 g, 4.6 mmol, 1.1 equiv.) in 100% ethanol (10 mL) was added dropwise at 25 °C. The solution immediately turned dark blue, and a purple precipitate formed. Stirring was continued for 30 minutes and then the precipitate was filtered off, washed with ethanol, and dried under vacuum. The filtrate was collected, reduced in volume to 10 mL, and a second crop of [Cu(Me-daptacn)](ClO$_4$)$_2$ was obtained.

Yield: 2.2 g (56 %)

UV-Vis (H_2O) λ (nm), (ε, L mol^{-1} cm^{-1}): 577 (113).

MS (FAB): 420.1 ([Cu(L)(ClO$_4^-$)]$^+$.

Analysis for [Cu($C_{13}H_{31}N_5$)](ClO$_4$)$_2$

Calc (%):	C: 30.04;	H: 6.01;	N: 12.47
Found (%):	C: 29.21;	H: 5.82;	N: 12.44

To a solution of [Cu(Me-daptacn)]$(ClO_4)_2$ (1.0 g, 1.8 mmol) in a mixture of water (50 mL) and methanol (950 mL) was added glyoxal (330 μL of a 40% solution, 2.0 mmol, 1.1 equiv.) The solution was refluxed overnight then cooled to room temperature. To this solution was added $NaBH_4$ (0.23 g, 4.5 mmol, 2.5 equiv.). The solution was then refluxed for 1 hour, over which time the color was observed to change to purple. The volume was reduced to 50 mL and the precipitate was filtered off, rinsed with methanol, and air dried. The filtrate was collected, evaporated to dryness under reduced pressure, and suspended in methanol (10 mL) to give a second crop of [Cu(Me-bicycloN$_5$)]$(ClO_4)_2$.

Yield: 1.2 g (57 %)

UV-Vis (H_2O) λ (nm), (ε, L mol^{-1} cm^{-1}): 277 (6831), 553 (155).

MS (FAB): 445.1 ([Cu(L)(ClO_4^-)]$^+$, 282 (LH^+).

Analysis for [Cu($C_{15}H_{33}N_5$)]$(ClO_4)_2$

Calc (%):	C: 33.00;	H: 6.09;	N: 13.47
Found (%):	C: 33.33;	H: 6.02;	N: 13.64

The free ligand 1-Methyl-1,5,8,12,17-pentaazabicyclo[10.5.2]nonadecane (Me-bicycloN$_5$) was obtained by dissolving [Cu(Me-bicycloN$_5$)]$(ClO_4)_2$ (0.78 g, 1.4 mmol) in distilled water (250 mL) and adding Na_2S (5 - 10 g). This solution was refluxed overnight. The resulting solution was colorless apart from a black precipitate of CuS. After filtration of the cooled mixture through a fine glass frit, the supernatant was taken to dryness. The residue was redissolved in aqueous 3 M NaOH (20 mL) and continuously extracted with $CHCl_3$ for 24 hours. The chloroform extract was dried over Na_2SO_4, filtered, and evaporated to dryness leaving a yellow oil which was further dried under vacuum. The free Me-bicycloN$_5$ ligand was not stored, rather used immediately to form the nickel complexes.

Yield: (0.34 g, 86%).

^{13}C NMR (300 MHz) ($CDCl_3$) : δ 26.9 ($CH_2\mathbf{C}H_2CH_2$); 45.9 ($\mathbf{C}H_3$), 48.1, 49.9, 51.9, 52.1, 56.2, 60.1 ($\mathbf{C}H_2NR_2$).

MS (CI): 284 (M + 1), 312 (M + 29), 325 (M + 41).

2.3.4.4 $[Ni(Me\text{-}bicycloN_5)](ClO_4)_2$ (11)

The free ligand Me-bicycloN$_5$ (0.134 g, 0.48 mmol) was dissolved in 100% ethanol (50 mL) and a solution of $Ni(ClO_4)_2 \cdot 6H_2O$ (180 mg, 0.49 mmol, 1.1 equiv.) in ethanol (10 mL) was added. The mixture was refluxed for 30 minutes, and after cooling to room temperature, the pink precipitate formed was filtered off, rinsed with ethanol, and air dried.

Yield: 150 mg (58 %)

UV-Vis (CH_3CN) λ (nm), (ε, L mol^{-1} cm^{-1}): 324 (16.3), 504 (9.5).

Analysis for $[Ni(C_{15}H_{33}N_5)](ClO_4)_2$

Calc (%):	C: 33.42;	H: 5.80;	N: 11.31
Found (%):	C: 32.97;	H: 5.94;	N: 12.20

2.3.5 De-Protection

2.3.5.1 1,4-di-(3-aminopropyl)-1,4,7-triazacyclononane (Daptacn) (12)

The ligand Bz-daptacn (0.10 g, 0.60 mmol) was dissolved in a solution of 4.4 % formic acid in methanol (25 mL) with stirring, under an N_2 atmosphere. The catalyst, 10 % Pd on activated charcoal (0.10 g), was added and the solution stirred at 25 °C overnight. The solution was filtered through celite to remove the charcoal, and evaporated to dryness. The residue was redissolved in aqueous 3M NaOH (20 mL) and continuously extracted

with $CHCl_3$ for 24 hours. The chloroform extract was dried over Na_2SO_4, filtered, and taken to dryness under reduced pressure. The product, a pale yellow oil was further dried under vacuum.

Yield: 80 mg (55 %).

^{13}C NMR: δ 30.9 ($CH_2CH_2CH_2$); 40.1 ($CH_2CH_2CH_2NH_2$), 56.2, 55.3, 55.6, 57.4 (CH_2NH_2).

MS (CI): 244 (M + 1)

2.3.5.2 1,5,8,12,17-pentaazabicyclo[10.5.2] nonadecane (BicycloN$_5$) (13)

The ligand Bz-daptacn (0.25 g, 0.60 mmol) was dissolved in a solution of 4.4 % formic acid in methanol (25 mL) with stirring, under an N_2 atmosphere. The catalyst, 10 % Pd on activated charcoal (0.25 g), was added and the solution stirred at 25 °C overnight. The solution was filtered through celite to remove the charcoal, and evaporated to dryness. The residue was redissolved in aqueous 3M NaOH (20 mL) and continuously extracted with $CHCl_3$ for 24 hours. The chloroform extract was dried over Na_2SO_4, filtered, and taken to dryness under reduced pressure. The product, a pale yellow oil was further dried under vacuum.

Yield: 180 mg (99 %).

^{13}C NMR: δ 27.0 ($CH_2CH_2CH_2$); 45.1, 46.4, 47.5,48.6, 53.7, 54.5 (CH_2NH_2).

MS (CI): 272 (M + 1)

2.3.5.3 [Ni(bicycloN$_5$)](ClO$_4$)$_2$ (14)

The free ligand bicycloN$_5$ (0.100 g, 0.37 mmol) was dissolved in 100% ethanol (50 mL) and a solution of $Ni(ClO_4)_2 \cdot 6H_2O$ (180 mg, 0.49 mmol, 1.1 equiv.) in ethanol

(10 mL) was added. The mixture was refluxed for 30 minutes, and after cooling to room temperature, the pink precipitate formed was filtered off, rinsed with ethanol, and air dried.

Yield: 150 mg (77 %)

UV-Vis (H_2O) λ (nm), (ε, L mol^{-1} cm^{-1}): 330 (12.0), 510 (7.5).

UV-Vis (H_2O) (lit.) λ (nm), (ε, L mol^{-1} cm^{-1}): 331 (14.5), 510, (9.0).[24]

Analysis for $[Ni(C_{14}H_{31}N_5)](ClO_4)_2$

Calc (%):	C: 31.90;	H: 5.92;	N: 13.28
Found (%):	C: 32.10;	H: 5.94;	N: 13.30

2.3.6 Synthesis of Tricyclo[9.14.9]N_6 Macrocycle

2.3.6.1 *N*-benzyl-(2,2'-diiodo-iminodiethane) (Bridging Ligand) (15)

Diethanolamine (8.8 g, 84.1 mmol) was dissolved in dry chloroform (250 mL) with Na_2CO_3 (1.5 g, 0.17 mol, 2 equiv.). Benzyl bromide (10 mL, 84.1 mmol, 1 equiv.) was added dropwise, and the solution was stirred for 2 hours. The Na_2CO_3 was filtered off, and the filtrate was evaporated to dryness under reduced pressure, leaving the crude product as a pale yellow oil.

Yield: 17.2 g (104 %).

^{13}C NMR: δ 55.8 ($\mathbf{C}H_2NR_2$), 59.2 ($\mathbf{C}H_2$-ϕ), 64.3 ($\mathbf{C}H_2OH$), 127.2, 129.3, 130.7, 131.5, 133.7 (**C**H (phenyl)).

MS (CI): 195 (M + 1)

The benzylated material (17.2 g, 84.1 mmol) was dissolved in dry dichloromethane (1 L) in a 2L, 2-neck round bottom flask. The solution was cooled to 0 °C under a stream of N_2 and 50 mL of triethanolamine was added through a dropping funnel. A solution containing p-toluensulfonyl chloride dissolved in CH_2Cl_2 (500 mL) was then added by

dropping funnel over a 1 hour period. The mixture was left to stir under N_2, overnight, gradually warming to room temperature. The triethylammonium chloride formed in the reaction was filtered off. The filtrate was washed with 500 mL of 2 M HCl and then with 500 mL of distilled water and finally with 500 mL of saturated Na_2CO_3 solution. The CH_2Cl_2 layer was dried over Na_2SO_4, filtered, and the solvent was removed by evaporation leaving a colorless crystalline product.

Yield: 33.0 g (95 %).

^{13}C NMR: δ 21.3, 21.7 (CH_3), 57.1 (CH_2NR_2), 63.0 (CH_2-ϕ), 66.7 (CH_2OTs), 126.0, 128.1, 129.5, 130.3, 131.2, 131.5, 133.2 (CH (phenyl)).

MS (CI): 506 (M + 1).

The ligand *N*-Bz-ditosyl-diethanolamine (10 g, 19.8 mmol) was dissolved in dmf (250 mL) with stirring, at 25 °C. NaBr (4.1 g, 39.6 mmol, 2 equiv.) was added and the solution was left to stir for several days. The white crystalline precipitate which formed was filtered off. The filtrate was taken to dryness under reduced pressure, leaving the product as a white powder, which was dried further under vacuum. The dibromo material was used without further characterization

Yield: 5.6 g (88 %).

The ligand *N*-Bz-dibromo-diethanolamine (5.4 g, 16.7 mmol) was dissolved in a mixture of acetone (100 mL) and water (5 mL). Sodium iodide (6.0 g, 36.8 mmol, 2 equiv.) was added, and the solution was left to stir for 2 hours at 25 °C. The solvent was taken to dryness under reduced pressure, and the residue was redissolved in distilled water (20 mL). It was then extracted with CH_2Cl_2 (3 x 50 mL fractions). The combined organic fractions were dried over Na_2SO_4, filtered, and evaporated to dryness.

Yield: 4.8 g (70 %).

^{13}C NMR: δ 55.0 (CH_2NR_2), 60.1 (CH_2-ϕ), 45.3 (CH_2I), 126.4, 129.1, 130.3, 130.7, 132.9 (CH (phenyl)).

MS (CI): 322 (M + 1)

2.3.6.2 High Dilution Reactions

High dilution reactions were carried out in 5 L 3-neck round bottom flask held firmly in a specially designed metal frame. Efficient mixing was achieved using a mounted 3/4 hp electric motor and stainless steel stir shaft aligned through the center neck of the reaction flask, and sealed with a teflon stir guide. This apparatus is similar to those already described in literature.[79] Reagents (dissolved in 50 mL dry CH_3CN) were dropped into the flask (containing ~ 3 L of dry CH_3CN) using plastic 50 mL syringes mounted in a specially designed holder driven by a stepping motor which could be used to control the rate of addition of the reagents. The addition of 50 mL of reagent typically took 8 - 10 hours. A condenser and nitrogen inlet were connect to one of the necks of the flask and the reaction mixture was heated to reflux under a nitrogen atmosphere. A pictorial representation of the high dilution experimental apparatus in shown in Figure 2.4.

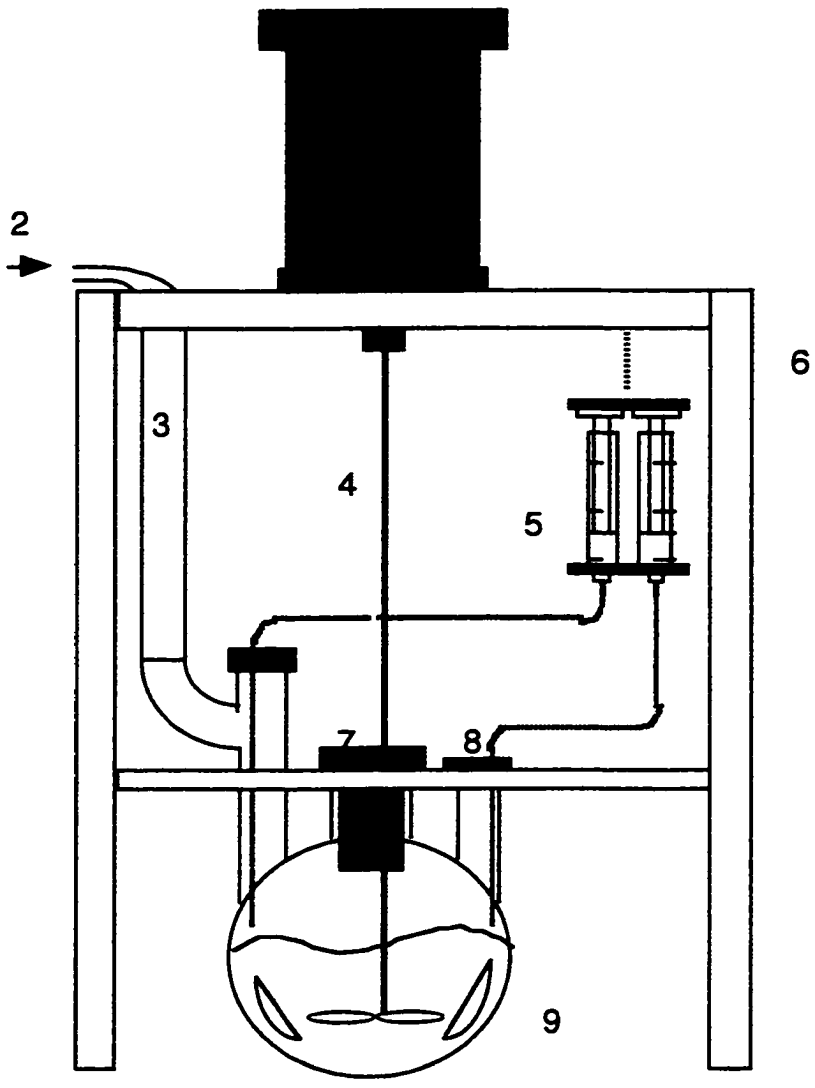

1. 3/4 hp electric motor
2. nitrogen inlet
3. condenser
4. stainless steel stir shaft
5. syringes / syringe holder / stepping motor
6. solid metal frame
7. teflon stir guide
8. rubber septa
9. 5 L, 3-neck RB flask

Figure 2.4 Apparatus used for high dilution reactions.

2.4 Synthesis of Nickel(II) Phenanthroline and Bipyridyl Complexes

The chelating ligands 1,10-phenanthroline (phen), 5-methyl-1,10-phenanthroline (5-Me-phen), 4,4'-dimethyl-1,10-phenanthroline (4,4'-Me_2-phen), 5-chloro-1,10-phenanthroline (5-Cl-phen), 5-nitro-1,10-phenathroline (5-NO_2-phen), and 2,2'-dipyridyl (bipy), were all obtained from the Aldrich Chemical Company. The nickel (II) complex of each of these ligands was prepared in the following manner: 3.5 equivalents of the appropriate ligand (0.5 g) was dissolved in 10 mL of methanol and added to 1 equivalent of $Ni(ClO_4)_2 \cdot 6\ H_2O$, also dissolved in 10 mL of methanol. The solution was stirred for 10 minutes at room temperature after which time the resulting precipitate was filtered off, washed with methanol followed by diethyl ether, and dried under vacuum. Yields were greater than 95%. These complexes were characterized by recording their UV-Vis spectra in CH_3CN and comparing to literature spectra.[80]

2.5 Potassium Tetrakis(μ-pyrophosphite-P,P')diplatinate(II) Dihydrate, $K_4[Pt_2(\mu\text{-}P_2O_5H_2)_4 \cdot 2H_2O$

The complex $Pt_2(pop)_4^{4-}$ was prepared by modifying a procedure in literature.[81] A solution of K_2PtCl_4 (0.8 g) and fresh 97% H_3PO_3 (3.0 g) in 5 mL H_2O was heated for 3 hours at 100°C, under an N_2 atmosphere. During the heating, the solution color gradually changed from red to brown, then to yellow-green. The solvent was removed by an N_2 flow while continuing to heat at 100°C. The solid was treated with methanol and acetone to remove any unreacted H_3PO_3. The crude product was purified by dissolving in a minimum amount of degassed water, and filtering through a medium porosity filter (10 to 20 μm), and a 0.45 μm Micron Sep membrane filter. Solutions of degassed methanol followed by acetone were quickly added to this bright yellow solution. A fine powder formed which was filtered under N_2, washed with methanol, acetone, and ether, and dried

under vacuum. The dry product was stored under N_2 and care was taken to avoid any exposure to moisture, in order to prevent oxidation.

Yield: 1.03 g (45%)

UV-Vis (H_2O) λ (nm), (ε, L mol^{-1} cm^{-1}): 369 (3.64 x 10^4).

UV-Vis (H_2O) (lit.) λ (nm), (ε, L mol^{-1} cm^{-1}): 370 (3.40 x 10^4).[82]

2.6 Synthesis of $[Cr([18]\text{-}aneN_6]Br_3$

The complex $[Cr([18]\text{-}aneN_6)]Br_3$ was prepared from the ligand [18]-$aneN_6{\cdot}3H_2SO_4$ supplied by the Aldrich Chemical Company ([18]-$aneN_6$ = 1,4,7,10,13,16-hexaazacyclooctadecane). The trisulfate salt was dissolved in water and made basic (pH ~ 13) with 2M sodium hydroxide solution. The free ligand was obtained as a colorless solid by continuously extracting the aqueous solution with chloroform. A solution of $CrCl_3.6H_2O$ (0.124 g, 0.5 mmol) was dissolved in 20 mL dmso at 190 °C. The volume of the solution was reduced to ~10 mL and a 0.5 mmol (0.134 g) solution of the free ligand in ethanol (5 mL) was added to the metal containing solution at 60 °C. The temperature was raised slowly to 170 °C during which time a yellow precipitate formed. Stirring was continued for 1 hr at 170 °C. The yellow solid was then filtered off and washed with ethanol and ether. After air-drying it was redissolved in water (~4 mL) at 50 °C and 2 mL of a saturated solution of sodium bromide was added. Yellow crystals were obtained on slow evaporation. The crystals were filtered off and dried under vacuum.

Yield: 0.28 g (70%)

UV-Vis (H_2O) λ (nm), (ε, L mol^{-1} cm^{-1}): 468 (227), 366, (92).

UV-Vis (H_2O) (lit.) λ (nm), (ε, L mol^{-1} cm^{-1}): 466 (227), 361, (103).[83]

Analysis for $[Cr(C_{12}H_{30}N_6)]Br_3$

Calc (%):	C: 26.19;	H: 5.49;	N: 15.27
Found (%):	C: 26.20;	H: 5.44;	N: 15.25

2.7 Synthesis of $Cr(sen)^{3+}$

2.7.1 Sen·6HCl

Crude 4,4',4"-ethylidenetris(3-azabutan-1-amine) (sen) was prepared following a procedure in literature.[84] The yellow oil of impure sen (50 g, 0.21 mol) was diluted with water (1 L), acidified (pH 3, HCl), and sorbed onto a column (5 x 50 cm) of Dowex 50W-X2 cation exchange resin (200 - 400 mesh) in the H^+ form. The column was washed thoroughly with water (1 L), followed by 1 M HCl (1 L). The material sen·6HCl, seen as a slightly lighter colored band on the column, was eluted off with 4 M HCl (1 L). The immediate front fraction of this band was discarded to ensure that no lower charged impurities were collected. The solvent was evaporated to dryness using a rotary evaporator and the residue was redissolved in warm water (10 ml). A pure sample of sen·6HCl,which crystallized on addition of ethanol and cooling, was filtered off, washed with ethanol, followed by diethyl ether, and dried under vacuum.

Yield: 32 g (34 %)

^{13}C NMR (300 MHz) (D_2O) : δ 18.5 (CH_3); 35.7, 46.3, 52.3 (CH_2); 36.6 (C quaternary).

2.7.2 $[Cr(sen)]Cl_3$

The compound sen·6HCl was converted to the free ligand in the following manner: The hexahydrochloride (3.0 g) was dissolved in a sodium ethoxide solution (formed by dissolving sodium metal (1.206, 6 equiv.) in 50 mL of methanol) while cooling in an ice bath under an atmosphere of nitrogen. The solution was warmed to room temperature and left to stir for 2 hours. A white precipitate was filtered off, leaving a clear yellow solution containing the free ligand.

The hexahydrate $CrCl_3 \cdot 6H_2O$ was dissolved in 20 mL of dmso in a 100 mL beaker, and heated to 170 °C on a hot plate, with magnetic stirring. After 20 minutes of boiling the volume had been reduced by half and the beaker was removed from the hot plate and allowed to cool to 50 °C. A solution of sen (free ligand) in methanol (50 mL, prepared as described above) was added dropwise and the beaker was again heated to 170 °C. The solution color turned from purple to brown and a yellow precipitate formed as the methanol was boiled off. After 20 minutes, the solution was cooled to room temperature and the yellow precipitate of $[Cr(sen)]Cl_3$ was filtered, washed thoroughly with ethanol followed by diethyl ether, and vacuum dried.

Yield: 1.9 g (56%)

The material $[Cr(sen)]Cl_3$ was purified by converting to the tribromide salt. This was achieved by dissolving $[Cr(sen)]Cl_3$ (1.0 g) in a minimum amount of water (5 mL) and adding a saturated solution of NaBr (10 mL), with stirring. The yellow crystals of $[Cr(sen)]Br_3$ could then be filtered off washed with diethyl ether and vacuum dried.

Yield: 0.8 g (95%)

UV-Vis (H_2O) λ (nm), (ε, L mol^{-1} cm^{-1}): 452 (93), 349 (63)

UV-Vis (H_2O) (lit.) λ (nm), (ε, L mol^{-1} cm^{-1}): 451 (97), 347, (65).[85]

Analysis for $[Cr(C_{11}H_{30}N_6)]Br_3$

Calc (%):	C: 24.55;	H: 5.58;	N: 15.62
Found (%):	C: 24.50;	H: 5.62;	N: 15.74

2.7.3 Separation Of Optical isomers of the $Cr(sen)^{3+}$ ion

2.7.3.1 (+)-$[Cr(sen)]Cl_3$

The complex $[Cr(sen)]Cl_3$ (1.49 g, 5.4 mmol) was dissolved in a minimum amount of distilled water (10 mL), in a 100 mL beaker with magnetic stirring, and d-tartaric acid ($[\alpha]_D = +12°$, 0.81g, 5.4 mmol) was added. Immediately after dissolution, $LiOH{\cdot}H_2O$ (0.45 g, 10.8 mmol) was added to this solution. After about 5 minutes, 100% ethanol (50 mL) was added dropwise, with continued stirring, to produce a yellow crystalline precipitate. The crude product, $Li\{(+)\text{-}[Cr(sen)]\}\{(+)\text{-tart}\}_2{\cdot}3H_20$, was filtered and collected. To this crude tartrate double salt was added 4 M HCl (0.88 mL), followed by 100% ethanol (11.5 mL). This solution was cooled in ice and the ensuing precipitate was collected in a Hirsch funnel. The product, $[Cr(sen)]Cl_3$ was washed with ethanol followed by diethyl ether, and vacuum dried.

Yield: 100 mg, 44%, ($[\alpha]_{546nm} = +70°$)

2.7.3.2 (-)-$[Cr(sen)]Cl_3$

The isomer (-)-$[Cr(sen)]Cl_3$ was isolated in the same manner as (+)-$[Cr(sen)]Cl_3$, as described above. The only difference was the addition of l-tartaric acid ($[\alpha]_D = -12°$) in place of d-tartaric acid, to isolate $Li\{(-)\text{-}[Cr(sen)]\}\{(+)\text{-tart}\}_2{\cdot}3H_20$ as the less soluble isomer.

Yield: 120 mg, 37%, ($[\alpha]_{546nm} = -22°$)

CHAPTER THREE

SYNTHESIS AND CHARACTERIZATION OF MACROBICYCLIC AND MACROTRICYCLIC LIGANDS

3.1 Introduction

An objective of this research project was to design and synthesize novel macrocyclic ligands which would exhibit unusual and useful properties when coordinated to transition metals. It was thought that an appropriately designed macrocyclic ligand could be used to control and study ground state reactivity including redox reactions and substitution kinetics. As well, it was hoped that formation of the chromium complexes of such novel ligands could be used to study the effects of coordination of macrocyclic ligands on the photophysical and photostereochemical properties of Cr(III) metal ion complexes.

The macrobicyclic complex 1,5,8,12,15-pentaazabicyclo[10.5.2]nonadecane, referred to here as bicycloN$_5$, consists of two ring systems 1,4,7-triazacyclononane ([9]-aneN$_3$) and 1,4,8,11-tetraazacyclotetradecane (cyclam) which have been "fused" together (Figure 3.1). The synthesis of this macrocyclic complex has been developed from the addition of two functional arms to [9]-aneN$_3$, followed by a template "ring-closure" reaction around copper.[24]

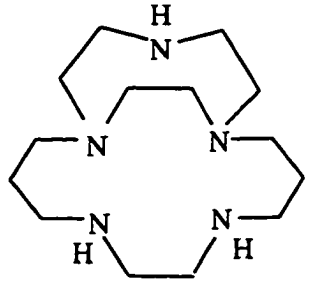

Figure 3.1 BicycloN$_5$ ligand.

The ligand BicycloN$_5$ was seen as a good starting point for the further synthetic investigation of nitrogen donor macrobicyclic complexes as well as an extension of the complexity of the ligand to form a macro tricyclic ligand. The target tricyclic ligand (Figure 3.2) consists of two [9]-aneN$_3$ rings fused together by cyclam. A transition metal complex

of this ligand would be coordinately saturated and extremely stable, and the metal ion would be held in a very defined environment within this rigid ligand framework. Properties such as these would make this a suitable candidate for an outer sphere redox reagent, since dissociation or substitution of the donor atoms would be unlikely, and the geometry of the metal ion would remain roughly constant before and after the electron transfer process. The energetics of the redox reaction would not be complicated by changes in coordination number or spin state, both of which would increase the barrier to electron transfer.

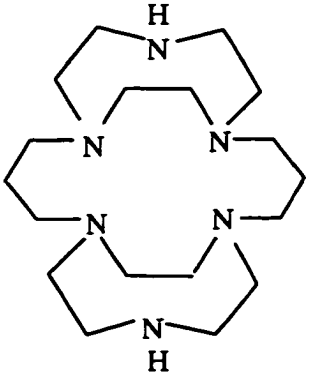

Figure 3.2 Tricyclo[9.14.9]N_6 target ligand.

3.2 Synthetic Strategy

For bicycloN_5 to be used as a precursor to the formation of the tricyclic ligand, sufficient quantity of this material was required. The synthesis of bicycloN_5 depends on the efficient bi-functionalization of 1,4,7-triazacyclononane as this is a key intermediate in formation of the bicyclic complex. The possible synthetic routes to bi-functionalized [9]-aneN_3 are summarized in Figure 3.3. Pathway (a) involves the reaction of [9]-aneN_3 with 2 mole equivalents of acrylonitrile, followed by reduction of the cyano groups to primary

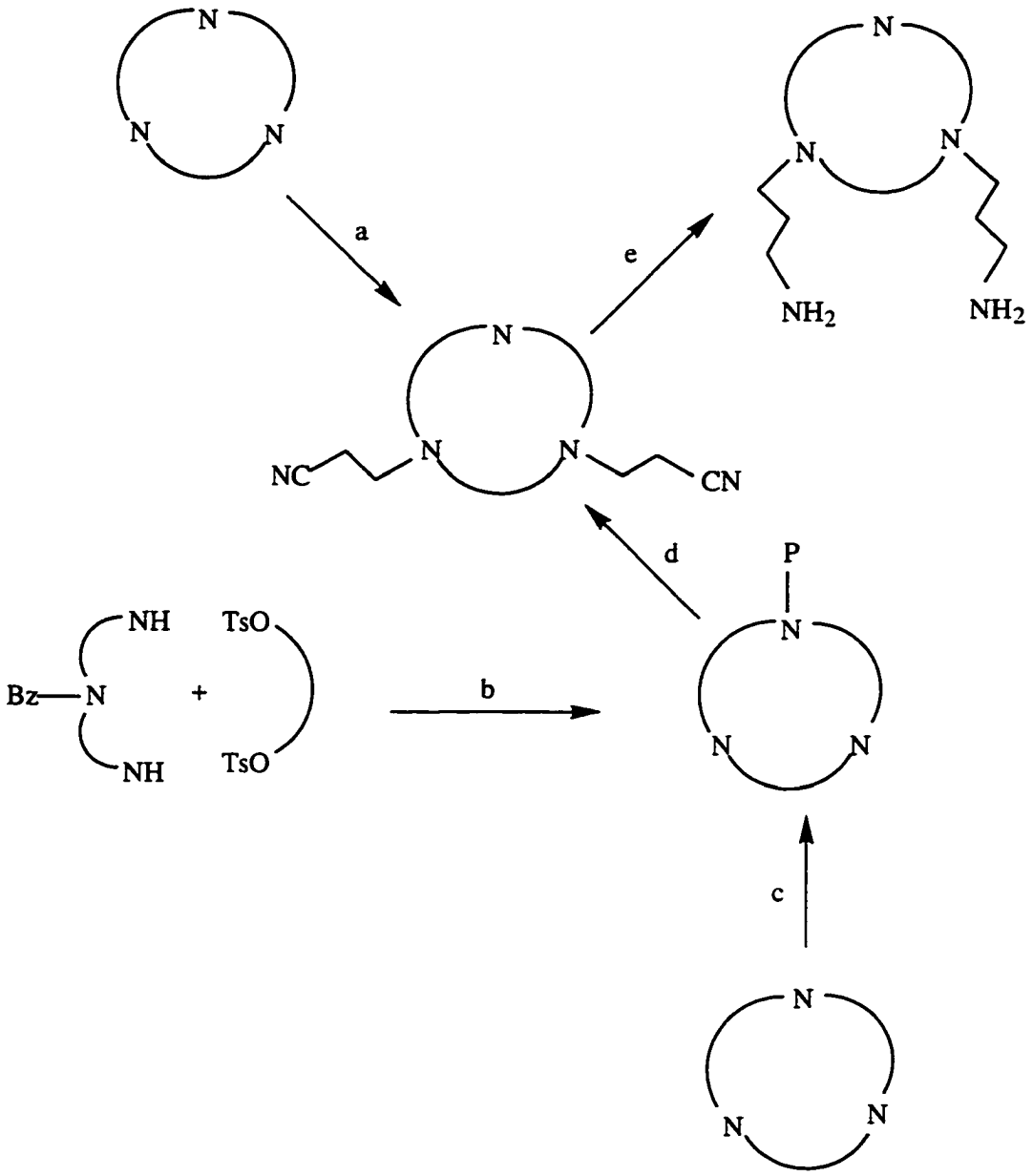

Figure 3.3 Possible synthetic routes to bi-functionalized [9]-aneN_3.

amines (pathway (e)). This route was used in the published synthesis of bicycloN$_5$,[23] developed by Fortier and McAuley and it was also initially used in this study. The difficulty with this synthesis, however, is that when such a reaction is carried out a mixture of mono- , di-, and tri- funtionalized products are formed and must be separated. This is depicted in Scheme 3.1. Copper (II) ion was added to the crude reaction mixture containing the mono-, di-, and tri-funtionalized products and they were separated on a Sephadex C-50 cation exchange column as their metal complexes. Separation of these ligands as their copper complexes was seen as more efficient than Fortier's procedure which separated the crude reaction mixture as their nickel complexes and then replaced the nickel with copper. This latter step was necessary because the subsequent ring closure template reaction used to form the bicyclic complex was found to proceed in the presence of copper (II) but not in the presence of nickel (II). A summary of the chromatographic separation of the copper complexes of the mono-, di-, and tri- functionalized products, referred to here as maptacn, daptacn, and taptacn (mono-, di-, and tri- (3-aminopropyl)-1,4,7-triazacyclononane), is given in Table 3.1.

Table 3.1 Results of the Sephadex separation of Cu(Xaptacn)$^{2+}$; X = m, d, t.

Band	[NaCl]	complex eluted	% yield
1	0 - 0.15 M	Cu(taptacn)$^{2+}$	20
2	0.15 - 0.3 M	Cu(daptacn)$^{2+}$	10
3	0.4 M	Cu(maptacn)$^{2+}$	5

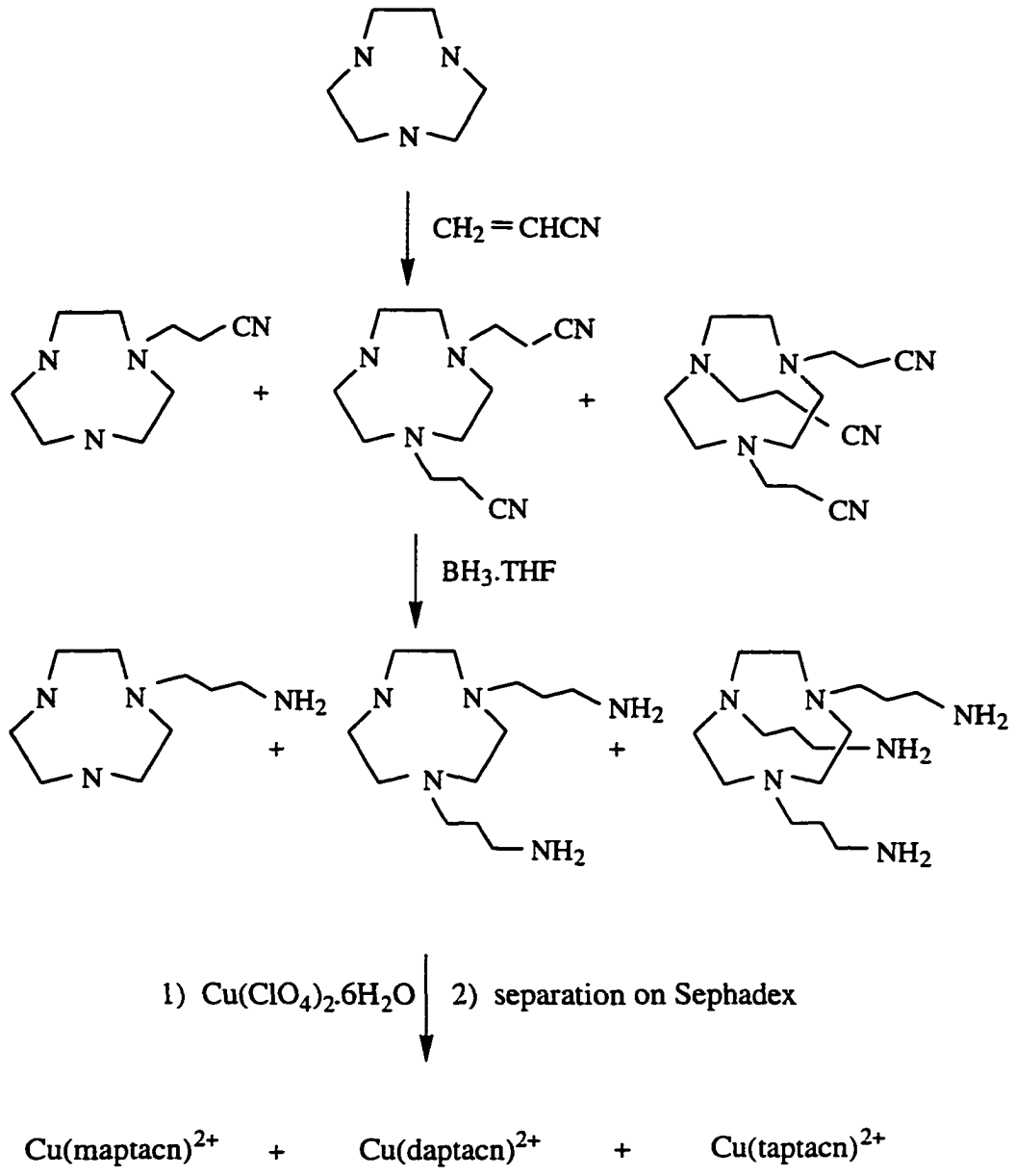

Scheme 3.1 Synthesis and isolation of mono-, di- and tri-functionalized [9]-aneN$_3$ ligands.

The overall percent yields of $Cu(taptacn)^{2+}$, $Cu(daptacn)^{2+}$, and $Cu(maptacn)^{2+}$, obtained from this difficult, tedious chromatographic separation, were found to be 20%, 10%, and 5% respectively. Clearly this is an inefficient synthetic route to bi-functionalized [9]-aneN_3, and for this reason an alternate route was sought.

Pathway (d) (Figure 3.3) seems a much more attractive, and more efficient synthesis of bi-functionalized [9]-aneN_3. This involves the synthesis of mono protected [9]-aneN_3 using a protecting group (P) followed by reaction to form the bi-functionalized molecule and the eventual removal of the protecting group. Two types of reaction can be envisioned for the synthesis of mono protected nonane. In pathway (b) the cyclisation reaction used to form the triazamacrocycle is carried out in the presence of the protecting group. This synthetic route had previously been investigated[86] and it was found that the conditions required to remove the tosyl (Ts) groups in the Richman-Atkins synthesis also removed the protecting group. A more feasible pathway to the formation of mono protected nonane involves the addition of a protecting group to the preformed triazamacrocylic ligand, pathway (c). An investigation of this synthetic pathway is described in Section 3.3.

3.3 Mono Protection of 1,4,7-triazacyclononane ([9]-aneN$_3$)

It was found that reacting 1,4,7-triazacyclononane with a slight excess of triphenyl methyl chloride[87] in the presence of a base (Li_2CO_3) resulted in the isolation of the mono protected product. Here one *N*-donor nitrogen is protected by a triphenylmethyl (trityl) group (Figure 3.4).

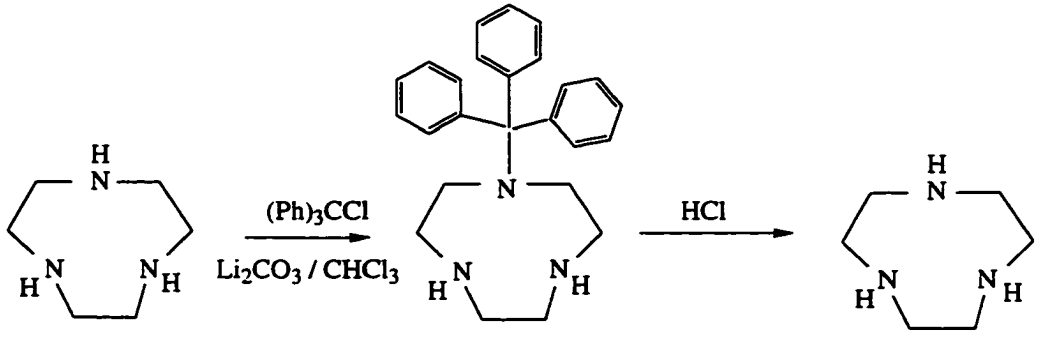

Figure 3.4 The mono protection and deprotection of [9]-aneN$_3$ with triphenylmethyl chloride.

This reaction was found to clearly favor the formation of mono-substituted product with a yield of 60%, as only a small amount of the di-substituted, and none of the tri-substituted products were detected. This may be a reflection of the steric influence of the bulky triphenylmethyl group which inhibits the addition of more than one of these groups to the nonane ring. This protecting group was found to be easily removed by stirring in acidic conditions to give back unprotected [9]-aneN$_3$.

An alternate procedure for protection of [9]-aneN$_3$ was obtained by following a method developed by Vachon and co-workers for the selective *N*-protection of medium-

ring triamines.[88] This short, efficient synthesis relies upon the introduction of a single *N*-formyl group masked as a tricyclic orthoamide within the triamine ring (Figure 3.5).

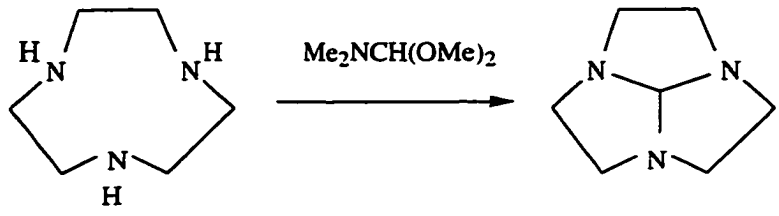

Figure 3.5 Orthoamide formation.

This approach has been used successfully by Schröder and co-workers[89] in the synthesis of bi-functional derivatives of [9]-aneN$_3$, where two pendant arms containing alcohol functional groups were added to nonane. It was thought that this would similarly provide an efficient route to the bi-functionalized daptacn molecule.

The reaction sequence for the mono protection of nonane via the formation of the orthoamide is shown in Scheme 3.2. The ligand 1,4,7-triazacyclononane was reacted with 1 equivalent of *N*,*N*'-dimethylformamide dimethyl acetal to give the desired orthoamide in 99% yield. Stirring this product in 3M HCl at room temperature, overnight, resulted in its unmasking by acid hydrolysis to give the *N*-formyl species. This derivative of [9]-aneN$_3$, obtained in 80% yield, contains one *N*-donor protected by a formyl (CHO) functional group. The *N*-formyl species was found to be reduced to the corresponding *N*-methyl derivative by reaction with 3 equivalents of LiAlH$_4$ in dry THF. Interestingly, the formyl group was found to be capable of withstanding reactions carried out in the presence of the less powerful reducing agent 1M BH$_3$.THF. In subsequent reactions carried out under these conditions the formyl group was found to be left unreacted.

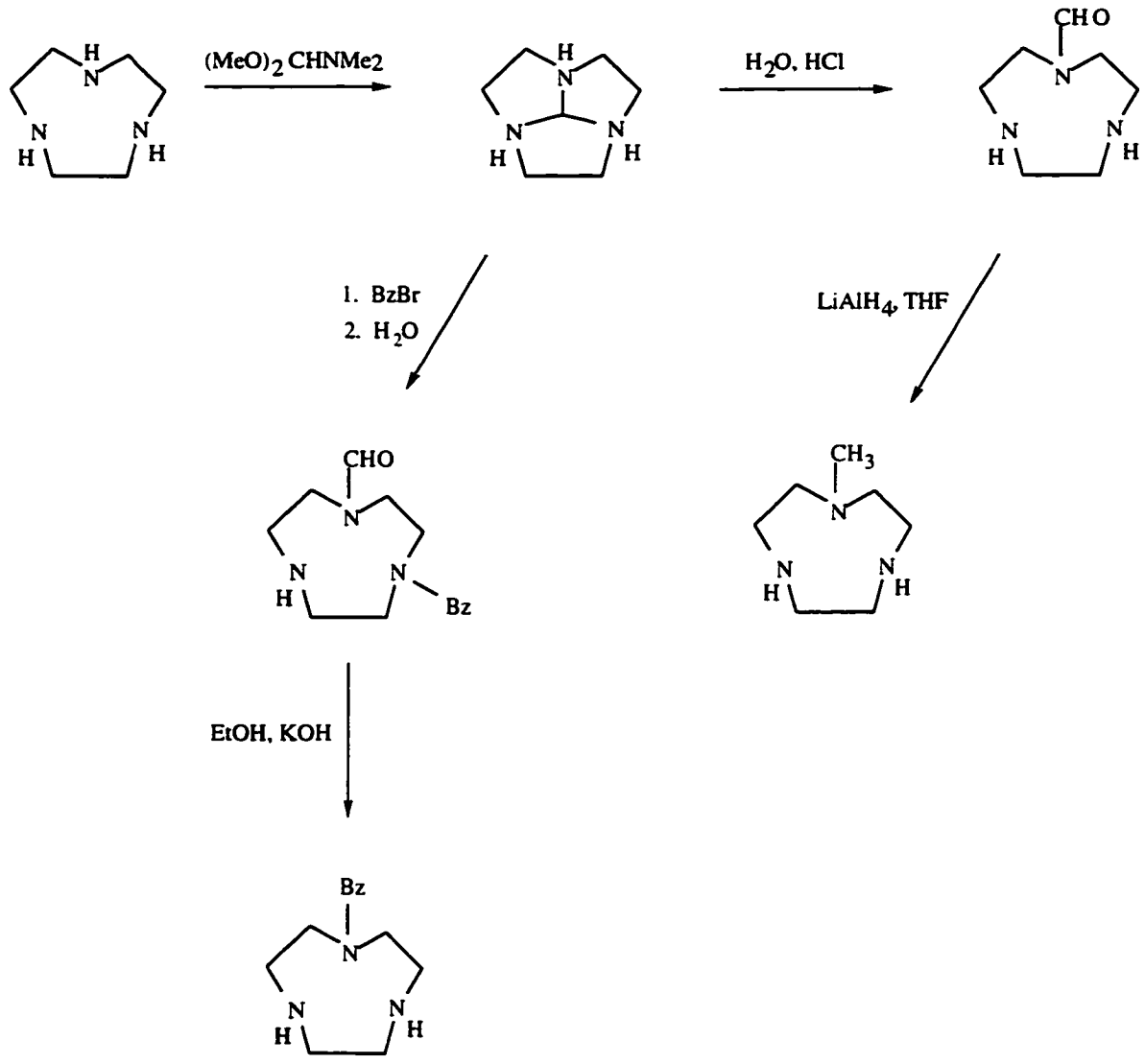

Scheme 3.2 Synthetic route to mono protected [9]-aneN_3.

The orthoamide was also reacted with 1 equivalent of benzyl bromide followed by hydrolytic un-masking to give a derivative of nonane which contained one *N*-formyl group and one *N*-benzyl group. The formyl group was easily removed by refluxing this product in an aqueous solution of NaOH (25 equivalents) for 24 hours. The mono benzylated derivative of nonane was obtained cleanly in 88% yield as a yellow crystalline solid.

This provides an efficient synthetic route to the mono protection of [9]-aneN_3 and can be used to obtain reasonable quantities of three different derivatives of nonane: *N*-formyl, *N*-methyl, and *N*-benzyl. These derivatives can then be utilized as building blocks in the formation of the bicyclic and tricyclic macrocyclic ligands. The chemical shifts observed in the ^{13}C NMR spectra of the three mono protected derivatives of nonane are summarized in Table 3.2. In the case of the formyl derivative, an additional single resonance is observed at 163.9 ppm corresponding to the carbon on the formyl group (**C**HO). For the methyl derivative an additional single line at 43.8 ppm is observed due to the methyl group (**C**H_3). For the benzyl derivative five additional lines are observed, one at 64.8 ppm which corresponds to the CH_2 carbon of the benzyl protecting group, and the other four signals, in the range 126 - 129 ppm which correspond to the aromatic ring carbons of the benzyl group. The identity of these compounds was also verified using chemical ionization (CI) mass spectroscopy.

Table 3.2 ^{13}C NMR data for [9]-aneN_3 and its mono protected derivatives.

Ligand	chemical shift (ppm)	# of C's	Assignment
[9]-aneN_3	47.1	6	CH_2NR_2
formyl-[9]-aneN_3	46.0	1	CH_2NR_2
	46.7	1	"
	48.4	1	"
	49.5	1	"
	50.2	1	"
	52.8	1	"
	163.9	1	CHO
methyl-[9]-aneN_3	43.8	1	CH_3
	45.7	1	CH_2NR_2
	49.9	1	"
	51.1	1	"
	57.4	1	"
	58.0	1	"
	60.9	1	"
benzyl-[9]-aneN_3	46.1	2	CH_2NR_2
	46.3	2	"
	52.6	2	"
	64.4	1	R_2NCH_2-ϕ
	126.7	2	CH (phenyl)
	126.9	2	"
	128.2	2	"
	129.1	2	"

3.4 Mono Protection of 1,4,8-triazacyclodecane ([10]-aneN$_3$)

It was deemed desirable to mono protect the ten member ring 1,4,8-triazacyclodecane ([10]-aneN$_3$). The formation of mono protected [10]-aneN$_3$ would provide a starting point for the synthesis of a different structural isomer of the bicyclic ligand (Figure 3.6) consisting of a ten-member ring fused to cyclam.

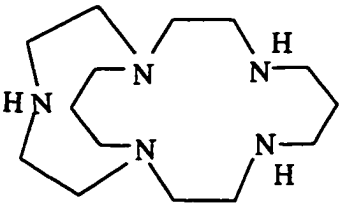

Figure 3.6 Macrobicyclic ligand derived from mono protected [10]-aneN$_3$.

There are conflicting literature reports on whether or not it is possible to form the orthoamide of the ten member ring [10]-aneN$_3$. Atkins[90] reported the formation of the orthoamide of [10]-aneN$_3$ in 91% yield. If this derivative could be isolated then the same strategy used to mono protect [9]-aneN$_3$ could be used. The presence of the extra methylene in the 10-member macrocyle would result in two possible isomers of the mono protected derivative, requiring that these isomers be separated. All attempts to form the orthoamide of [10]-aneN$_3$ following the same procedure described for [9]-aneN$_3$ (Section 3.3), using [10]-aneN$_3$, failed. This supports the observations made by Vachon[88] that the orthoamide can be formed for the nine member ring, [9]-aneN$_3$, and the twelve-member ring, [12]-aneN$_3$, but not for the ten member ring, [10]-aneN$_3$.

An alternative synthesis in which [10]-aneN$_3$ can be selectively mono protected is described in Scheme 3.3. In this procedure, diethylenetriamine and diethyl malonate

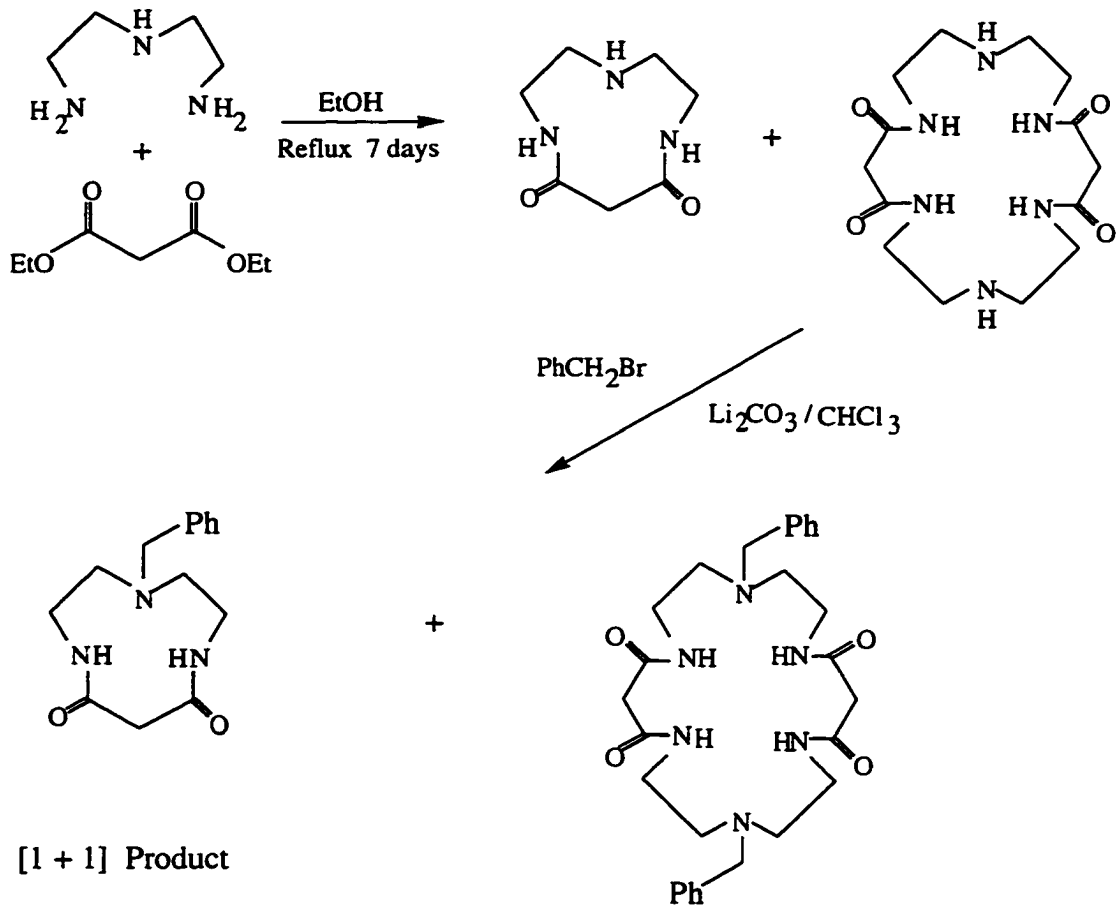

Scheme 3.3 Synthetic route to mono protected [10]-aneN$_3$.

(1 equiv.) are refluxed in 2 L of ethanol for 7 days and the ensuing condensation reaction gives a diamide macrocyclic product. This product can then be selectively protected at the amine nitrogen by reaction with a suitable protecting group such as benzyl bromide or tosyl chloride. The final step is to isolate by chromatography the ten member macrocycle from any other products which may have formed in the condensation reaction. A similar procedure had been used successfully within our group for the formation of a mono tosylated derivative of the twelve member ring [12]-aneN_3. Separation on a silica column (elution with methanol in dichloromethane 30% v/v) of the crude reaction mixture obtained from the reaction of diethylenetriamine and diethyl malonate resulted in the isolation of a white solid (0.5 g) which was identified by mass spectroscopy (CI : 535 g $mole^{-1}$ (M + 1)) as the macrocyclic eighteen-member, dibenzylated, [2 + 2] cyclisation product (Figure 3.7).

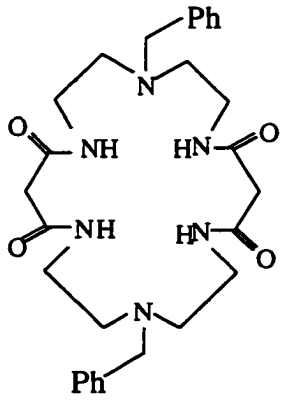

Figure 3.7 [2 + 2] Cyclisation product

An oil was also obtained from the chromatographic separation and the desired ten-member [1 +1] cyclisation product could not be cleanly separated from this. This uncharacterizable oil (~ 5 g) likely contained a mixture of the ten-member macrocyclic product as well as other higher molecular weight cyclisation products also formed from the condensation reaction.

3.5 Addition of Functional Arms to Mono Protected [9]-aneN$_3$

Reaction of both the *N*-benzyl and the *N*-methyl derivatives of [9]-aneN$_3$ with acrylonitrile followed by diborane reduction resulted in the addition of two functional propylamine arms to each of these complexes. In both cases the protecting group remained attached while the other two nitrogens in the macrocyclic ring added acrylonitrile in a Michael addition. Neither the *N*-methyl nor the *N*-benzyl group was affected by the refluxing 1M BH_3.THF conditions of the reduction step used to convert the cyano groups to amines. The chemical shifts observed in the ^{13}C NMR spectra of *N*-benzyl-daptacn and *N*-methyl-daptacn are summarized in Table 3.3. Both spectra exhibited three lines due to the ring carbons and three lines due to the pendant arm carbons in addition to the carbon resonances due to the corresponding protecting groups. This indicated that there is a plane of symmetry in both of these molecules. This is similar to the ligand daptacn which exhibits 6 lines in its ^{13}C NMR spectrum. The identity of these compounds was also verified using mass spectroscopy (CI).

The option of removing the benzyl protecting group at this stage would result in the formation of the ligand daptacn. It is desirable, however, to leave the protecting group attached in order to form the protected derivatives of the bicyclic ligands, which could then be used in subsequent reactions to form the tricyclic ligand. The removal of the benzyl protecting group is discussed in Section 3.8.

Copper (II) ions were added to each of these two derivatives of daptacn, one containing an *N*-methyl group, the other containing an *N*-benzyl group, to form their metal complexes. This is depicted in Scheme 3.4. The two bi-functional complexes formed, [Cu(Me-daptacn)]$(ClO_4)_2$, and Cu(Bz-daptacn)$(ClO_4)_2$, were obtained in good yields (56% and 84% respectively). This has proven to be a more simple and efficient synthetic

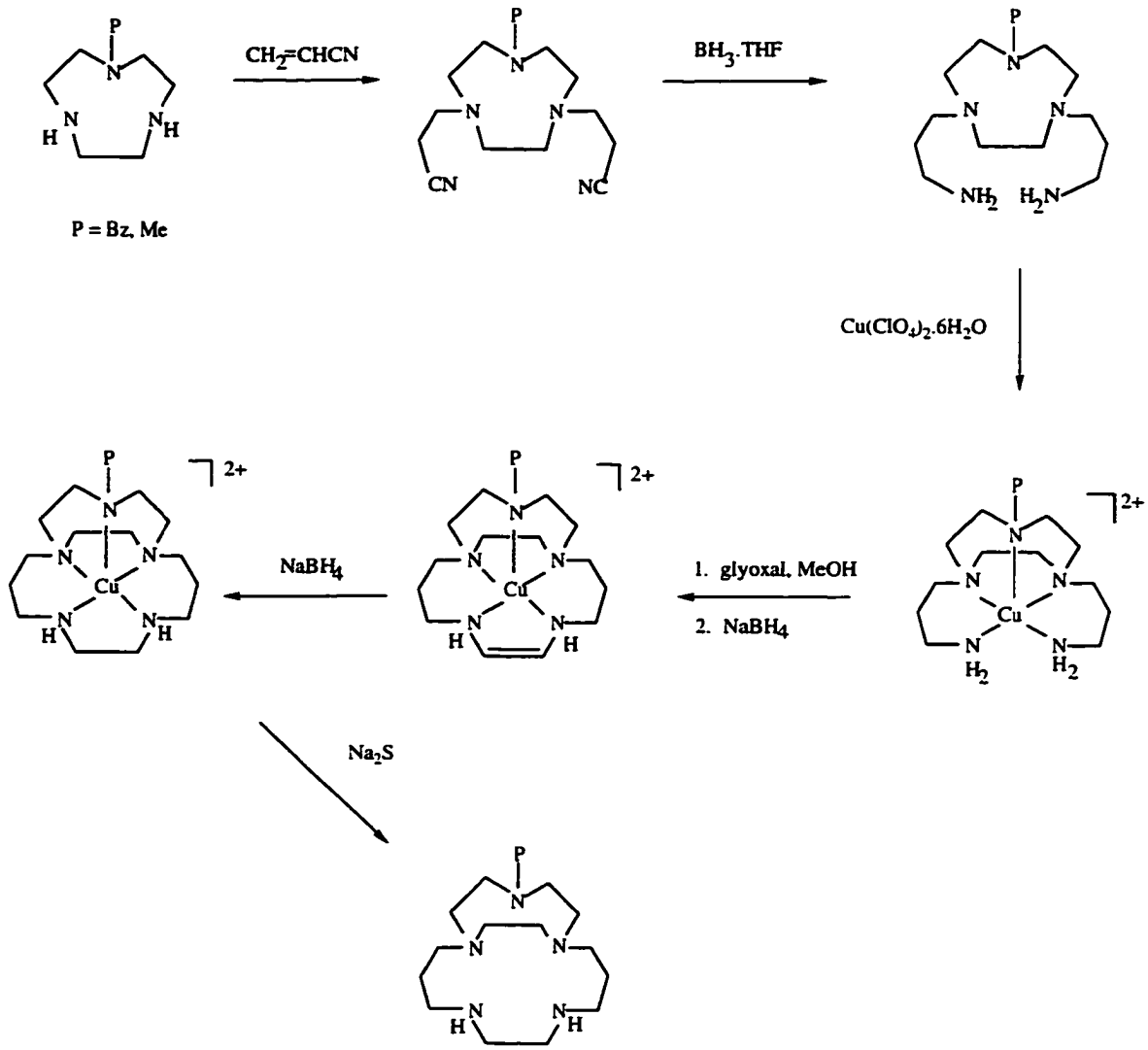

Scheme 3.4 Synthetic route to macrobicyclic ligands.

Table 3.3 ^{13}C NMR data for the bi-functionalized [9]-aneN_3 ligands.

Ligand	Chemical shift (ppm)	# of C's	Assignment
daptacn	30.9	2	$H_2CCH_2CH_2$
	40.1	2	$CH_2CH_2CH_2NH_2$
	56.2	2	CH_2NR_2
	55.3	2	"
	55.6	2	"
	57.4	2	"
Me-daptacn	28.5	2	$CH_2CH_2CH_2$
	38.9	2	$CH_2CH_2CH_2NH_2$
	42.8	1	CH_3
	48.5	2	CH_2NR_2
	49.9	2	"
	52.7	2	"
	62.1	2	"
Bz-daptacn	30.9	2	$CH_2CH_2CH_2$
	40.5	2	$CH_2CH_2CH_2NH_2$
	55.2	2	CH_2NR_2
	55.3	2	"
	55.6	2	"
	56.4	2	"
	64.5	1	CH_2-ϕ
	126 - 129	6	CH (phenyl)

route to bi-functional [9]-aneN$_3$ than the tedious chromatographic separation of maptacn, daptacn, and taptacn where daptacn is obtained in only 10% yield.

3.6 Synthesis of Macrobicyclic Ligands

3.6.1 Synthetic Strategy

The synthesis of the macrobicyclic complexes followed the procedure outlined by Fortier and McAuley[24] (Scheme 3.4). The two copper complexes, [Cu(Me-daptacn)](ClO$_4$)$_2$ and [Cu(Bz-daptacn)](ClO$_4$)$_2$ were converted to the corresponding macrobicyclic complexes by condensation with glyoxal in a methanol/water mixture. Subsequent reduction with NaBH$_4$ resulted in the isolation of the fully reduced macrobicyclic complexes, [Cu(Me-bicycloN$_5$)](ClO$_4$)$_2$ and [Cu(Bz-bicycloN$_5$)](ClO$_4$)$_2$. It was found that when this reduction step was not carried out carefully, by ensuring that there was a sufficient excess of the reductant NaBH$_4$, an intermediate complex corresponding to an enamine product was isolated (Figure 3.8).

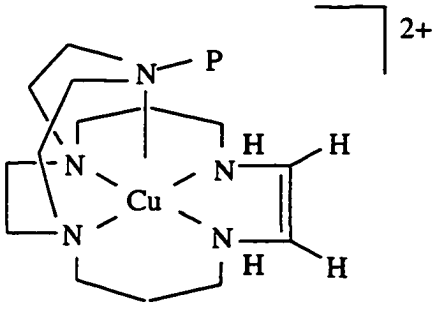

Figure 3.8 Enamine complex formed from incomplete reduction by NaBH$_4$: P = Me, Bz.

The mechanism for the formation of this enamine complex has been investigated for the $Cu(bicycloN_5)^{2+}$ complex.[24] It has been proposed that the enamine intermediate is formed by incomplete reduction of an imidate intermediate. The imidate intermediate results from the addition of MeOH across a C=N bond after the condensation with glyoxal. These steps are shown in Figure 3.9.

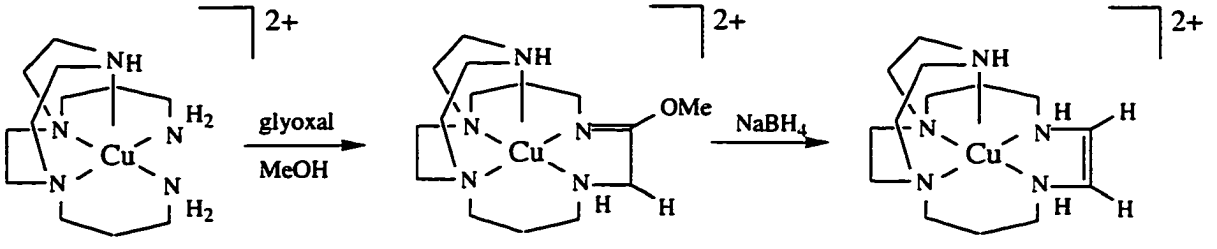

Figure 3.9 Formation of the imidate and enamine intermediates.

Copper (II) ions were removed from the bicyclic metal complexes by reaction with Na_2S to give the free ligands Me-$bicycloN_5$ and Bz-$bicycloN_5$. The chemical shifts observed in the ^{13}C NMR spectra for both theses ligands are summarized in Table 3.4, along with the ^{13}C NMR data for the $bicycloN_5$ ligand. All three spectra exhibited 7 lines of roughly equal intensity corresponding to the fourteen CH_2's of the macrocylic framework. A plane of symmetry in these ligands results in half of the CH_2's being chemically equivalent, hence 7 lines are observed. In the spectra of the *N*-methyl bicyclic ligand the CH_3 resonance was found at 45.9 ppm. This was clearly identified from the ^{13}C DEPT experiment where the CH_2 resonances are inverted 180 ° from the CH and CH_3 resonances. In the spectrum of the *N*-benzyl bicyclic ligand, the characteristic lines due to the benzyl protecting group (126 - 129 ppm CH phenyl, 61 ppm CH_2-ϕ) were clearly distinguishable. In addition, mass spectroscopy (FAB) was used to verify the identity of the copper (II) complexes $[Cu(Me\text{-}bicycloN_5)](ClO_4)_2$ and $[Cu(Me\text{-}bicycloN_5)](ClO_4)_2$.

Table 3.4 ^{13}C NMR data for the macrobicyclic ligands.

Ligand	Chemical shift (ppm)	# of C's	Assignment
bicycloN$_5$	26.9	2	$CH_2CH_2CH_2$
	45.0	2	CH_2NR_2
	46.4	2	"
	47.4	2	"
	48.6	2	"
	53.6	2	"
	54.5	2	"
Me-bicycloN$_5$	26.9	2	$CH_2CH_2CH_2$
	45.9	1	CH_3
	48.1	2	CH_2NR_2
	49.9	2	"
	51.9	2	"
	52.1	2	"
	56.2	2	"
	60.1	2	"
Bz-bicycloN$_5$	26.1	2	$CH_2CH_2CH_2$
	47.6	2	CH_2NR_2
	49.0	2	"
	52.3	2	"
	53.9	2	"
	56.7	2	"
	56.9	2	"
	61.4	1	CH_2-ϕ
	126 - 129	6	CH (phenyl)

3.6.2 Metal Complexes of Macrobicyclic Ligands and Solution Studies

3.6.2.1 UV-Vis Spectra

The electronic spectra of the nickel and copper metal complexes of the ligands Me-bicycloN$_5$ and Bz-bicycloN$_5$ were recorded and compared to the spectra of species for the ligand bicycloN$_5$. The copper (II) spectra are similar to Cu(bicycloN$_5$)$^{2+}$ and consistent with these complexes all being five-coordinate. It is interesting to compare the spectra of the bicyclic ligands with their open chain daptacn analogs. The d-d transitions are found at slightly higher energy in the copper bicyclic complexes. The difference reflects the increase in crystal field stabilization energy (CFSE) upon formation of the macrocyclic ring. From a comparison of the band positions and molar absoprtivities observed in the spectra of the nickel complexes it is evident that Ni(Me-bicycloN$_5$)$^{2+}$ and Ni(Bz-bicycloN$_5$)$^{2+}$ are both six coordinate like Ni(bicycloN$_5$)$^{2+}$. A solvent molecule occupies the sixth coordination site. The protecting groups, both methyl and benzyl, do not appear to prevent the apical donor nitrogen, to which they are attached, from coordinating to the Cu^{2+} and Ni^{2+} metal centers.

Both Ni(Me-bicycloN$_5$)$^{2+}$ and Ni(Me-bicycloN$_5$)$^{2+}$ were found to be readily oxidized to nickel (III) using NO^+ in dry acetonitrile. Other methods which have been used to form Ni(bicycloN$_5$)$^{3+}$, include electrochemical oxidation as well as a variety of chemical oxidants: i) 3 M HNO_3, ii) $Co^{III}(H_2O)_6^{3+}$ in acidic aqueous media, and iii) $Na_2S_2O_8$ in neutral aqueous media. The electronic spectra of the Ni(Me-bicycloN$_5$)$^{3+}$ and Ni(Bz-bicycloN$_5$)$^{3+}$ are similar to that of Ni(bicycloN$_5$)$^{3+}$ (Table 3.5) and are characteristic of Ni^{III} complexes with macrocyclic ligands.[91] Strong charge transfer (CT) bands are observed around 300 nm ($\varepsilon \sim 1 \times 10^4$ M^{-1} cm^{-1}), and a weak d-d transition around 660 nm ($\varepsilon \sim 30$ M^{-1} cm^{-1}). The nickel (III) complexes of Me-bicycloN$_5$ and Bz-bicycloN$_5$ were found to be stable in acetonitrile for days.

Table 3.5 Electronic spectra of nickel (II)/(III) and copper (II) complexes with N5 macrobicyclic ligands.

Complex	λ_{max}, nm (ε, $M^{-1}\,cm^{-1}$)	ref.
$Cu(daptacn)^{2+}$	578 (106)	86
$Cu(Me\text{-}daptacn)^{2+}$	577 (113)	a
$Cu(Bz\text{-}daptacn)^{2+}$	571 (149)	a
$Cu(bicycloN_5)^{2+}$	276 (5700) 567 (145)	86
$Cu(Me\text{-}bicycloN_5)^{2+}$	277 (6831) 553 (155)	a
$Cu(Bz\text{-}bicycloN_5)^{2+}$	278 (5618) 546 (149)	a
$Ni(bicycloN_5)^{2+}$	331 (14.5) 510 (9.0) [b]	86
$Ni(Me\text{-}bicycloN_5)^{2+}$	324 (16.3) 504 (9.5) [c]	a
$Ni(Bz\text{-}bicycloN_5)^{2+}$	328 (sh) 523 (13.6) [c]	a
$Ni(bicycloN_5)^{3+}$	262 (sh) 303 (1.06×10^4) 380 (sh) 665 (37) [b]	86
$Ni(Me\text{-}bicycloN_5)^{3+}$	258 (sh) 315 (8.80×10^3) 373 (sh) 657 (23) [c]	a
$Ni(Bz\text{-}bicycloN_5)^{3+}$	242 (sh) 321 (6.19×10^{-3}) 383 (sh) 670 (30) [c]	a

a = this work. b = in H_2O. c = in CH_3CN.

3.6.2.2 Cyclic Voltammetry

Cyclic voltammetry of the complexes $Ni(Me\text{-}bicycloN_5)^{2+}$ and $Ni(Bz\text{-}bicycloN_5)^{2+}$ in acetonitrile (0.1 M $(n\text{-}Bu)_4NPF_6$ media, scan rate = 100 mV s^{-1}) showed a reversible one electron wave at 0.75 V and 0.73 V respectively (versus $Fc^{+/0}$) (Table 3.6). The CV of $Ni(Me\text{-}bicycloN_5)^{3+/2+}$ is shown in Figure 3.10, this wave corresponds to the $Ni^{III/II}$

couple. It is well documented that replacement of a secondary amine donor with a tertiary amine in a tetraaza macrocyclic ring destabilizes the nickel (III) state by approximately 100 mV per tertiary amine.[91] Comparison of the $E_{1/2}$ values of Ni(Me-bicycloN$_5$)$^{3+/2+}$ and Ni(Bz-bicycloN$_5$)$^{3+/2+}$ with the $E_{1/2}$ value for Ni(bicycloN$_5$)$^{3+/2+}$ (0.63 V vs. $Fc^{+/0}$) shows that the nickel (III) has been destabilized by 120 mV by the conversion of the secondary apical donor nitrogen to a tertiary nitrogen by the addition of the methyl group, and by 100 mV for addition of the benzyl group.

Table 3.6 Electrochemical data for the $Ni^{III/II}$ couple of the nickel bicyclic complexes in acetonitrile (versus $Fc^{+/0}$).

Complex	$E_{1/2}$, V	$E_C - E_A$, mV	reference
Ni(bicycloN$_5$)$^{3+/2+}$	0.63 (reversible)	80 (reversible)	86
Ni(Me-bicycloN$_5$)$^{3+/2+}$	0.75 (reversible)	75 (reversible)	this work
Ni(Bz-bicycloN$_5$)$^{3+/2+}$	0.73 (reversible)	70 (reversible)	this work

3.6.2.3 ESR Spectroscopy

The nickel (III) complexes Ni(Me-bicycloN$_5$)$^{3+}$ and Ni(Bz-bicycloN$_5$)$^{3+}$ were found to be ESR active. The ESR spectrum of Ni(Bz-bicycloN$_5$)$^{3+}$ is shown in Figure 3.11. This spectrum is characteristic of a low spin d^7 ion in a distorted octahedral environment. It has been shown for the Ni(bicycloN$_5$)$^{3+}$ complex that the ESR spectrum is sensitive to the counter ion present which occupies the sixth coordination site.[86] The ESR spectra of [Ni(Bz-bicycloN$_5$)](ClO$_4$)$_2$ and [Ni(Me-bicycloN$_5$)](ClO$_4$)$_2$ were recorded in frozen CH_3CN (77 K) and g values for Ni(Bz-bicycloN$_5$)$^{3+}$ and Ni(Me-bicycloN$_5$)$^{3+}$ as

perchlorates and are given in Table 3.7 together with the corresponding value for the $Ni(bicycloN_5)^{3+}$ ion.

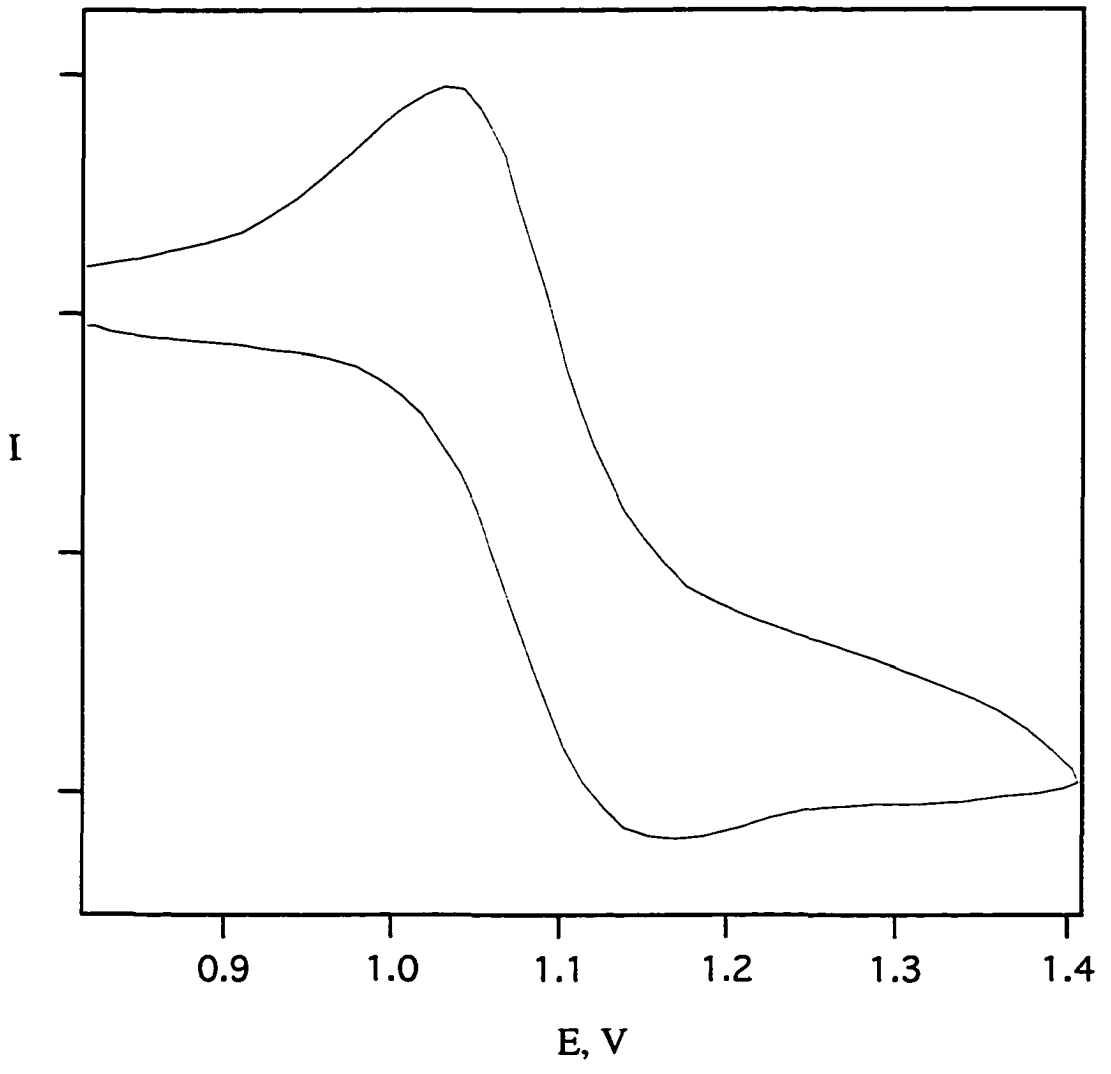

Figure 3.10 The CV of $[Ni(Bz\text{-}bicycloN_5)](ClO_4)_2$ in acetonitrile: 0.1 M $(n\text{-}Bu)_4NPF_6$ media, scan rate = 100 mV s^{-1} (vs. $Fc^{+/0}$).

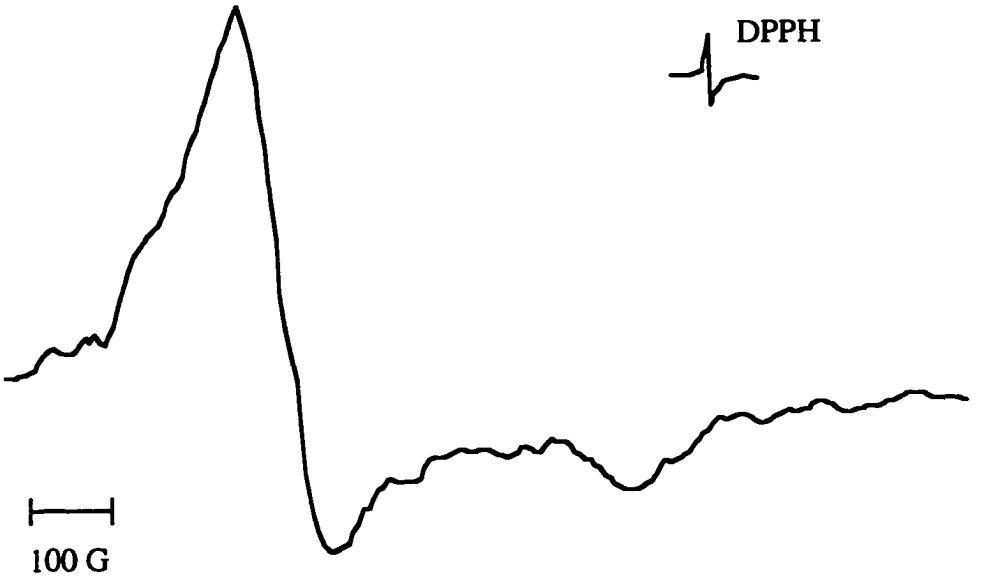

Figure 3.11 ESR spectrum of $Ni(Bz\text{-}bicycloN_5)^{3+}$ in frozen (77 K) acetonitrile matrix: counter ion = ClO^{4-}.

Table 3.7 g values for nickel (III) bicyclic complexes recorded in acetonitrile at 77 K: counter ion = ClO_4^-.

Complex	$g_\perp$	$g_\parallel$
$Ni(bicycloN_5)^{3+}$	2.170	2.025
$Ni(Me\text{-}bicycloN_5)^{3+}$	2.167	2.029
$Ni(Bz\text{-}bicycloN_5)^{3+}$	2.168	2.026

3.7 Synthesis of a Macrotricyclic Ligand

3.7.1 Synthetic Strategy

Two types of reactions can be envisioned for the formation of the target six-nitrogen donor macro tricyclic ligand (Figure 3.2) The first strategy involves the reaction of a bi-functionalized mono protected nonane derivative with a second mono protected nonane molecule, under conditions of high dilution. The two nonane units would be fused together through the two functional arms, forming the macrotricyclic ligand. This ligand could then be de-protected at both of the apical nitrogen donor positions. This approach is depicted by reaction a) in scheme 3.5. A second strategy involves the capping of the parent protected bicyclic complex Bz-bicycloN$_5$, also under conditions of high dilution, using an appropriate *N*-protected bridging ligand. This approach is depicted by reaction **b**) in Scheme 3.5. Both of these strategies were used in attempts to form the desired macrotricyclic target ligand.

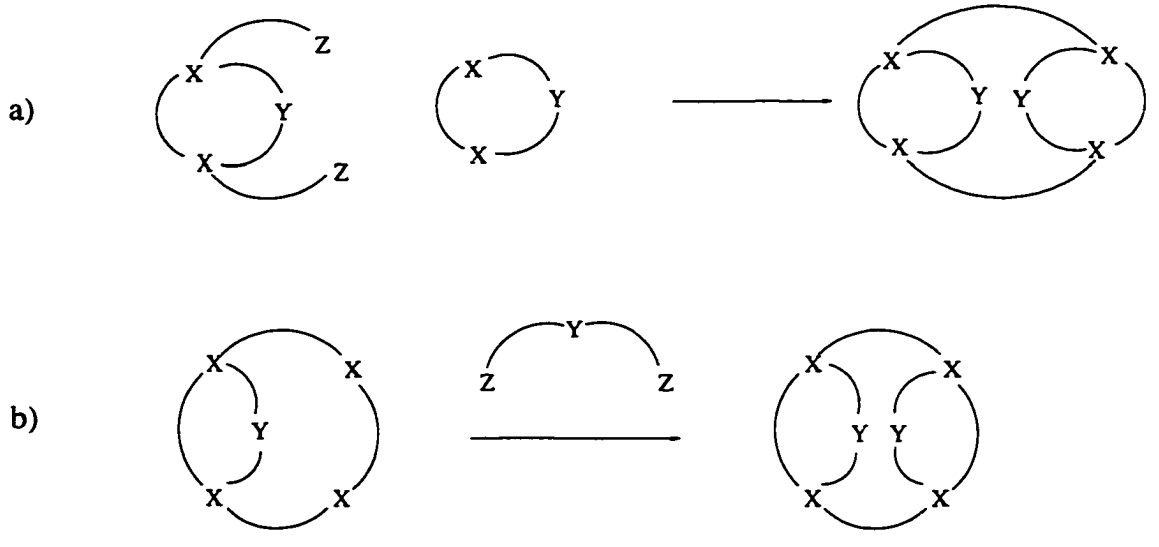

Scheme 3.5 Possible synthetic routes to macro tricyclic ligand; X = N, NH, Y = N-Bz.

Two possible isomers of the target macro tricyclic ligand tricyclo[9.14.9]N_6 may be formed. The *anti* and the *syn* isomers are illustrated in Figure 3.12.

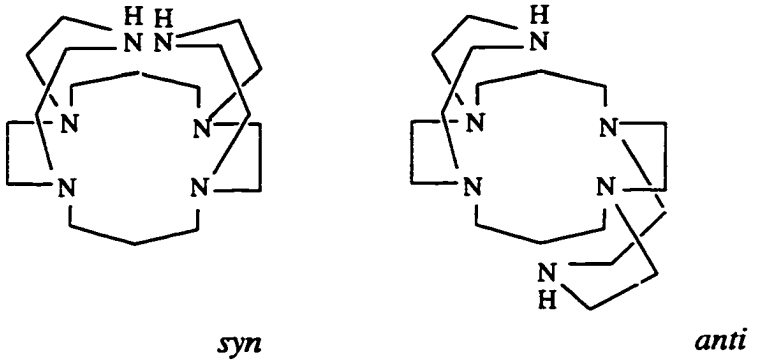

syn *anti*

Figure 3.12 *Syn* and *anti* isomers of the tricyclo[9.14.9]N_6 ligand.

It has been shown that the 14-member cyclam ring on which this tricyclic ligand is based can have five different conformations which arise due to the chirality of the coordinated nitrogen centers. These are: trans-I (++++), trans-II (+-++), trans-III (+--+), trans-IV (++--), and trans-V (+-+-), where "+" indicates that the hydrogen or substituent on the N atom is above the plane of the macrocycle and "-" indicates that it is below. This terminology was first introduced by Bosnich et al.[19] and is depicted in Figure 3.13.

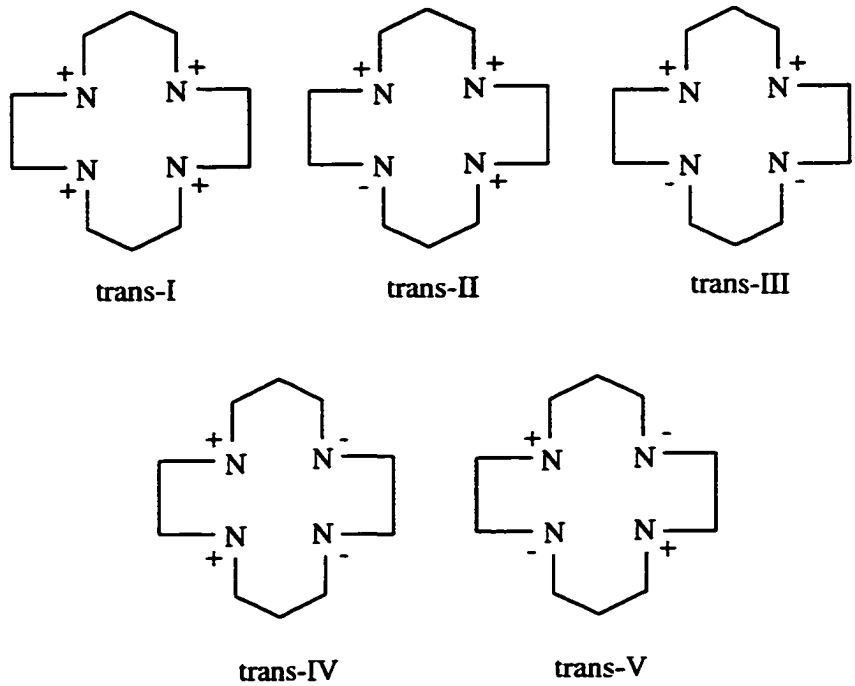

Figure 3.13 Possible ring conformations of cyclam.

For the bicyclic ligands, the presence of the fused 9-member ring forces both substituents on one of the 5-member chelate rings to be on the same side of the macrocycle, this means that conformers trans-III and trans-V are not possible. Of the remaining three possible conformers a molecular mechanics study[92] on cyclam itself has shown that the trans-I form has the lowest relative strain energy. The crystal structure of the copper complex of the bicyloN$_5$ enamine complex described in Section 3.6.1 (Figure 3.9) shows that this complex does indeed adopt the trans-I configuration. If this is the preferred conformation of the bicyclic complex in solution, then reaction of this complex with a bridging ligand should favor the formation of the *syn* isomer of the tricyclic ligand. Here the apical donor nitrogens are found on the same side of the 14-member ring forming a macrocyclic ligand which can probably be best described as a "nest" for a coordinating transition metal ion. The possibility that the tricyclic ligand will adopt the trans-IV configuration can not be discounted. This would lead to the formation of the anti isomer of the tricyclic ligand.

Here, the apical donors are on opposite sides of the 14-member ring. This macrocyclic ligand would be described as a "vice" as it would hold a coordinating transition metal ion securely in an octahedral environment. Isolation of both of these isomers of the tricyclic ligand was deemed desirable as both would exhibit interesting coordination chemistry.

3.7.2 High Dilution Reactions

Attempts were made to link two [9]-aneN$_3$ molecules, each protected at one of the *N*-donor nitrogens by the triphenyl methyl protecting group, using the reagent malonyl dichloride. It was thought that two equivalents of this reactive electrophile could be readily added to [9]-aneN$_3$ at the two *N*-donor nitrogens available for reaction. This would lead to a diamide complex having the two propyl arms, each functionalized by a reactive acid chloride group. The presence of the amide group enhances the rigidity of the functional arms holding them in an orientation favorable to cyclisation when reacted with a second [9]-aneN$_3$ molecule. Perhaps the best analogy for this pre-orientation of the functional amide arms is to compare them to the pincers of a crab.[93]

The reaction sequence is shown in Scheme 3.6. An excess amount of malonyl dichloride was reacted with triphenyl methyl [9]-aneN$_3$ in dry chloroform containing Li_2CO_3. The undissolved material was filtered off and the solvent and excess malonyl dichloride were removed under reduced pressure. This material was immediately reacted with 2 equivalents of *N*-trityl-[9]-aneN$_3$ in 2 L of dry chloroform. High dilution conditions were used to enhance the desired cyclisation reaction and minimize unwanted side reactions. The experimental apparatus used for the high dilution reactions is described in Section 2.3.6.2. Two equivalents of monoprotected nonane reagent were added to allow for the fact that H^+ was being generated by the reaction. Half of the monoprotected nonane would act as a base to mop up the H^+ ions. Once the amines of the macrocycle ring

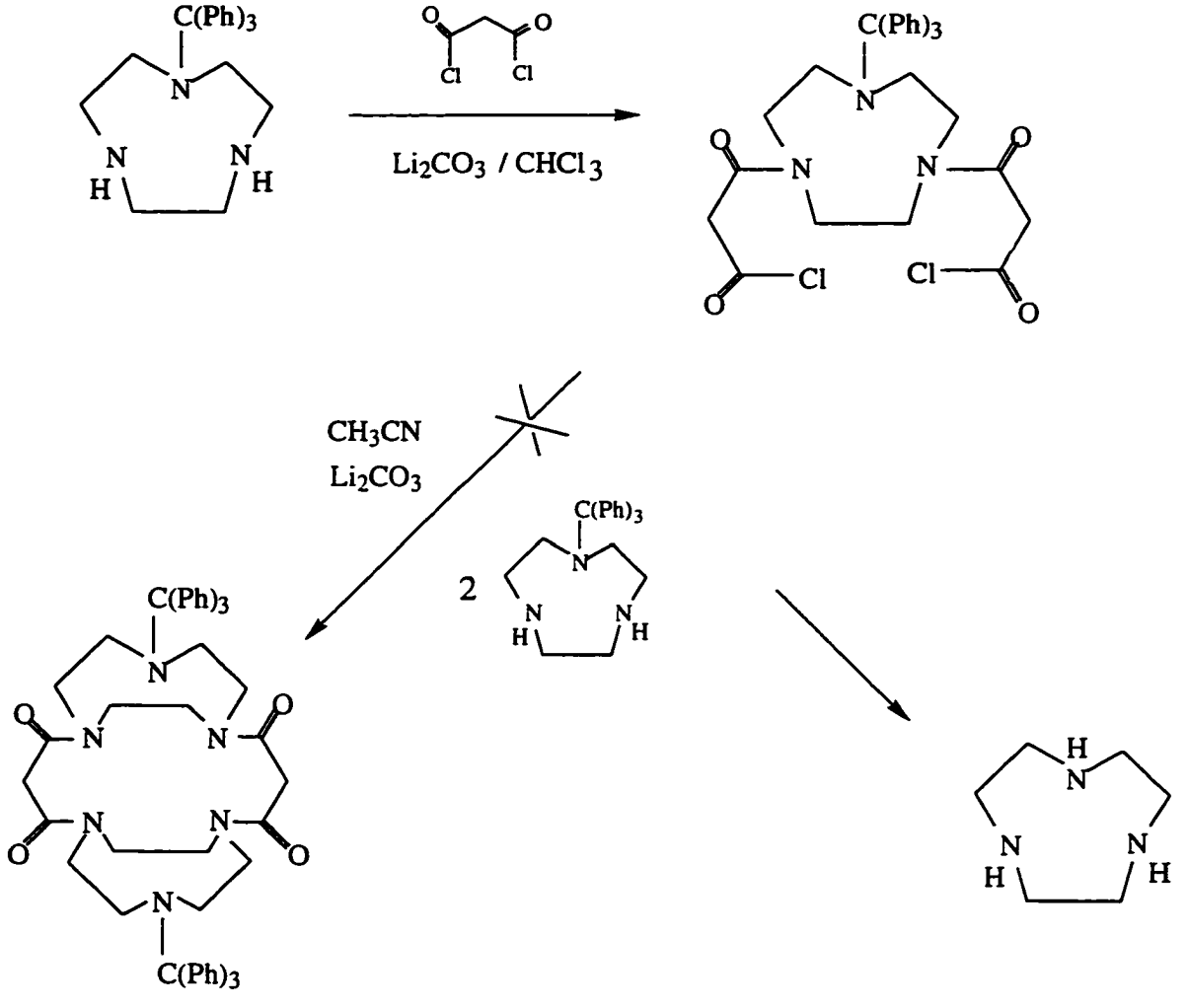

Scheme 3.6 High dilution coupling reaction of *N*-trityl-[9]-aneN_3 using malonyl dichloride.

become protonated, they are incapable of reacting. After 12 hours of vigorous stirring a white precipitate had formed which was filtered off and dried. The ^{13}C NMR spectrum of this material showed the presence of both methylene (CH_2) and amide ($R_2N(CO)R$) carbons. The mass spectrum did not correspond to the predicted molecular weight of the tricyclic tetra amide product. Attempts to reduce this material to the fully saturated molecule using BH_3.THF were unsuccessful, and the amide peaks were still observed in the ^{13}C NMR. Evaporation of the filtrate from this reaction gave a yellow oil which ^{13}C NMR showed to contain both de-protected [9]-aneN_3 and the free triphenyl methyl protecting group. It was apparent that the trityl protecting group was not robust enough to withstand the reaction conditions used. Hydrolysis of the acid chloride arms prior to the high dilution reaction likely resulted in sufficiently acidic conditions to cleave the trityl protecting group. This would explain why the desired tricyclic reaction product was not isolated.

This coupling strategy was repeated using the *N*-formyl-[9]-aneN_3 and *N*-benzyl-[9]-aneN_3 derivatives as starting materials. It was thought that the formyl and benzyl groups would provide suitable protection for the donor nitrogen of the macrocyclic ring and be much more stable to acid, and harder to displace than the trityl protecting group, and therefore should have a much better chance of withstanding the reaction conditions. The compound *N*-formyl [9]-aneN_3 was reacted with an excess of the reagent 3-chloro propionyl chloride in the presence of K_2CO_3 in dichloromethane. This resulted in the addition of two functional arms to the nonane ring (Scheme 3.7). The identity of this material was verified by ^{13}C NMR and mass spectroscopy (CI). In this case, the formyl group was found to withstand these reaction conditions and was left unaffected. Using chloro propionyl chloride rather than malonyl dichloride was found to have two advantages: first, the problem of hydrolysis of the acid chloride functional arms (when malonyl dichloride is used) would be eliminated and this would allow for the isolation and characterization of the bi-functional ligand to make sure that the protecting group had not

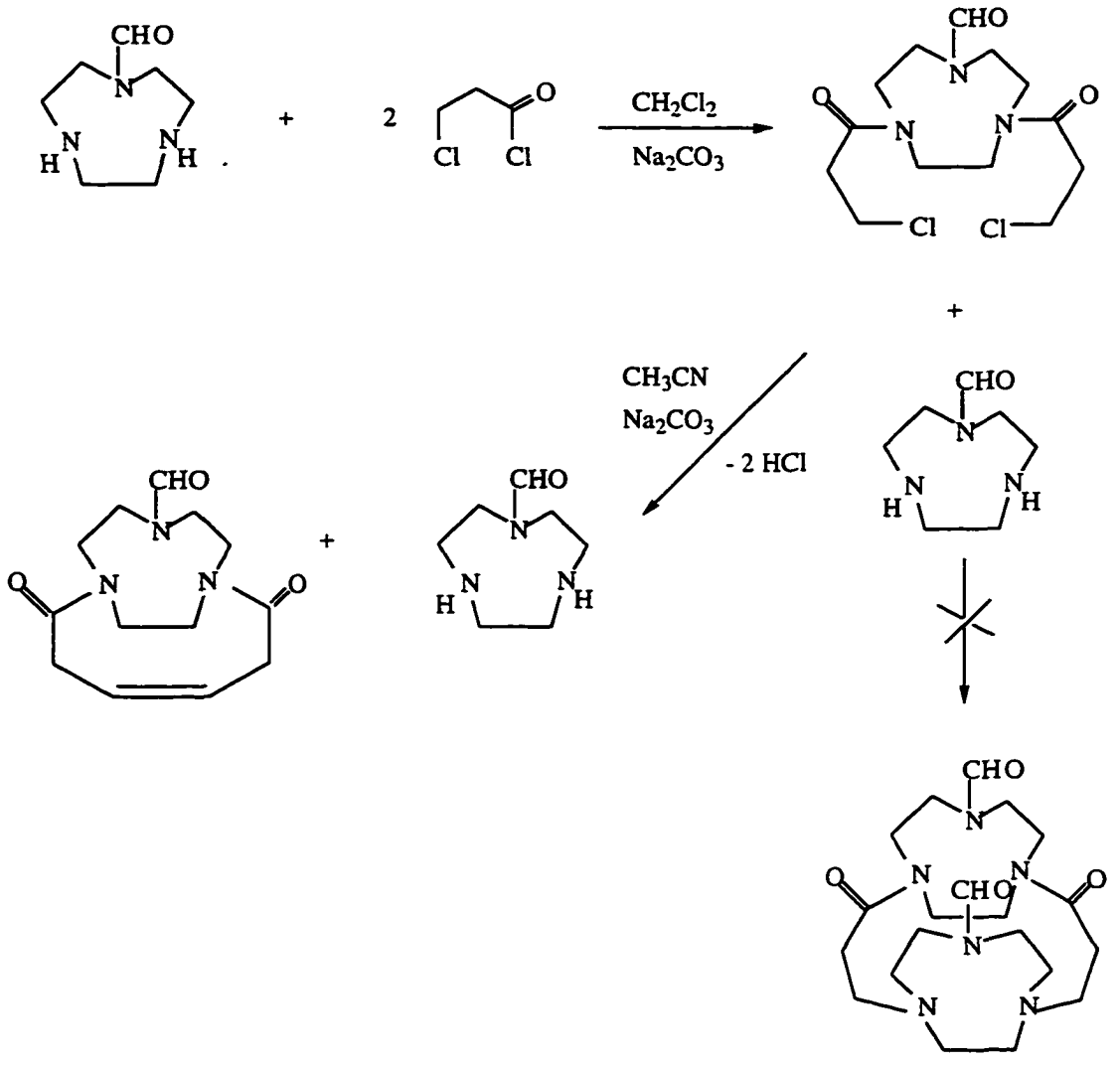

Scheme 3.7 High dilution coupling reaction of *N*-formyl-[9]-aneN_3 using 3-chloro propionyl chloride.

been removed prior to the high dilution reaction; second, the tricyclic product formed would contain only two amide groups, making it easier to be reduced to the saturated macrocycle. The same reaction was carried out on the *N*-benzyl-[9]-aneN_3 derivative to give its bi-functionalized product (Figure 3.14). The benzyl protecting group remained attached and was found to be resilient to these reaction conditions.

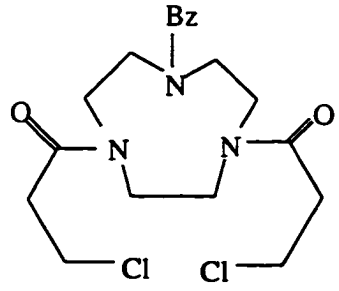

Figure 3.14 Product of the reaction of *N*-benzyl-[9]-aneN_3 with chloropropionyl chloride.

The bi-functional [9]-aneN_3 molecule having two propyl chloro amide arms was reacted with a second *N*-formyl [9]-aneN_3 molecule in dry CH_3CN (2.5 L) containing Na_2CO_3, under high dilution conditions. Bradshaw[93] has shown that bis α-chloro amide electrophiles can react efficiently with amines to form cyclized products. This type of reaction has been used successfully within our group to form the bicyclic isomer [10]-aneN_4O from the reaction of [10]-aneN_2O and *N,N'*-bis(α-chloro amido) diamino propane.[94,95] It was hoped that the electrophile used in this reaction, the bi-functional [9]-aneN_3 molecule (having an additional carbon in the functional arm), would react in a similar fashion. After filtering off the Na_2CO_3 and reducing the volume of the reaction mixture a solid white precipitate was filtered off and collected. This material was identified as the self condensed reaction product. Here, the two functional arms have reacted in an intramolecular fashion to ring-close and form a bicyclic complex which consists of a nine-member ring fused to a ten-member ring containing a double bond (Figure 3.15).

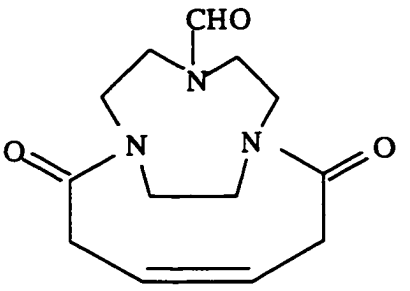

Figure 3.15 Self-condensed reaction product obtained from high dilution coupling reaction.

This type of internal cyclisation has been observed with compounds containing bis α-chloro amide arms.[96] The desired tricyclic reaction product was not detected or isolated from this reaction. For this reason this coupling reaction was not attempted using the *N*-benzyl-[9]-aneN_3 derivative and a different approach was used instead.

In the alternate strategy, (reaction b, scheme 3.5) the tricyclic ligand is formed from the protected bicyclic ligand Bz-bicycloN_5 using an appropriate bridging ligand. Since the benzyl protecting group attached to the bicyclic ligand ensures that there are only two nitrogens available for reaction, the tricyclic ligand should be the favored product. This reaction was carried out in high dilution conditions in order to minimize the chance that the bridging ligand link two Bz-bicycloN_5 molecules forming unwanted side products. This synthetic route has the advantage that the tricyclic ligand formed contains no amide groups and therefore no reduction step is required. Only the removal of the benzyl protecting groups would be required.

The bridging ligand was synthesized from diethanolamine by the reaction sequence shown in Scheme 3.8a. The central nitrogen of the bridging ligand was protected with a benzyl protecting group to ensure that no reaction occurred at this atom in the high dilution reaction. The two OH groups were replaced via the di-tosylate to form the di-bromide and

the di-iodide ligands. Iodide is a better leaving group than bromide and should provide the best chance of success for the reaction, for this reason the di-iodo bridging ligand (*N*-benzyl-2,2'-diiodo-iminodiethane) was used (Figure 3.16).

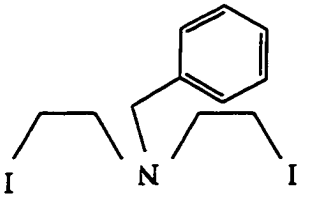

Figure 3.16 Bridging ligand.

The reaction of Bz-bicycloN$_5$ and this bridging ligand was carried out in acetonitrile in high-dilution in the presence of the base Na_2CO_3 (Scheme 3.8b). Optimum yields have been reported in the cyclisation of bi-functional iodides with bi-functional amines, when the base sodium carbonate is used in acetonitrile.[96,97] After filtering off the Na_2CO_3 and removing the solvent from the reaction mixture, a solid white material remained. ^{13}C NMR showed this material to contain both bridging ligand and Bz-bicycloN$_5$. $NiCl_2.6H_2O$ was added to this material in methanol so that the reaction products could be isolated as their metal complexes on a Sephadex column. The yellow-green solution was seen to separate into two bands on the Sephadex column and both these fractions were collected. The first band, the major component, was evaporated to give a pink material. This was identified by FAB mass spectroscopy as the nickel complex of the unreacted bicyclic ligand [Ni(Bz-bicycloN$_5$)]Cl_2. The second band, the minor component, was evaporated to give a yellow-green material. This material was found to have the correct molecular weight, by FAB mass spectroscopy, for the nickel complex of the expected tricyclic reaction product: [Ni((Bz)$_2$-tricycloN$_6$)]Cl_2, ([Ni(L)(Cl^-)]$^+$: 613 g/mole). Subsequent elemental analysis of this material was also indicative of the tricyclic reaction product:

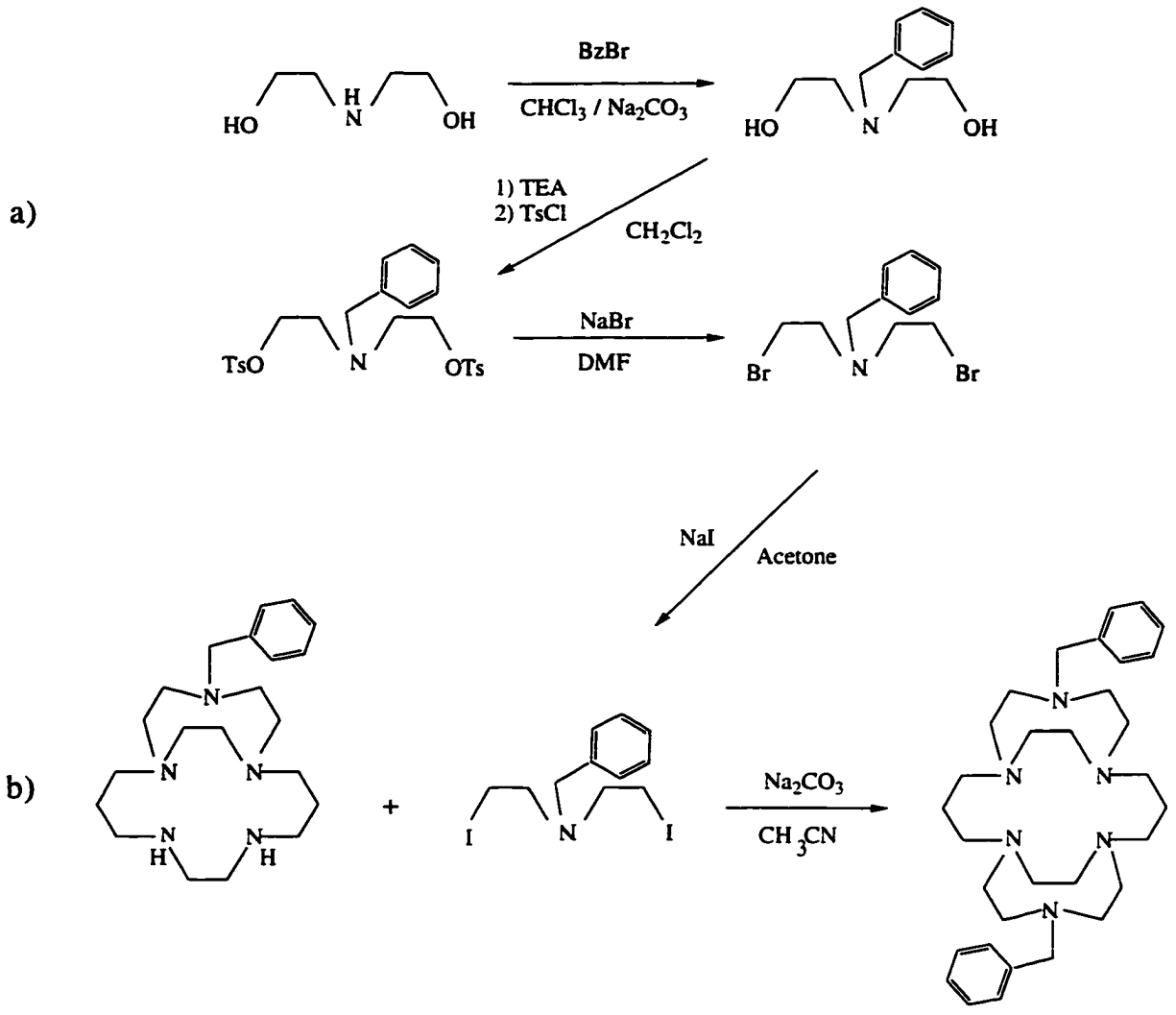

Scheme 3.8 a) Formation of the bridging ligand. b) High dilution reaction of bridging ligand with Bz-bicycloN$_5$ in Na_2CO_3/CH_3CN.

$[Ni(C_{32}H_{50}N_6)]Cl_2$, (calculated (%): C: 59.29; H: 7.72; N: 12.97; Found (%): C: 59.31; H: 7.56; N: 13.11). Unfortunately very little of this material was obtained (~10 mg) and this would not allow for removal of the metal to record the ^{13}C NMR of the free tricyclic ligand. The possibility exists that this material is a mixture of the *syn* and *anti* isomers of the tricyclic ligand, and that these isomers were unresolved on the Sephadex column. Alternatively, it is possible that the isomers were resolved on the column but due to the small amounts of material obtained only one isomer was detected. The *anti* isomer, which provides an octahedral environment for the nickel, might be expected to have a lower molar absorptivity than the *syn* isomer and may be harder to detect visually on the column. There is also the possibility that only one isomer was preferentially formed from the bridging reaction.

3.8 De-protection

Removal of the *N*-benzyl protecting group from the ligand Bz-daptacn was attempted by stirring a methanol solution containing the ligand and an excess amount of a palladium catalyst on activated charcoal (10% Pd-C), at room temperature under an atmosphere of H_2 (50 psi) (Scheme 3.9a). Even after 4 days it was found that the benzyl protecting group was left unaffected. This result is consistent with reports that the cleavage of benzylamines using H_2/Pd-C is often very slow.[98] An alternate method for cleavage of the benzyl group has been developed which involves catalytic transfer hydrogenation with formic acid. Here formic acid is used as the hydrogen donor instead of H_2.[99] Stirring the Bz-daptacn ligand in a methanol solution containing 4.4 % CHOOH and an excess of 10% Pd-C catalyst at room temperature, overnight, did indeed result in the clean removal of the benzyl protecting group. The yield of daptacn was 55% for this step. This reaction was also used to de-protect the macrobicyclic ligand Bz-bicycloN$_5$ (Scheme 3.9b). The clean

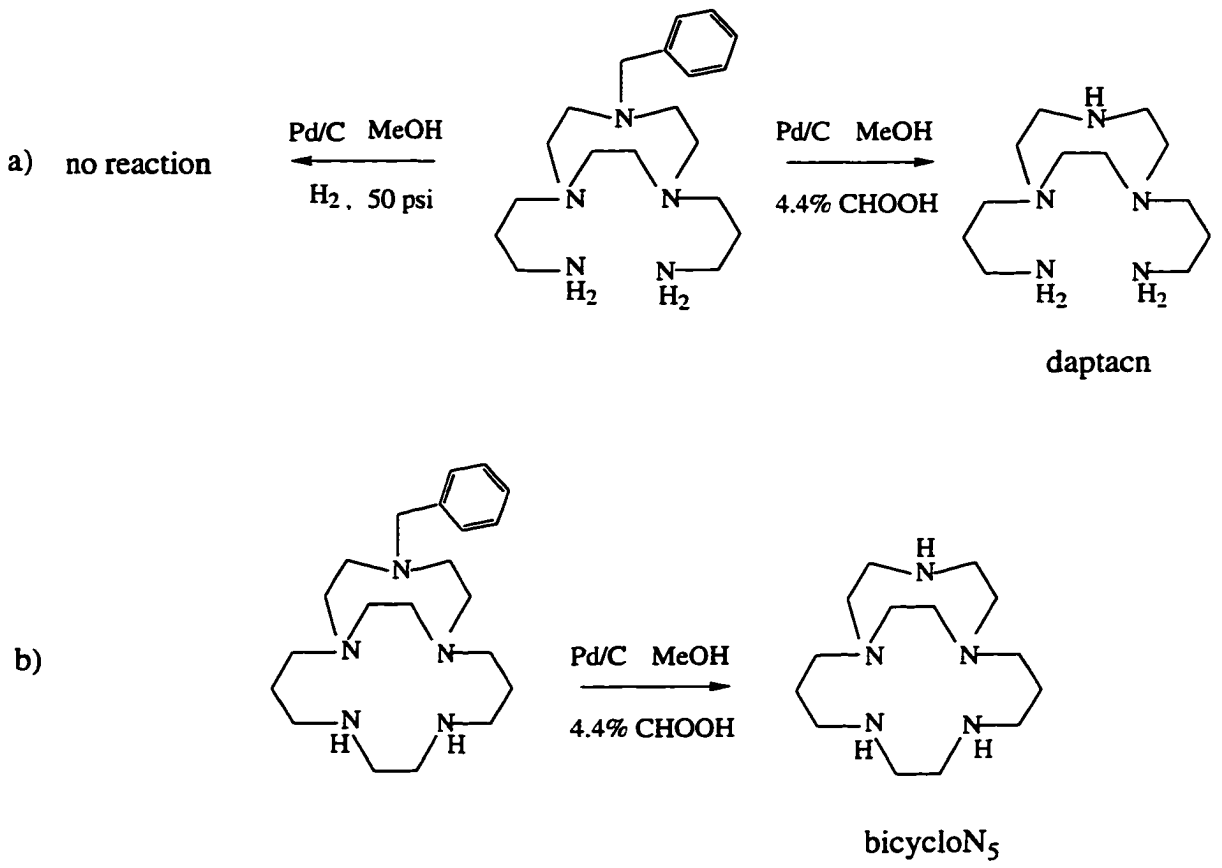

Scheme 3.9 The de-protection of a) Bz-daptacn and b) Bz-bicycloN$_5$.

bicycloN$_5$ product was obtained with a yield of 99% for this step. The ^{13}C NMR chemical shifts observed for this complex are given in Table 3.4. Unfortunately, there was too little of the tricyclic reaction product to remove the nickel and attempt to de-protect the free macrotricyclic ligand.

3.9 Conclusions

The macrocyclic ligand 1,4,7-triazacyclononane can be efficiently mono protected using a procedure which involves the formation an orthoamide intermediate. The same procedure could not be used to form the corresponding mono protected derivative of the ten member ring [10]-aneN$_3$. Reaction of the *N*-formyl, *N*-methyl and *N*-benzyl derivatives of nonane, obtained by this procedure, resulted in the bi-functionalization of nonane through the addition of two pendant arms. The bicyclic complexes Cu(Me-bicycloN$_5$)$^{2+}$ and Cu(Bz-bicycloN$_5$)$^{2+}$ were formed from the ring closure reaction of Cu(Me-daptacn)$^{2+}$ and Cu(Bz-daptacn)$^{2+}$ with glyoxal. The nickel complexes of these bicyclic ligands, Ni(Me-bicycloN$_5$)$^{2+}$ and Ni(Bz-bicycloN$_5$)$^{2+}$, were prepared and exhibited similar abilities to stabilize Ni(III) as the parent bicyclic complex Ni(bicycloN$_5$)$^{2+}$. Attempts to couple two [9]aneN$_3$ units through the functional arms to form the macro tricyclic ligand were unsuccessful. Reaction of Bz-bicycloN$_5$ with a bridging ligand showed limited success, forming the target tricyclic product tricyclo[9-14-9]N$_6$ in low yield (~ 10 mg).

CHAPTER FOUR

QUENCHING OF THE EXCITED STATE OF $^3Pt_2(pop)_4^{4-}$ By Ni(II) MACROCYCLIC COMPLEXES

4.1 Introduction

In this chapter the ability of a macrocyclic ligand to stabilize a less common oxidation state of a transition metal, in this case Ni(III), is utilized in the study of a series of photoinduced electron transfer reactions.

The well known diplatinum(II) complex $K_4Pt_2(\mu\text{-}P_2O_5H_2)_4$, more commonly referred to as *platinum pop*, and abbreviated as $Pt_2(pop)_4^{4-}$ has become an important tool used by the inorganic photochemist. Since its discovery[100,96] the unique photochemical and photophysical properties of this complex have made it very useful in the study of photoinduced electron transfer reactions, both oxidative[101] and reductive[102] in nature, as well as in the study of excited state atom transfer processes.[103] Other studies in our laboratory have looked at the salt effects and specific cation effects in the quenching of $^*Pt_2(pop)_4^{4-}$ by a series of acidopentacycanocobalt(III) complexes and found evidence for both oxidative electron transfer and atom transfer mechanisms.[104]

Until now, all of the examples of bimolecular reductive quenching of the excited state of $Pt_2(pop)_4^{4-}$ have been limited to reactions with organic amines. It was thought that the Ni(II) macrobicyclic complexes described in Chapter 3 might interact with the excited state of $Pt_2(pop)_4^{4-}$ to provide the first example of reductive quenching of $^*Pt_2(pop)_4^{4-}$ by a transition metal coordination complex. It was predicted that the macrocyclic complex would reductively quench the $Pt_2(pop)_4^{4-}$ excited state and that the macrocyclic ligand would stabilize the Ni(III) quenching product long enough to be observed by conventional spectroscopic techniques. It was hoped that by extending the quenching study to include a series of related Ni(II) complexes having varying $Ni^{III/II}$ reduction potentials both the kinetic and thermodynamic aspects of the quenching process could be investigated.

4.2 Properties of the $Pt_2(pop)_4^{4-}$ Ion

The lantern-type structure of $Pt_2(pop)_4^{4-}$ involves two planar d^8-d^8 platinum(II) metal centers bridged by four μ-$P_2O_5H_2^{2-}$ groups as shown in Figure 4.1. The electronic absorption spectrum (Figure 4.3) of the $Pt_2(pop)_4^{4-}$ complex in aqueous solution has absorption bands at λ_{max}, nm (ε, M^{-1} cm^{-1}): 368 ($3.4x10^4$) and 453 (115) which have been assigned to the singlet (allowed) $^1A_{1g} \rightarrow {}^1A_{2u}$ transition and the triplet (spin forbidden) $^1A_{1g} \rightarrow {}^3A_{2u}$ transition, respectively.[105,106.101,102] Excitation of a room temperature aqueous solution of $Pt_2(pop)_4^{4-}$ at 370 nm results in an intense green emission at 514 nm which originates from the triplet $^3A_{2u}$ excited state and has a rather long lifetime ($\tau \geq 9$ μs in aqueous solution at 22.0 °C). It is because of its long lifetime at ambient temperature and high quantum yield of formation ($\emptyset$ = 1.0) that the triplet excited state of $Pt_2(pop)_4^{4-}$ is a useful chemical reagent for the study of bimolecular quenching reactions. A feature of these excited states is that the transfer of an electron from a $1a_{2u}$ antibonding (d_z^2, σ^*) orbital to a $2a_{1g}$ bonding (p_z, σ) orbital results in a net increase of intermetallic bond order between the two platinum metal centers.

The $^3A_{2u}$ excited state is both a strong one electron reductant and a strong one electron oxidant. From the energy diagram shown in Figure 4.2 it is apparent that the triplet excited state has an excited electron in the $2a_{1g}$ orbital which can easily be removed by an oxidant. The triplet excited state also has a vacancy in the $1a_{2u}$ orbital that can readily accept a single electron from an appropriate reductant. The excited state potentials for $^*Pt_2(pop)_4^{4-}$ have been obtained from its reactions with added oxidants and reductants, measured versus a saturated calomel electrode (SCE), and are given in Figure 4.4.[103]

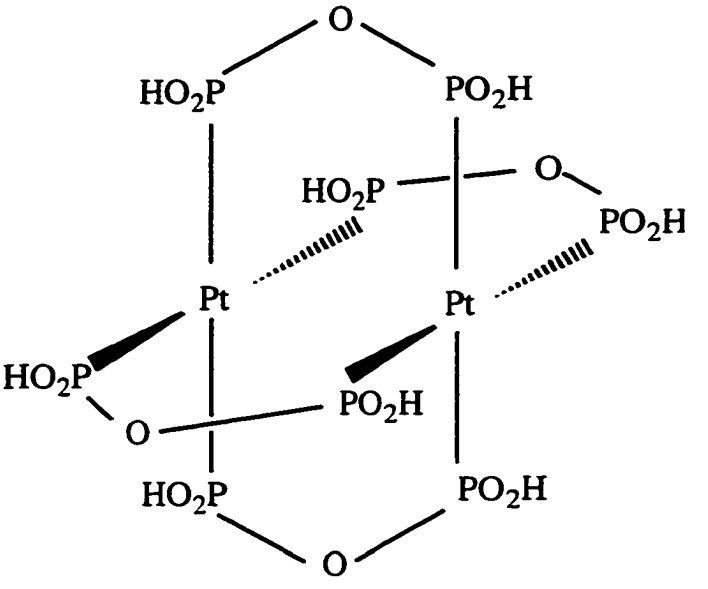

Figure 4.1 Diagram of $Pt_2(pop)_4^{4-}$ structure.

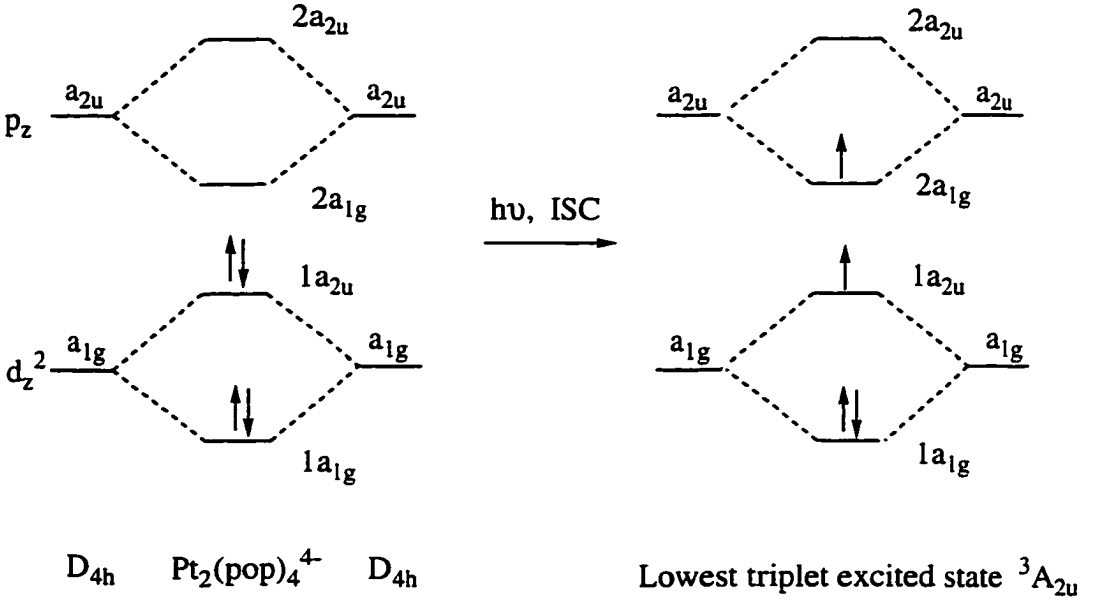

Figure 4.2 Energy level diagram of the ground state and triplet state of $Pt_2(pop)_4^{4-}$.

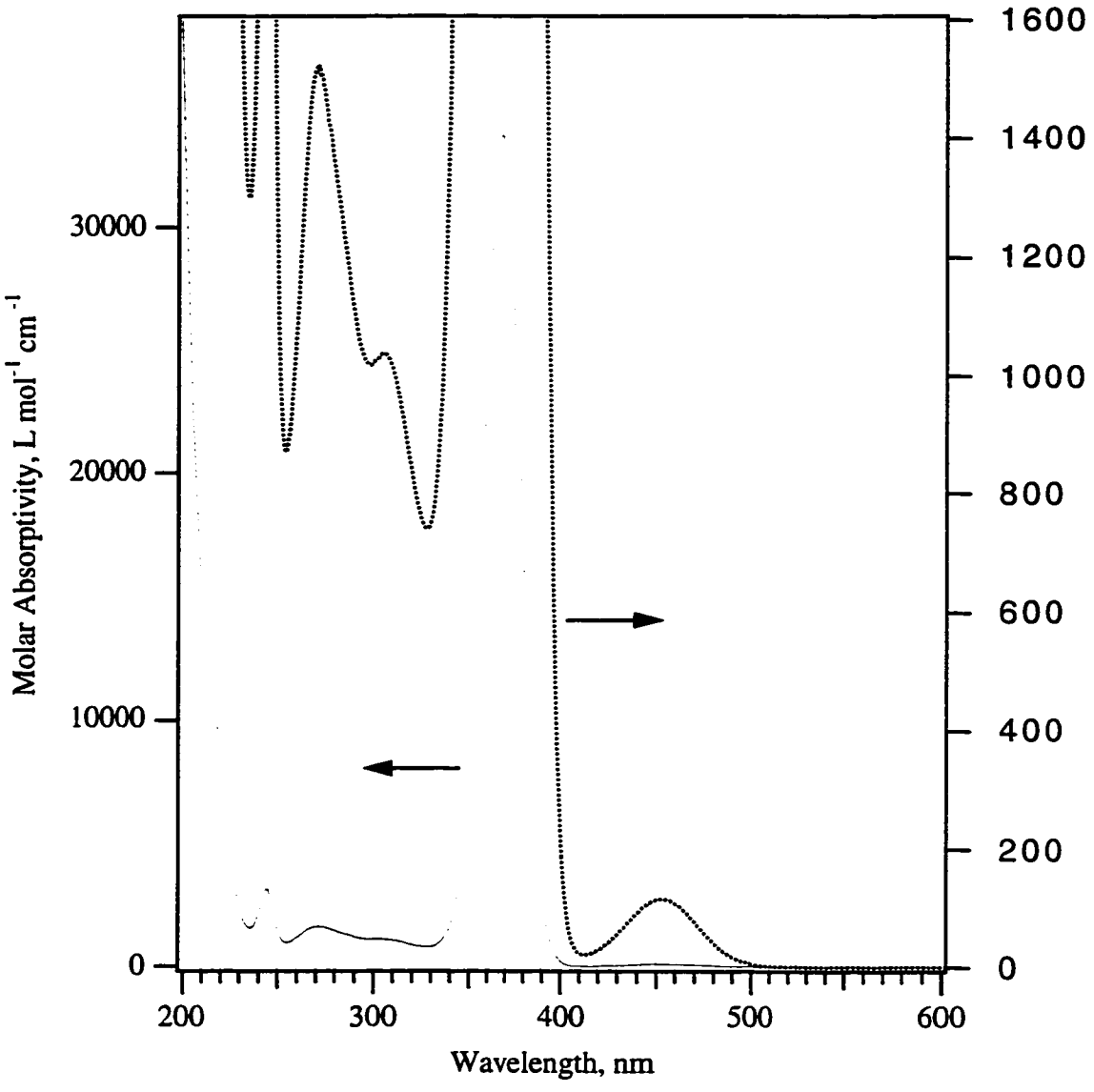

Figure 4.3 Electronic absorption spectra of $Pt_2(pop)_4^{4-}$ in aqueous solution.

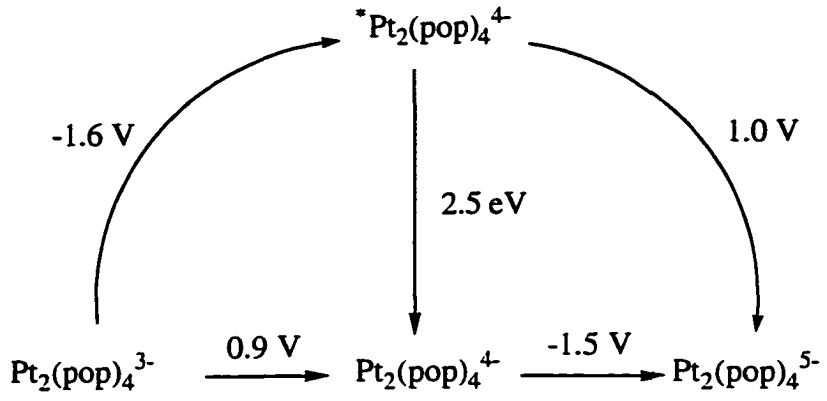

Figure 4.4 Excited state potentials for $Pt_2(pop)_4^{4-}$ (vs SCE).

4.3 Ni(II) Complexes Used to study the quenching of $*Pt_2(pop)_4^{4-}$

The Ni(II) complexes used to study the bimolecular quenching of $*Pt_2(pop)_4^{4-}$ included two of the bicyclic complexes described in Chapter 3: $[Ni(bicycloN_5)](ClO_4)_2$, $[Ni(Bz\text{-}bicycloN_5)](ClO_4)_2$. Four additional Ni(II) macrocyclic complexes were also used: The bicyclic ligand $[Ni(bicycloN_4O)](ClO_4)_2$ (16), which has an oxygen in place of a nitrogen at the apical donor site,[107] was kindly provided by Dr T. Rodopoulous. Samples of the complexes $[Ni(cyclam)](ClO_4)_2$ (17), $[Ni(cyclam\text{-}diene\text{-}Me_2)](ClO_4)_2$ (18), and $[Ni(TIM)](ClO_4)_2$ (19) (where cyclam-diene-Me_2 = Me_2[14]4,7-dieneN_4, and TIM = Me_4[14]1,3,8,10-tetraeneN_4) were prepared by their published literature procedures[108-110] and provided by other members of our group. The structures of these ligands are shown in Figure 4.5.

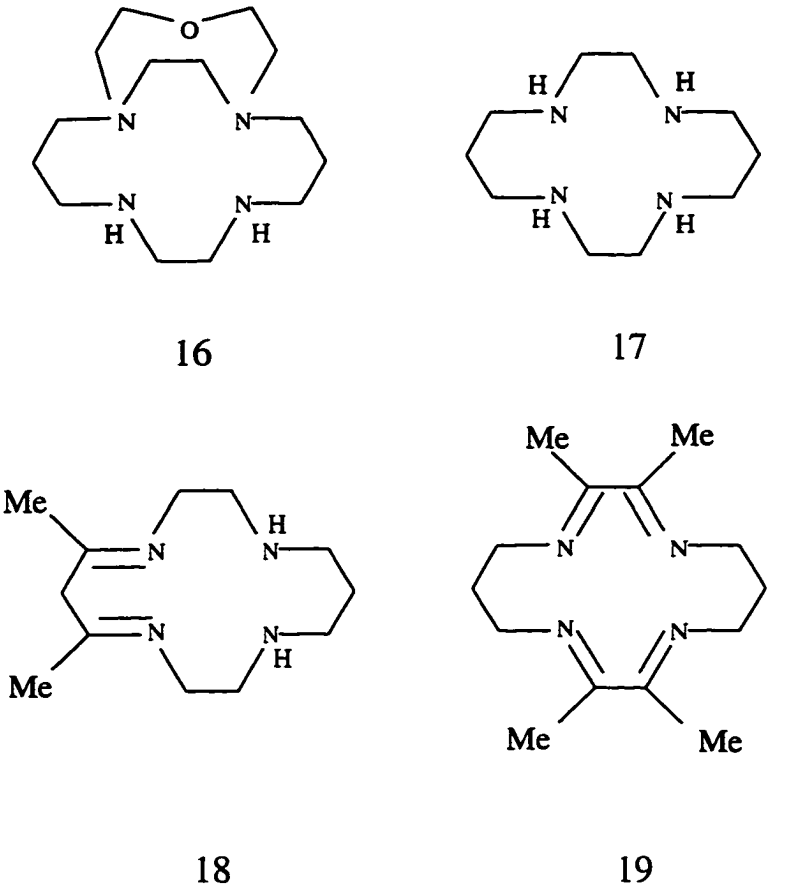

Figure 4.5 Structures of Ni(II) complexes used to quench the excited state $^*Pt_2(pop)_4^{4-}$.

In addition to these macrocyclic Ni(II) complexes, a series of substituted Ni(II) tris phenanthroline and tris bipyridyl complexes were also prepared. This included: $Ni(phen)_3^{2+}$, $Ni(4,4'\text{-}Me_2\text{-}bipy)_3^{2+}$, $Ni(5\text{-}Cl\text{-}phen)_3^{2+}$, and $Ni(5\text{-}NO_2\text{-}phen)_3^{2+}$ (where phen = 1,10-phenanthroline, and bipy = 2,2'-bipyridyl).

The redox potentials of each of these Ni(II) complexes has been measured using cyclic voltammetry and Table 4.1 lists the values of the $Ni^{III/II}$ reduction potentials (vs NHE). All together, these ten Ni(II) complexes provide different reduction potentials which span a range of almost 1.3 V, from 0.55 V to 1.82 V.

Table 4.1 Electrochemical data: $Ni^{III/II}$ reduction potentials of complexes used in the quenching study of $^*Pt_2(pop)_4^{4-}$.

Ni(II) Complex	E°, V (vs NHE)	Reference
$Ni(cyclam\text{-}diene\text{-}Me_2)^{2+}$	0.55	111
$Ni(cyclam)^{2+}$	0.98	112
$Ni(bicycloN_5)^{2+}$	1.03	86
$Ni(bicycloN_4O)^{2+}$	1.17	113
$Ni(Bz\text{-}bicycloN_5)^{2+}$	1.18	this work
$Ni(TIM)^{2+}$	1.31	111
$Ni(4,4'\text{-}Me_2\text{-}bipy)_3^{2+}$	1.51	80
$Ni(phen)_3^{2+}$	1.64	80
$Ni(5\text{-}Cl\text{-}phen)_3^{2+}$	1.75	80
$Ni(5\text{-}NO_2\text{-}phen)_3^{2+}$	1.82	80

4.4 Results

4.4.1 Quenching Rate Constants

Quenching experiments were carried out in 0.010 M $HClO_4$ media with solutions having $A_{370} \approx 1$ and $Pt_2(pop)_4^{4-} \approx 3 \times 10^{-5}$ M. No self-quenching of the phosphorescence was observed under these conditions, consistent with the report by Kalyanasundaram[114] that no self-quenching occurs when the concentration of $Pt_2(pop)_4^{4-}$ is less than 1×10^{-4} M. Under these acidic conditions more than 90% of the platinum pop exists as the undissociated (or protonated) 4- anion (pK_a values of: $pK_{a1} = 3.0$, $pK_{a2} = 8.0$ have been reported for $Pt_2(pop)_4^{4-}$).

In a thoroughly degassed solution, and in the absence of any quencher, the lifetime of $Pt_2(pop)_4^{4-}$ was found to be in the range of 9 μs, which is in good agreement with the literature value.[82,105,115] The addition of aliquots (5 - 20 μL) of a solution containing the Ni(II)-complex quencher (~ 1×10^{-3} M in 0.01 M $HClO_4$) resulted in a decrease in the measured lifetime. According to the Stern-Volmer equation (SV) (Section 1.6.3, eq. 1.12) the quenching rate constant k_q can be calculated by dividing the slope obtained from a SV plot of $^\circ\tau/\tau$ vs quencher concentration [Q] by the initial lifetime $^\circ\tau$. A typical SV plot obtained for this series of quenching experiments is shown in Figure 4.6 and in all cases good straight lines were observed from which k_q could be calculated. The second order rate constants k_q were measured for the quenching of the excited state of $Pt_2(pop)_4^{4-}$ by each of the ten Ni(II) complexes and were found to be in the range 10^{10} to 10^8 M^{-1} s^{-1}. The values of k_q are given in Table 4.2.

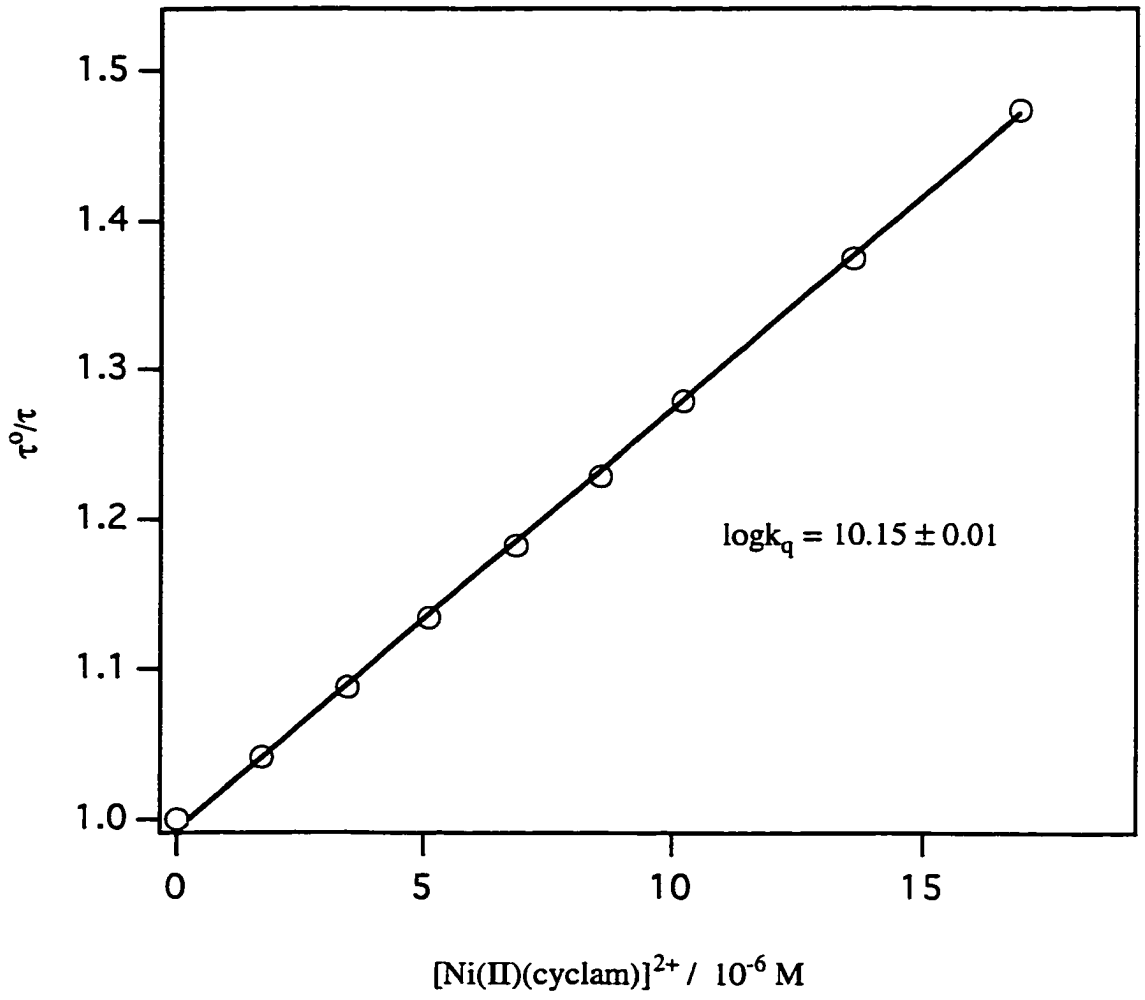

Figure 4.6 Typical Stern-Volmer plot: quenching of $^{*}Pt_2(pop)_4^{4-}$ by $Ni(cyclam)^{2+}$ in 0.01 M $HClO_4$ aqueous media: $\mu = 0.01$, $T = 22 \pm 1$ °C.

Table 4.2 Rate constants for the quenching of $^*Pt(pop)_4^{4-}$ by Ni(II) complexes: $\mu = 0.01$ M, T = 22 ± 1 °C.

Ni(II) Quencher	ΔG, eV	k_q, $M^{-1}s^{-1}$	k_q', $M^{-1}s^{-1}$ a)
$Ni(cyclam\text{-}diene\text{-}Me_2)^{2+}$	-0.97	$(1.48 \pm 0.03) \times 10^{10}$	$(3.70 \pm 0.05) \times 10^{11}$
$Ni(cyclam)^{2+}$	-0.54	$(1.41 \pm 0.03) \times 10^{10}$	$(1.66 \pm 0.05) \times 10^{11}$
$Ni(bicycloN_5)^{2+}$	-0.49	$(1.32 \pm 0.03) \times 10^{10}$	$(9.21 \pm 0.05) \times 10^{10}$
$Ni(bicycloN_4O)^{2+}$	-0.35	$(1.50 \pm 0.03) \times 10^{10}$	$(5.66 \pm 0.05) \times 10^{11}$
$Ni(Bz\text{-}bicycloN_5)^{2+}$	-0.34	$(1.23 \pm 0.03) \times 10^{10}$	$(6.10 \pm 0.05) \times 10^{10}$
$Ni(TIM)^{2+}$	-0.21	$(1.07 \pm 0.02) \times 10^{10}$	$(3.50 \pm 0.04) \times 10^{10}$
$Ni(4,4'\text{-}Me_2\text{-}bipy)_3^{2+}$	-0.01	$(2.95 \pm 0.07) \times 10^{9}$	$(3.65 \pm 0.08) \times 10^{9}$
$Ni(phen)_3^{2+}$	0.12	$(1.48 \pm 0.04) \times 10^{9}$	$(1.63 \pm 0.06) \times 10^{9}$
$Ni(5\text{-}Cl\text{-}phen)_3^{2+}$	0.23	$(1.05 \pm 0.03) \times 10^{9}$	$(1.12 \pm 0.08) \times 10^{9}$
$Ni(5\text{-}NO_2\text{-}phen)_3^{2+}$	0.30	$(5.89 \pm 0.10) \times 10^{8}$	$(6.11 \pm 0.11) \times 10^{8}$

a) Quenching rate constant corrected for diffusional effects.

The value of the bimolecular rate constant k_q was found to depend on the redox potential of the Ni(II) complex used to quench $^*Pt_2(pop)_4^{4-}$. Two distinct types of behavior can be observed: For the first five complexes listed in Table 4.2 the value of k_q does not vary significantly with the $Ni^{III/II}$ redox potential. These quenching rates are greater than 1×10^{10} M^{-1} s^{-1}, suggesting that these quenching reactions have reached a diffusion controlled limit. For the remaining five Ni(II) complexes listed in Table 4.2, the value of log k_q is found to decrease as the $Ni^{III/II}$ redox potential increases. The dependence of the quenching rate constant k_q on E° provides strong evidence that the quenching reaction is occurring by an electron transfer process.

4.4.2 UV-Visible Spectroscopic Studies

To identify the quenching products and establish the mechanism of the quenching reaction, ie. electron transfer versus energy transfer, changes in the UV-Vis absorption spectrum were monitored under conditions of steady state irradiation. A thoroughly dearated aqueous solution containing the nickel(II) complex $[Ni(cyclam)](ClO_4)_2$ (~1 x 10^{-4} M) and $Pt_2(pop)_4^{4-}$ (A_{370} ~ 1, 1 x 10^{-5} M) in 0.01 M $HClO_4$ and 0.1 M Na_2SO_4 was irradiated at λ = 370 nm for varying lengths of time. After each time interval the UV-Vis spectrum was immediately recorded. It has been shown that the addition of sulfate stabilizes the Ni(III) species through complex formation.[91] It was thought that the addition of sulfate here would stabilize the Ni(III) quenching product long enough to be observed for this quenching reaction. The difference spectra for the quenching reaction are shown in Figure 4.7. The notable features of this plot are the bleaching of the $Pt_2(pop)_4^{4-}$ absorption band at 370 nm and the corresponding growth of a band at 295 nm. The electronic spectra for $Ni(cyclam)(SO_4)^+$ in acetonitrile, obtained from literature,[116] shows two bands, one at 370 nm (ε = 6000 M^{-1} cm^{-1}) and the other at 295 nm (ε = 11000 M^{-1} cm^{-1}). Therefore, the band observed to develop at 295 nm was assigned to the formation of the quenching product $Ni(cyclam)SO_4^+$. This supports the conclusion that the quenching mechanism involves reductive quenching of the excited state of $Pt_2(pop)_4^{4-}$ by $Ni(cyclam)^{2+}$. The net reaction is expressed in equation 4.1:

$$Ni(cyclam)SO_4 + {}^*Pt_2(pop)_4^{4-} \rightarrow Ni(cyclam)SO_4^+ + Pt_2(pop)_4^{5-} \qquad (4.1)$$

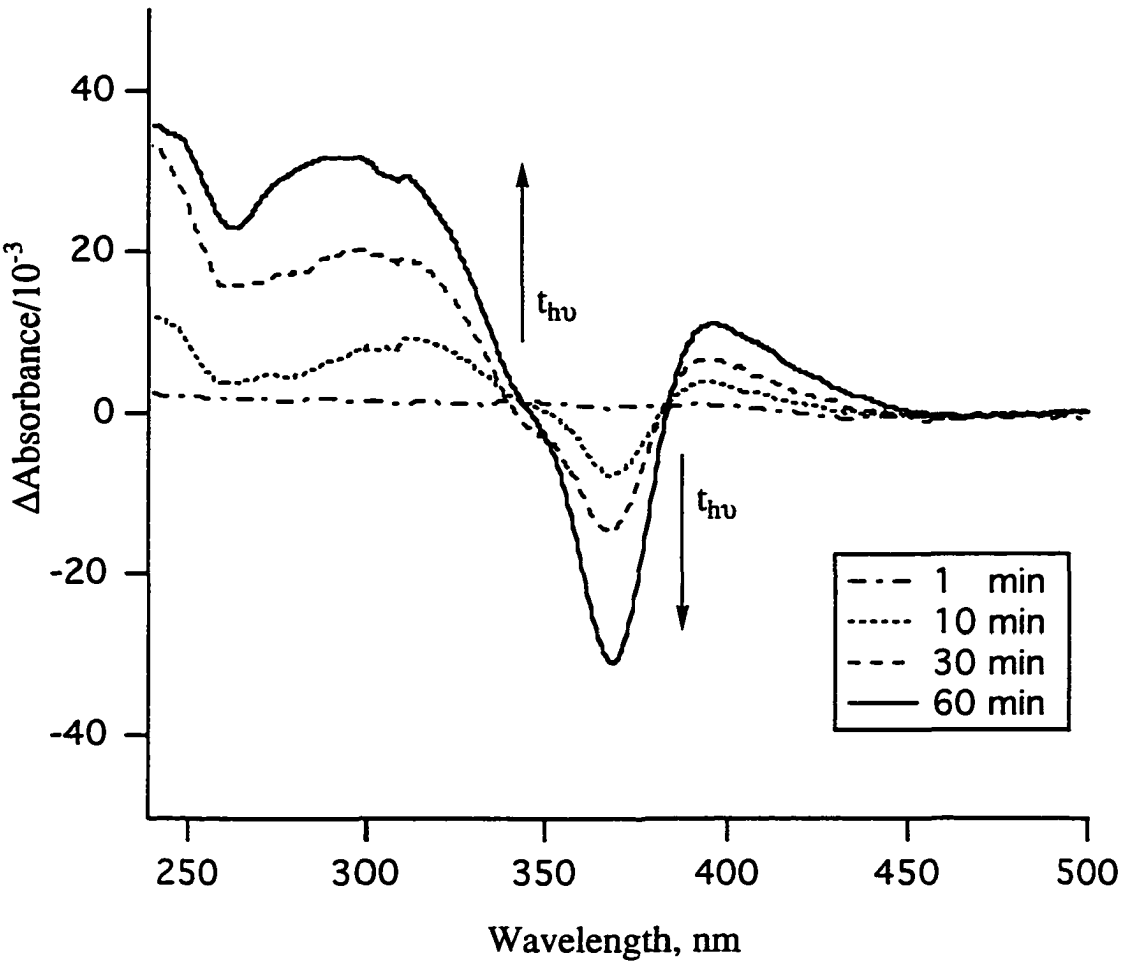

Figure 4.7 Absorbance changes for quenching of $^*Pt_2(pop)_4^{4-}$ by $Ni(cyclam)^{2+}$ in 0.1 M Na_2SO_4 and 0.010 M $HClO_4$ aqueous solution. $\lambda_{irrad.}$ = 370 nm. Irradiation time = 1, 10, 30, and 60 minutes, with N_2 stirring.

It was observed that when the identical quenching reaction between $^*Pt_2(pop)_4^{4-}$ and $Ni(cyclam)^{2+}$ was carried out in oxygenated solutions the change in absorbance at 295 nm (ΔA_{295}) was enhanced. Figure 4.8 shows the change in absorbance with increasing irradiation time for an aqueous 0.010 M $HClO_4$ solution mixed by O_2, instead of N_2, bubbling. The value of ΔA_{295} at 295 nm after 60 minutes of irradiation was found to be 0.032 in the deareated (N_2) solution, and 0.055 in the aerated (O_2) solution. This indicates that there is nearly a two-fold increase in the yield of the $Ni(cyclam)SO_4$ quenching product when oxygen is present in the solution. One likely explanation for this result is that the residual oxygen scavenges the reduced quenching product, $Pt_2(pop)_4^{5-}$, thus preventing it from reacting in a back electron transfer step to form $Ni(cyclam)SO_4^+$ and increasing the yield of the Ni(III) quenching product which is able to escape from the caged complex. Oxygen would be reduced to form O_2^- which, under these acidic conditions, would quickly lead to the formation of hydrogen peroxide (H_2O_2). This is shown in equation 4.2:

$$O_2 + Pt_2(pop)_4^{5-} \rightarrow O_2^- + Pt_2(pop)_4^{4-} \qquad (4.2)$$
$$O_2^- \ldots + H^+ \rightarrow H_2O_2$$

Assuming that no bulk recombination occurs, the quantum yield of product formation $\Phi_{product}$ can be expressed as :

$$\Phi_{product} = \Phi_{isc}\, \eta_q\, \eta_{ce} \qquad (4.3)$$

where is Φ_{isc} the intersystem crossing quantum yield, η_q is the quenching efficiency, and η_{ce} is the cage escape efficiency (Figure 1.10). For the quenching reaction of $^*Pt_2(pop)_4^{4-}$ (~ 1×10^{-5} M) and $Ni(cyclam)SO_4$ (~ 1×10^{-4} M), $\Phi_{product}$ was determined to be 2.8×10^{-4} in deaerated solution (0.01 M $HClO_4$) and 5.3×10^{-4} in aerated solution (the light

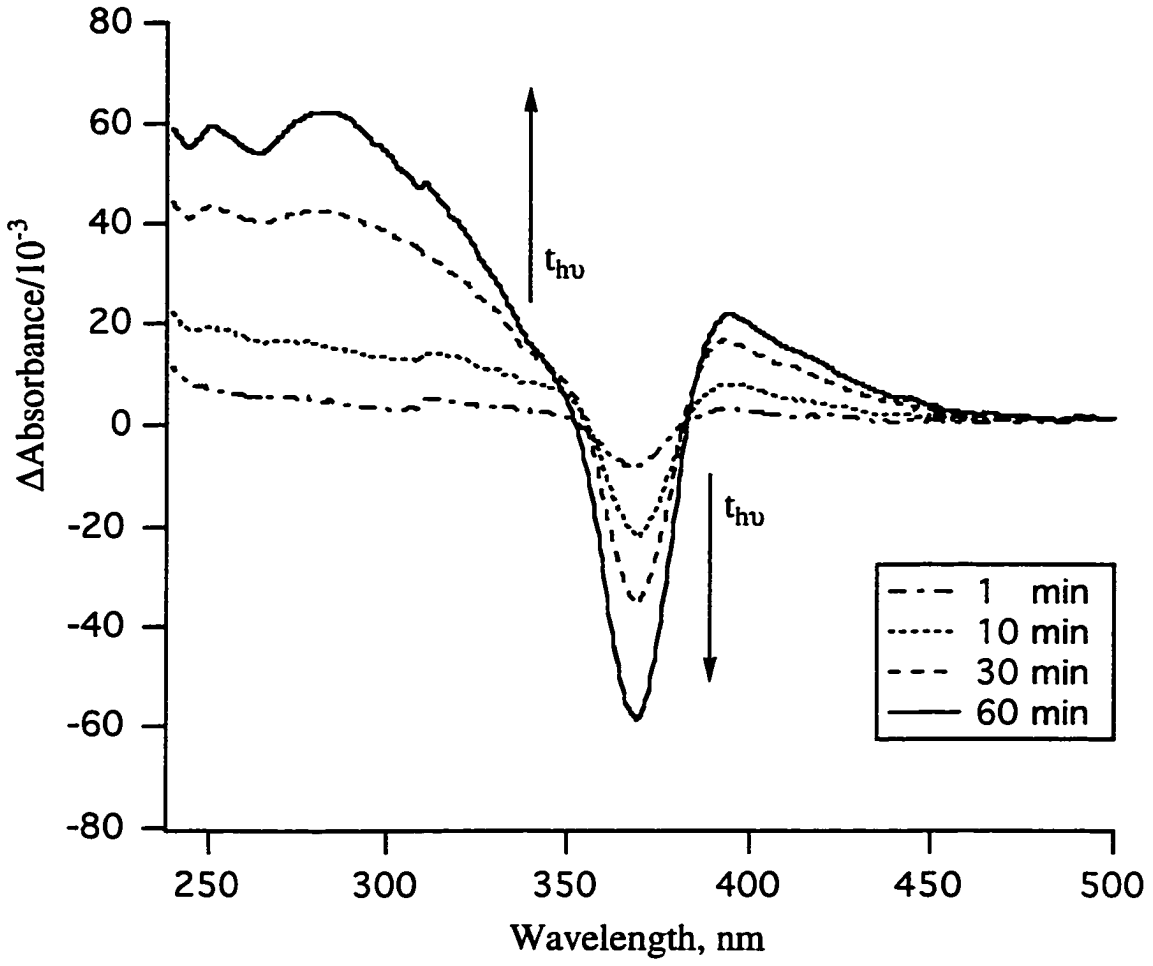

Figure 4.8 Absorbance changes for quenching of $^*Pt_2(pop)_4^{4-}$ by $Ni(cyclam)^{2+}$ in 0.1 M Na_2SO_4 and 0.010 M $HClO_4$ aqueous solution. $\lambda_{irrad.}$ = 370 nm. Irradiation time = 1, 10, 30, and 60 minutes, with O_2 stirring.

intensity I_o was determined by ferrioxalate actinometry). According to the literature,[117] the main $Pt_2(pop)_4^{4-}$ absorption is $^1A_{1g} \rightarrow {}^1A_{2u}$ which intersystem crosses to the corresponding triplet state $^3A_{2u}$ with a yield approaching unity, i.e. $\Phi_{isc} = 1.0$. Using the relationship shown in equation 4.4 the cage escape efficiency η_{ce} may be calculated.

$$\eta_{ce} = \frac{\Phi_{product}}{\Phi_{isc}\eta_q} = \Phi_{product}\frac{1 + k_q\tau^o[Q]}{k_q\tau^o[Q]} \qquad (4.4)$$

The cage escape efficiency η_{ce} was calculated to be 0.028 in the absence of oxygen, and 0.054 in the presence of oxygen. A cage escape efficiency of less than 1.0 can be attributed to the competing processes of back reaction, and quenching to the ground state. The low cage escape efficiency found for this quenching reaction is probably an indication of efficient back electron transfer within the {Pt..Ni} caged complex.

4.4.3 Laser Flash Photolysis Studies

It was thought that laser flash photolysis with transient absorption detection could provide further details about the quenching reaction. It might be possible to measure the back-electron transfer rate by following the disappearance of the Ni(III) quenching product on a very short time scale (< μs). Figure 4.9 shows the transient absorption changes seen after a 30 mJ, 355 nm laser flash excitation of $Pt_2(pop)_4^{4-}$ containing sufficient $Ni(cyclam)^{2+}$ to quench the emission lifetime by about 30% (~4 x 10^{-5} M) in 0.1 M Na_2SO_4 and 0.010 M $HClO_4$ degassed aqueous media. Immediately after the laser flash (4 μs) a decrease in the concentration of $Pt_2(pop)_4^{4-}$ was observed by the loss of absorbance at 370 nm. Associated with the bleaching of $Pt_2(pop)_4^{4-}$ was the formation of two new peaks at 325 nm and 460 nm. These absorbances can be assigned to the $^*Pt_2(pop)_4^{4-}$ $^3A_{2u}$ triplet excited state. After 17 μs the ΔAbsorbance at 460 nm had returned to the baseline

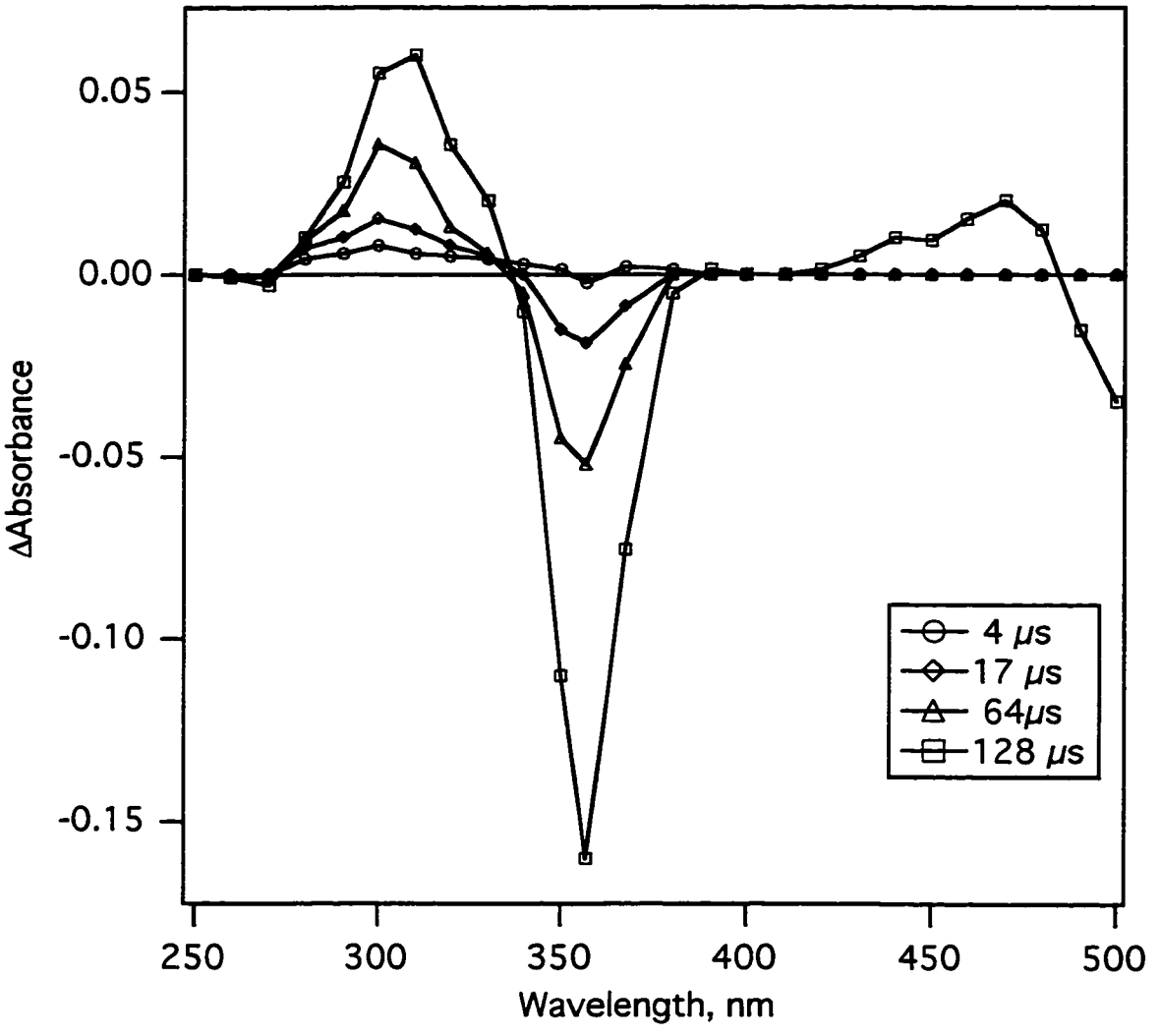

Figure 4.9 Transient (ΔAbsorbance) spectra for the laser flash photolysis (λ=355 nm), 30 mJ of a solution containing $Pt_2(pop)_4^{4-}$ and $Ni(cyclam)^{2+}$ in 0.1 M Na_2SO_4 and 0.010 M $HClO_4$ aqueous solution (deaerated).

indicating that the triplet $^*Pt_2(pop)_4^{4-}$ complex has disappeared. On this timescale there remains a transient absorbance signal with an absorbance maximum at 310 nm. This absorbance has been assigned to the oxidized platinum species $Pt_2(pop)_4^{3-}$.[82] Absorbance changes due to the expected quenching products $Ni(cyclam)SO_4^+$ (λ = 295, 370 nm) and $Pt_2(pop)_4^{5-}$ (λ = 420 nm) were not detected under these conditions. A summary of the absorbance maxima (λ) and molar absorptivities (ε) of these platinum species are given in Table 4.3.

The formation of the oxidized species $Pt_2(pop)_4^{3-}$ is consistent with a report by Che[118] that $Pt_2(pop)_4^{4-}$ readily undergoes photoionization leading to the formation of $Pt_2(pop)_4^{3-}$ and solvated electrons (e^-_{solv}). At a pulse energy of 30 mJ, photoionization would be the dominant process. Under the acidic conditions used, e^-_{solv} would rapidly produce hydrogen atoms (H) which, like e^-_{solv}, is also a strong reductant.

The interference caused by the photoionization of $Pt_2(pop)_4^{4-}$ is a significant difficulty in these flash photolysis experiments. There are two possible ways to alleviate this problem. One way would be to change the excitation wavelength from 355 nm to a region where $^3Pt_2(pop)_4^{4-}$ does not absorb as strongly, but unfortunately this was not an option. The other is to reduce the pulse energy used. In order to determine over what range photoionization had an effect, the transient absorbance (ΔA) of the $^*Pt_2(pop)_4^{4-}$ triplet excited state was monitored as a function of laser pulse energy. Figure 4.10 shows ΔA_{460} as a function of laser pulse energy over the range 0 $\rightarrow$ 50 mJ. A curve is obtained which was found to be linear up to a pulse energy of ~5 mJ and reached a maximum (saturation) at a pulse energy of ~20 mJ. This indicates that if interference by photoionization is to be avoided, a laser pulse energy of < 5 mJ should be used. Unfortunately a pulse energy this low is not practical for the study of the Ni(II) quenching system as the quenching products $Ni(cyclam)(SO_4)^+$ and $Pt_2(pop)_4^{5-}$ would not be detectable due to their lower molar absorptivities (refer to table 4.3) than $Pt_2(pop)_4^{3-}$ which absorbs more strongly in the same region of the spectrum.

Table 4.3 Absorbance maxima and molar absorptivities of the platinum and nickel(III) species and the solvated electron.

Species	λ, nm (ε, M^{-1} cm^{-1}) [18,82]
$Pt_2(pop)_4^{3-}$	310 (76000)
$Pt_2(pop)_4^{4-}$	370 (34000)
$Pt_2(pop)_4^{5-}$	420 (13000)
$^*Pt_2(pop)_4^{4-}$ ($^3A_{2u}$)	325 (12000)
"	460 (15000)
$Ni(cyclam)SO_4^+$	295 (11000)
e^-_{solv}	720 (15800)

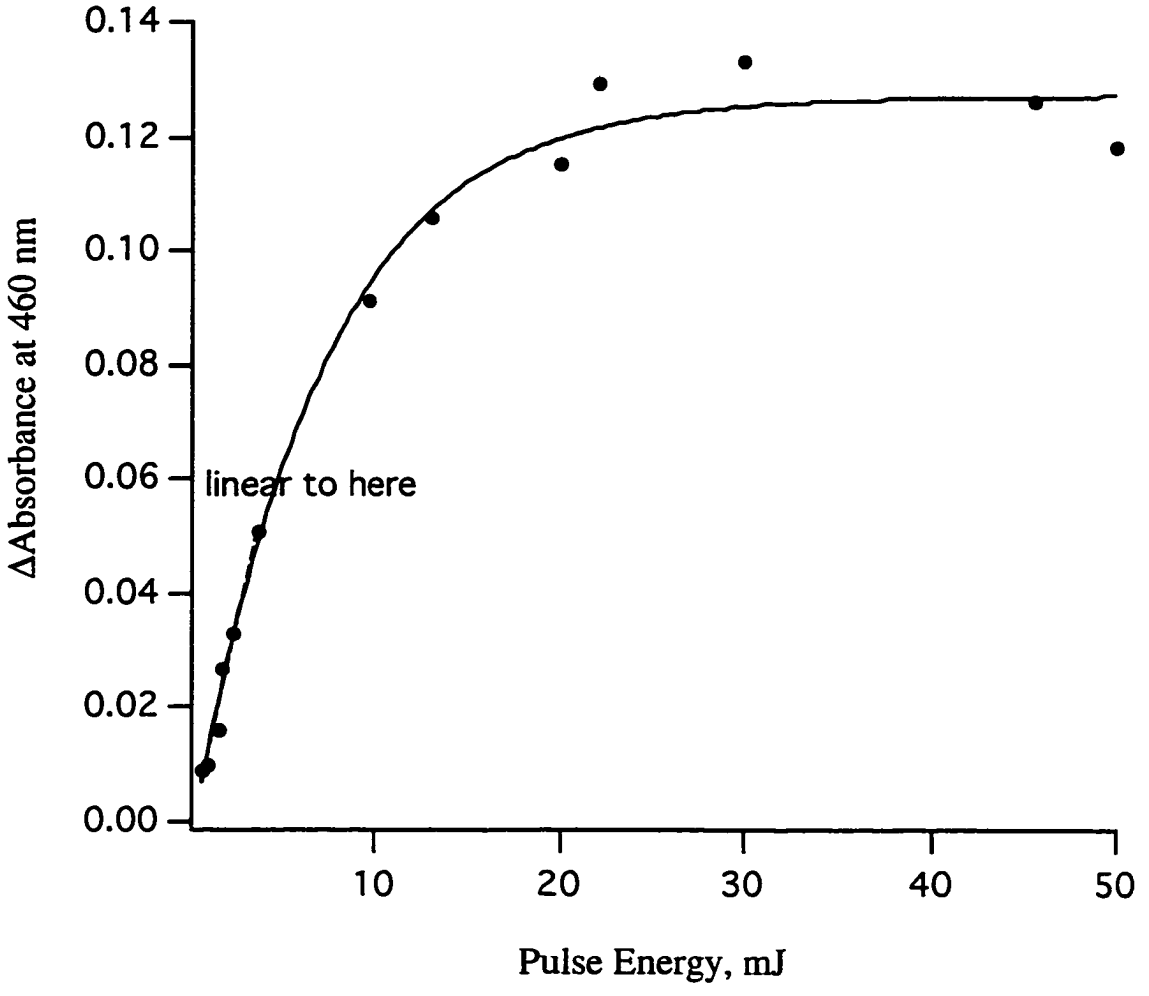

Figure 4.10 Dependence of the $^{*}Pt_2(pop)_4^{4-}$ $^3A_{2u}$ excited state (ΔA_{460}) on laser pulse energy.

4.4.4 Rehm-Weller Behavior

The steps involved in the bimolecular reductive quenching of the excited state of $Pt_2(pop)_4^{4-}$ by the Ni(II) complexes may be expressed by the following equation:

$$D^* + Q \underset{k_{-d}}{\overset{k_d}{\rightleftharpoons}} \{D^*.....Q\} \underset{k_{-e}}{\overset{k_e}{\rightleftharpoons}} \{D^-.....Q^+\} \underset{k'_d}{\overset{k'_{-d}}{\rightleftharpoons}} D^- + Q^+ \qquad (4.5)$$

Where k_d, k'_d, k_{-d}, and k'_{-d} are the rate constants for diffusion and dissociation of the precursor and successor complex, and k_e and k_{-e} are the rate constants for the forward and back electron transfer step within the encounter complex. As described in Chapter 1 (Section 1.6.3) a kinetic analysis of this scheme leads to the expression:

$$k_q = \frac{k_d}{1 + \frac{k_d}{k_e^\circ e^{\Delta G^\ddagger/RT}} + \frac{k_d}{k'_{-d}} e^{\Delta G/RT}} \qquad (4.6)$$

which relates the observed quenching rate constant k_q to the activation barrier ($\Delta G^\ddagger$) and the free energy change (ΔG) of the reaction. The frequency factor k_e° is defined as:

$$k_e^\circ = \kappa \frac{kT}{h} \qquad (4.7)$$

where κ is the transmission coefficient, k is Boltzman's constant, and h is Planck's constant.

The free energy change (ΔG) of the overall electron transfer reaction can be estimated from the standard potentials of the two redox couples involved:[119]

$$\Delta G = E(Q^{+}/Q) - E(^{*}D/D^{-}) + W_p - W_r \quad (4.8)$$

Here the value W_r is the electrostatic work term for bringing the charged reactants together in the precursor complex, and W_p is the corresponding work term for the successor complex. The work terms are often neglected, particularly in cases where one of the reactants is uncharged. For the reaction studied here, however, involving 2+ and a 4- reactants and 3+ and 5- products, the contribution of the work terms can not be neglected.

The values of ΔG for the reactions between $^{*}Pt_2(pop)_4^{4-}$ and each of the Ni(II) quenchers are given in Table 4.2. These values were determined using the estimated $Pt_2(pop)_4^{4-*/5-}$ redox couple (1.34 V (versus NHE))[120], the $Ni^{3+/2+}$ redox couples, and the calculated work terms for reactants and products (refer to Table 4.6). A plot of $\log k_q$ versus ΔG shows classic Rehm-Weller behavior (Figure 4.11). The value of $\log k_q$ increases as the driving force for the reaction increases and ΔG becomes more negative. This can be classified as the "normal" region where the reactions are endergonic in nature. At greater driving forces a plateau is reached, where $\log k_q$ is independent of the value of ΔG. In this region, the reactions are exergonic in nature and a diffusion controlled limit for the quenching rate, k_d, is reached. Marcus type behavior predicts that, with increasing driving force, eventually a decrease in $\log k_q$ should occur (the "inverted" region). Over the range of ΔG values studied for this series of Ni(II) quenchers, no evidence for the Marcus inverted region was observed.

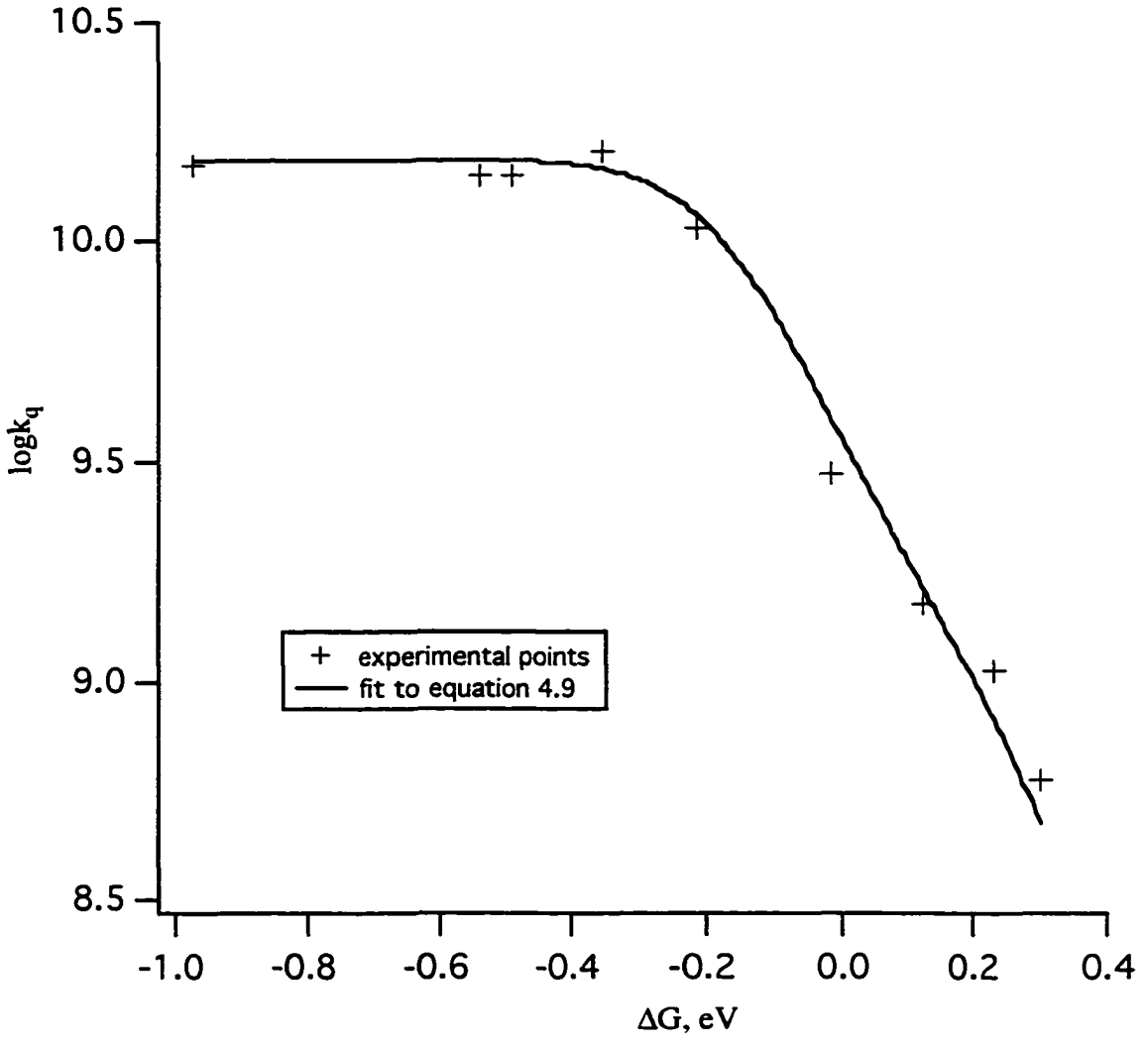

Figure 4.11 Rehm-Weller behavior: Plot of quenching rate log k_q vs driving force ΔG.

The plot of $\ln k_q$ versus ΔG (Figure 4.11) was fitted to the function given in equation 4.9 using a computer modeling program (Igor Pro 3.05 software, Wavemetrics). The temperature was taken as T = 298 K. Four variables v_1, v_2, v_3, and v_4 were defined and given reasonable initial values, the fitting program then applied these initial values to this function and refined the four unconstrained variables to obtain a line which gave the best fit to the experimental points. The line obtained from this fit is shown in Figure 4.11.

$$k_q = \frac{v_1}{1 + (v_2 e^{-\Delta G‡/RT}) + v_4 e^{\Delta G/RT}} \tag{4.9}$$

$\Delta G‡$ was defined in terms of the variable v_3 by the function:[121]

$$\Delta G‡ = \Delta G + \frac{v_3}{\ln 2} \ln\left\{1 + \exp\left[\frac{\Delta G \ln 2}{v_3}\right]\right\} \tag{4.10}$$

A summary of the values obtained for v_1, v_2, v_3, and v_4 obtained from this fitting procedure is given in Table 4.4.

Table 4.4 Parameters obtained from fitting of the Rehm-Weller plot.

parameter	equivalent to	value
v1	k_d	$(1.54 \pm 0.04) \times 10^{10}\ s^{-1}$
v2	k_{-d}/k_e°	39 ± 1
v3	$\Delta G‡(0)$	0.15 ± 0.01 eV
v4	k_{-d}/k'_{-d}	$(8.8 \pm 0.1) \times 10^{-2}$

As seen by comparing eq. 4.6 with eq. 4.9 the variables v_1, v_2, v_3 and v_4 are equivalent to the values of k_d, k_{-d}/k_e°, $\Delta G^\ddagger(0)$, and k_{-d}/k'_{-d} (Table 4.4). The intrinsic barrier $\Delta G^\ddagger(0)$ for the electron transfer reaction is therefore determined to be 14 ± 1 kJ mol^{-1} for this series of quenchers. The reorganizational energy λ is expected to be four times this value (eq. 1.23), and is therefore determined to be 57 ± 4 kJ mol^{-1}.

The diffusion-controlled rate constants k_d, k_{-d}, k'_d, and k'_{-d} can be calculated from the Debye-Smoluchowski and Debye-Eigen equations for the diffusion of charged particles. This treatment has been outlined by Chiorboli and co-workers[122] who give the relevant equations in c.g.s units, and by Kirk and Cai[123] who have presented these equations in SI units.

In order to calculate the theoretical values of k_d, k_{-d}, k'_d, and k'_{-d} for the quenching reaction of $^*Pt_2(pop)_4^{4-}$ and the Ni(II) complexes, values for the radii of the reactants are required. To allow for the fact that reactants may not be truly spherical their radii were estimated from the equation:

$$r = 0.5(d_x d_y d_z)^{1/3} \qquad (4.11)$$

where d_x, d_y, and d_z are the dimensions measured along the three molecular axis. For $K_4[Pt_2(pop)_4]$ these were measured from a space filling model generated by Chem-3D (CambridgeSoft) giving a value of $r(Pt_2(pop)_4^{4-}) = 0.43$ nm. The dimensions of the nickel complex were estimated from the crystallography data[124] available for $[Ni(bicycloN_4O)](ClO_4)_2$, giving a value of $r(Ni(complex)^{2+}) = 0.28$ nm. The radii of the main counter ions were taken as $r_{K+} = 0.13$ nm and $r_{ClO_4^-} = 0.29$ nm respectively. Other values used in these calculations included: k_B, Boltzmann's constant (1.381×10^{-23} J K^{-1}); N, Avagadro's number (6.0022×10^{23} mol^{-1}); e, charge of an electron (1.602×10^{-19} C); ε°, vacuum permittivity (8.854×10^{-12} J^{-1} C^2 m^{-1}); D, the static dielectric constant of

water at 298 K (78.54); η, the viscosity of water at 298 K (1.002×10^{-3} N s m^{-2}); T, the temperature (298 K); and Z_A and Z_B are the charges of the reactants (-4 and +2 respectively for the calculation of k_d and k_{-d}, and -5 and +3 respectively for the calculation of k'_d and k'_{-d}). The calculated values of k_d, k_{-d}, k'_d, and k'_{-d} are given in Table 4.5.

Table 4.5 Calculated values of the rate constants k_d, k_{-d}, k'_d, and k'_{-d}: ionic strength $\mu = 0.01$, T = 298 K.

k_d	1.6×10^{10} M^{-1} s^{-1}
k_{-d}	2.2×10^{8} M^{-1} s^{-1}
k'_d	1.9×10^{10} M^{-1} s^{-1}
k'_{-d}	3.2×10^{7} M^{-1} s^{-1}

The calculated value of 1.6×10^{10} $M^{-1}s^{-1}$ for the diffusional rate constant k_d is in excellent agreement with the value obtained from the computer fit of $(1.54 \pm 0.04) \times 10^{10}$ M^{-1} s^{-1}. The frequency factor k_e° was estimated using the ratio $k_{-d}/k_e^\circ = 39$ which was obtained from the fitting procedure together with the calculated value $k_{-d} = 2.23 \times 10^8$ M^{-1} s^{-1}. k_e° was found to have a value of 5.7×10^6 s^{-1}. Applying this value to equation 4.7 leads to an estimation of the transmission coefficient of $\kappa \sim 1 \times 10^{-6}$. According to theory[125-127] a value of $\kappa = 0$ falls under the *nonadiabatic* limit for electron transfer and in this case the electronic interaction between the reactants is weak and the rate determining step is the electron transfer at the transition state geometry. This differs from an *adiabatic* reaction, $\kappa = 1$, where there is strong electronic coupling between the reactants and the rate determining step is the nuclear motion that leads to the transition-state geometry.

Somewhere between these two extremes lies an intermediate region which is called "weakly adiabatic" ($0 < \kappa < 1$).

The small transmission coefficient ($\kappa \sim 1 \times 10^{-6}$) estimated for this series of quenching reactions falls within the weakly adiabatic domain for electron transfer. This small value can be the result of either electronic factors resulting from poor overlap of the donor and acceptor orbitals, or nuclear factors which arise from changes in the coordination geometries of the reactants associated with the transfer of the electron. For this series of electron transfer reactions between the nickel quenchers and $^*Pt_2(pop)_4^{4-}$ a small value for κ may indicate that a tunnelling mechanism, where the electron must tunnel through the barrier separating the donor and acceptor, is important.

4.4.5 The $Pt_2(pop)_4^{4-*/5-}$ Ion Excited State Potential

It has been shown that excited state redox potentials can be estimated by electron transfer quenching using Marcus-Hush theory.[128] This procedure was used by Nagle et al.[120] to estimate the redox potential of the $Pt_2(pop)_4^{4-*/5-}$ couple from a study of the quenching of $^*Pt_2(pop)_4^{4-}$ by a series of aromatic amines in methanol. An estimate of 1.34 V (vs. NHE) was determined. It was thought that the series of quenching reactions between $Pt_2(pop)_4^{4-}$ and the Ni(II) complexes could provide a second determination for the value of the excited state redox couple $Pt_2(pop)_4^{4-*/5-}$.

In this treatment the quenching rate constants, k_q, are corrected for diffusional effects using equation 4.12:

$$\frac{1}{k_q} = \frac{1}{k_q'} + \frac{1}{k_d} \qquad (4.12)$$

The corrected rate constants k_q' are listed in Table 4.2. To calculate these rates, the value $k_d = 1.54 \times 10^{10}\ M^{-1}s^{-1}$, obtained from the computer fitting to our experimental data, was used.

According to the theory, two limiting cases for the quenching rate constant k_q' can be identified, based upon the relative importance of back electron transfer to ground state or excited state $Pt_2(pop)_4^{4-}$:

$$Pt_2(pop)_4^{5-}\ldots\ Ni^{3+} \rightarrow Pt_2(pop)_4^{4-}\ \ldots\ Ni^{2+} \qquad (4.13)$$

$$Pt_2(pop)_4^{5-}\ldots\ Ni^{3+} \rightarrow {}^*Pt_2(pop)_4^{4-}\ \ldots\ Ni^{2+} \qquad (4.14)$$

Case I: Back electron transfer to give ground state $Pt_2(pop)_4^{4-}$ is faster than back electron transfer to give the excited state and equation 4.13 dominates. In this case a logarithmic expression can be obtained which relates the corrected quenching rate constant k_q' to the reduction potentials of the nickel couples, E(Ox/Red), and the excited state potential of ${}^*Pt_2(pop)_4^{4-}$, $E(Pt^{4-*}/Pt^{5-})$. This expression is given in equation 4.16:

$$RT\ \ln k_q' = RT\ln k_q'(0) - \frac{\Delta G_{et}}{2} \qquad (4.15)$$

$$RT\ \ln k_q' = RT\ln k_q'(0) - \frac{E(Ox/Red)}{2} + \frac{1}{2}[E(Pt^{4-*/5-}) + W_p - W_r)] \qquad (4.16)$$

Here the value $k_q'(0)$ is the electron transfer rate constant for the hypothetical quencher for which the free energy change of the electron transfer step is zero, i.e. $\Delta G_{et} = 0$. The value of kq'(0) is equivalent to the product $\nu_{et}K_d$, where ν_{et} is the frequency factor and K_d is the equilibrium constant for the formation of the precursor complex ($K_d = k_d/k_{-d}$).

Case II: Back electron transfer to give the excited state is the rapid process and equation 4.14 dominates. In this case the logarithmic expression relating k_q' and the reduction potentials takes the following form:

$$RT \ln k_q' = RT\ln k_q'(0) - \Delta G_{et} \quad (4.17)$$

$$RT \ln k_q' = RT\ln k_q'(0) - E(Ox/Red) + [E(Pt^{4-*/5-}) + W_p - W_r)] \quad (4.18)$$

It follows that if a plot of $RT\ln k_q'$ versus E(Ox/Red) for a related series of quenchers has a linear region of slope = 1/2, the free energy dependence in equation 4.16 is established and case I type behavior is obtained. Similarly, a linear region of slope = 1 is evidence for case II type behavior (from eq. 4.18).

A plot of $\ln k_q'$ versus the E(Ox/Red) values for this series of Ni^{II} quenchers is shown in Figure 4.12. The data points appear to be reaching an asymptotic limit at higher $Ni^{III/II}$ redox potentials, unfortunately this linear portion of the plot could not be developed further due to a lack of Ni(II) complexes having E(Ox/Red) values >1.82 V. It is clear however, that this region is fit better by a straight line of slope = 1/2, than by a line with slope = 1 (shown by the dotted line on the graph). This indicates that this series of quenching reactions fall into the category of case I and is in accord with back electron transfer to form ground state $Pt_2(pop)_4^{4-}$ being the dominant process.

The excited state redox potential $E(Pt^{4-*/5-})$ was determined following the same procedure used by Nagle:[120] A potential may be defined, E(0)(Ox/Red), for a hypothetical quencher for which $\Delta G_{et} = 0$. This E(0)(Ox/Red) value may be interpolated from the plot of $RT\ln k_q'$ vs. E(Ox/Red) if an independent estimate of $k_q'(0)$, the corrected rate constant for the quenching reaction between the hypothetical quencher and $Pt_2(pop)_4^{4-}$, can be made. It follows from equation 4.16 that once RTlnkq'(0) is known the value of

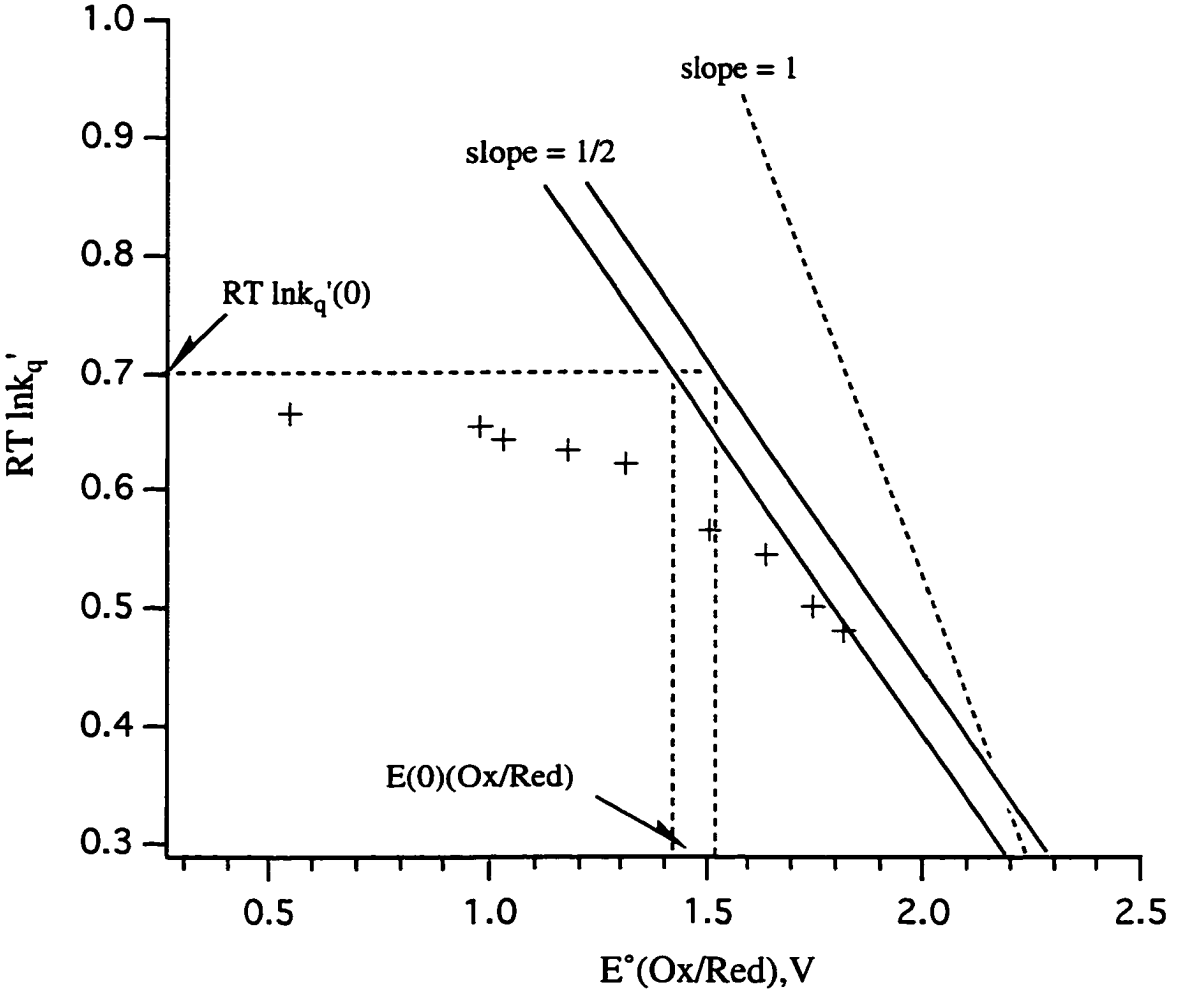

Figure 4.12 Plot of RTlnk$_q$' vs E°(Ox/Red) for the series of Ni(II) quenchers used.

E(0)(Ox/Red) can be read from the graph and can then be used to calculate the excited state redox potential $E(Pt^{4-*/5-})$ from the following relationship:

$$E(Pt^{4-*/5-}) = E(0)(Ox/Red) - (W_p - W_r) \quad (4.19)$$

Assuming that the product $\nu_{et}K_d$ and the reorganizational barrier $\Delta G^{\ddagger}$ ($\lambda/4$) remain reasonably constant throughout the series of quenchers then the value of $k_q'(0)$ may be estimated by the following equation:

$$\ln k_q'(0) = \frac{1}{2} \ln k_{11}k_{22} + \frac{(W_{11} + W_{22} - 2W_r)}{2RT} \quad (4.20)$$

which is derived from the Marcus "cross-reaction" equation[43,43], $k_q' = (k_{11}k_{22}K_{et})^{1/2}$. Here $K_{et} = k_e/k_{-e} = 1$ ($\Delta G_{el} = 0$), and k_{11} and k_{22} are the self-exchange rate constants for the quencher and excited state couples, W_{11} and W_{22} are the electrostatic work terms for bringing together the reactants for the two self exchange reactions, respectively. Thus, an estimate of $\ln k_q'(0)$ could be made for this series of Ni^{II} quenchers from their self-exchange rate constants. The electron transfer self-exchange rate for $Pt_2(pop)_4^{4-*/5-}$ has been estimated to have a maximum value of 2×10^3 M^{-1} s^{-1}.[120] The self-exchange rates of the nickel complexes were estimated using the self-exchange rate constant measured for $Ni(cyclam)^{2+}$, a value of 2×10^{-3} M^{-1} s^{-1}.[129] The values of the work terms (W) were calculated using the following equation.

$$W_i = \frac{Z_A Z_B e^2}{\varepsilon_s (r(Ni(cyclam)^{2+}) + r(Pt_2(pop)_4^{4-}))} \quad (4.21)$$

where Z_A, Z_B, e, r_{Ni}, and r_{Pt} all have the same meanings and values as described in Section 4.4.4. The calculated electrostatic work terms are summarized in Table 4.6:

Table 4.6 Electrostatic work terms used to calculate the excited state redox potential $Pt_2(pop)_4^{4-*/5-}$.

W_{11} ($Pt^{4-*/5-}$)	0.42 eV
W_{22} ($Ni^{2+/3+}$)	0.20 eV
W_r (Pt^{4-*}/Ni^{2+})	-0.21 eV
W_p (Pt^{5-}/Ni^{3+})	-0.39 eV

These values, together with the electron transfer self-exchange rates, were applied to equation 4.20 to give an estimate of $k_q'(0) = 1.07 \times 10^{12}$ s^{-1}. The two solid straight lines (slope = 1/2) shown in Figure 4.12 represent our estimated upper and lower limits for the asymptote to this portion of the quenching plot. Using these two lines and the estimated value for RTlnkq'(0) a range of 1.42 to 1.52 V was determined for E(0)(Ox/Red). Correcting these value for the work terms W_p and W_r, using equation 4.19, gave an estimated range for the value of the excited state redox potential $Pt_2(pop)_4^{4-*/5-}$ of 1.24 to 1.34 (vs. NHE). This is in excellent agreement with and provides support for the previous literature value of 1.34 V (vs. NHE), estimated by Nagle.

4.5 Conclusions

It has been shown that the excited state $^*Pt_2(pop)_4^{4-}$ can be quenched by Ni(II) macrocyclic complexes. Evidence for the formation of an oxidized Ni(III) quenching product supports a mechanism involving reductive quenching of the "platinum-pop" excited

state. This is the first reported example of $^*Pt_2(pop)_4^{4-}$ being reductively quenched by a transition metal complex.

By extending the quenching study to include a series of related Ni(II) complexes, having varying redox potentials, the dependence of the quenching rate constant k_q on the driving force ΔG was determined. This showed classic Rehm-Weller type behavior. Computer fitting allowed for the determination of the reorganizational barrier for electron transfer, $\Delta G^{\ddagger}(0) = 14 \pm 1$ kJ mol^{-1}, for this series of Ni(II) quenchers.

Unfortunately, laser flash photolysis was not useful in probing the mechanistic details of the quenching reaction due to complications caused by photoionization resulting in the formation of the oxidized species $Pt_2(pop)_4^{3-}$.

An estimate of the excited state redox potential $Pt_2(pop)_4^{4-*/5-}$ was made using the data from this series of Ni(II) quenching experiments in aqueous media, and a range of 1.24 to 1.34 V (vs. NHE) was determined. This is in excellent agreement with the literature value.

CHAPTER FIVE

PHOTOCHEMISTRY AND PHOTOPHYSICS OF Cr(III) MACROCYCLIC COMPLEXES

5.1 Introduction

Macrocyclic ligands have been studied for their ability to place constraints on Cr(III) metal ion complexes which alter their photochemical and photophysical properties. As described in Section 1.7.5, it has been established that reaction pathways can be modified by steric factors associated with the presence of multidentate ligands. It has also been suggested that photophysical properties such as emission lifetime, τ, may be dependent on the nature of the coordinated macrocyclic ligand. This has led to the concept that properly designed macrocyclic ligands may be usefully employed to alter and control, to "tune", the photophysical and photochemical behavior of Cr(III) complexes.[130-132]

With this is mind, an investigation of the photophysics and photochemistry of a constrained Cr(III) macrocyclic complex, 1,4,7,10,13,16-hexaazacyclooctadecane, $Cr([18]\text{-ane}N_6)^{3+}$, was undertaken. This complex was then compared to another constrained Cr(III) complex containing the ligand 4,4',4"-ethylidynetris(3-azabutan-1-amine), more commonly referred to as sen. The structures of these ligands are shown in Figure 5.1. The photophysical and photochemical properties of $Cr(sen)^{3+}$ have previously been reported by Endicott and co-workers[130], and in their study a correlation was drawn between trigonal distortion in the complex and an unusually short doublet emission lifetime. $Cr(sen)^{3+}$ is best viewed as a $Cr(en)_3^{3+}$ complex capped at a trigonal face by a neopentyl group. This capping imposes a twist angle on the ligand which in turn induces a trigonal strain in the complex.

In addition to verifying Endicott's results for the photophysical and photochemical properties of $Cr(sen)^{3+}$, a detailed study of the photostereochemistry of this complex, something not previously investigated, was undertaken. The chelate nature of the sen ligand results in two optically active enantiomeric forms of $Cr(sen)^{3+}$ which can be represented by Λ and a Δ. This offered the possibly of probing the photostereochemical

pathways involved in the photoreaction by following the changes in optical activity of the resolved starting material and of the photoproducts. Section 5.3 of this Chapter deals with the separation and identification of these photoproducts.

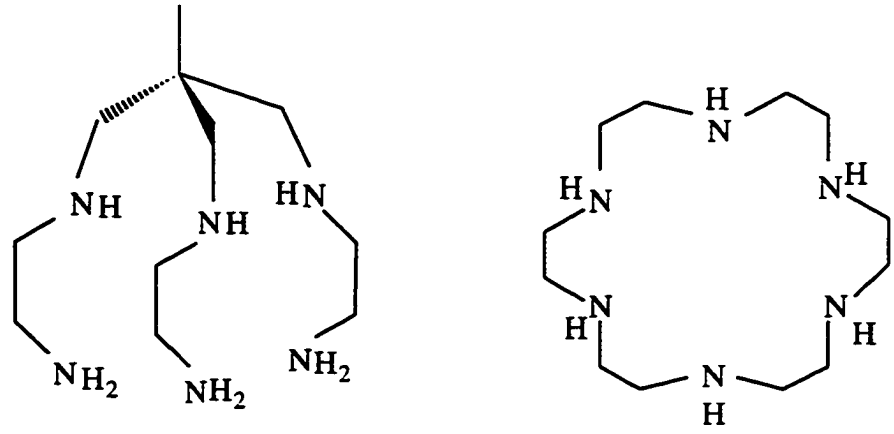

Sen [18]-aneN$_6$

Figure 5.1 Structures of the macrocyclic ligand [18]-aneN$_6$ and the ligand sen.

5.2 Photophysics and Photochemical Reactivity of Cr([18]-aneN$_6$)$^{3+}$ and Cr(sen)$^{3+}$

5.2.1 Quantum Yield and Lifetime Determination

Irradiation of [Cr([18]-aneN$_6$)]Br$_3$ in 1 x 10^{-3} M aqueous $HClO_4$ solution at λ = 436 nm into the first quartet resulted in a slight change in the UV-Vis absorption spectrum over 20 minutes of irradiation (Figure 5.2). This indicates that there is some conversion of the complex to aquated photoproduct. The pH stat method (Section 2.2.6.3) was used to

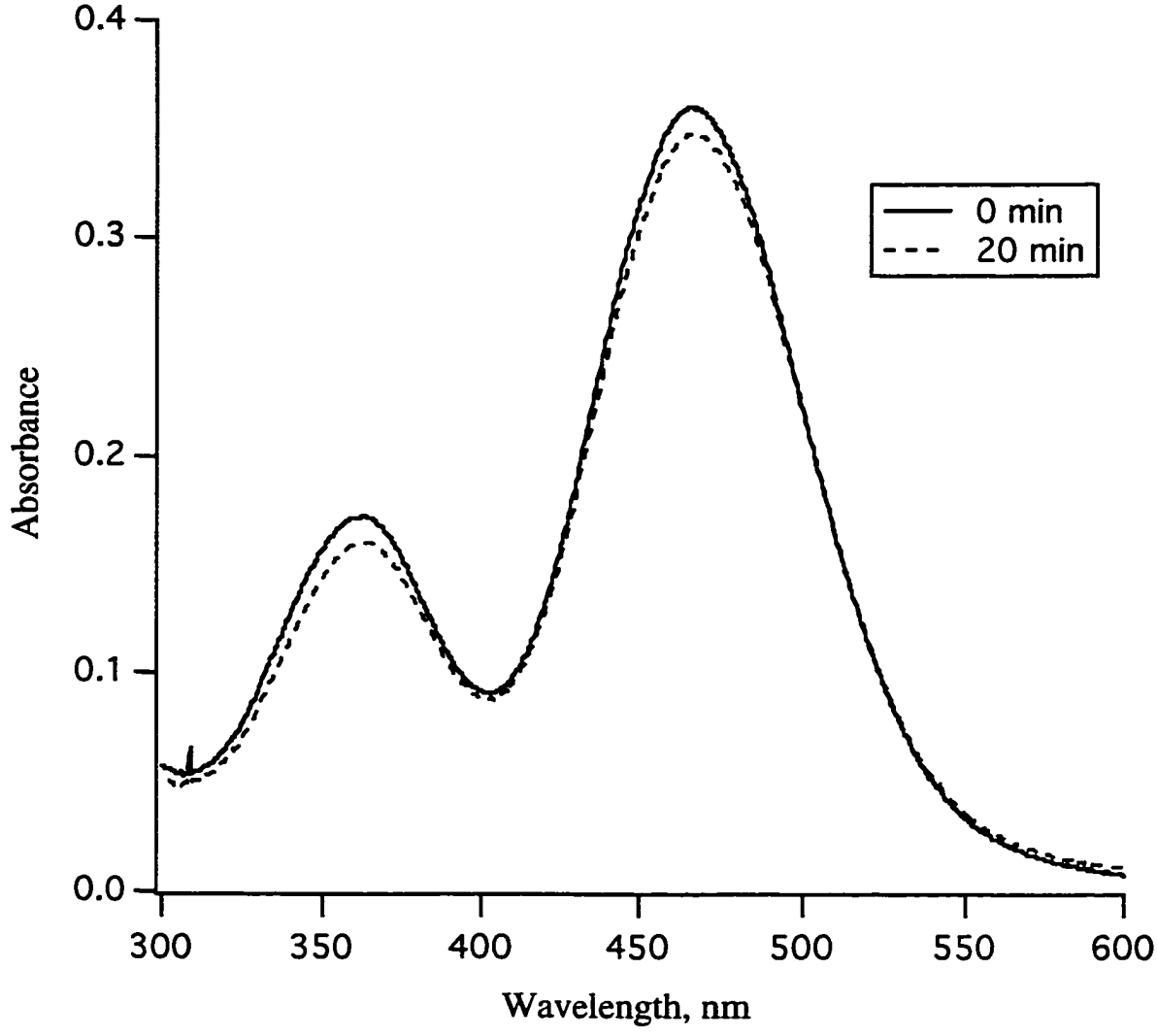

Figure 5.2 UV-Vis spectrum of $[Cr([18]\text{-}aneN_6)]Br_3$ (1.6×10^{-3} M), irradiation at $\lambda = 436$ nm in 1×10^{-3} M $HClO_4$.

determine the quantum yield of photoreaction. In this method the photolysis of a photoreactive Cr(III) amine complex in acid media leads to aquation and protonation of one of the amine ligands. The addition of a standard acid solution is used to maintain a constant pH throughout the photolysis and the volume of acid added can be used to calculate the quantum yield for the photoreaction. For $Cr([18]\text{-}aneN_6)^{3+}$ no proton uptake was detected during irradiation at $\lambda = 436$ nm. This gives an upper limit for the photoreaction of $Cr([18]\text{-}aneN_6)^{3+}$ of $\emptyset_{rxn} = 1.0 \times 10^{-3}$. A small value for $\emptyset_{rxn}$ is not surprising considering the nature of this macrocyclic ligand. This hexaaza macrocyclic ligand effectively wraps itself around the chromium metal. The crystal structure[83] of this complex shows that it has S_6 symmetry, and more importantly, that there is no open site for a nitrogen donor to easily dissociate to allow for substitution by an incoming water molecule.

Irradiation into the first quartet band of $[Cr(sen)]Br_3$ in an aqueous 1×10^{-3} M $HClO_4$ solution at $\lambda = 436$ nm confirmed Endicott's results[124] that this complex is photoreactive. The photoreaction was followed over time by monitoring the changes in the UV-Vis spectrum. A gradual red shift of the spectrum, with good isosbestic points, was observed as the aquated photoproduct was formed in greater amounts (Figure 5.3). The quantum yield for the formation of photoproduct was measured by the pH stat method. The plot of proton uptake versus photolysis time was found to be curved (Figure 5.4), the result of the absorbance decrease from photolysis, and the corrected quantum yield was calculated according to the procedure given in Appendix I. A value of $\emptyset_{rxn} = 0.10 \pm 0.01$ was obtained which is in excellent agreement with the published value of $\emptyset_{rxn} = 0.10$.[130]

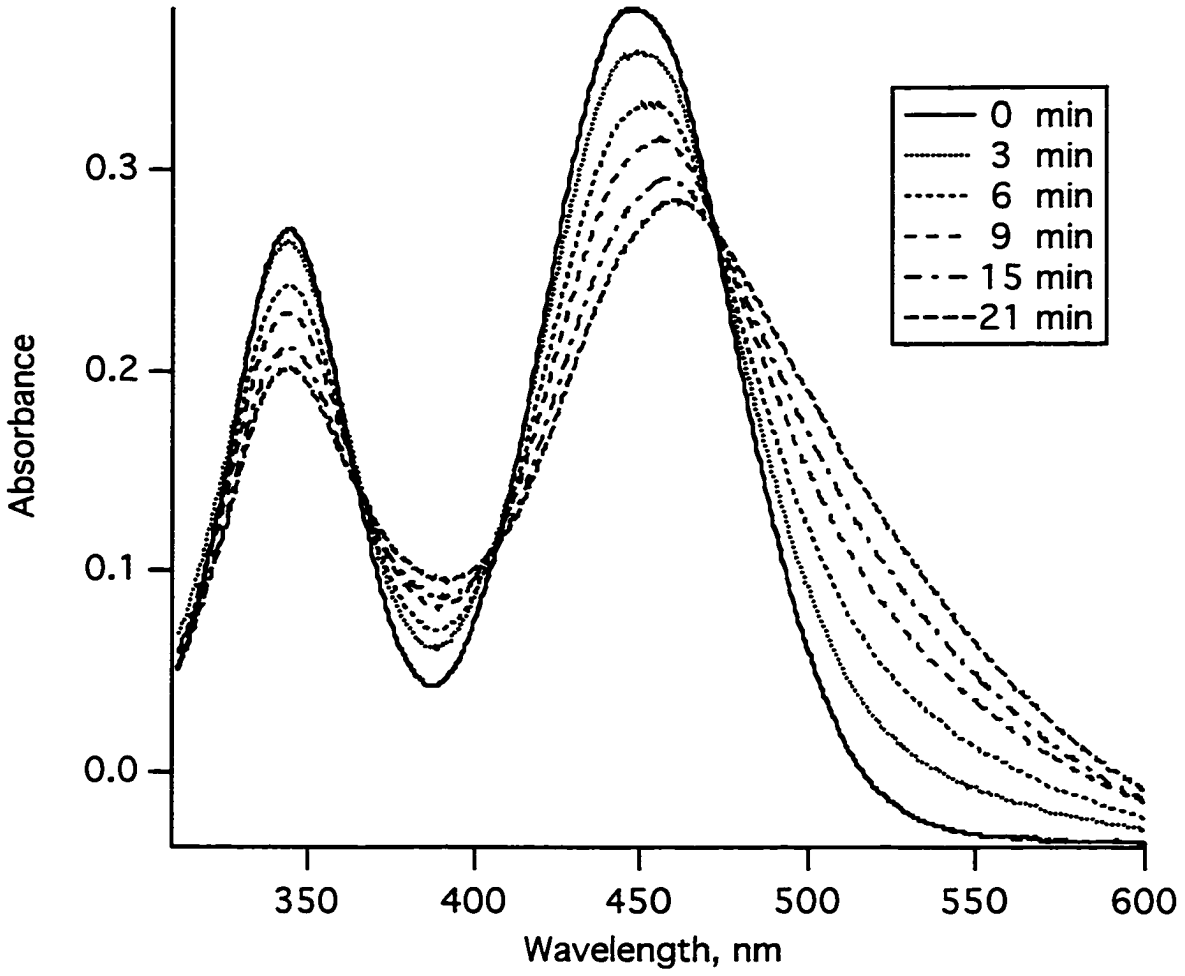

Figure 5.3 UV-Vis spectrum of $[Cr(sen)]Br_3$ (3.8×10^{-3} M), irradiation at $\lambda = 436$ nm in 1×10^{-3} M $HClO_4$.

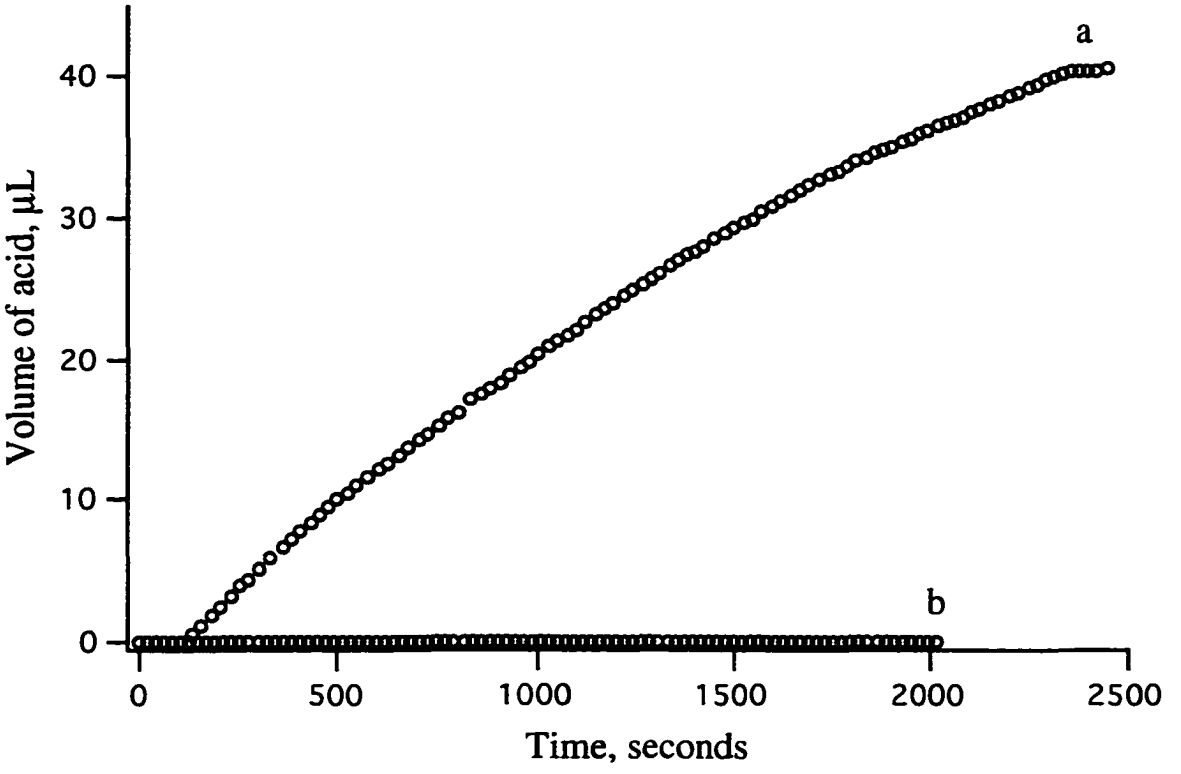

Figure 5.4 pH stat trace for a) $[Cr(sen)]Br_3$ and b) $[Cr([18]\text{-}aneN_6)]Br_3$ at $\lambda = 436$ nm irradiation in 1 x 10^{-3} M $HClO_4$.

5.2.2 Emission Properties of [Cr([18]-aneN$_6$)]Br$_3$ and [Cr(sen)]Br$_3$

The doublet (^{2}E) emission of [Cr([18]-aneN$_6$)]Br$_3$ (~ 1 x 10^{-3} M), cooled to 77 K in dmso/water (1:1) glass media, was found to have an intense maximum at λ = 692 nm corresponding to the 0-0 transition ($^2E \rightarrow {}^4A_2$) (Figure 5.5). The emission signal became sufficiently weak as the sample was allowed to warm to higher temperature (298 K) that it was not observed. This is similar to the observations made by Endicott for the emission spectrum of Cr(sen)$^{3+}$ which were confirmed here: Cr(sen)$^{3+}$ was found to have a emission maximum at λ = 676 nm in dmso/water (1:1) at 77 K which was not observed at higher temperature (298 K). The room temperature (298 K) ^{2}E emission for both of these complexes was found to be too weak to allow for the measurement of the lifetime (τ) using the conventional nitrogen laser apparatus (described in Section 2.2.6.5).

5.2.3 Laser Flash Photolysis Studies

Laser flash photolysis with conductivity detection can be used as an accurate technique for measuring the doublet excited state lifetime of chromium (III) complexes. As well, this technique can be used to provide a direct method of measuring the fraction of the photoreaction that proceeds via the quartet excited state (the *fast* process) and the fraction that proceeds via the doublet excited state (the *slow* process). A typical conductivity decay curve is shown in Figure 5.6a for the flash photolysis of Cr(NH$_3$)$_6^{3+}$ in 1 x 10^{-3} M HClO$_4$ at an irradiation wavelength of λ = 355 nm. Upon photolysis the complex takes up a proton in acidic aqueous media (eq. 5.1).

$$Cr(NH_3)_6^{3+} + H_3O^+ \xrightarrow{h\upsilon} Cr(NH_3)_5(H_2O)^{3+} + NH_4^+ \qquad (5.1)$$

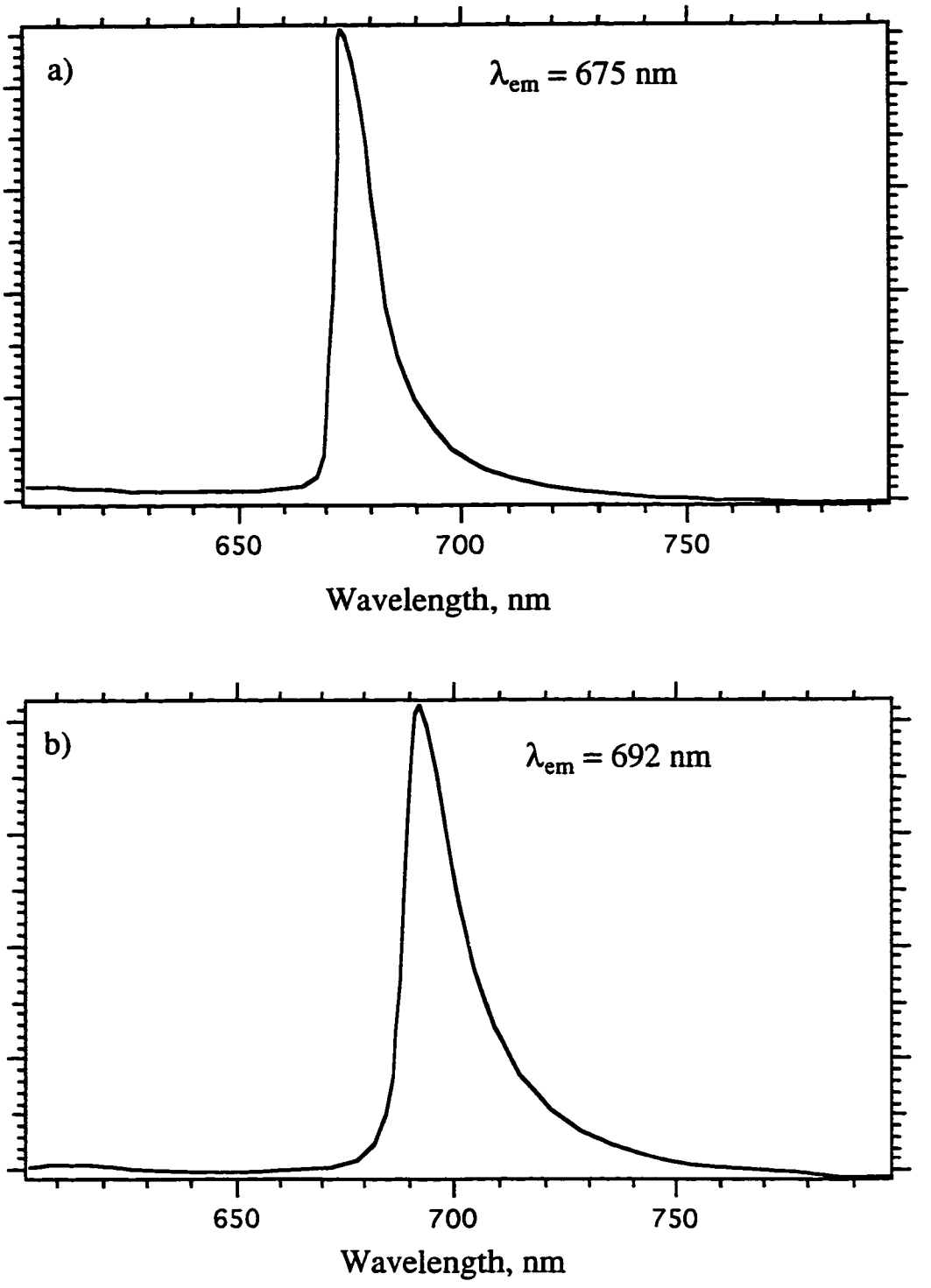

Figure 5.5 Emission spectra of a) $[Cr(sen)]Br_3$ and b) $[Cr([18]\text{-}aneN_6)]Br_3$: dmso/water (50:50) mixture, glassy media at 77 K.

The ionic conductivity of the starting material and the photoproduct are expected to be about the same whereas that of H_3O^+ is much higher than these ions and also greater than NH_4^+. Therefore, under the experimental conditions used (section 2.2.6.4) a drop in conductivity associated with the reaction can be measured on the time scale of the photoreaction. This can then be related to the lifetime of the excited state involved. The conductivity decay trace for $Cr(NH_3)_6^{3+}$ clearly shows that there are two components to the photoreaction leading to a double exponential decay (refer to Figure 5.6). The first component occurs on a slow time scale (μs), having a lifetime of 2.2 μs at 22 ± 1 °C, and corresponds to reaction via the doublet state. This decay curve does not extrapolate back to the baseline at t = 0; there is an initial baseline shift in the conductivity signal. This indicates that there is a fast component to the photoreaction (< μs) that occurs during the laser pulse and corresponds to photoreaction occurring via the quartet excited state which is in competition with the process populating the doublet excited state. The 1:3 ratio of these two components correspond to 25% of the photoreaction occurring via the quartet state and 75% occurring via the doublet state in the case of $Cr(NH_3)_6^{3+}$.

Laser flash photolysis with conductivity detection was used to confirm the unreactive nature of $Cr([18]\text{-}aneN_6)^{3+}$ and the short doublet excited state lifetime of $Cr(sen)^{3+}$. Laser flash photolysis of an aqueous solution of $Cr([18]\text{-}aneN_6)^{3+}$ in 1 x 10^{-3} M $HClO_4$ at λ = 355 nm resulted in no overall conductivity decay signal. This is consistent with the observations that this complex has a very low quantum yield for photoreaction, $Ø_{rxn}$. The low conversion of complex to photoproducts did not produce a significant enough conductivity change to be detectable by this method.

The conductivity decay trace for the flash photolysis of $Cr(sen)^{3+}$ in 1 x 10^{-3} M $HClO_4$ at λ = 355 nm is shown in Figure 5.6b. The lifetime of 524 ns was measured from the conductivity decay signal and was found to depend on the concentration of acid $[H^+]$ present in the solution. Increasing the acid concentration to 4 x 10^{-3} M $[H^+]$ caused the lifetime to decrease to 163 ns. Attempts to measure lifetimes shorter than 163 ns by

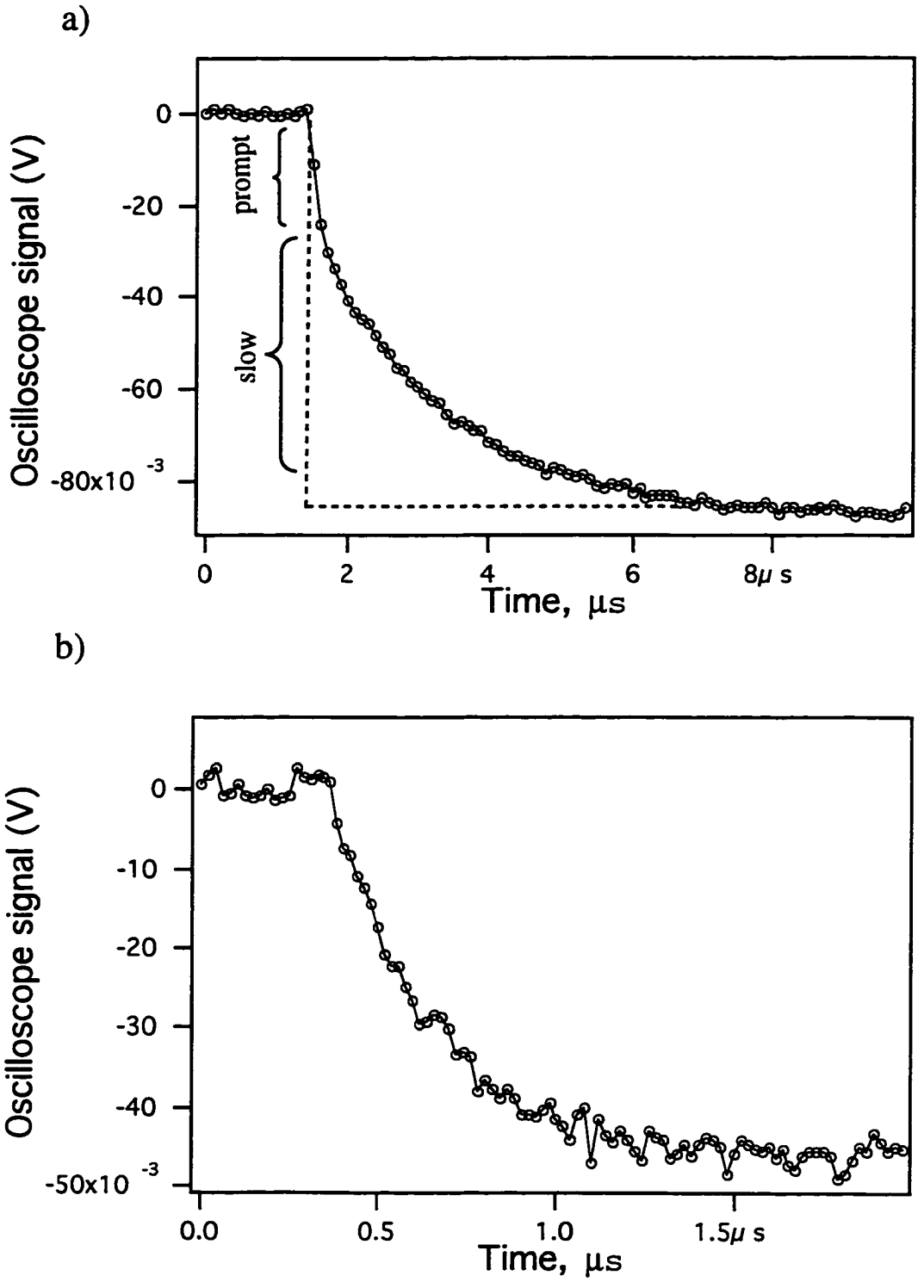

Figure 5.6 Laser flash photolysis decay trace of a) $Cr(NH_3)_6^{3+}$ and b) $Cr(sen)^{3+}$ in aqueous 1 x 10^{-3} M $HClO_4$ media, λ = 355 nm.

increasing the acid concentration (> 4 x 10^{-3} M) were limited by the inability of the experimental apparatus to operate in solutions of such high conductivity. The lifetime associated with proton uptake was found to be linearly dependent on $[H^+]$ throughout the accessible concentration range, indicating that the results were rate-limited by the step of protonating the sen ligand (eq. 5.2).

$$Cr(sen)^{3+} + H_3O^+ \xrightarrow{k_{H+}} Cr(senH)H_2O^{4+} \qquad (5.2)$$

A plot of the reciprocal lifetime (τ^{-1}) versus $[H^+]$ is shown in Figure 5.7. The slope of the straight line fit of this data gives an estimate of $k_{H+} = 1.4 \pm 0.1 \times 10^9\ M^{-1}\ s^{-1}$ for the protonation rate constant of $Cr(sen)^{3+}$. This is about an order of magnitude slower than the rate constant $k_{H+} = 4.3 \times 10^{10}\ M^{-1}\ s^{-1}$ reported for the protonation of free amine.[133] The slower protonation rate observed for $Cr(sen)^{3+}$ may suggest that k_{H+} can be reduced by steric factors associated with the limited angle of access of a proton to the liberated base, in this case a dangling amine arm which is still attached to the metal center. Waltz and co-workers have measured the rate constant for the protonation of $Cr(en)_2(en)H_2O^{3+}$ and found it to be $3.6 \times 10^9\ M^{-1}\ s^{-1}$.[134] The protonation rate of this species has also been measured in our laboratory under similar conditions used to measure k_{H+} for $Cr(sen)^{3+}$ and a value of $2.2 \times 10^9\ M^{-1}\ s^{-1}$ was determined,[135] which is consistent with the value of k_{H+} measured for $Cr(sen)^{3+}$. The LFP results confirmed the extremely short doublet excited state lifetime (< 163 ns) of $Cr(sen)^{3+}$.

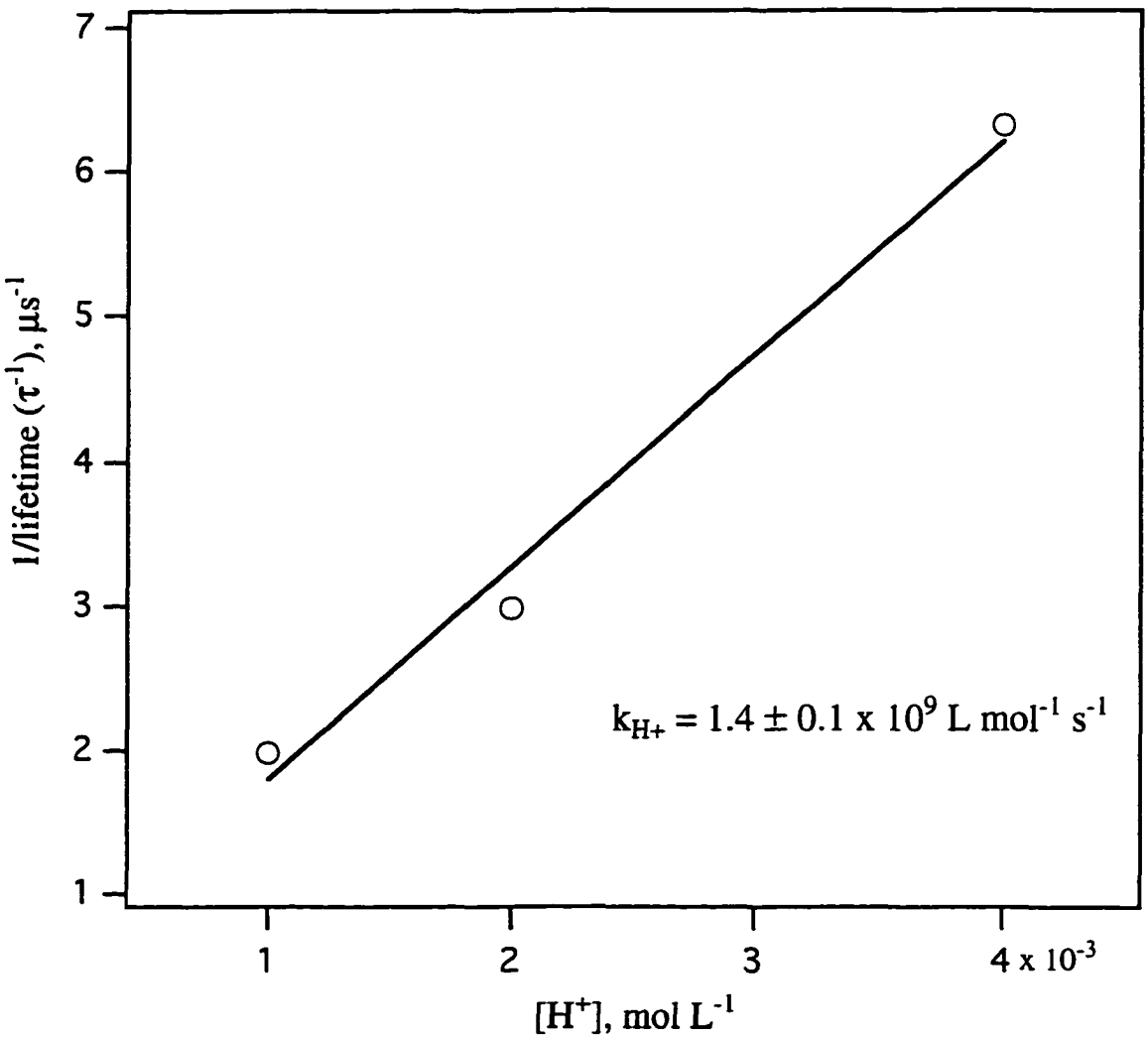

Figure 5.7 pH dependence of conductivity lifetime: plot of τ^{-1} versus [H^+].

5.2.4 Temperature Dependence of the Doublet (^2E) Lifetime

The ^2E emission lifetime of Cr(III) complexes are found to be temperature dependent.[59] The observed relaxation behavior of the doublet state may often be expressed by the following relationship:[136]

$$\tau^{-1} = k = k_{lim} + k(T) \qquad (5.3)$$

where τ is the observed lifetime, k_{lim} is the limiting low temperature (nearly temperature independent) relaxation rate constant and k(T) represents the thermally activated relaxation behavior. A typical plot of $\ln(\tau^{-1})$ versus temperature (T) for Cr(III) complexes exhibits a low temperature region where k_{lim} dominates and the relaxation rate decreases only slightly with increasing temperature. Eventually, a temperature is reached (usually referred to as the onset temperature) where k(T) begins to dominate and the lifetime decreases linearly with increasing temperature (high temperature region). This high temperature region is often fitted to a simple Arrhenius function:

$$k(T) = A\exp(-E_a/RT) \qquad (5.4)$$

where A is the pre-exponential factor, E_a is the activation energy, and R is the gas constant. A single exponential decay in the high temperature region of an Arrhenius plot of ln(k(T)) versus T^{-1} is suggestive of a single process deactivating the ^2E excited state. The value of the activation energy (E_a) for this process can be determined from the slope of the straight line in this region of the Arrhenius plot. The value of the pre-exponential factor (A) can be determined from the y-intercept.

The emission lifetime, τ, was measured over a temperature range of 77 to 273 K for $Cr([18]\text{-ane}N_6)^{3+}$ and $Cr(sen)^{3+}$ in dmso/water (1:1). The temperature dependence of the

emission lifetime for $Cr(en)_3^{3+}$ was also recorded in dmso/water (1:1) under similar conditions for comparison. At 77 K $Cr(([18]\text{-}aneN_6))^{3+}$ was found to have a lifetime of 162 μs, while $Cr(sen)^{3+}$ had a lifetime of 157 μs at this temperature, similar to the value of 171 μs measured by Endicott. The emission lifetime decreased with increasing temperature. An Arrhenius plot of ln(k(T)) versus T^{-1} for all three complexes is shown in Figure 5.8. The onset temperature for the thermally activated decay of the ^2E excited state was found to follow the order: $Cr([18]\text{-}aneN_6)^{3+}$ (143 K) < $Cr(sen)^{3+}$ (167 K) < $Cr(en)_3^{3+}$ (200 K). The low temperature region of these plots were fitted to straight lines in order to determine the values of k_{lim} the temperature independent decay rate constant. These values of k_{lim} were then used to correct the thermally activated decay rate constant k(T) according to the equation:

$$k(T)' = k(T) - k_{lim} \qquad (5.5)$$

The logarithm of the corrected decay rate constant ln(k(T)') was plotted against T^{-1} for the high temperature region of the Arrhenius plot. These plots are shown in Figures 5.9 a,b,c for $Cr(([18]\text{-}aneN_6))^{3+}$, $Cr(sen)^{3+}$, and $Cr(en)_3^{3+}$ respectively. Each of these high temperature decays were fitted by straight lines and in all three cases good fits were obtained. Values for the activation energies were determined from the slopes of these lines and were: $Cr([18]\text{-}aneN_6)^{3+}$, $E_a = 34.2 \pm 1.4$ kJ mol^{-1}; $Cr(sen)^{3+}$, $E_a = 33.9 \pm 0.9$ kJ mol^{-1}; $Cr(en)_3^{3+}$, $E_a = 48.5 \pm 1.0$ kJ mol^{-1}. Values of A, the pre-exponential factor, were determined by calculating the y-intercept of these straight lines. The values obtained are summarized in Table 5.1. The results for $Cr(sen)^{3+}$ are in agreement with the observations made by Endicott that the thermally activated ^2E decay of $Cr(sen)^{3+}$ in dmso/water medium has an onset temperature of 180 K and an activation energy of $E_a = 29$ kJ mol^{-1}. The activation energy determined for $Cr(en)_3^{3+}$ is also in excellent agreement with Endicott's measurement of $E_a = 48.7$ kJ mol^{-1} determined in dmso.[137]

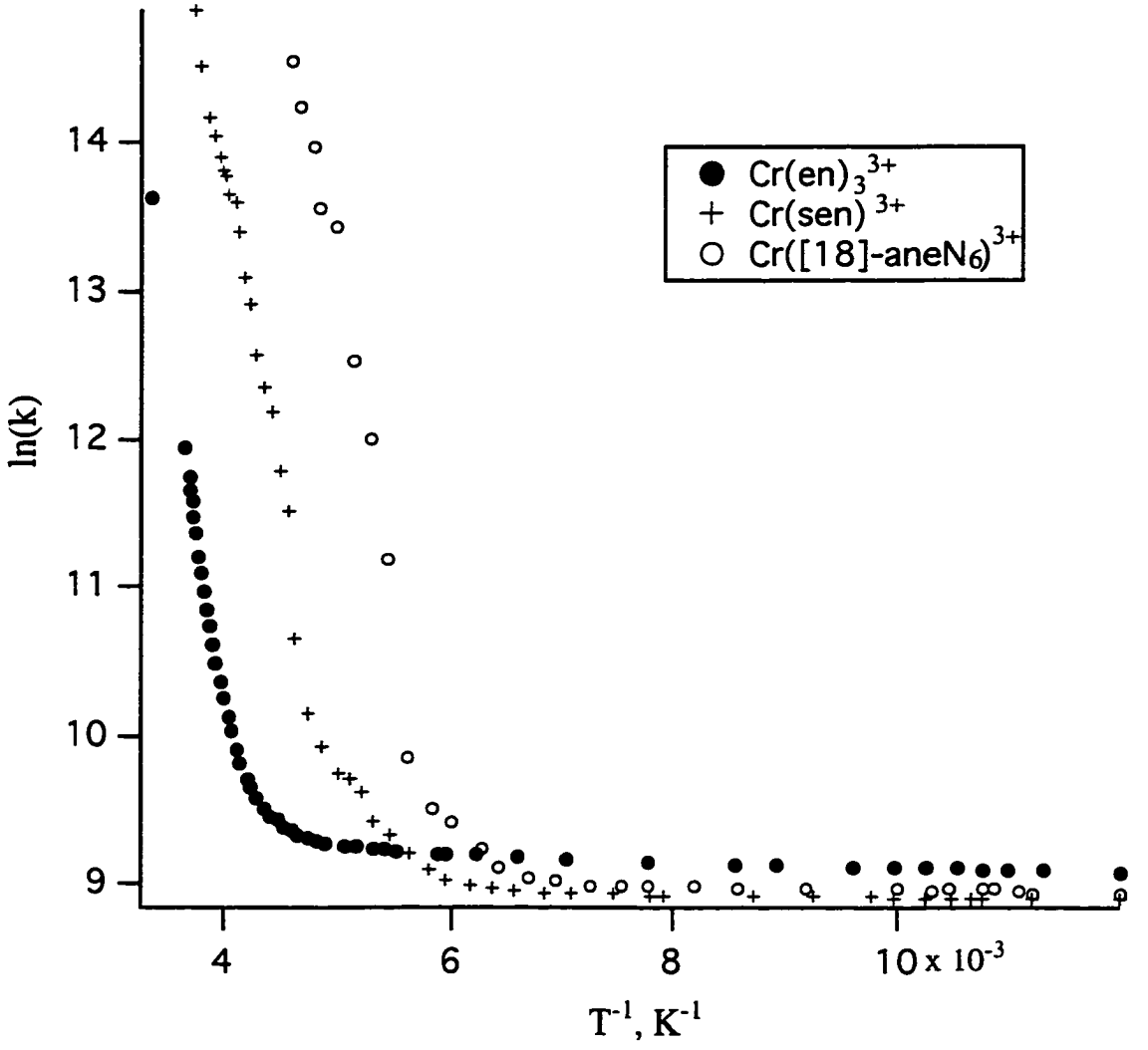

Figure 5.8 Plot of ln(k) vs T^{-1} for $Cr([18]\text{-}aneN_6)^{3+}$, $Cr(sen)^{3+}$, and $Cr(en)_3^{3+}$ in dmso/water (1:1).

For both $Cr([18]\text{-}aneN_6)^{3+}$ and $Cr(sen)^{3+}$ deviations from linearity were observed over a portion of the reciprocal temperature range (Figures 5.9 a,b). This phenomenon has been observed in the temperature dependence studies of other Cr(III) hexaam(m)ine complexes and has been attributed to the transition of the matrix in which the complexes are frozen from glass to fluid as the sample warms up.[59,85,137] The phase transition region has been reported to be ~180 K for $Cr(sen)^{3+}$ in both dmso/water (1:1)[85] and LiCl/water,[137]. The deviations from linearity observed here were found to occur over two different temperature ranges (measured in (1:1) dmso/water) depending on the complex: 190 - 220 K for $Cr(sen)^{3+}$ and 165 - 180 K for $Cr([18]\text{-}aneN_6)^{3+}$. The difference between these temperature ranges is too large to be attributed to errors in the temperature measurement (T ± 1 °C) and indicates that this phenomenon is influenced by more than just a simple phase transition of the solvent and may also depend on the nature of the complex, perhaps involving hydrogen bonding between the Cr(III) amine complex ions and the neighboring solvent molecules.[137,138]

Table 5.1 Activation parameters for the thermal deactivation of the Cr(III) hexamine complexes.

Complex	Medium	A, s^{-1}	E_a, kJ mol^{-1}	Reference
$Cr([18]\text{-}aneN_6)^{3+}$	dmso/H_2O	(3.3 ± 1.7) x 10^{14}	34.2 ± 1.4	a
$Cr(sen)^{3+}$	dmso/H_2O	(4.4 ± 2.5) x 10^{14}	33.9 ± 0.9	a
$Cr(sen)^{3+}$	dmso/H_2O	9 x 10^{14}	29	85
$Cr(en)_3^{3+}$	dmso/H_2O	(2.5± 1.4) x 10^{14}	48.5 ± 1.0	a
$Cr(en)_3^{3+}$	dmso	(1.4 ± 1.1) x 10^{14}	48.7 ± 1.2	137

a = this work.

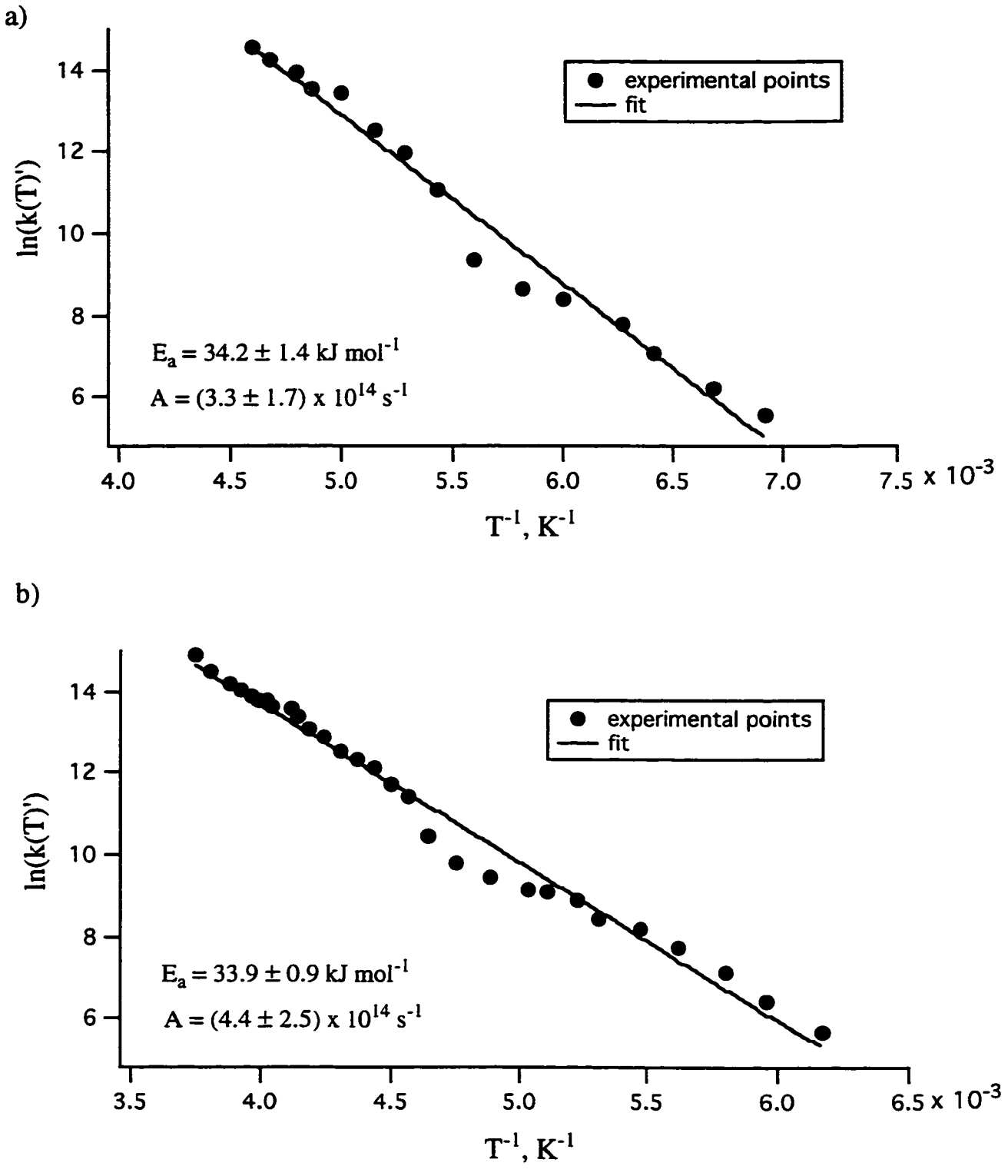

Figure 5.9 a,b Plot of ln(k(T)') vs T^{-1} for a) $Cr([18]\text{-ane}N_6)^{3+}$, b) $Cr(sen)^{3+}$.

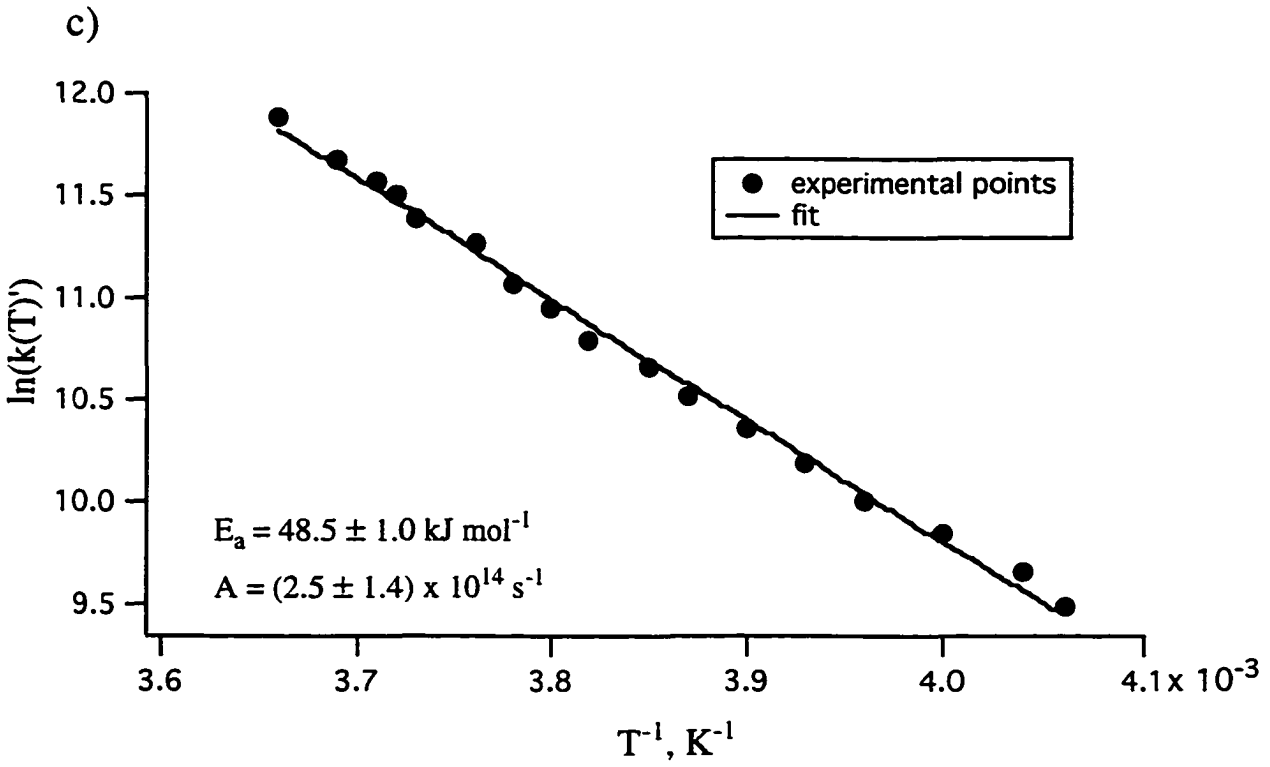

Figure 5.9 c Plot of ln(k(T)') vs T^{-1} for $Cr(en)_3^{3+}$.

Extrapolation of the straight line fitting obtained for $Cr([18]\text{-}aneN_6)^{3+}$ and $Cr(sen)^{3+}$ to 293 K allowed for an estimation to be made of their ambient ^2E emission lifetimes. A value of 0.6 ns was estimated for the ^2E lifetime of $Cr(sen)^{3+}$ at 293 K, which is in agreement with the prediction made by Endicott of a lifetime of 0.1 ns (298 K). The ^2E lifetime of $Cr([18]\text{-}aneN_6)^{3+}$ was estimated to be 17 ns at 293 K. Both of these complexes exhibit strikingly different photophysical properties to $Cr(en)_3^{3+}$ which is more typical of a CrN_6 unit. Its emission lifetime measured at 77 K, in dmso/water (1:1) was found to be 120 μs, and upon warming to room temperature has a much longer lifetime of 1.6 μs (293 K). The activation energies E_a observed for both $Cr([18]\text{-}aneN_6)^{3+}$ and $Cr(sen)^{3+}$ are significantly smaller than the activation energy observed for $Cr(en)_3^{3+}$, more typical of a chromium(III) am(m)ine complex (40 - 50 kJ mol^{-1}). For $Cr(en)_3^{3+}$ the value of E_a is considered to be of the magnitude to be expected for the E(Q°/D°) spacing, consistent with reverse intersystem crossing being the dominant process deactivating the doublet state.

5.2.5 Stereochemical Perturbations of ^2E Lifetime

The estimated ambient ^2E emission lifetimes of both $Cr([18]\text{-}aneN_6)^{3+}$ (17 ns at 293 K) and $Cr(sen)^{3+}$ (0.6 ns at 293 K) are many orders of magnitude shorter than the lifetime of $Cr(en)_3^{3+}$ (1.7 μs at 298 K). The question arises; why are the emission lifetimes of these complexes so much shorter? A model has been proposed by Endicott[130] which attributes the unusually short lifetime of $Cr(sen)^{3+}$ to the introduction of trigonal strain imposed through the capping of $Cr(en)_3^{3+}$ with the neopentyl moiety. According to this model the trigonal distortion from octahedral geometry imposed by the ligand facilitates access to an efficient thermally activated nonradiative relaxation channel from the ^2E state in ambient solutions to the ground state. A twist angle θ can be defined to indicate the amount

of twist between the two N_3 faces at each end of the ethylenediamine ligand (divided by a factor of two)[139] where $\theta = 30°$ indicates an octahedral environment for the central ion and $\theta = 0°$ indicates a trigonal prism (Figure 5.10).

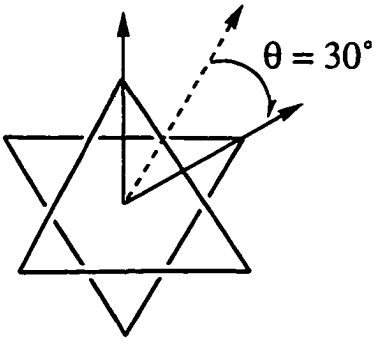

Figure 5.10 Definition of twist angle: Octahedral complex $\theta = 30°$, trigonal prismatic $\theta = 0°$.

Using angular overlap calculations Endicott estimated that the surface crossing which leads to the deactivation of the doublet state occurs with a transition state having a twist angle of $\theta = 15°$. This was based on calculations for $Cr(NH_3)_6^{3+}$ where the molecule distorts along a trigonal distortion coordinate from octahedral (O_h) to trigonal prismatic (D_{3h}) coordination geometry. The ground-state geometry of $Cr(sen)^{3+}$, determined from its x-ray structure, has a twist angle of 25.4°. Comparison of the ambient emission lifetimes for a series of hexaam(m)ine chromium(III) complexes, having different degrees of trigonal distortion, was used to support the claim that the coordination of the ligand can cause a dramatic decrease in the lifetime of the complex. Endicott drew a correlation between the thermally activated nonradiative relaxation rate, k(T), and the change in steric energy within the ligand that was calculated for a trigonal twist from the ground-state geometry to a geometry in which the twist angle is 15°. This correlation was used to explain the short doublet lifetime of the $Cr(sen)^{3+}$ complex. It was also used to explain the long lifetime

(180 μs at 298 K) observed for $Cr(TAP[9]aneN_3)^{3+}$ which has a rigid octahedral coordination geometry (θ =30°) and resists twisting, and the short lifetime (4×10^{-3} μs at 298 K) of the sterically strained $Cr(TAE[9]aneN_3)^{3+}$ molecule where θ = 27° (structures of the ligands $TAP[9]aneN_3$ and $TAE[9]aneN_3$ are shown in Figure 5.11). Table 5.2 gives the twist angle and room temperature ^2E emission lifetimes for this series of Cr(III) hexaam(m)ine complexes.

Table 5.2 ^2E emission lifetimes of hexaam(m)ine Cr(III) complexes.

Complex	Twist angle, θ °	τ, μs (298 K)	Reference
$Cr([9]aneN_3)^{3+}$	30	30.2	140
$Cr(TAE[9]aneN_3)^{3+}$	27	4×10^{-3}	132
$Cr(TAP[9]aneN_3)^{3+}$	30	179	132
$Cr(NH_3)_6^{3+}$	30	2.2	140
$Cr(en)_3^{3+}$	26.7	1.6 [b]	140
$Cr(sen)^{3+}$	25.4	6×10^{-4} [b]	a
$Cr([18]\text{-}aneN_6)^{3+}$	30	1.7×10^{-2} [b]	a
$Cr(diamsar)^{3+}$	25	$< 1 \times 10^{-2}$ [b]	141
$Cr(sar)^{3+}$	25	$< 1 \times 10^{-2}$ [b]	141
$Cr(sep)^{3+}$	25	10	142

a = this work b = 293 K

The crystal structure of $[Cr([18]\text{-}aneN_6)]Br_3$ shows that this complex has S_6 symmetry, and more importantly, that it has a twist angle of $\theta = 30°$ and no trigonal distortion. Therefore its short ^2E lifetime would appear to contradict the model proposed by Endicott which was used to explain the short lifetime of $Cr(sen)^{3+}$. The crystal structure of $Cr([18]\text{-}aneN_6)^{3+}$ indicates that while there is no trigonal distortion, there is a compression of the two N_3 faces towards each other resulting in a "flattening" of this octahedral molecule. The bite angle of the five member ring subtended at the central Cr atom was measured to be 81.9°.[143] It seems reasonable to suggest that the short doublet lifetime of $Cr([18]\text{-}aneN_6)^{3+}$ may be manifested in this distortion which flattens the complex, imposed by the coordination of the ligand, rather than a trigonal distortion as suggested for $Cr(sen)^{3+}$.

The unreactive nature of $Cr([18]\text{-}aneN_6)^{3+}$ should lead to the expectation of a long doublet lifetime for this complex if direct chemical reaction were the major process deactivating the doublet excited state. This can be related to studies of the photoinert Cr(III) cage-type complexes $Cr(sep)^{3+}$, $Cr(sar)^{3+}$, and $Cr(diamsar)^{3+}$. Where sep = 1,3,6,8,10,13,19-octaazabicyclo-[6-6-6]-eicosane; sar = 3,6,10,13,16,19-hexaazabicyclo[6.6.6]-eicosane; and diamsar = 1,8-diamino-3,6,10,13,16,19-hexaazabicyclo[6.6.6]-eicosane. The structures of these ligands are shown in Figure 5.11. A study by Endicott[142] found similar absorption and emission spectra and emission lifetimes for $Cr(sep)^{3+}$ and $Cr(en)_3^{3+}$ and $Cr(NH_3)_6^{3+}$ and this was taken as evidence for a common mechanism, namely surface crossing to a ground state intermediate as the most probable pathway for the deactivation of the doublet state. Sargeson et al.[141] found contradictory results for the structurally related complexes $Cr(sar)^{3+}$ and $Cr(diamsar)^{3+}$. These macrocyclic cage complexes were found to have considerable spectroscopic differences, and much shorter ambient emission lifetimes than that reported for $Cr(sep)^{3+}$ (Table 5.2) and this was interpreted in favor of back intersystem crossing as the likely pathway for deactivation of the doublet excited state. The authenticity of the $Cr(sep)^{3+}$

sample was questioned due to lack of a published crystal structure. The short emission lifetime observed for $Cr([18]\text{-}aneN_6)^{3+}$ is similar to the observation made by Sargeson for $Cr(sar)^{3+}$ and $Cr(diamsar)^{3+}$ and contrasts the long lifetime reported for $Cr(sep)^{3+}$. The complex $Cr(diamsar)^{3+}$ is reported to be twisted about the C_3 axis toward a trigonal prism by $10 \pm 2°$, and a similar distortion is expected for $Cr(sar)^{3+}$ and $Cr(sep)^{3+}$.[141] This corresponds to a twist angle of $\theta = 25°$, equivalent to the trigonal distortion found in $Cr(sen)^{3+}$. According to Endicott's model, the short emission lifetimes observed for $Cr(diamsar)^{3+}$ and $Cr(sar)^{3+}$ would be explained by this trigonal distortion, it would also predict that $Cr(sep)^{3+}$ should have a much shorter lifetime than is reported.

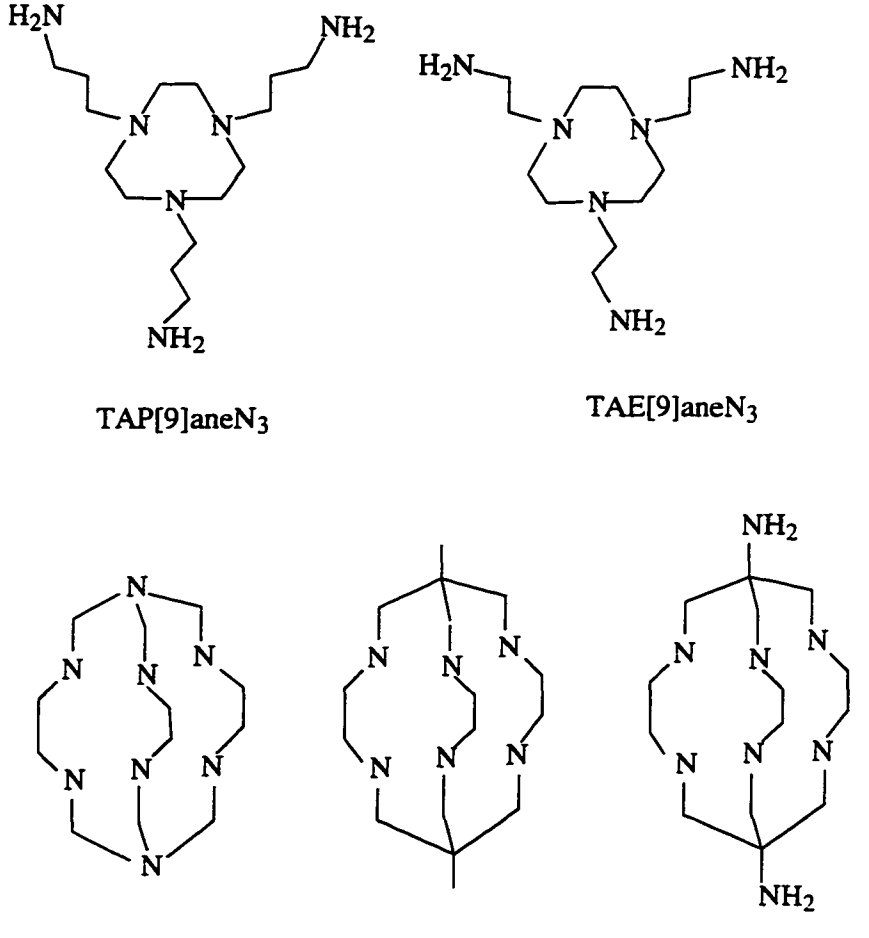

Figure 5.11 Structures of macrocyclic ligands used in the Cr(III) photophysical studies.

5.2.6 Direct Doublet (^2E) Irradiation of $Cr(sen)^{3+}$

Since the fast and slow components of the photoreaction of $Cr(sen)^{3+}$ could not be determined from LFP conductivity measurements because of the short ^2E lifetimes, an alternative method of probing the extent of participation of the quartet and doublet excited states was sought. The excited state participation in the photochemical reactions of Cr(III) complexes can be investigated by two different methods:[58] i) The addition of suitable quenchers to quench the 'slow' component of the photoreaction, and ii) comparison of the photochemical yield upon direct irradiation into the quartet and doublet excited states.

Quenching experiments have proven successful in examining simultaneously the effect of quencher on photochemical reaction and the emission of the doublet state.[144] The best example of this is the complex $Cr(CN)_6^{3-}$ which, in dmf, emits with a long ^2E lifetime and at the same time photosubstitutes with a quantum yield of 0.11. The doublet emission is quenched by both water and oxygen, but complete quenching of the doublet emission leaves the quantum yield of the photoreaction unchanged. This establishes without question that this molecule does not react from its doublet excited state. Quenching experiments of other Cr(III) complexes are not so clear. For the majority of Cr((III) complexes η_{isc} appears to lie in the range 0.5 - 1.0, and the energy spacing between the relaxed doublet and quartet excited states (E(Q°/D°)), although not known with certainty, is sufficiently small that thermal repopulation of the quartet excited state from the doublet, reverse intersystem crossing, is likely the dominant doublet decay process. For $Cr(sen)^{3+}$ such quenching experiments are not feasible due to the short doublet lifetime of this complex. Instead method ii) comparison of the quantum yield (Φ_{rxn}) upon direct irradiation into the quartet and doublet excited states was investigated.

In early experiments involving direct doublet irradiation the idea was that if reaction was occurring from the doublet excited state and if the quartet to doublet intersystem crossing yield was less than unity, then an increase in photochemical yield would be seen

on direct doublet irradiation. A study[145] of the direct doublet irradiation of $Cr(en)_3^{3+}$ failed to resolve the question of doublet versus quartet excited state reactivity. The photochemical quantum yield was found to be the same (within experimental error) whether the complex was irradiated into its quartet or into the doublet absorption band. This result can be interpreted in three different ways; i) reaction occurs from the doublet excited state and the intersystem crossing efficiency is equal to 1.0; ii) reaction occurs from the quartet state, but quartet and doublet excited states are near equilibrium; and iii) reaction occurs from both excited states and there is coincidental equality of doublet and quartet yields.

The quantum yield of photoreaction $\emptyset_{rxn}$ for $Cr(sen)^{3+}$ for irradiation into the lowest quartet excited state, $^4T_2 \leftarrow {}^4A_2$ ($\lambda_{irradiation} = 436$ nm), was determined to be $\emptyset_{rxn} = 0.10 \pm 0.01$ at 22 °C (section 5.2.1). Measuring the value of $\emptyset_{rxn}$ for irradiation directly into the doublet excited state was a much more difficult process. The doublet absorption band is found at $\lambda = 675$ nm (Figure 5.12). This band is sharp, due to the similar geometry of the doublet excited state complex and quartet ground state complex, and has a low molar absorptivity due to the spin forbidden nature of the transition. Determining the amount of light absorbed purely by the doublet excited state of $Cr(sen)^{3+}$ at $\lambda = 675$ nm was complicated by the fact that there appeared to be a tailing component from the absorption of the lowest lying quartet state. The molar absorptivity ε_{675} was determined from the absorption spectrum at a wavelength of 675 nm and measured from the baseline of the spectrum. A value of $\varepsilon_{675} = 0.42\ M^{-1}\ cm^{-1}$ was obtained and this value was used in subsequent photolysis experiments to calculate the quantum yield of photoreaction, $\emptyset_{rxn}$. For the quartet excited state to absorb this far along the red edge of its absorption band would require the involvement of a much higher energy vibrational state of the ground state. The 0-0 transition for $Cr(sen)^{3+}$ can be estimated from the point in the spectrum where the quartet absorption band drops to 5% of its maximum value, ~ 520 nm. According to the Boltzman equation the probability of a transition for a single mode occurring to the quartet excited state at 675 nm, involving a vibrational level which has an

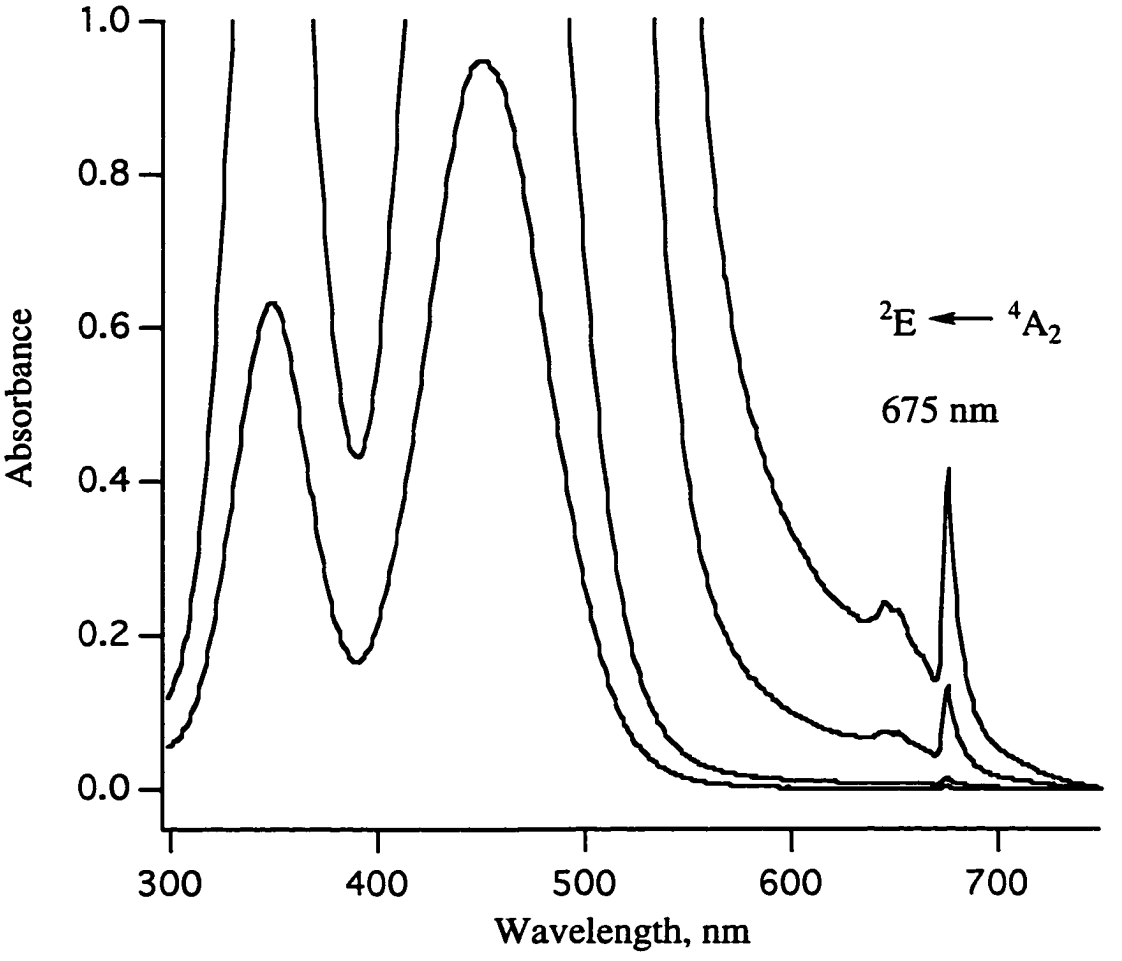

Figure 5.12 UV-Vis spectrum showing the doublet absorbance at 675 nm of [Cr(sen)]Br_3.

energy difference of $\Delta E \sim 6.5$ kK, would be extremely low unless it involved many additional vibrational modes in the molecule.

Irradiation at 675 nm was achieved using a tunable dye (Rhodamine 640 dye) laser pumped by an argon ion laser at 514 nm. A specially designed flow cell having a path length of 10 cm and an internal diameter of 3 mm was filled with a filtered (0.45 μm) aqueous solution of $[Cr(sen)]Br_3$ (~4×10^{-2} M) in 1×10^{-3} M $HClO_4$. The 10 cm flow cell was specifically designed to maximize the path length, necessary due to the low ε_{675} value, in order to increase the amount of light absorbed at 675 nm. The greater complex concentration required for absorption at 675 nm had the advantage that several photolysis runs could be performed on the same solution while still remaining below 5% total decomposition. A typical plot of volume acid added versus photolysis time, obtained from the pH stat method for determining the quantum yield for the reaction (Φ_{rxn}), is shown in Figure 5.13. The good linearity of this plot indicated that the experimental apparatus was working as anticipated, responding to the photoreaction of the complex. The excitation power was determined by monitoring the light transmitted through the back of the flow cell using a power meter (Scientech 365). A decrease in power was observed which corresponded to the absorbance of the solution at 675 nm. This was maximized by tuning the dye laser to adjust the irradiation wavelength in order to ensure that Φ_{rxn} was measured while irradiating into the maximum of the doublet absorption band (difficult due to the sharpness of this band). To ensure that this was indeed the case, the quantum yield was measured as a function of irradiation wavelength over a short range ($\lambda_{irradiation}$ = 670 nm - 680 nm) to ensure that a maximum value was obtained for Φ_{rxn}. For an excitation power of 30 mW a photochemical quantum yield of $\Phi_{rxn} = 0.08 \pm 0.01$ was obtained for direct doublet irradiation at $\lambda_{irradiation}$ = 675 nm, at 22 ± 1 °C. The quantum yield was measured for the irradiation of a solution of $Cr(sen)^{3+}$ (1×10^{-4} M) at 514 nm, under identical conditions and the expected value for quartet irradiation of $\Phi_{rxn} = 0.10$ was obtained.

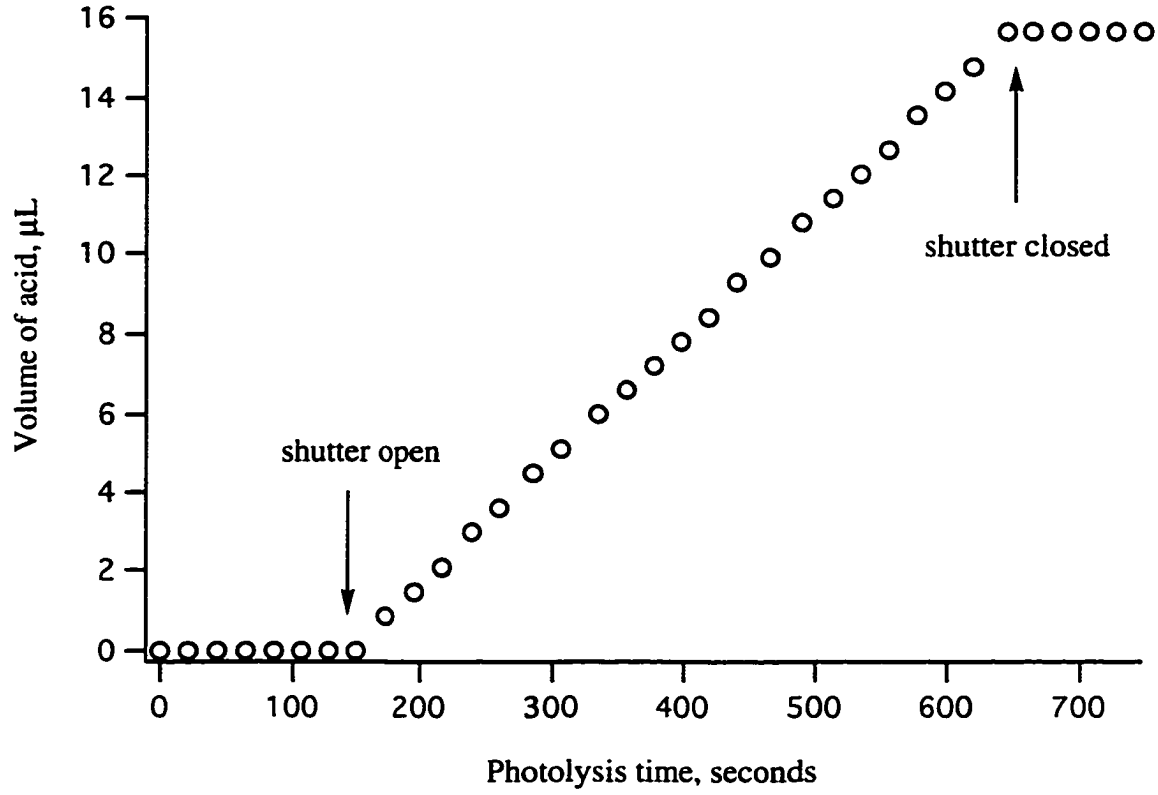

Figure 5.13 Plot of volume acid added vs irradiation time, obtained from the pH stat method for the photolysis of $Cr(sen)^{3+}$ at $\lambda_{irradiation}$ = 675 nm in 1 x 10^{-3} M $HClO_4$.

Similar values of $\emptyset_{rxn} = 0.10 \pm 0.01$ for irradiation at 514 nm over 6 measurements were calculated based on the power readings (corrected for reflections). This indicated that there was about a 10% error in the absolute power calibration. A schematic diagram of the experimental apparatus is given in Section (2.2.6.3).

The observation that the quantum yield for the photoreaction of $Cr(sen)^{3+}$ decreases upon direct doublet irradiation is a novel result, there are no other reports of a decrease in $\emptyset_{rxn}$ upon doublet irradiation. The excited state processes for a Cr(III) complex are shown in Figure 5.14. A detailed analysis of the kinetics[146] of these processes leads to an expression for the fast component of the photochemical reaction:

$$\emptyset_{rxn}^{(fast)} = (1 - \eta_{pisc})\eta_{QR} \qquad (5.6)$$

where η_{pisc} is the efficiency of prompt intersystem crossing, and η_{QR} is the efficiency of quartet reaction. For the slow component of the reaction:

$$\emptyset_{rxn}^{(slow)} = \frac{(\eta_{pisc} + (1 - \eta_{pisc})\eta_{isc})(\eta_{DR} + \eta_{risc} \times \eta_{QR})}{1 - \eta_{isc}\eta_{risc}} \qquad (5.7)$$

where η_{isc} is the efficiency of intersystem crossing and η_{DR} is the efficiency of doublet reaction. The factor $1 - \eta_{isc}\eta_{risc}$ in the denominator allows for multiple passes through the doublet excited state. Several possible analyses can be presented to explain the decrease in $\emptyset_{rxn}$ observed for direct doublet irradiation: i) direct reaction occurs from both the quartet and doublet excited states and the doublet reactive pathway is less efficient; ii) a component of the photoreaction occurs from higher vibrational levels of the quartet excited

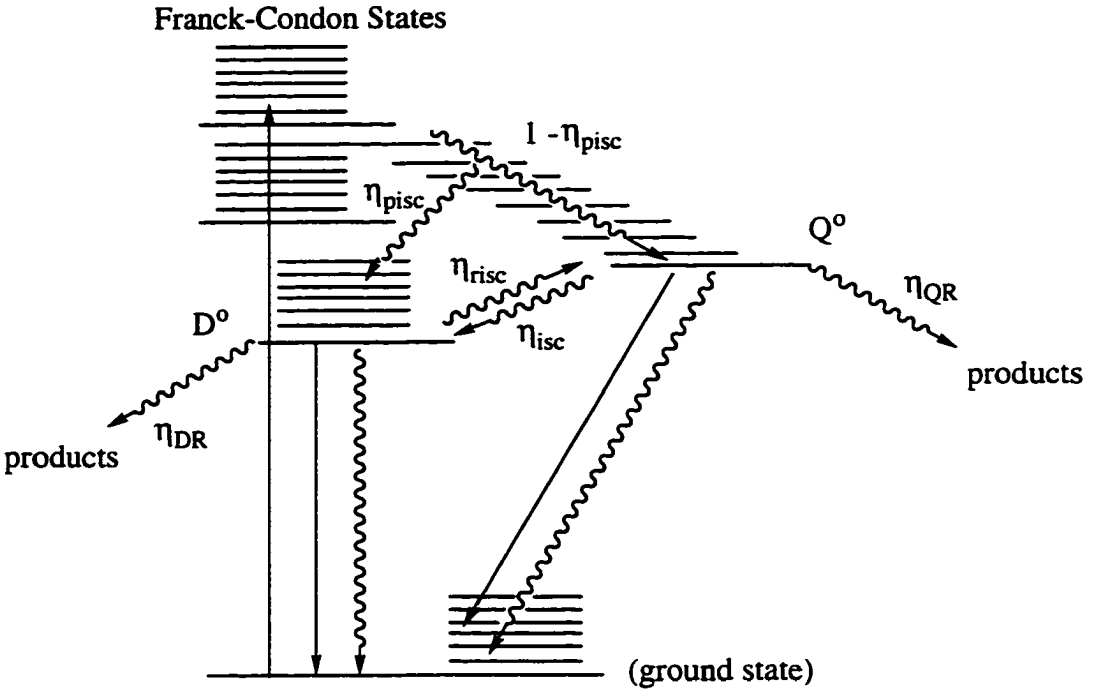

Figure 5.14 Excited state processes for a Cr(III) complexes: η_{isc}, efficiency of intersystem crossing; η_{risc}, efficiency of reverse intersystem crossing; η_{pisc}, efficiency of prompt intersystem crossing; η_{QR}, efficiency of quartet reaction, η_{DR}, efficiency of doublet reaction.

state and this component is removed when irradiating directly into the doublet excited state; iii) photoreaction occurs via surface crossing from the doublet excited state to a ground state intermediate and this process is competitive with non-radiative decay (Endicott's model); iv) reaction occurs from the quartet excited state and the slow component of the photoreaction occurs via reverse intersystem crossing from the doublet excited state where the efficiency of reverse intersystem crossing is less than unity ($\eta_{risc} < 1$). Due to the evidence in support of reversed intersystem crossing and reaction via the quartet excited state[145,147,148] model iv) is favored here and is used in the following discussion to explain the results obtained for quartet and doublet irradiation. This analysis is presented as an illustration only, in order to show how a decrease in the quantum yield could be obtained upon direct doublet irradiation. It should be noted that this interpretation does not, however, distinguish between model iv) and model iii) (Endicott's model) where reaction is proposed to occur from a ground state intermediate.

Flash photolysis with conductivity detection has been used to measure the fast and slow components of the photoreaction of $Cr(en)_3^{3+}$ and has established that the doublet and the quartet excited states are populated with efficiencies of 70% and 30% respectively, the result of intersystem crossings. Due to its short lifetime no such determination can be made for $Cr(sen)^{3+}$, instead the 70/30 ratio observed for $Cr(en)_3^{3+}$ was taken as an estimate for the efficiency of population of the doublet and quartet excited states when $Cr(sen)^{3+}$ is irradiated into its quartet absorption band. After the initial 0.7/0.3 population of D° and Q° in Scheme 5.15a the fast component of the reaction occurs from the quartet state with an efficiency of $\eta_{QR} = 0.08$ while the slow component occurs through intersystem crossing and reverse intersystem crossing between the doublet and quartet excited states. Efficiencies for these processes are: $\eta_{isc} = 0.92$ and $\eta_{risc} = 0.52$. Reaction occurs only from the quartet excited state, no doublet reaction occurs ($\eta_{DR} = 0$). Using equations 5.6 and 5.7 this leads to a calculated value of 0.10 for $\emptyset_{rxn}$, which is in excellent agreement with the observed value of 0.10 ± 0.01. Irradiation at a wavelength of 675 nm populates

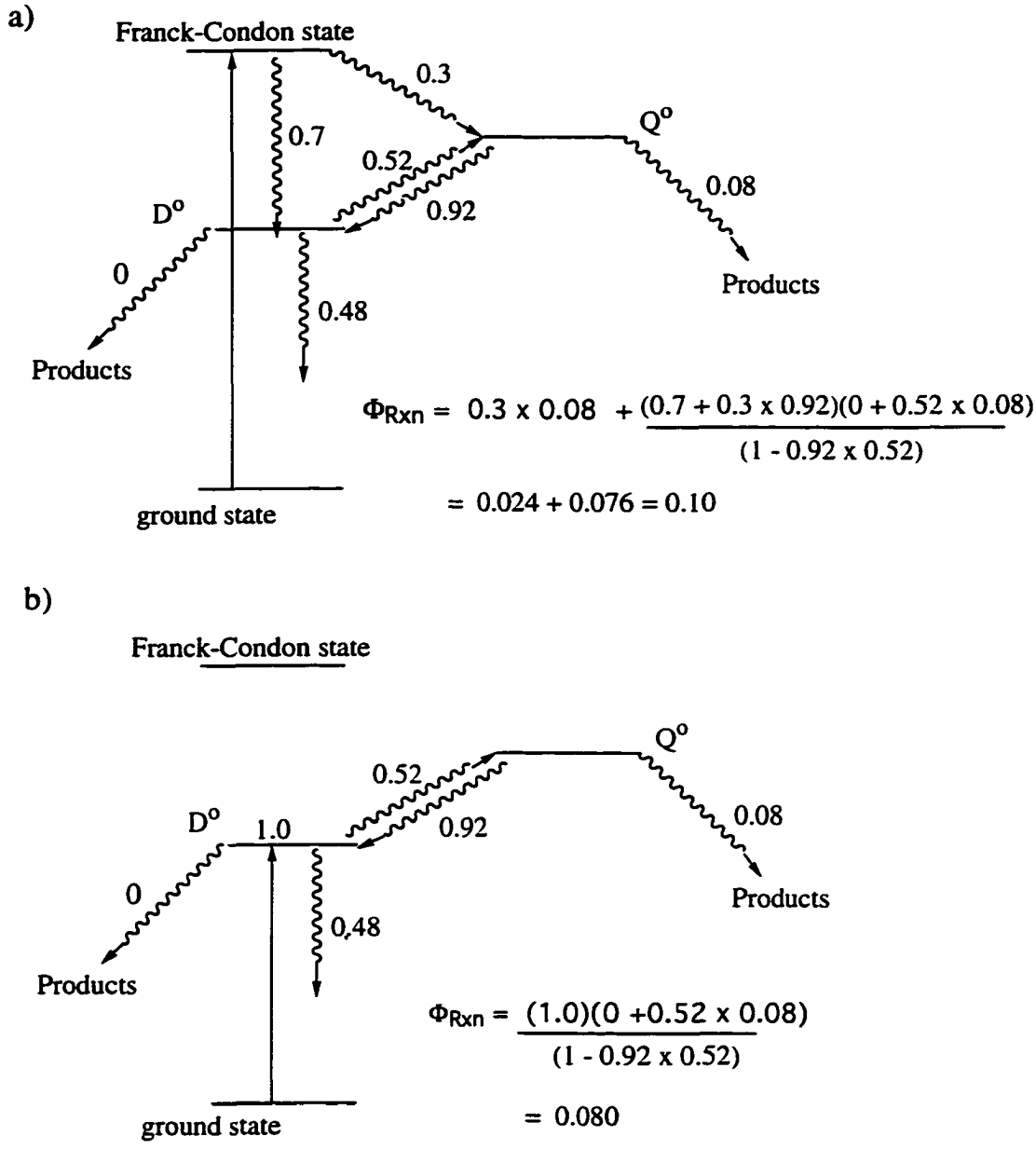

Figure 5.15 Scheme showing excited state participation for $Cr(sen)^{3+}$.

a) Irradiation $\lambda_{irradiation}$ = 436 nm populates the relaxed doublet (D°) and quartet (Q°) excited states with efficiencies of 70% and 30% respectively.

b) Irradiation at = 675 nm populates the relaxed doublet excited state (D°) with 100% efficiency.

the doublet excited state 100% and eliminates the fast component of the photoreaction which occurs directly from the quartet excited state (Scheme 5.15b). Using the same values for η_{isc}, η_{pisc},η_{risc}, η_{QR},and η_{DR} a value of 0.080 is calculated for $\emptyset_{rxn}$, which is also in agreement with the observed value of 0.08 ± 0.01. The value for the intersystem crossing efficiency $\eta_{isc} = 0.92$, used in this modeling, is slightly lower than the value measured for $Cr(en)_3^{3+}$, $\eta_{isc} = 1.0 \pm 0.01$.[145,149]

This model needs to be reconciled with the observations made for the temperature dependence of the doublet emission lifetime (Section 5.2.4). A value of less than 1.0 for the efficiency of reverse intersystem crossing, in this case $\eta_{risc} = 0.52$, indicates that there is another process deactivating the doublet excited state. If both of these processes are important and each exhibit an temperature dependence, than the thermally activated decay rate constant k(T)' is better described by a two-term function:[59]

$$k(T)' = k(T)_1 + k(T)_2 = A_1\exp(-E_{a1}/RT) + A_2\exp(-E_{a2}/RT) \qquad (5.8)$$

Where $k(T)_1$ and $k(T)_2$ are the individual thermally activated decay rate constants, A_1 and A_2 are the pre-exponential factors, and E_{a1} and E_{a2} are the activation energies of the two respective processes. It was found that the plot of ln(k(T)') versus T^{-1} for $Cr(sen)^{3+}$ shown in Figure (5.9a) was fit quite well by this two-term function. This was achieved by defining an equation of the form given in equation 5.8, where A_1, A_2, Ea_1, and Ea_2 were defined as unconstrained variables and given reasonable initial values. The fitting program refined these initial values to obtain the best fit to the data points (this is shown in Figure 5.16a). This gave values of $A_1 = (1.2 \pm 1.0) \times 10^{15}$ s^{-1} and $Ea_1 = 45 \pm 1$ kJ mol^{-1} for one of the two deactivation processes, and $A_2 = (5.4 \pm 1.2) \times 10^{11}$ s^{-1} and $Ea_2 = 29 \pm 1$ kJ mol^{-1} for the other process. An activation energy of 45 kJ mol^{-1} is of the magnitude typically observed for Cr(III) amine complexes and can be associated the E(Q°/D°) energy

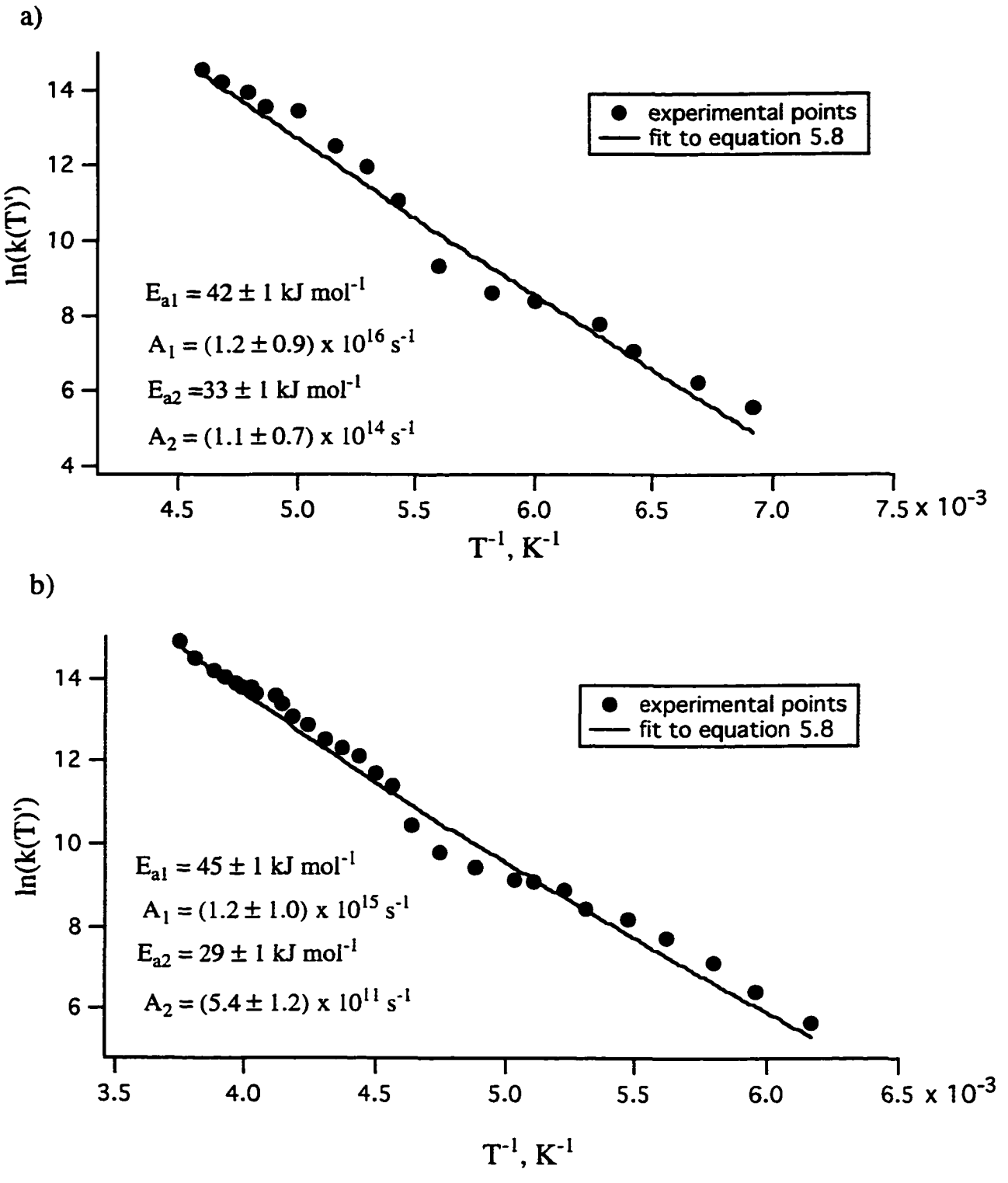

Figure 5.16 Fitting of ln(k(T)') vs T^{-1} plot for a) $Cr([18]\text{-}aneN_6)^{3+}$, b) $Cr(sen)^{3+}$ to equation 5.8.

gap and back intersystem crossing as the deactivation process. The second process, having an activation energy of 29 kJ mol^{-1}, can be associated with nonradiative deactivation of the doublet excited state to the ground state. This is in good agreement with an activation energy of E_a = 32 kJ mol^{-1} which has been measured for the complex $Cr(CN)_6^{3-}$.[150] In this case a large E(Q°/D°) energy gap inhibits back intersystem crossing from the doublet to the quartet excited state and the dominant relaxation process for the doublet excited state is nonradiative decay.

The individual rate constants $k(T)_1$ and $k(T)_2$ (eq. 5.8) were calculated from the pre-exponential factors and the activation energies obtained from the fitting and were found to be $k(T)_1 = (1.6 \pm 1.0) \times 10^7\ s^{-1}$ and $k(T)_2 = (4.5 \pm 1.0) \times 10^6\ s^{-1}$. These two rate constants were then used to obtain an estimate for the efficiency of reverse intersystem crossing, a value of $\eta_{risc} = 0.72 \pm 0.10$. This is slightly higher than the value of η_{risc} = 0.52 which was used in the modeling.

The temperature dependance data obtained for $Cr([18]\text{-}aneN_6)^{3+}$ was also fitted to a two term Arrhenius type function. The plot of ln(k(T)') versus T^{-1} for $Cr([18]\text{-}aneN_6)^{3+}$ was found to be fit quite well by equation 5.8 using the same fitting procedure that was used for $Cr(sen)^{3+}$ (Figure 5.16b). This gave values of $A_1 = (1.2 \pm 0.9) \times 10^{16}\ s^{-1}$ and an activation energy of $E_{a1} = 42 \pm 1$ kJ mol^{-1} for the process associated with back intersystem crossing from the doublet to the quartet excited state, and $A_2 = (1.1 \pm 0.7) \times 10^{14}\ s^{-1}$ and an activation energy of 33 ± 1 kJ mol^{-1} for the process associated with nonradiative deactivation of the doublet excited state.

5.3 Photostereochemistry of $Cr(sen)^{3+}$

The chelating nature of the sen ligand gives rise to two stereoisomers when complexed to a Cr(III) metal ion. These two enantiomers of $Cr(sen)^{3+}$ labeled Λ and Δ,

corresponding to left-handed and right-handed "propellers", are depicted in Figure 5.17. Theoretical examination of the photoaquation reaction of each of these two isomers leads to the identification of three possible outcomes for the photoreaction to $Cr(senH)H_2O^{4+}$ product.

1) Substitution of an amine by a water molecule may occur with no ligand migration (pathway a) and therefore no stereochemical change is involved. This would lead to the stereoretentive products: $\Lambda \rightarrow \Lambda$-*cis* and $\Delta \rightarrow \Delta$-*cis* (Here *cis* distinguishes the relationship between the dangling amine arm and the water substituent).
2) Substitution of an amine by water may occur with an associated ligand migration (pathway b) resulting in a change in stereochemistry. This would lead to the optically inactive *trans* aquated product (Here the dangling arm is *trans* to the water substituent).
3) Substitution of an amine by water may involve ligand migration which leads to racemization (pathway c) to give a product which has the opposite stereochemistry to the starting material: $\Lambda \rightarrow \Delta$-*cis* and $\Delta \rightarrow \Lambda$-*cis*.

A detailed study by Cimolino and Linck[151] of the stereochemistry of the photoaquation of the related optically active complex $Cr(en)_3^{3+}$ has shown that the stereochemistry can be used as a probe to investigate the excited state pathway of the photosubstitution reaction. The product distribution for the photoaquation of Λ-$Cr(en)_3^{3+}$ was determined to be 7% Δ-*cis*-$[Cr(en)_2(enH)H_2O)]^{4+}$, 28% Λ-*cis*-$[Cr(en)_2(enH)H_2O)]^{4+}$, and 65% *trans*-$[Cr(en)_2(enH)H_2O)]^{4+}$. These values were obtained by the ion exchange chromatographic separation of the photoproducts from the starting material, and the identification of each of these products by measuring their molar rotations. This product ratio was found to be the same for doublet and quartet irradiation

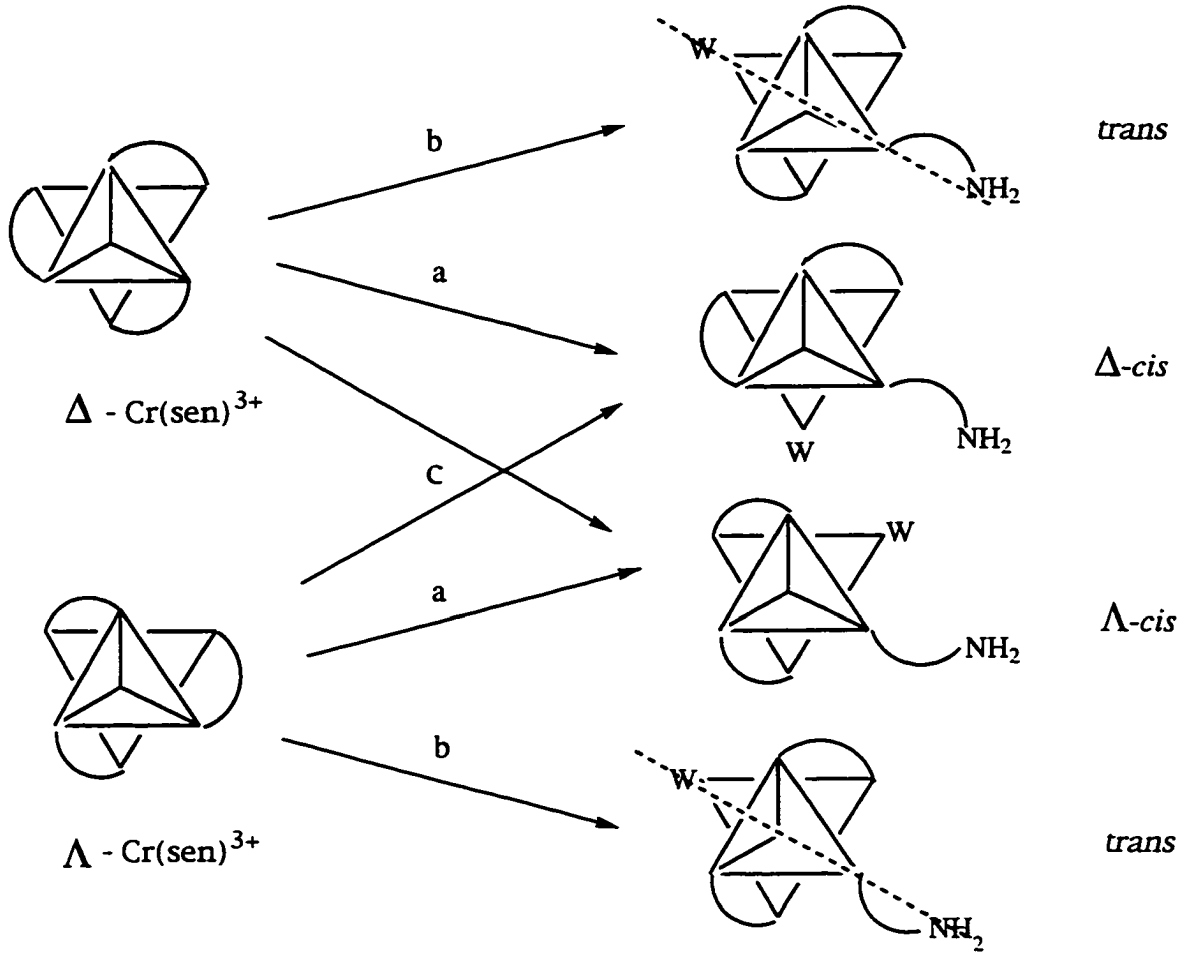

Figure 5.17 Photoreactive pathways of Λ and Δ stereoisomers of $Cr(sen)^{3+}$:
a) stereoretentive, b) stereochemical change, c) racemization.

and contrasted the thermal reaction which gave 100% Λ-*cis*-$[Cr(en)_2(enH)H_2O)]^{4+}$, the stereoretentive product. These results have since been interpreted[58] in terms of the symmetry rules (Section 1.7.4) developed by Vanquickenbourne and Ceulemans[64] and are found to be consistent with the predictions made by this model.

In applying the VC symmetry rules to predict the photoaquation products of $Cr(sen)^{3+}$, it appears that the neopentyl cap of the sen ligand may restrict the number of modes of reaction compared to $Cr(en)_3^{3+}$. A pictorial representation of the photoaquation of Λ-$Cr(sen)^{3+}$ is shown in Figure 5.18. This complex contains six nitrogen donors each of which are equally labilized upon irradiation into the lowest energy quartet state. Three of these nitrogen donors are held in place by the neopentyl cap of the sen ligand framework (denoted by * in Figure 5.18) and therefore will not be expected to be substituted due to the constraints placed on them by the sen ligand. This leaves the remaining three nitrogen donors to be photoaquated. From the symmetry of this complex all three orthogonal planes in which excitation can occur can be treated as equivalent and each plane contains two nitrogen donors which may be dissociated from the chromium metal center. Dissociation and protonation of the nitrogen labeled (1) would not be expected to lead to photoaquated product. One of the trans edges of the ground state trigonal bipyramidal intermediate which is formed is blocked by the in-plane ethylenediamine component of the ligand while the other trans edge contains two nitrogens both held in place by the neopentyl cap of the sen ligand. Due to the constraints placed on them by the ligand, neither of these two donors can undergo the required ligand motion to allow for the substitution of a water molecule. Loss of the nitrogen donor labeled (2) would result in a ground state trigonal bipyramidal intermediate which can undergo the process of edge displacement at only one of its two edges trans to the leaving group, in the plane of the vacant t_{2g} and occupied e_g orbitals. This would lead to the optically inactive *trans*-$[Cr(senH)H_2O]^{4+}$ product. The other trans edge contains two nitrogen donors which are both held in place by the neopentyl cap of the

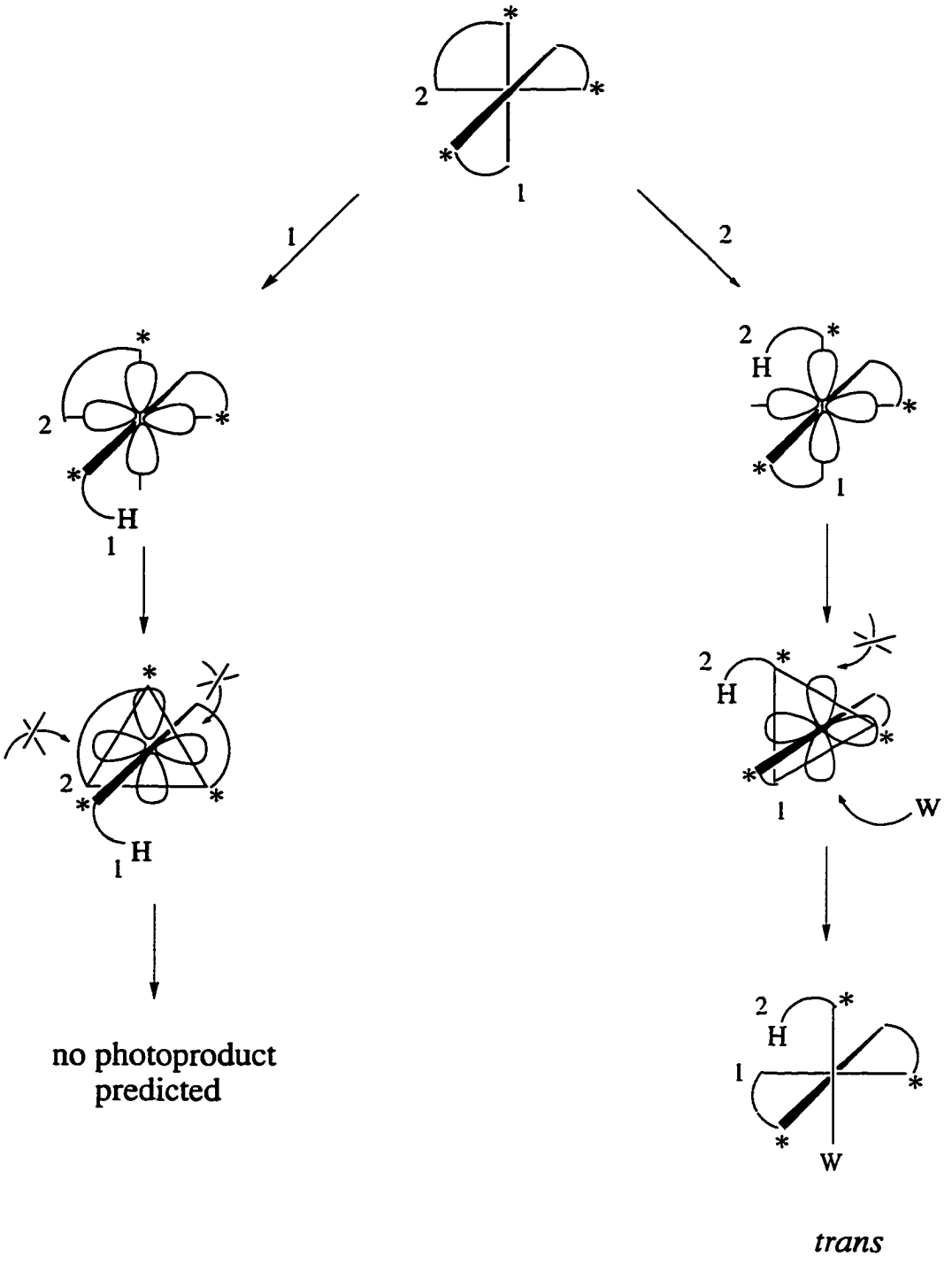

Figure 5.18 Symmetry rules for the photoaquation of Λ-Cr(sen)$^{3+}$ (* denotes donor nitrogen linked to neopentyl cap of the sen ligand).

sen ligand and therefore can not undergo the necessary ligand migration for displacement to occur from this side of the molecule.

Therefore, the symmetry rules established by VC theory would predict that the photoaquation of the stereoisomers of $Cr(sen)^{3+}$, Λ-$Cr(sen)^{3+}$ and Δ-$Cr(sen)^{3+}$, should produce only one photoproduct, *trans*-$[Cr(senH)H_2O]^{4+}$, and that there should be a loss of optical activity associated with the photolysis.

5.3.1 Resolution of Λ and Δ Stereoisomers of $Cr(sen)^{3+}$

In order to investigate the photoaquation of Λ-$Cr(sen)^{3+}$ and Δ-$Cr(sen)^{3+}$ the stereoisomers had to first be resolved from a racemic mixture, obtained from the synthesis of $Cr(sen)^{3+}$. Attempts were made to separate the Λ and Δ isomers of $Cr(sen)^{3+}$ on a Sephadex ion-exchange column by addition of the resolving agent d-tartrate^{2-} to the aqueous eluent. This technique has been used successfully to separate the stereoisomers Λ-$Co(sen)^{3+}$ and Δ-$Co(sen)^{3+}$.[152] The d-tartrate ion forms a unique face-to-face close contact interaction, through hydrogen bonding, with the Λ-$Co(sen)^{3+}$ stereoisomer which results in the chiral discrimination necessary to separate the two isomers on the ion exchange column. For $Cr(sen)^{3+}$ however, a single band containing both isomers was observed to move down the Sephadex column, when eluting with 0.1 M Na_2-d-tartrate, and the Λ and Δ forms remained unresolved. This chromatographic separation was also attempted using the resolving agent antimony-d-tartrate (Sb-d-tartrate^{2-}, 0.1 M). The Sb-d-tartrate^{2-} ion has been shown to be more effective than d-tartrate^{2-} at separating the isomers of $Co(en)_3^{3+}$ due to a larger difference between the association constants of the ion pairs (K_Λ and K_Δ) formed.[153,154] It was hoped that this would also be true for $Cr(sen)^{3+}$, but unfortunately the isomers Λ-$Cr(sen)_3^{3+}$ and Δ-$Cr(sen)_3^{3+}$ still remained

unresolved on the Sephadex column when an eluent containing 0.1 M Sb-d-tartrate^{2-} was used.

The stereoisomers of Cr(sen)$^{3+}$ were instead separated by the formation and selective crystallization of their diastereomers following a procedure by Galsbol[155] which has been used for the separation of the isomers Λ-Cr(en)$_3^{3+}$ and Δ-Cr(en)$_3^{3+}$. In this case, the Δ enantiomer of Cr(en)$_3^{3+}$ was found to form the less soluble diastereomer with the d-tartrate^{2-} ion and precipitated out first. The less soluble diastereomer was identified as the (+)$_D$-form, where (+)$_D$ indicates that this isomer has a positive optical rotation at the sodium D line (λ = 589 nm). The success of the enantiomeric separation of [Cr(sen)]Cl$_3$ was established by measuring the optical rotation of an aqueous solution of the two isomers. The wavelength dependence of the optical rotation [α] (also known as the optical rotary dispersion (ORD)) of these two enantiomers is shown in Figure 5.19. The optical rotation is given by the following equation:

$$[\alpha] = \frac{\alpha}{c\ L} \tag{5.6}$$

where α is the rotation (measured in degrees), c is the concentration (g mL^{-1}), and L is the pathlength of the polarimeter cell (10 cm). Figure 5.18 shows that the resolution of the (-)$_D$-isomer was not as good as that obtained for the (+)$_D$-isomer. The dashed line represents the expected values for the optical rotation for the (-)$_D$-isomer if the optical purity had been the same as obtained for the (+)$_D$-isomer. Table 5.3 compares the measured optical rotation of the two stereoisomers of Cr(sen)$^{3+}$ to the literature values for the stereoisomers of Cr(en)$_3^{3+}$.

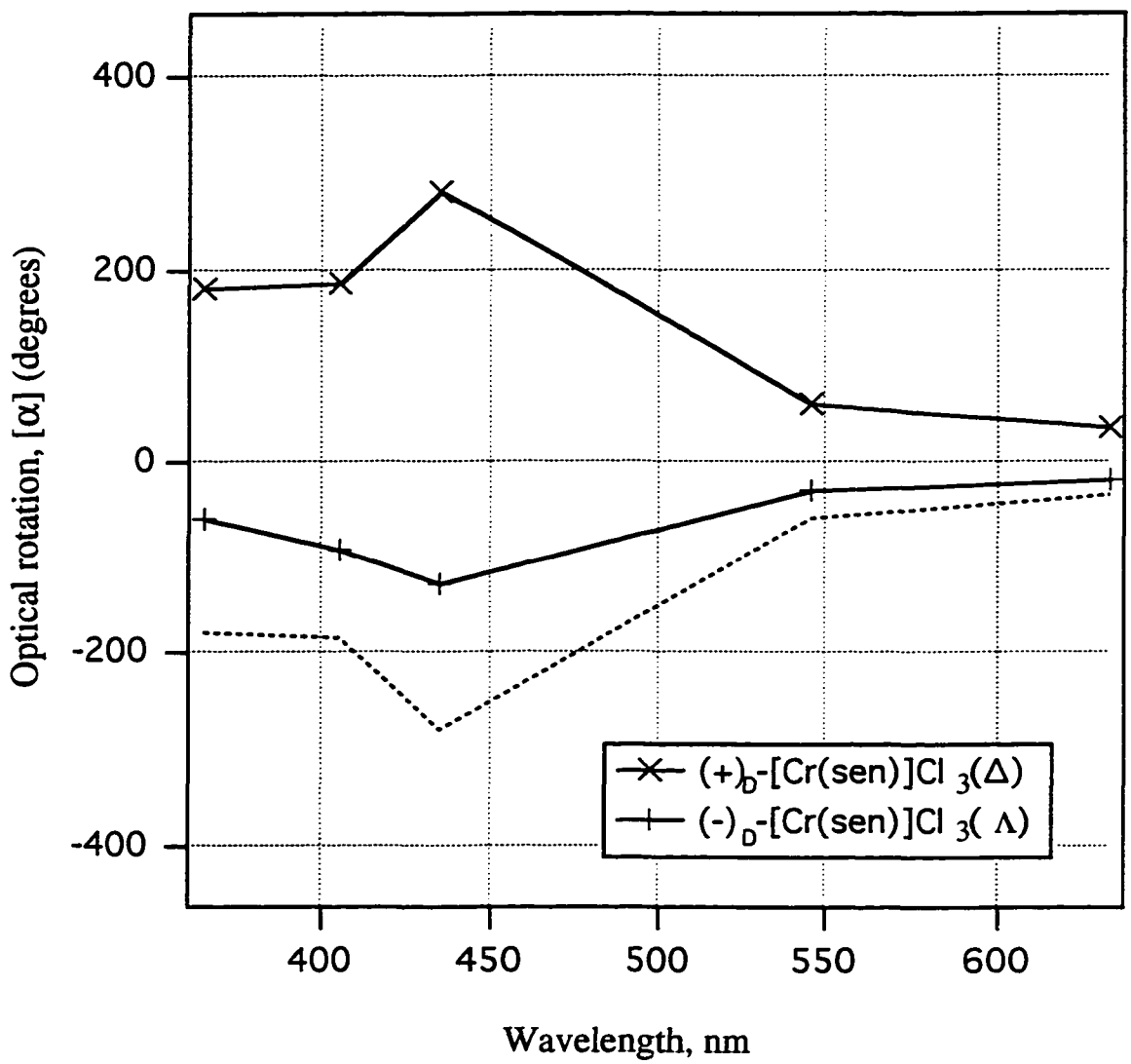

Figure 5.19 Optical rotary dispersion (ORD) of the stereoisomers $(+)_D$-$[Cr(sen)]Cl_3$ and $(-)_D$-$[Cr(sen)]Cl_3^{3+}$.

Table 5.3 Optical rotational values [α] (a = this work).

Complex	365 nm	405 nm	435 nm	546 nm	589 nm	633 nm	ref.
$(+)_D$-$[Cr(sen)]Cl_3$	180	186	281	60	43	35	a
$(-)_D$-$[Cr(sen)]Cl_3$	-60	-65	-127	-30	-22	-19	a
$(+)_D$-$[Cr(en)_3]Cl_3$	-829	-	-	223	103	-	155
$(-)_D$-$[Cr(en)_3]Cl_3$	810	-	-	-218	-122	-	155

By analogy to the assignments of Δ and Λ made for $Cr(en)_3^{3+}$, the isomer $(+)_D$-$[Cr(sen)]Cl_3$, obtained as the less soluble diastereomer which formed with the d-tartrate^{2-} ion, would be assigned as the Δ-$[Cr(sen)]Cl_3$ stereoisomer, while $(-)_D$-$[Cr(sen)]Cl_3$, the more soluble isomer, would be assigned as the Λ–$[Cr(sen)]Cl_3$ stereoisomer.

5.3.2 HPLC Product Analysis for the Photolysis and Thermolysis of $Cr(sen)^{3+}$

Aqueous solutions of the stereoisomers Δ-$[Cr(sen)]Cl_3$ and Λ-$[Cr(sen)]Cl_3$, and racemic $[Cr(sen)]Cl_3$ (~ 2 x 10^{-2} M, in 0.01 M $HClO_4$) were photolysed by irradiation at a wavelength of λ = 488 nm (laser power ~ 10 mW), with constant stirring. Conversion of the starting material to photoproducts was kept to less than 10% to minimize any secondary photolysis. Changes in the UV-Vis spectrum were recorded over irradiation intervals of 1, 5, 10, and 15 minutes and a typical UV-Vis spectrum of the absorbance changes is shown in Figure 5.20, for the photolysis of the racemic $[Cr(sen)]Cl_3$ solution.

Analysis of the photoproducts formed in the photolysis reaction was carried out using a modification of a reversed-phase HPLC chromatography technique[156] which employs the ion interaction reagent butanesulfonate, incorporated into the eluent. This technique has been used successfully to separate cationic metal complexes having charges ranging from 1+ to 5+.[157] [158,159] It was thought that addition of the resolving agent d-tartrate^{2-} (50 mM) to the eluent might also provide the necessary chiral discrimination to resolve the optically active forms of both $Cr(sen)^{3+}$ and its photoproduct(s) on the HPLC column. Injection (50 μL) of an aqueous solution gave a peak having a retention time of ~ 8 minutes. This peak was broad and had a definite shoulder in the case of the racemic mixture of $[Cr(sen)]Cl_3$ (t_R = 8.6 minutes) and was much narrower and sharper when the resolved isomers Δ-$[Cr(sen)]Cl_3$ and Λ-$[Cr(sen)]Cl_3$ were injected. The Λ-isomer was

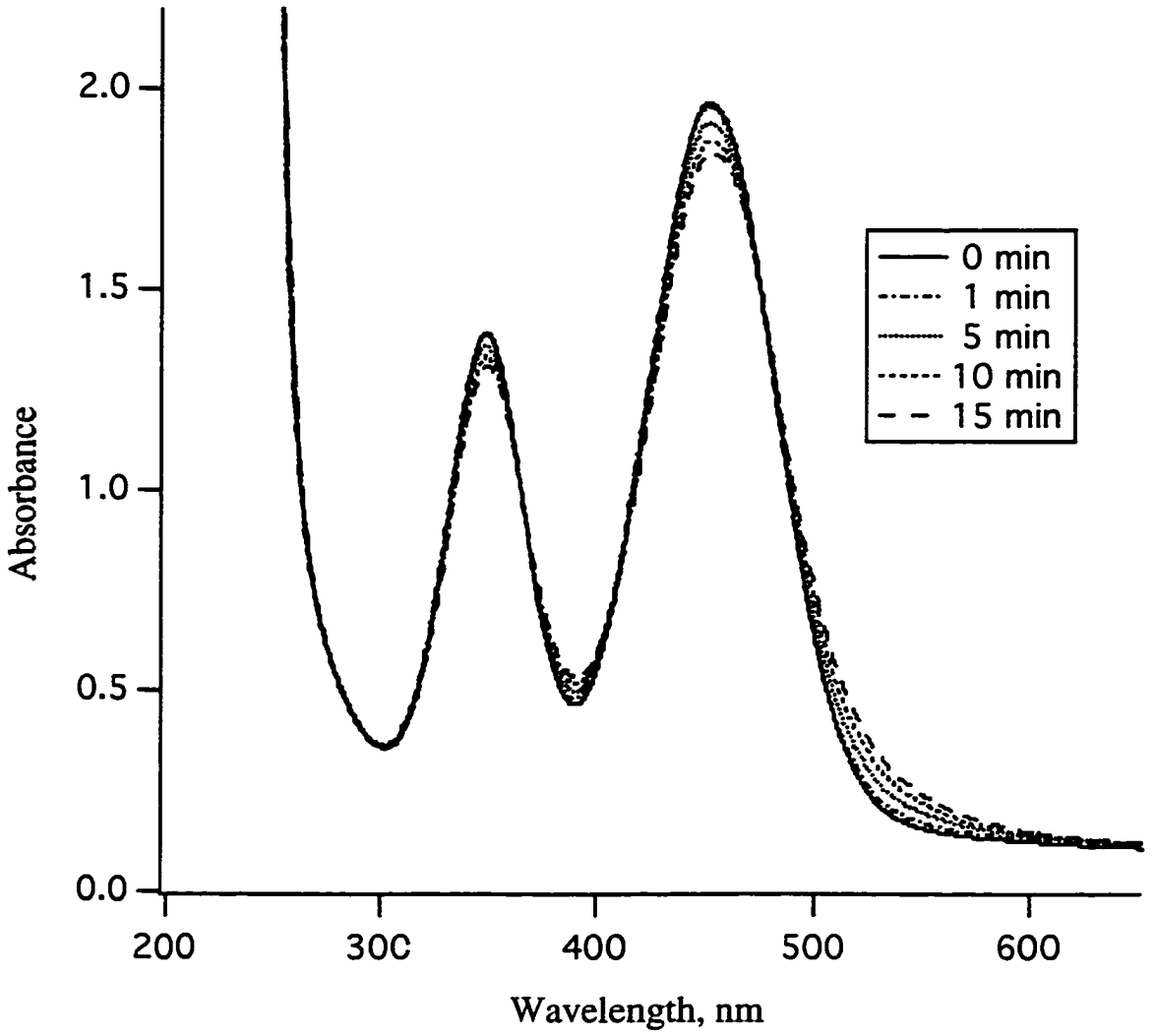

Figure 5.20 Absorbance changes in the UV-Vis spectrum for the photolysis of a racemic mixture ($\Lambda + \Delta$) of $[Cr(sen)]Cl_3$ (2×10^{-2} M) at an irradiation wavelength of $\lambda = 488$ nm.

found to elute first and had a slightly shorter retention time (t_R = 8.4 minutes) than the Δ-isomer (t_R = 8.8 minutes). This indicated that some resolution of the stereoisomers had been achieved by adding d-tartrate^{2-} to the eluent. As the photolysis of these complexes proceeded three new peaks were seen to develop which corresponded to the formation of at least three photoproducts, all of which eluted faster than the parent complex. Similar results were obtained regardless of whether the complex being photolysed was Δ-[Cr(sen)]Cl_3, Λ-[Cr(sen)]Cl_3, or racemic [Cr(sen)]Cl_3. The HPLC chromatograms for the photolysis of these three compounds are shown in Figures 5.22-24. The areas of each of the photoproduct peaks, eluting at t_R = 3.4, 3.9, and 5.6 minutes respectively, were measured as a function of irradiation time and showed that the three photoproducts peaks were being formed in a ratio of 1 : 1 : 2 (assuming all of the photoproducts have the same molar absorptivities at λ = 250 nm). To aid in the identification of the photoproducts which corresponded to these three chromatographic peaks, the corresponding thermal reactions were carried out. Aqueous solutions of the stereoisomers Δ-[Cr(sen)]Cl_3 and Λ-[Cr(sen)]Cl_3, and racemic [Cr(sen)]Cl_3 (~ 2 x 10^{-2} M, in 0.01 M $HClO_4$) were heated to 70 °C using a quartz cell (1 cm) in a thermostated cell holder. These solutions were rigorously kept in the dark to ensure that no unwanted photoreaction occurred. After 1, 5, 10, and 15 minutes of thermolysis the UV-Vis spectrum was recorded and a sample (50 μL) was injected into the HPLC chromatograph. A representative UV-Vis spectrum, showing the absorbance changes for the thermolyisis of a racemic mixture of [Cr(sen)]Cl_3, is given in Figure 5.21. The chromatograms for the thermal reactions (Figures 5.22-24) all show the development of the peak at t_R = 5.6 minutes and the absence of the other two peaks at t_R = 3.4 and t_R = 3.9 minutes. The peak at t_R = 5.6 minutes was found to be significantly broader in the case of the thermal reaction regardless of whether the resolved complexes or the racemic complex was thermolysed. The thermal reaction is expected to proceed with complete stereoretention and for this reason the peak at t_R = 5.6 minutes can be identified as the stereoretentive product: Δ-*cis*-Cr(senH)H_2O^{4+} for the thermolysis of

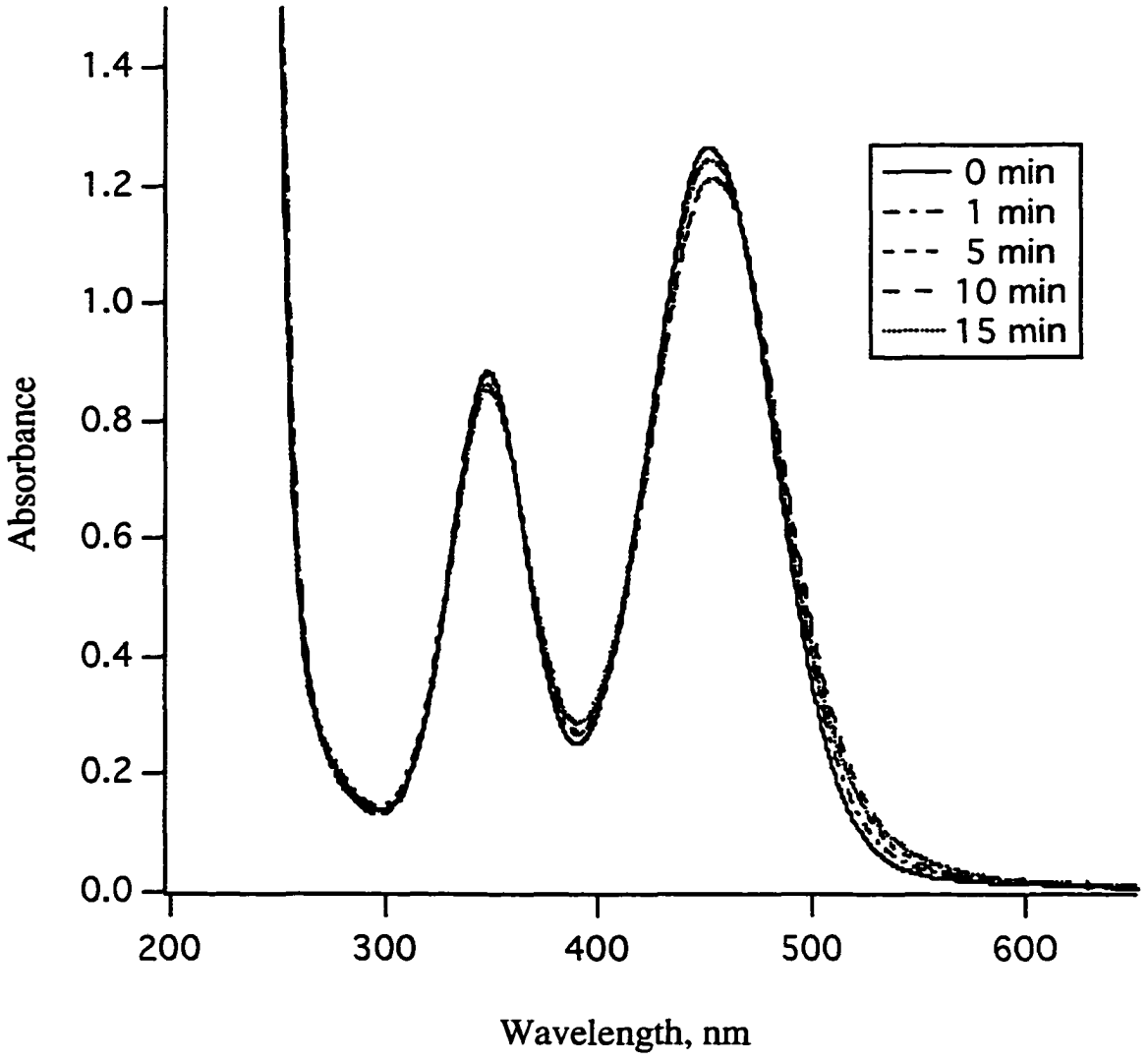

Figure 5.21 Absorbance changes in the UV-Vis spectrum for the thermolysis of a racemic mixture ($\Lambda + \Delta$) of $[Cr(sen)]Cl_3$ (2×10^{-2} M) at 70 °C.

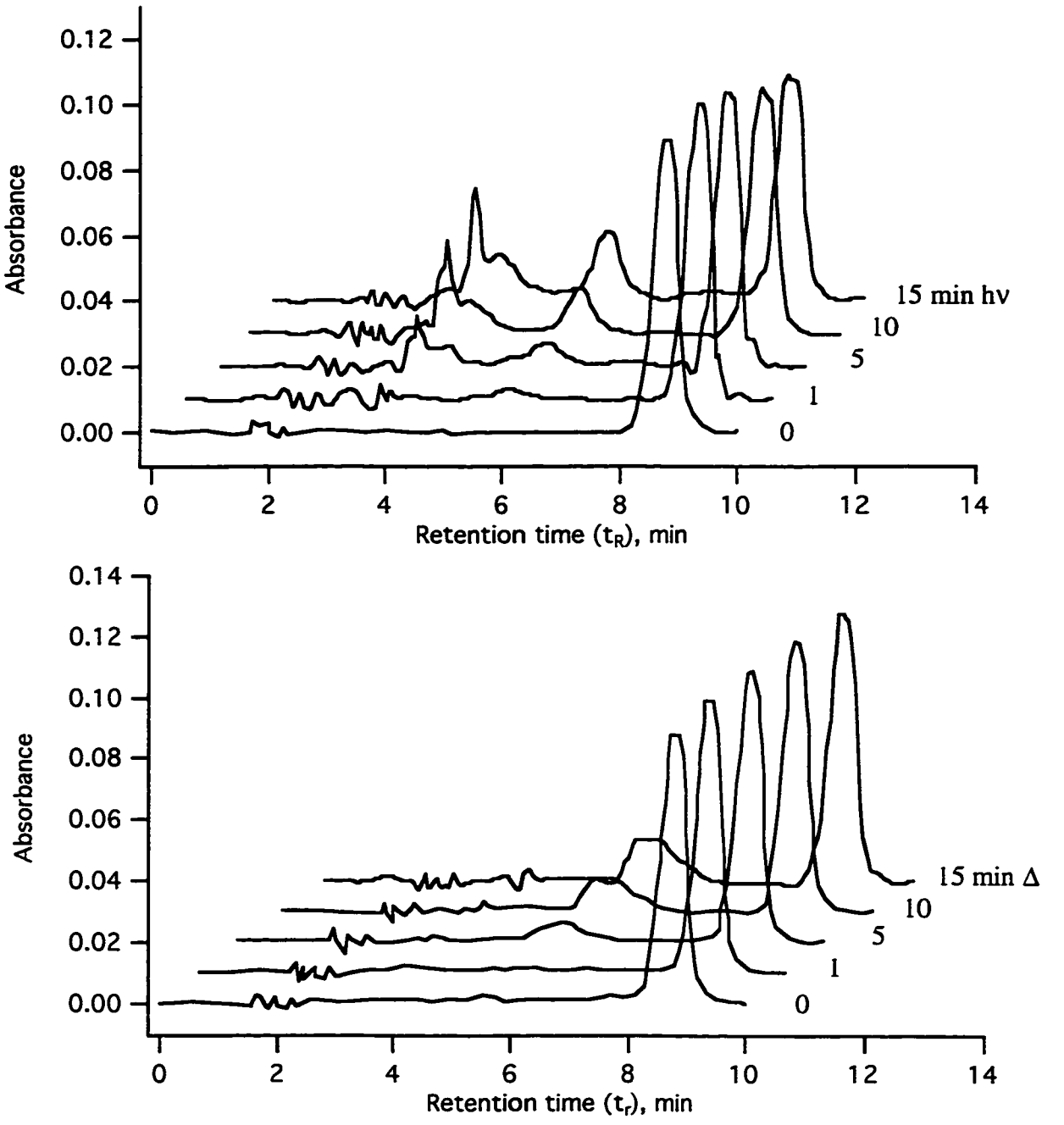

Figure 5.22 HPLC chromatograms: a) photolysis and b) thermolysis of a racemic mixture (Λ + Δ) of $[Cr(sen)]Cl_3$ (2×10^{-2} M). Conditions: eluent: 25 mM butanesulfonate, 25 mM triethylamine, 25 mM d-tartaric acid in 7.5 % MeOH at pH 3.6; Flow rate: 1.5 mL min^{-1}; detection wavelength: $\lambda = 250$ nm .

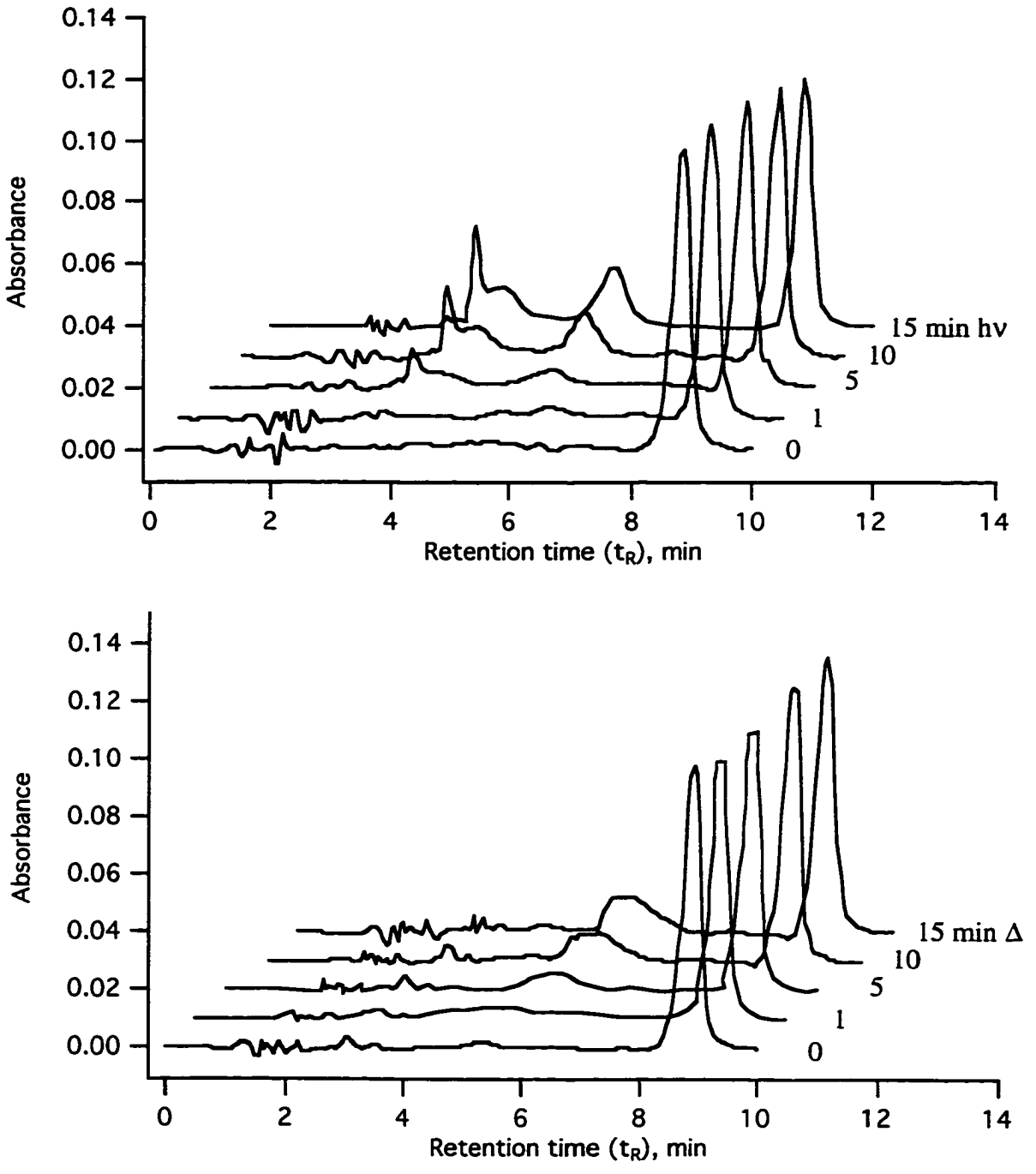

Figure 5.23 HPLC chromatograms: a) photolysis and b) thermolysis of Δ-[Cr(sen)]Cl_3 (2×10^{-2} M). Conditions: eluent: 25 mM butanesulfonate, 25 mM triethylamine, 25 mM d-tartaric acid in 7.5 % MeOH at pH 3.6; Flow rate: 1.5 mL min^{-1}; detection wavelength: $\lambda = 250$ nm .

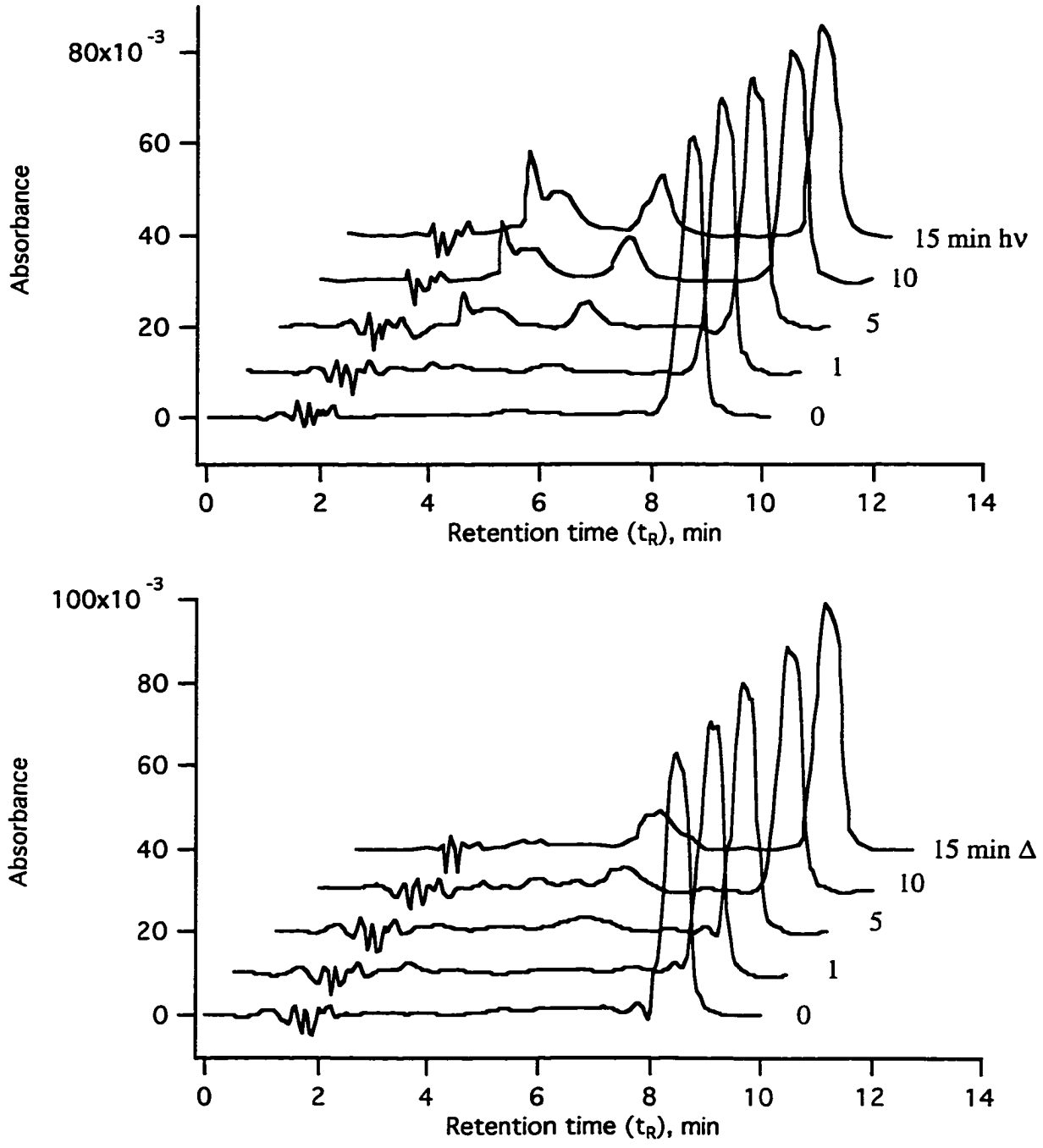

Figure 5.24 HPLC chromatograms: a) photolysis and b) thermolysis of Λ-[Cr(sen)]Cl_3 (1 x 10^{-3} M). Conditions: eluent: 25 mM butanesulfonate, 25 mM triethylamine, 25 mM d-tartaric acid in 7.5 % MeOH at pH 3.6; Flow rate: 1.5 mL min^{-1}; detection wavelength: $\lambda = 250$ nm .

Δ-[Cr(sen)]Cl_3, Λ-*cis*-Cr(senH)H_2O^{4+} for the thermolysis of Λ-[Cr(sen)]Cl_3, and a mixture of both Λ-*cis*-Cr(senH)H_2O^{4+} and Δ-*cis*-Cr(senH)H_2O^{4+} isomers for the thermolysis of the racemic mixture of [Cr(sen)]Cl_3. Unfortunately, the isomers Λ-*cis*-Cr(senH)H_2O^{3+} and Δ-*cis*-Cr(senH)H_2O^{4+} were not resolved by this HPLC technique and for this reason no conclusion can be drawn as to whether this photoreaction was occurring stereoretentively or whether photoracemization was occurring: Δ-Cr(sen)$^{3+}$ → Δ-*cis*-Cr(senH)H_2O^{4+}, Λ-Cr(sen)$^{3+}$ → Λ-*cis*-Cr(senH)H_2O^{4+}. It is surprising that the peak at t_R = 5.6 min. is observed at all in the photolysis reactions. According to the symmetry rules outlined in Figure 5.18, neither the Δ-*cis*-Cr(senH)H_2O^{4+} nor the Λ-*cis*-Cr(senH)H_2O^{4+} products are allowed by VC theory. Of the additional two peaks formed in the photolysis reaction, one a sharp peak at t_R = 3.4 min. and the other a broad peak at t_R = 3.9 min. (both absent in the thermolysis reaction), one of these peaks can be assigned to the predicted photoproduct *trans*-Cr(senH)H_2O^{3+} while the other peak is left unassigned.

5.3.3 Optical Rotation Studies for the Photolysis and Thermolysis of Cr(sen)$^{3+}$

The effect of both thermal and photoaquation on the optical rotation [α] was investigated. An aqueous solution of Δ-[Cr(sen)]Cl_3 (~ 1 x 10^{-2} M in 0.01 M $HClO_4$) was either irradiated at a wavelength of 488 nm or heated at 70 °C and the value of [α] was monitored as a function of time. Both the photolysis and the thermolysis reactions were carried out in a 1 cm quartz cell, with stirring. The solution was then transferred to a micropolarimeter cell and the optical rotation was measured using a polarimeter. In the case of the thermal reaction the optical rotation, [α], was found to remain constant at all wavelengths (633, 589, 546, 435, 405, 365 nm) over 30 minutes of thermolysis at 70 °C.

This is consistent with the expectation that the thermal reaction should be stereoretentive and indicates that the starting material Δ-[Cr(sen)]Cl_3 and the thermal aquo product Δ-*cis*-Cr(senH)H_2O^{4+} have similar optical rotations. When Δ-[Cr(sen)]Cl_3 was photolysed the optical rotation was found to decrease with irradiation time. This is shown in Figure 5.25. The loss of optical rotation associated with the photoaquation reaction is consistent with the formation of the optically inactive *trans*-Cr(senH)H_2O^{4+} product. The loss of optical rotation may also be the result of photoracemization of $Cr(sen)^{3+}$, but because this HPLC technique did not result in sufficient separation of the stereoisomers of the photoproducts this can not be determined with certainty.

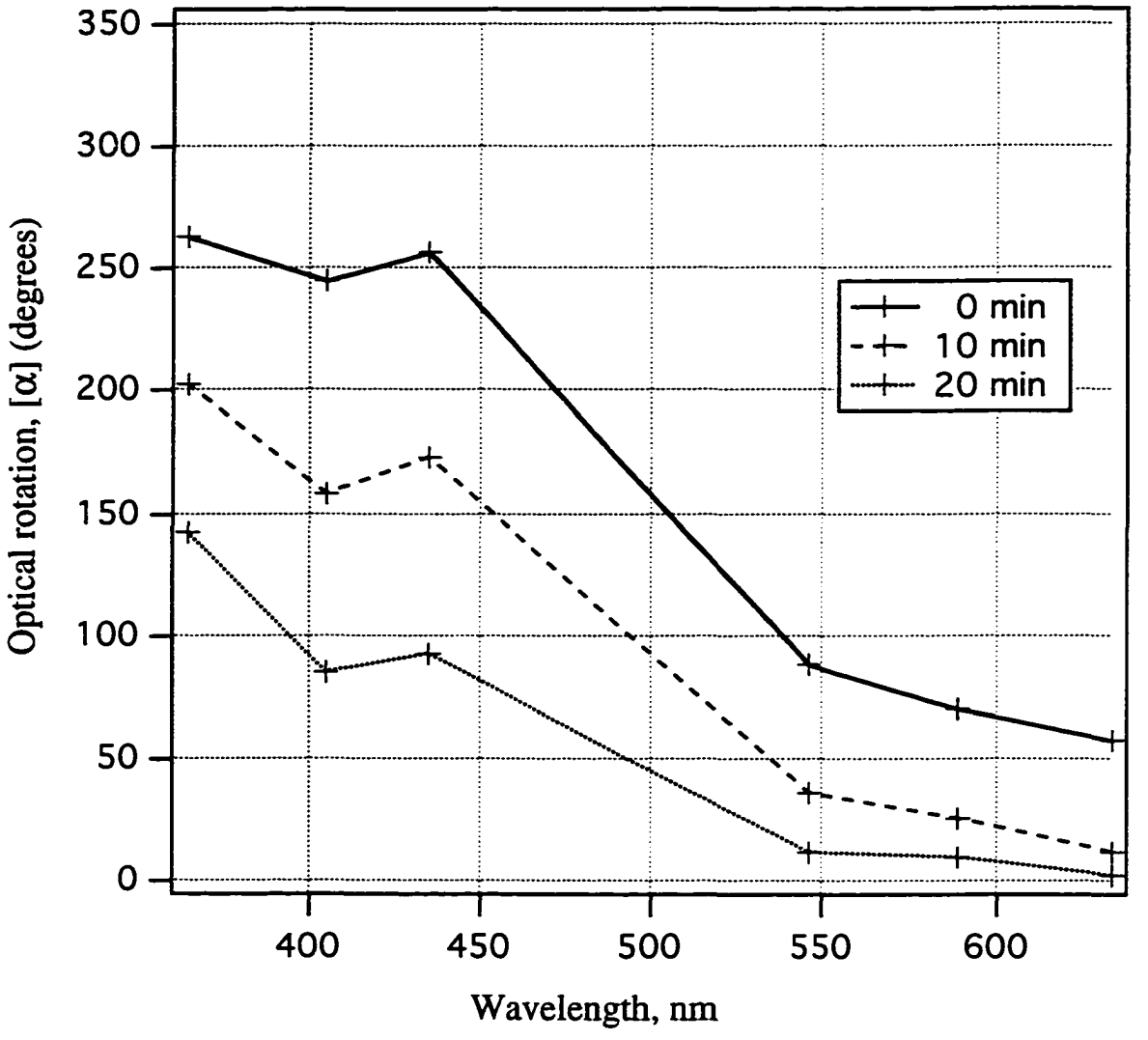

Figure 5.25 Changes in optical rotation of Δ-[Cr(sen)]Cl_3 (1 x 10^{-2} M in 0.01 M $HClO_4$) with photolysis at an irradiation wavelength of $\lambda = 488$ nm.

5.4 Discussion

The complex $Cr([18]\text{-}aneN_6)^{3+}$ provides a further example of the effects that a coordinated ligand can have on Cr(III) photochemical and photophysical behavior. The unreactive nature of this complex ($\emptyset_{rxn} < 1.0 \times 10^{-3}$) likely results from there being no primary nitrogen which can easily dissociate from the metal ion center. Any photoreaction would involve the dissociation of a secondary nitrogen which is linked through two positions to the macrocyclic ring. This is shown in Figure 5.26 from the structure generated using the modeling program Chem-3D (CambridgeSoft). The hydrogen atoms are left off for clarity. The hypothetical photoproduct $Cr([18]\text{-}aneHN_6)H_2O^{4+}$ was found to minimize with a strain energy of 268 kJ mol^{-1}, which is lower than the strain energy of 345 kJ mol^{-1} calculated for the parent $Cr([18]\text{-}aneN_6)^{3+}$ complex. The secondary nitrogen labeled N_B is dissociated to allow for the incoming water molecule (W) and nitrogen N_A migrates from position A to position B.

The results obtained for direct irradiation into the doublet excited state of $Cr(sen)^{3+}$ may help to elucidate the excited state deactivation processes involved in these Cr(III) complexes. A model can be suggested in which there are two competitive processes deactivating the doublet excited state: nonradiative decay directly to the ground state, and reverse intersystem crossing from the doublet excited state to the quartet excited state. The possibility of several different mechanisms (decay channels) contributing to k(T), the thermally activated doublet decay rate constant, has been suggested in the study of several families of Cr(III) complexes.[160] Waltz et al.[161-163] has shown that studies of the effects of solvent, temperature, and pressure on the spectroscopic, photophysical, and photochemical properties of Cr(III) complexes, to determine such parameters as volumes of activation ($\Delta V^{\ddagger}$) and solvent dependencies, can provide an effective manner in which to determine the relative importance of competitive decay processes. This has provided evidence for reverse intersystem crossing, non-radiative decay, and in the case of *cis*-

$Cr(cyclam)(NH_3)_2^{3+}$ the formation of an intermediate as important deactivation pathways. Undoubtedly, the decay channel that dominates will be different in different classes of complexes and there will be some complexes in which two or more pathways may contribute, as is suggested here for $Cr(sen)^{3+}$.

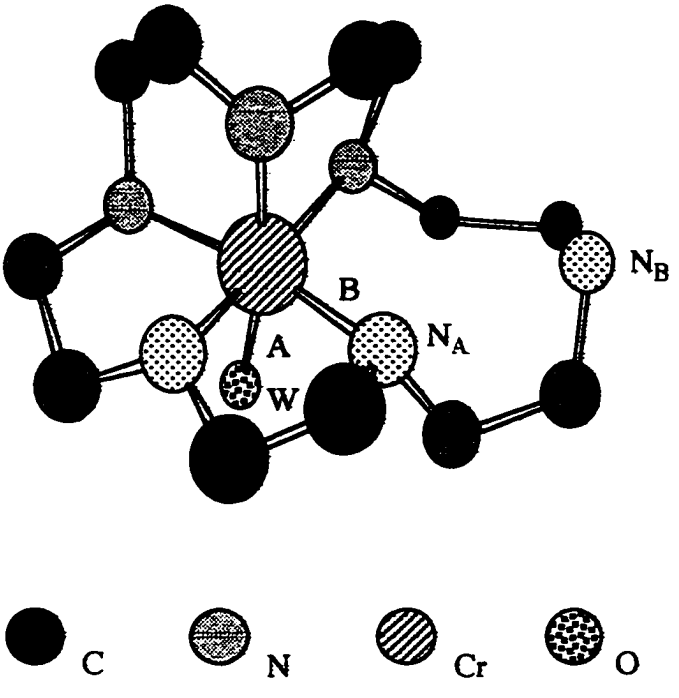

Figure 5.26 Model generated using Chem-3D for the theoretical photoproduct $Cr([18]\text{-ane}HN_6)H_2O^{4+}$ (W = water).

The photostereochemical study of $Cr(sen)^{3+}$ has shown that using symmetry rules to predict the photoproducts of this complex, such as those given by the Vanquickenbourne and Ceuleman's theory, can be more complicated than anticipated. In the case of $Cr(sen)^{3+}$ the predicted photochemistry, based on octahedral symmetry, may be an over simplification of the actual situation and it may be necessary to account for the true symmetry of the complex in order to explain all of the photochemical products formed. The identification of three photoproduct peaks from the HPLC chromatograms of the photolysis of $Cr(sen)^{3+}$ corresponds to the formation of at least four photoproducts. Three of the possible photoproducts can be assigned as Λ-*cis*-$Cr(senH)H_2O^{4+}$, Δ-*cis*-$Cr(senH)H_2O^{4+}$, and *trans*-$Cr(senH)H_2O^{4+}$. The isomers Λ-*cis*-$Cr(senH)H_2O^{4+}$, Δ-*cis*-$Cr(senH)H_2O^{4+}$ were not resolved by the HPLC chromatographic technique and correspond to one of the three photoproduct peaks while *trans*-$Cr(senH)H_2O^{4+}$ corresponds to the other. This leaves one photoproduct peak unassigned. The additional photoproduct might arise from the dissociation of one of the secondary donor nitrogen of the sen ligand. Figure 5.27 shows the model generated using Chem-3D for the hypothetical photoproduct $Cr(senH)H_2O^{4+}$, formed by the dissociation of one of the secondary nitrogen donors (N_B) followed by a migration of the sen ligand (the primary nitrogen labeled N_A moves from position A to position B) associated with the addition of the incoming water molecule (W). This ligand migration would result in the formation of a 9-member ring within the photoproduct which would include the chromium metal center and the protonated amine. This structure was found to minimize with a strain energy of 212 kJ mol^{-1} which is just slightly greater than the strain energy of 194 kJ mol^{-1} calculated for the parent $Cr(sen)^{3+}$ complex. While there is currently no experimental evidence to verify the formation of this complex (a difficult task that would require its chromatographic isolation followed by a crystal structure determination) it does, however, provide a possible explanation as to how a fourth photoproduct could be obtained from the photolysis of $Cr(sen)^{3+}$.

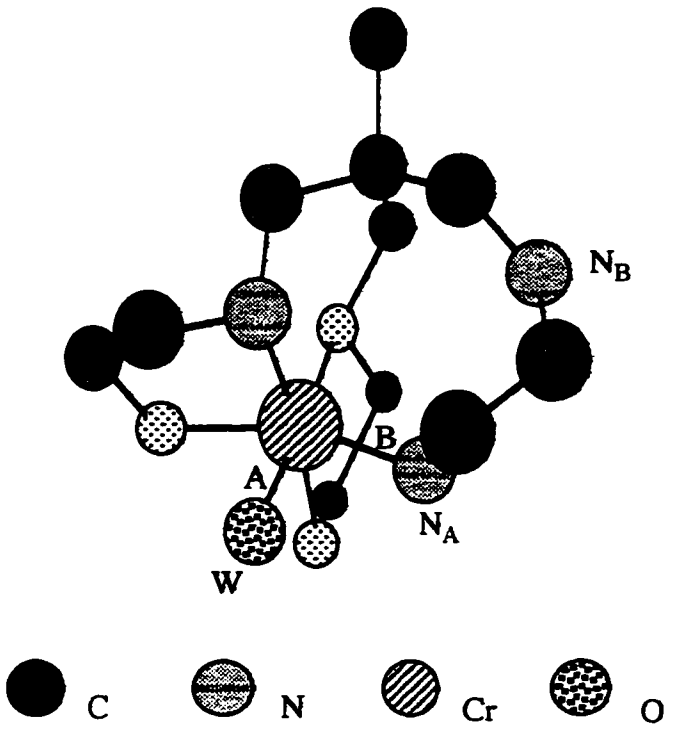

Figure 5.27 Model generated using Chem-3D for the theoretical photoproduct $Cr(senH)H_2O^{4+}$, formed from the dissociation of a secondary nitrogen donor (N_B), W = water.

5.5 Conclusions

The photophysical and photochemical properties of the macrocyclic complex $Cr([18]\text{-}aneN_6)^{3+}$ has been investigated, along with the complex $Cr(sen)^{3+}$, and compared with the behavior of other Cr(III) hexaam(m)ine complexes.

The macrocyclic complex $Cr([18]\text{-}aneN_6)^{3+}$ was found to be unreactive, and an upper limit for the quantum yield for reaction of this complex was estimated to be $\emptyset_{rxn} = 1.0 \times 10^{-3}$. The complex $Cr([18]\text{-}aneN_6)^{3+}$ was found to have similar photophysical properties to the photoreactive complex $Cr(sen)^{3+}$ and this included having an unusually short room temperature emission lifetime: estimated to be 17 ns (293 K) for $Cr([18]\text{-}aneN_6)^{3+}$ and 0.6 ns (293 K) for $Cr(sen)^{3+}$. The short ambient emission lifetime of $Cr([18]\text{-}aneN_6)^{3+}$ contradicts a model proposed by Endicott which ascribes the unusually short emission lifetime of $Cr(sen)^{3+}$ to a thermally activated nonradiative decay channel from the doublet excited state to the ground state, facilitated by trigonal distortion in the complex imposed by the coordination of the ligand. In the case of $Cr([18]\text{-}aneN_6)^{3+}$ the short emission lifetime may be explained by a distortion in which the octahedral molecule is "flattened", rather than being the result of a trigonal distortion.

The photoreactivity of $Cr(sen)^{3+}$ was verified and the quantum yield for reaction, $\emptyset_{rxn} = 0.10 \pm 0.01$, was measured (for irradiation into the quartet absorption band) which is in good agreement with the published value. Direct irradiation into the doublet absorption band of $Cr(sen)^{3+}$ at $\lambda = 675$ nm produced a decrease in quantum yield, $\emptyset_{rxn} = 0.08 \pm 0.01$. This result can be explained in terms of a model in which there are two competitive processes deactivating the doublet excited state; reverse intersystem crossing to the quartet excited state with an efficiency $\eta_{risc} = 0.52$, and nonradiative decay back to the ground state. By fitting the temperature dependence data of the emission lifetime for $Cr(sen)^{3+}$ to a two term Arrhenius equation, estimates for the activation energies of these two processes, 45 ± 1 kJ mole^{-1} and 29 ± 1 kJ mole^{-1} respectively, were obtained. The

temperature dependence data of the emission lifetime for $Cr([18]\text{-}aneN_6)^{3+}$ were also fit to a two term Arrhenius equation and this gave estimates for the activation energies of 42 ± 1 kJ $mole^{-1}$ and 33 ± 1 kJ $mole^{-1}$ respectively, for the two competitive processes of nonradiative decay and reverse intersystem crossing, deactivating the doublet excited state.

The photostereochemistry of $Cr(sen)^{3+}$ was investigated by following the photoreaction of the racemic complex and the resolved Λ and Δ stereoisomers chromatographically. Attempts to develop an HPLC technique that could be used to separate these stereoisomers using the chiral resolving agent d-$tartrate^{2-}$ was found to produce only limited success in separating the isomers of the starting complex $Cr(sen)^{3+}$, and did not resolve the stereoisomers of the photoproducts. Comparison of the HPLC results, obtained for the photolysis and the thermal reaction of $Cr(sen)^{3+}$, led to the identification of three photoproduct peaks corresponding to the formation of four photoproducts. The formation of this number of photoproducts for the photolysis of $Cr(sen)^{3+}$ can not easily be accounted for by applying the symmetry rules of VC theory.

CHAPTER SIX

CONCLUDING REMARKS AND FUTURE DIRECTIONS

The exceptional properties that macrocyclic ligands can impart on their transition metal ion complexes has been revealed in this study. As new synthetic methodologies are developed it can be expected that the range and complexity of the accessible macrocyclic ligands will increase. For this reason it becomes ever more important to be able to understand, predict, and even control the properties of macrocyclic transition metal complexes. This will undoubtedly lead to important and useful applications of these complexes.

The high dilution conditions used to form the tricyclo[9.14.9]N_6 macrocyclic ligand should be investigated further in order to increase the yield of the tricyclic complex to obtain useful quantities of this material. This may involve identifying a more efficient base to use in the reaction of the bicyclic complex and the bridging ligand. The transition metal complexes of both the *syn* and *anti* isomers of the de-protected form of the tricyclic ligand would yield interesting studies of the effect of ligand structure on coordination geometry, electronic and ESR spectra, and redox processes. This would complement an on going investigation in our laboratory of the properties of two analogous tricyclic ligands tricyclo[12.14.12]N_6 and tricyclo[10.14.10]N_4O_2 (Figure 6.1) and help to determine the effects of varying the donor atom and ring size on the coordination geometry and properties of these complexes. Continuing the search for an efficient synthetic method of mono protecting [10]-aneN_3 could provide a similar synthetic route to another tricyclic complex tricyclo[10.14.10]N_6 (Figure 6.1) which could also be compared to this series of macrocyclic complexes.

The isolation of the *syn* isomer of the tricyclo[9.14.9]N_6 macrocyclic ligand could lead to a novel 'cage-type' complex on bridging the two apical donor nitrogens with a propyl group (Figure 6.2). Here a coordinated transition metal would be encapsulated within the ligand framework and this would undoubtedly produce very interesting coordination geometry and redox properties.

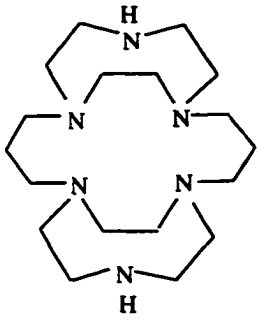

tricyclo[9.14.9]N_6

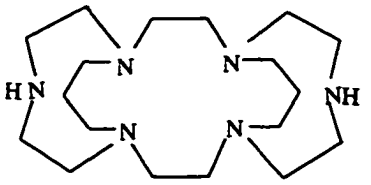

tricyclo[10.14.10]N_6

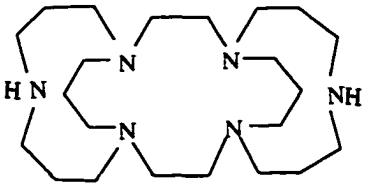

tricyclo[12.14.12]N_6

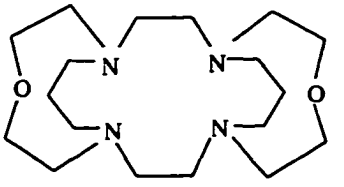

tricyclo[10.14.10]N_4O_2

Figure 6.1 Series of possible tricyclic macrocyclic ligands.

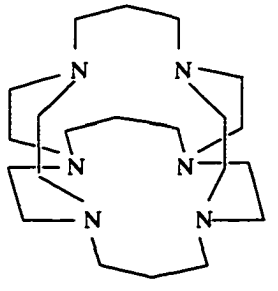

Figure 6.2 Proposed cage complex derived from tricyclo[9.14.9]N_6.

An investigation of the palladium (II) complexes of the bicycloN_5 ligands prepared here is in progress. It is hoped that, in a similar manner to the Ni(II) complexes, these macrobicyclic ligands will impose five coordinate geometry in the palladium(II) complex and stabilize the Palladium(III) oxidation state. This would allow for the study of the substitution kinetics at the open sixth coordination site at the Pd(III) metal centers, a unique situation which has not previously been investigated.

The quenching study involving the Ni(II) macrocyclic complexes provides the first example of the reductive quenching of the excited state of $Pt_2(pop)_4^{4-}$ by a transition metal coordination compound. The rich photochemistry exhibited by the complex $Pt_2(pop)_4^{4-}$ makes it useful tool for researchers to study excited state processes such as electron and energy transfer and it should find even more useful applications in the future.

Identifying more examples of Cr(III) macrocyclic complexes which have short doublet emission lifetimes may add to the growing evidence that photophysical properties can be influenced by the coordination imposed by the ligand. This would include identifying other complexes in which there is a "flattening" of the molecule as this may help to distinguish the effects of other types of distortion from trigonal distortions. Studies of this type may lead to the ultimate goal of being able to tune the photochemical and photophysical properties of Cr(III) complexes. It would be interesting to re-evaluate the photophysical properties of an authenticated sample of the macrocyclic cage complex $Cr(sep)^{3+}$ to verify whether or not this complex has a short ambient doublet excited state lifetime. Several efforts to repeat the synthsis of this complex, however, have been unsuccessful.[164] The formation of the chromium(III) complex of the macrocyclic ligand shown in Figure 6.2 would provide a complex which would have unusual coordination geometry and it would be interesting to compare the properties of this complex with other Cr(III) cage complexes such as $Cr(sar)^{3+}$ and $Cr(diamsar)^{3+}$.

The HPLC results obtained for the photolysis of $Cr(sen)^{3+}$ exemplifies the difficulties involved in a study of this nature. It is hard to design an experiment that

unambiguously identifies the photostereochemical pathways involved in a photoreaction. Further investigation of $Cr(sen)^{3+}$ is required to resolve the exact stereochemical nature of the photoproducts formed. This may require the development of a more sophisticated chromatographic technique, perhaps using a chiral HPLC column, which is capable of unambiguously resolving the stereoisomers of the starting material and the photoproducts and their detection. This may provide the necessary understanding to develop a model which can be used to predict the photoreactivity of constrained Cr(III) complexes of this type.

REFERENCES

(1) Melson, G. A. *Coordination Chemistry of Macrocyclic Compounds*; Plenum: N.Y., **1979**.

(2) Bailar, J. C. In *Coordination Chemistry*; Ed., A. E. M., Ed.; Van Nostrand Reinhold Co., **1971**; Vol. 1.

(3) Hedley, E. P. In *Inorganic Chemistry*; London Press, **1989**.

(4) Moser, F. H.; Thomas, A. L. *Phthalocyanine Compounds*; Reinhold Publishing Corp., **1963**.

(5) Curtis, N. F. *J. Chem. Soc.* **1960**, 4409.

(6) Peterson, C. J. *J. Am. Chem. Soc.* **1967**, *89*, 7017.

(7) Lindoy, L. F. *The Chemistry of Macrocyclic Complexes*; Cambridge University Press: Cambridge, 1989.

(8) Cabbinus, D. K.; Margerum, D. W. *J. Am. Chem. Soc.* **1969**, *91*, 6540.

(9) Micheloni, M.; Paoletti, P.; Lever, A. B. P. *Inorg. Chem.* **1976**, *15*, 1502.

(10) Munro, D. *Chem. Ber.* **1977**, 100.

(11) Kodama, M.; Kimura, E. J. *J. Chem. Soc., Dalton Trans.* **1983**, 2341.

(12) Martel, A. E.; Hancock, R. D.; Motekaitis, R. J. *Coord. Chem. Rev.* **1994**, *133*, 39.

(13) Busch, D. H. *Acc. Chem. Res.* **1978**, *11*, 392.

(14) Billo, E. J. *Inorg. Chem.* **1984**, *23*, 236.

(15) Busch, D. H. *Acc. Chem. Res.* **1978**, *11*, 392 - 400.

(16) Hancock, R. D.; McDougal, G. J. *J. Am. Chem. Soc.* **1980**, *102*, 6551.

(17) Endicott, T. F.; Durham, B. In *Coordination Chemistry of Macrocyclic Compounds*; Melson, G. A., Ed.; Plenum Press: New York, **1979**; pp 393.

(18) Haines, R. I.; McAuley, A. *Coord. Chem. Rev.* **1981**, *39*, 77.

(19) Bosnich, B.; Poon, C. K.; Tobe, M. L. *Inorg. Chem.* **1965**, *4*, 1102.

(20) Barefield, E. K.; Wagner, F.; Herlinger, A. W.; Dahl, A. R. *Inorg. Synth.* **1975**, *16*, 220.

(21) Atkins, T. J.; Richman, J. E.; Öettle, W. F. *Org. Synth.* **1978**, *58*, 86.

(22) Richman, J. E.; Atkins, T. J. J. *J. Am. Chem. Soc.* **1974**, *96*, 2268.

(23) Lehn, J. M. *Pure and Applied Chem.* **1964**, *52*, 2441.

(24) Fortier, D. G.; McAuley, A. *J. Am. Chem. Soc.* **1990**, *112*, 2640.

(25) Benchini, A.; Bianchi, A.; Chimichi, S.; Campomlini, M.; Dapporto, P.; Garci-Espana, E.; Micheloni, M.; Nardi, N.; Paoli, P.; Valtancoli, B. *Inorg. Chem.* **1991**, *30*, 3687.

(26) Wieghardt, K.; Schmidt, W.; Herrmann, W.; Kuppers, H. J. *Inorg. Chem.* **1983**, *25*, 2953.

(27) McAuley, A.; Norman, P. R.; Olubuyide, O. *Inorg. Chem.* **1984**, *23*, 1938.

(28) Balzani, V.; Moggi, L. *Coord. Chem. Rev.* **1990**, *97*, 313-326.

(29) Sykora, J.; Sima, J. *Coord. Chem. Rev.* **1990**, *107*, 1-225.

(30) Balzani, V. *Tetrahedron* **1992**, *48*, 10443-10514.

(31) Balzani, V.; Ballardini, R.; Bolletta, F.; Gandolfi, M. T.; Juris, A.; Maestri, M.; Manfrin, M. F.; Moggi, L.; Sabbatini, N. *Coord. Chem. Rev.* **1993**, *125*, 75-88.

(32) Balzani, V.; Carassiti, V. *Photochemistry of Coordination Compounds*; Acedemic Press: London, **1970**.

(33) Gilbert, A.; Baggott, J.; Wagner, P. J. *Essentials of Molecular Photochemistry*; CRC Press: Boca Raton, Ann Arbor, Boston, London, **1991**.

(34) Lever, A. B. P. *Inorganic Electronic Spectroscopy*; Second ed.; Elsevier: New York, **1984**.

(35) Scandola, F.; Balzani, V. *J. Chem. Educ.* **1983**, *60*, 814-823.

(36) Evans, D. H.; O'Connell, K. M.; Peterson, R. A.; Kelly, M. J. *J. Chem. Educ.* **1983**, *60*, 290-293.

(37) Balzani, V.; Moggi, L.; Manfrin, M. F.; Bolletta, F. *Coord. Chem. Rev.* **1975**, *15*, 321-433.

(38) Balzani, V.; Bolletta, F.; Scandola, F. *J. Am. Chem. Soc.* **1980**, *102*, 2152.

(39) Rehm, D.; Weller, A. *Isr. J. Chem.* **1970**, *8*, 259.

(40) Sutin, N. *Prog. Inorg. Chem.* **1983**, *30*, 441.

(41) Cannon, R. D. *Electron Transfer Reactions*; Butterworth: London, **1980**.

(42) Marcus, R. A. *J. Phys. Chem.* **1965**, *43*, 1261.

(43) Marcus, R. A. *Ann. Rev. Phys. Chem.* **1964**, *15*, 155.

(44) Clark, C.; Hoffman, M. Z. *J. Phys. Chem.* **1996**, *100*, 7526.

(45) Miller, J. R.; Closs, G. L. *J. Am. Chem. Soc.* **1984**, *106*, 3047.

(46) Closs, G. L.; Miller, J. R. *Science* **1988**, *240*, 440.

(47) Wasielewski, M. R.; Niemczuk, M. P. *J. Am. Chem. Soc.* **1984**, *106*, 5043.

(48) Zinato, E. in *Concepts of Inorganic Photochemistry*; eds. W. Adamson and P. Fleischauer, Wiley: New York, **1975**; Vol. Chapt. 4.

(49) Jamieson, M. A.; Serpone, N.; Hoffman, M. Z. *Coord. Chem. Rev.* **1981**, *39*, 121-179.

(50) Hollebone, B. R.; Langford, C. H.; Serpone, N. *Coord. Chem. Rev.* **1981**, *39*, 181-224.

(51) Kirk, A. D. *Coord. Chem. Rev.* **1981**, *39*, 225-263.

(52) Kirk, A. D. *Comments Inorg. Chem.* **1993**, *14*, 89-121.

(53) Adamson, A. W.; Waltz, W. L.; Zinato, E.; Watts, D. W.; Fleischauer, P. D.; Lindholm, R. D. *Chem. Rev.* **1968**, *68*, 541-585.

(54) Endicott, J. F.; Ramasami, T.; Tamilarasan, R.; Lessard, R. B.; Ryu, C. K. *Coord. Chem. Rev.* **1987**, *77*, 1-87.

(55) Garner, C. S.; House, D. A. In *Transition Metal Chemistry*; Carlin, R. L., Ed.; Marcel Dekker Inc.: New York, **1970**; Vol. 6; pp 59-295.

(56) Mønsted, L.; Mønsted, O. *Coord. Chem. Rev.* **1981**, *94*, 109.

(57) Fleischauer, P. D.; Adamson, A. W.; Sartori, G. *Prcgr. Inorg. Chem.* **1972**, *17*, 1-56.

(58) Kirk, A. D. *J. Chem. Educ.* **1983**, *60*, 853-852.

(59) Forster, L. S. *Chem. Rev.* **1990**, *80*, 331-353.

(60) Zinato, E. *J. Am. Chem. Soc.* **1969**, *91*, 1076.

(61) Adamson, A. W. *J. Phys. Chem* **1967**, *71*, 798-808.

(62) Zink, J. I. *J. Amer. Chem. Soc.* **1974**, *96*, 4464-4470.

(63) Kirk, A. D. *Mol. Photochem.* **1973**, *5*, 127-150.

(64) Vanquickenborne, L. G.; Ceulemans, A. *Coord. Chem. Rev.* **1983**, *48*, 157-202.

(65) Vanquickenborne, L. G.; Ceulemans, A. *Inorg. Chem.* **1978**, *17*, 2730-2736.

(66) Vanquickenborne, L. G.; Ceulemans, A. *J. Am. Chem. Soc.* **1978**, *100:2*, 475-483.

(67) Kirk, A. D. *J. Am. Chem. Soc.* **1971**, *93*, 283-285.

(68) Manfrin, M. F.; Moggi, L.; Castelvetro, V.; Balzani, V.; Hosseini, M. W.; Lehn, J. M. *J. Am. Chem. Soc.* **1985**, *107*, 6888-6892.

(69) Kirk, A. D.; Moss, K. C.; Valentin, J. G. *Can. J. Chem.* **1971**, *49*, 1525-1528.

(70) Kutal, C.; Adamson, A. W. *Inorg. Chem.* **1973**, *12*, 1990-191994.

(71) a) Mønsted, L., *unpublished work.* b) Kirk, A. D.; Heyd, D. *Inorg. Chem.* **1991**, *30*, 2453 - 2457.

(72) Parker, C. A. "Measurement of Light by Chemical Methods" In *Photoluminescence of Solutions*; Elsevier Publishing Co.: Amsterdam, London, New York, **1968**; pp 208.

(73) Kirk, A. D.; Namasivayam, C. *Anal. Chem.* **1983**, *55*, 2428-2429.

(74) Demas, J. N.; Bowman, W. D.; Zalewski, E. F.; Velapoldi, R. A. *J. Phys. Chem.* **1981**, *85*, 2766-2771.

(75) Hamai, S.; Hirayama, F. *J. Phys. Chem.* **1983**, *87*, 83-89.

(76) Demas, J. N. *Excited State Lifetime Measurements*; Academic Press: New York, London, Paris, San Diego, San Francisco, São Paulo, Sydney, Tokyo, Toronto, 1983.

(77) McAuley, A.; Norman, P. R.; Olubuyide, O. *Inorg. Chem.* **1984**, *23*, 1938.

(78) Richman, J. E. A., T. J. *J. Am. Chem. Soc.* **1974**, *96*, 2268.

(79) Karbach, S.; Lohr, W.; Vogtle, F. *J. Chem. Res. (S)* **1981**, 314-15.

(80) Brodovitch, J. C.; Haines, R. I.; McAuley, A. *Can.J. Chem.*, **1981**, *59*, 1610 - 1614.

(81) Alexander, K. A.; Bryan, S. A.; Dickson, M. K.; Hedden, D.; Roundhill, D. M.; Che, C.-M.; Butler, L. G.; Gray, H. B. *Inorg. Synth.* **1986**, *24*, 211-213.

(82) Roundhill, D. M.; Gray, H. B.; Che, C.-M. *Acc. Chem. Res.* **1989**, *22*, 55-61.

(83) Chandrasekhar, S.; Fortier, D. G.; McAuley, A. *Inorg. Chem.* **1993**, *32*, 1424 - 1429.

(84) Geue, R. J.; Searle, G. H. *Aust. J. Chem.* **1983**, *36*, 927 - 35.

(85) Endicott, J. F.; Perkovic, M. W. *Inorg. Chem.* **1991**, *30*, 3140.

(86) Fortier, D. G. *Ph.D. Thesis* **1988**, *University of Victoria.*

(87) Greene, T. W.; Wuts, P. G. M. *Protective Groups in Inorganic Synthesis*; John Wiley & Sons, Inc.: New York, **1991**.

(88) Weisman, G. R.; Vachon, D. J.; Johnson, V. B.; Gronbeck, D. A. *J. Chem. Soc., Chem. Commun.* **1987**, 886.

(89) Blake, A. J.; Fallis, I. A.; Gould, R. O.; Parsons, S.; Ross, S. A.; Schröder, M. *J. Chem. Commun.* **1994**, 2467.

(90) Atkins, T. J. *J. Am. Chem. Soc.* **1980**, *102*, 6364.

(91) Haines, R. I.; McAuley, A. *Coord. Chem. Rev.* **1981**, *39*, 77 - 119.

(92) Connolly, P. J.; Billo, E. J. *Inorg. Chem.* **1987**, *26*, 3224.

(93) Bradshaw, J. S. *Heterocyclic Chem.* **1989**, *26*, 1431.

(94) Rodopoulos, T. *unpublished results* **1996**.

(95) Beveridge, K. A.; McAuley, A.; Xu, C. *Inorg. Chem.* **1991**, *30*, 2074.

(96) Ingham, A. *Ph.D. Thesis* **1996**, *University of Victoria.*

(97) Kulstad, S.; Malmsten, L. A. *Acta Chem. Scand. B* **1979**, *33*, 469.

(98) Zervas, L.; Theodoropoulos, D. M. *J. Org. Chem.* **1982**, *47*, 1324.

(99) El Amin, B.; Anantharamaiah, G. M.; Royer, G. P.; Means, G. E. *J. Org. Chem.* **1979**, *44*, 3443.

(100) Sperline, R. P.; Dickson, M. K.; Roundhill, D. M. *J. Chem. Soc. Chem. Commun.* **1977**, 62-63.

(101) Che, C.-M.; Cho, K.-C. *J. Chem. Soc. Chem. Comm.* **1987**, 133-134.

(102) Heuer, W. B.; Totten, M. D.; Rodman, G. S.; Hebert, E. J.; Tracy, H. J.; Nagle, J. K. *J. Am. Chem. Soc.* **1984**, *106*, 1163-1164.

(103) Roundhill, D. M.; Shen, Z.-P.; King, C.; Atherton, S. J. *J. Phys. Chem.* **1988**, *92*, 4088-4094.

(104) Kirk, A. D.; Cai, L. Z. *Chem. Commun.* **1997**, 523-524.

(105) Che, C.-M.; Butler, L. G.; Gray, H. B. *J. Am. Chem. Soc.* **1981**, *103*, 7796-7797.

(106) Fordyce, W. A.; Brummer, J. G.; Crosby, G. A. *J. Am. Chem. Soc.* **1981**, *103*, 7061-7064.

(107) Beveridge, K. A.; McAuley, A.; Xu, C. *Inorg. Chem.*, **1994**, *30*, 2074.

(108) Barefield, E. K. *Inorg. Chem.* **1972**, *11*, 2273.

(109) Cummings, S.; Seivers, R. E. *J. Am. Chem. Soc.* **1970**, *92*, 215.

(110) Barefield, E. K.; Busch, D. H. *Inorg. Chem.* **1971**, *10*, 1216.

(111) Lovecchio, F. V.; Gore, E. S.; Busch, D. H. *J. Am. Chem. Soc.* **1974**, *96*, 3109.

(112) Buttafava, A.; Fabbrizzi, L.; Perotti, L.; Poggi, A.; Poli, G.; Seghi, B. *Inorg. Chem.* **1986**, *25*, 1456.

(113) Xu, C. *Ph.D. Thesis* **1991**, *University of Victoria.*

(114) Kalyanasundaram, K. *Coord. Chem. Rev.* **1982**, *46*, 159-244.

(115) Fetterolf, M.; Friedman, A. E.; Yang, Y.-Y.; Offen, H.; Ford, P. C. *J. Phys. Chem.* **1988**, *92*, 3760-3763.

(116) Zeigerson, E.; Ginsburg, G.; Schwartz, N.; Luz, Z.; Meyerstein, D. *J. Chem. Soc. Chem. Commun.* **1979**, 241.

(117) Horvath, O.; Stevenson, K. L. *Charge Transfer Photochemistry of Coordination Compounds*; VCH Publishers, Inc.: New York, Weinham, Cambridge, **1993**.

(118) Cho, K. C.; Che, C. M. *Chem.Phys.Lett.* **1986**, *124*, 313.

(119) Scandola, F.; Balzani, V.; Schuster, G. B. *J. Am. Chem. Soc.* **1981**, *103*, 2519-2523.

(120) Nagle, J.; Heuer, W. B.; Totten, M. D.; Rodman, G. S.; Hebert, E. J.; Tracy, H. J. *J. Am. Chem. Soc.* **1984**, *106*, 1163-1164.

(121) Balzani, V.; Scandola, F.; Orlandi, G.; Sabbatini, N.; Indelli, M. T. *J. Am. Chem. Soc.* **1981**, *103*, 3378.

(122) Chiorboli, C.; Indelli, M. T.; Scandola, M. A. R.; Scandola, F. *J. Phys. Chem.* **1988**, *92*, 156-163.

(123) Cai, L.-Z.; Kneeland, D. M.; Kirk, A. D. *J. Phys. Chem.* **1997**, *101*, 3871-3879.

(124) Fortier, D. G.; McAuley, A. *J. Am. Chem. Soc.* **1990**, *112*, 1990.

(125) Meyer, T. J. *Progr. Inorg. Chem.* **1983**, *30*, 389-440.

(126) *Fundamental Concepts of Photoinduced Electron Transfer*; Kavarnos, G. J., Ed.; Springer-Verlag: New York, **1990**; Vol. 156, pp 21-58.

(127) Balzani, V.; Bolletta, F.; Ciano, M.; Maestri *J. Chem. Educ.* **1983**, *60*, 447-450.

(128) Bock, C. R.; Connor, J. A.; Gutierrez, A. R.; Meyer, T. J.; Whitten, D. G.; Sullivan, B. P.; Nagle, J. K. *J. Am. Chem. Soc.* **1978**, *101*, 4815.

(129) McAuley, A.; Macartney, D. H.; Oswald, T. *J. Chem. Soc., Chem. Commun.* **1982**, 274.

(130) Perkovic, M. W.; Heeg, M.; Endicott, J. F. *Inorg. Chem.* **1991**, *30*, 3140.

(131) Endicott, J. F.; Lessard, R. B.; Lynch, D.; Perkovic, M. W.; Ryu, C. K. *Coord. Chem. Rev.* **1990**, *97*, 65-79.

(132) Perkovic, M. W.; Endicott, J. F. *J. Phys. Chem.* **1990**, *94*, 1217-1219.

(133) Eigen, M. *Agnew. Chem.* **1963**, *75*, 489.

(134) Waltz, W. L.; Lilie, J.; Lee, S. H. *Inorg. Chem.* **1984**, *23*, 1768-1775.

(135) Irwin, G. *unpublished results.*

(136) Forster, L. S.; Murrow, D.; Fulcaloro, A. F. *Inorg. Chem.* **1990**, *36*, 3706.

(137) Allsopp, S. R.; Cox, A.; Kemp, T. J.; Reed, W. J. *J.C.S. Faraday* **1980**, *76*, 162.

(138) Gaith, A. M.; Forster, L. S.; Rund, J. V. *Inorg. Chem.* **1987**, *26*, 2493.

(139) Kepert, D. L. *Inorganic Stereochemistry*; Springer-Verlag: New York, **1982**.

(140) Perkovic, M. W.; Heeg, M. J.; Endicott, J. F. *Inorg. Chem.* **1991**, *30*, 3140 3147.

(141) Comba, P.; Mau, A. W. H.; Sargeson, A. M. *J. Phys. Chem.* **1985**, *89*, 394-396.

(142) Ramasami, T.; Endicott, J. F.; Brubaker, G. R. *J. Phys. Chem.* **1983**, *87*, 5057-5059.

(143) Chandrasekhar, S.; Fortier, D. G.; McAuely, A. *Inorg. Chem.* **1993**, *32*, 1424.

(144) Adamson, A. W.; Fleischauer, P. D. *Concepts of Inorganic Photochemistry*; John Wiley & Sons, Inc.: New York, London, Sydney, Toronto, **1975**.

(145) Kirk, A. D.; Scandola, M. A. R. *J. Phys. Chem.* **1982**, *86*, 4141-4143.

(146) Porter, G. B. In *Concepts of Inorganic Photochemistry*; Adamson, A. W., Fleischauer, P. D., Eds.; John Wiley & Sons, Inc.: New York, London, Sydney, Toronto, 1975; pp 37-80.

(147) Vincze, L.; Friesen, D. A.; Mezyk, S. P.; Waltz, W. L. *Inorg. Chem.* **1992**, *31*, 4950 - 4958.

(148) Linck, N. J.; Berens, S. J.; Magde, D. M.; Linck, R. G. *J. Phys. Chem.* **1983**, *87*, 1733 - 1737.

(149) Bolletta, F.; Maestri, M.; Balzani, V. *J. Phys. Chem.* **1976**, *80*, 2498.

(150) Wasgestian, H. F. *Z. Physik. Chem. Neue Folge* **1969**, *67*, 39-50.

(151) Cimolino, M. C.; Linck, R. G. *Inorg. Chem.* **1980**, *20*, 3499-3503.

(152) Okazaki, H.; Sakaguchi, U.; Yoneda, H. *Inorg. Chem.* **1983**, *22*, 1539.

(153) Taura, T.; Nakazawa, H.; Yoneda, H. *Inorg. Nucl. Chem. Letters* **1977**, *13*, 603.

(154) Yoneda, H. *J. Chromatogr.* **1985**, *313*, 59.

(155) Galsbol, F. *Inorg. Synth.* **1970**, *12*, 274.

(156) Kirk, A. D.; Hewavitharana, A. K. *Anal. Chem.* **1988**, *60*, 797-801.

(157) Kirk, A. D.; Fernando, S. R. L. *Inorg. Chem.* **1992**, *31*, 656 - 661.

(158) Kirk, A. D.; Ibrahim, A. M. *Inorg. Chem.* **1988**, *27*, 4567-4574.

(159) Kirk, A. D.; Ibrahim, A. M. *Inorg. Chem.* **1990**, *29*, 4848-4850.

(160) Lessard, R. B.; Endicott, J. F. *Inorg. Chem.* **1989**, *28*, 2574-2583.

(161) Friesen, D. A.; Lee, S. H.; Lilie, J.; Waltz, W. L.; Vincze, L. *Inorg. Chem.* **1991**, *30*, 1975.

(162) Friesen, D. A.; Lee, S. H.; Nashiem, R. E.; Mezyk, S. P.; Waltz, W. L. *Inorganic Chemistry* **1995**, *34*, 4026-4031.

(163) Vincze, L.; Friesen, D. A.; Mezyk, S. P.; Waltz, W. L. *Inorg. Chem.* **1992**, *31*, 4950.

(164) Kirk, A. D. *personal communication* .

APPENDIX 1

1) Quantum yield determination for irradiation of $Cr(sen)^{3+}$ at $\lambda = 436$ nm.

i) Ferrioxalate actinometry to determine I_0 (see section 2.2.6):

$$I_0 = \left[\frac{A_p - A_d}{\varepsilon_{510}\, l}\right]\left[\frac{V_T}{\Phi\, f_a\, t}\right]$$

$$I_0 = \left[\frac{0.25 - 0.01}{1.105 \times 10^4\ M^{-1}\ cm^{-1} \times 1\ cm}\right]\left[\frac{0.02500\ L}{1.11 \times 0.5 \times 30\ s}\right]$$

$I_0 = 3.29 \times 10^{-8}$ einstein s^{-1}

I_0 was taken as the average of three determinations measured for irradiation times, t , of 15, 30, and 45 seconds.

time (s)	A_p	A_d	I_0 (einstein s^{-1})
15	0.13	0.01	3.30×10^{-8}
30	0.25	0.01	3.29×10^{-8}
45	0.37	0.01	3.29×10^{-8}
			3.29×10^{-8}

ii) Correction of I_0 for window reflectance:

A window reflectance of ~4% is estimated[76], therefore 96% of the light is transmitted through the front face of the cell. The back face of the cell reflects 4% of the light back to the solution being irradiated.

$$I_0' = (0.96 \times I_0) + (0.04 \times 10^{-A} \times I_0)$$

$= (0.96 \times 3.29 \times 10^{-8}$ einstein $s^{-1}) + (0.04 \times 10^{-0.45} \times 3.29 \times 10^{-8}$ einstein $s^{-1})$

$= 3.20 \times 10^{-8}$ einstein s^{-1}

iii) Determination of $\emptyset_{rxn}$ from pH stat method:

The experimental proton uptake curve shown in Figure 5.4 was fitted to the quadratic expression $y = ax^2 + bx + c$ (Igor Pro 3.05 software, Wavemetrics) where the coefficients a, b, c are variables. The initial slope was obtained as the coefficient, b, of the first order term. The rate of thermal proton uptake can be estimated from linear regression on sections of the proton uptake plot before and after the photolysis and subtracted from the initial slope to obtain the total corrected initial proton uptake rate. In this case the proton uptake due to thermal reactions was found to be negligible. A plot of a straight line having the initial slope is shown in Figure A1, this was used to determine the total volume of acid added over the irradiation time A corrected volume of 60 µL of of acid was determined for a photolysis time of 2255 s.

$$\emptyset_{rxn} = \frac{\text{moles of product formed}}{\text{moles of photons absorbed}}$$

moles of product formed = (volume acid added) x (acid concentration)

$= 60.0 \times 10^{-6}$ L x 0.09427 mol L^{-1}

$= 5.66 \times 10^{-6}$

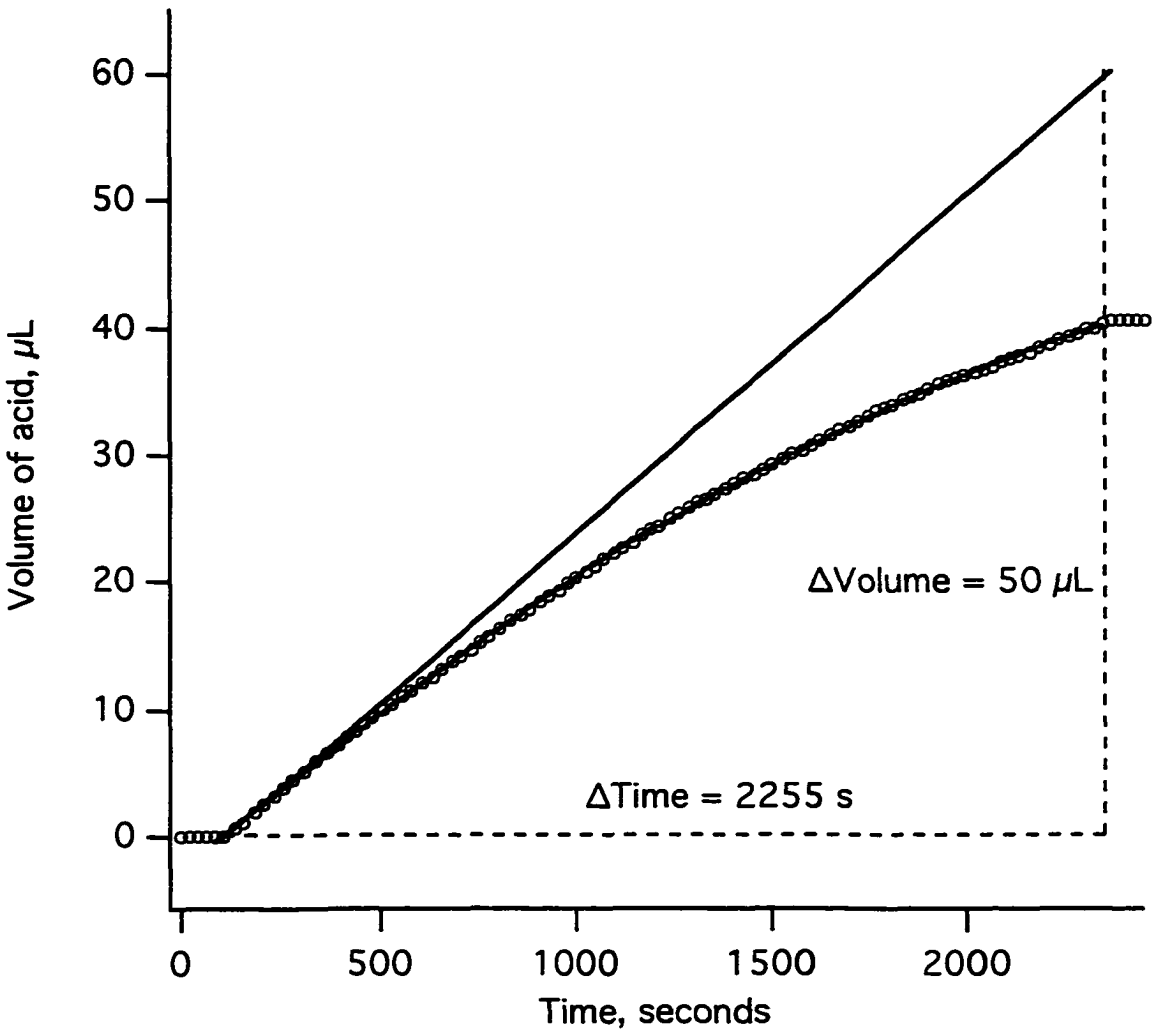

Figure A2 Plot of volume of acid added versus irradiation time for the photolysis of [Cr(sen)]Br_3 at $\lambda = 436$ nm, corrected for secondary photolysis.

moles of photons absorbed $= I_0 \times (1-10^{-A}) \times$ (photolysis time)

$= 3.90 \times 10^{-8}$ einstein $s^{-1} \times (1 - 10^{-0.45}) \times 2255$ s

$= 5.7 \times 10^{-5}$

$$\Phi_{rxn} = \frac{5.66 \times 10^{-6} \text{ mol}}{5.7 \times 10^{-5} \text{ mol}}$$

$$\Phi_{rxn} = 0.10$$

2) Quantum yield determination for irradiation of $Cr(sen)^{3+}$ at $\lambda = 675$ nm.

i) Power meter reading used to determine I_0:

$$\text{energy of 1 photon, } E_{675} = \frac{hc}{\lambda} = \frac{6.626 \times 10^{34} \text{ J s} \times 3.00 \times 10^{8} \text{ m s}^{-1}}{6.75 \times 10^{-7} \text{ m}}$$

$= 2.95 \times 10^{19}$ J

energy of 1 mole of photons $= 2.95 \times 10^{19}$ J photon^{-1} x 6.02×10^{23} photon mol^{-1}

$= 1.78 \times 10^{5}$ J

power reading, 33 mW $= 33 \times 10^{-3}$ J s^{-1}

$$I_0 = \frac{33 \times 10^{-3} \text{ J s}^{-1}}{177590 \text{ J mol}^{-1}}$$

$I_0 = 1.85 \times 10^{-7}$ einstein s^{-1}

ii) Correction of I_0 for window reflectance:

$$I_0' = (0.96 \times I_0) + (0.04 \times 10^{-A} \times I_0)$$

$$= (0.96 \times 1.85 \times 10^{-7} \text{ einstein } s^{-1}) + (0.04 \times 10^{-0.09} \times 1.85 \times 10^{-7} \text{ einstein } s^{-1})$$

$$= 1.83 \times 10^{-7} \text{ einstein } s^{-1}$$

iii) Determination of Φ_{rxn} from pH stat method:

$$\Phi_{rxn} = \frac{\text{moles of product formed}}{\text{moles of photons absorbed}}$$

moles of product formed = (volume acid added) x (acid concentration)

$$= 15.6 \times 10^{-6} \text{ L} \times 0.09427 \text{ mol } L^{-1}$$

$$= 1.47 \times 10^{-6}$$

moles of photons absorbed = $I_0 \times (1-10^{-A}) \times$ (photolysis time)

$$= 1.83 \times 10^{-7} \text{ einstein } s^{-1} \times (1 - 10^{-0.09}) \times 537 \text{ s}$$

$$= 1.8 \times 10^{-5}$$

$$\Phi_{rxn} = \frac{1.47 \times 10^{-6} \text{ mol}}{1.8 \times 10^{-5} \text{ mol}}$$

$$\Phi_{rxn} = 0.078$$

Quantum yield was measured as a function of dye laser micrometer setting to ensure that a maximum value of Φ_{rxn} was obtained, corresponding to irradiation into the doublet peak maximum at 675 nm. A plot of Φ_{rxn} versus micrometer setting is shown in Figure A2.

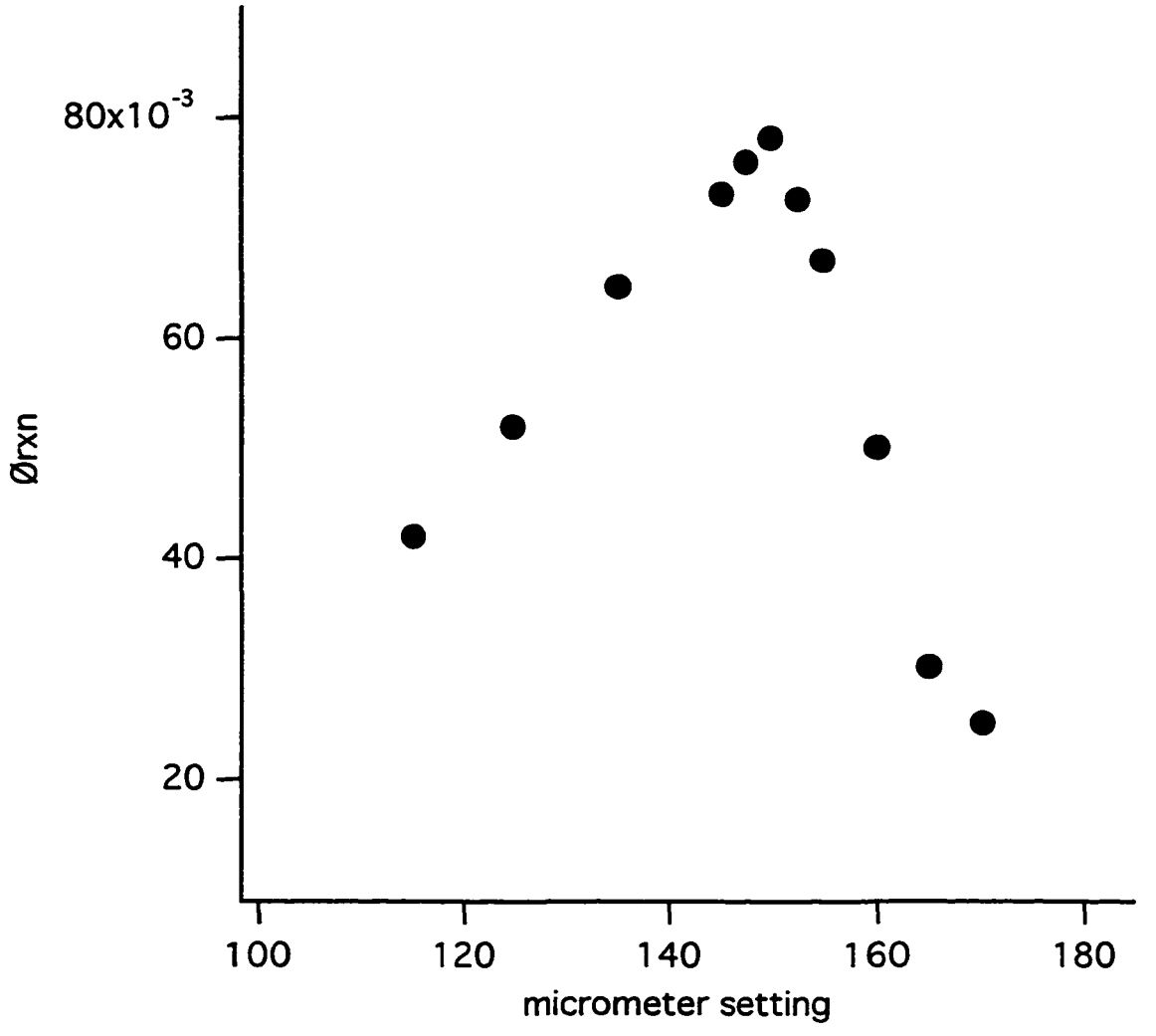

Figure A2 Direct doublet irradiation of $Cr(sen)^{3+}$: quantum yield, $Ø_{rxn}$, as a function of dye laser micrometer setting.